EXPERIMENTAL AND THEORETICAL STUDIES ON ELECTROSTATIC SPRAYING FROM A SINGLE ORIFICE

by

NESLI ZILER, B.Sc., M.Sc.,

November 1988

A thesis submitted for the degree of Doctor of Philosophy of the University of London and for the Diploma of Membership of Imperial College.

Department of Chemical Engineering
and Chemical Technology,
Imperial College,
London, S.W.7.

To my family

Statement

This thesis is based on work carried out in the department of Chemical Engineering and Chemical Technology at Imperial College, London, and is the original and independent work of the author except where specifically acknowledged in the text.

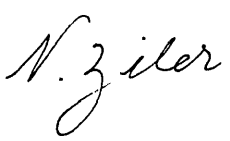

N. Ziler

(Candidate)

ACKNOWLEDGEMENT

I am indebted to and would like to sincerely thank my supervisors Professor Anita I. Bailey of the Department of Chemical Engineering at Imperial College, and Dr. Tharwat F. Tadros of the Agrochemicals Division of I.C.I., for their guidance, sound advice and moral support during this work. I would also like to thank Dr. Ighan Hayati of the Department at Imperial College for his many helpful suggestions.

My thanks also to members of staff at the Chemical Engineering Department, particularly Mr. K. Gurney, for his help in building the apparatus, and Mr. L. Moulder for his photographic assistance.

I am grateful to Dr. M.J.M. Bernal of the Department of Mathematics, Imperial College, for advice on the numerical solution of the equations and also to Mr. P. Winn and Mr. N. Fletcher for their experimental help at I.C.I.

I would like to express my appreciation to my family and friends, who gave me much encouragement and support.

This research was supported financially by I.C.I., Agrochemicals Division, at Jealot's Hill, and by S.E.R.C.

CONTENTS

LIST OF FIGURES

LIST OF SYMBOLS

Latin letters

A - area
c_l - length of the capillary
c_m - charge to mass ratio
d - diameter of drops
d_d - diameter of the top disc
E - electric field intensity
E_n - electric field in the normal direction
E_t - electric field in the tangential direction
E_l - electric field within a pulsating liquid
E_r - radial field outside the jet
e_e - electric energy
e_s - surface tension energy
e_t - total energy of a system containing many droplets
e_p - total energy of the parent drop
F - force per unit volume of liquid
$f(\theta)$ - function of θ
g - acceleration of gravity
H - height
I_o - Ohmic current
I_c - convection current
I_t - total current
J - current density
k - conductivity
k_w - wavenumber
L - length of capillary

l - distance between the top disc and the earthed collector

m_d - mass of a drop

M - mass flowrate

n - number of charges per unit volume

n_j - number of jets formed

N - number of drops

p - polarization per unit volume

p - pressure of the jet

p_s - pressure of the surroundings

Q - bound charge or charge on a parent drop

q - charge on a drop

q_a - charge density in the bulk

q_v - charge per unit volume

q_o - initial charge in the volume of a liquid before a field is applied

r - radial direction of a cylinder

r_c - radius of capillary

r_j - radius of jet

r_o - radius of spherical charge injection electrode

r_g - radius of earthed collector

r_a - radius of a jet disturbed from the equilibrium

r_p - radius of drop

R - radial direction for a cone

R_p - radius of parent drop

s - radius of the outside wall electrode

t - time

T_n - normal electric stress

T_t - tangential elctric stress

u_i - velocity of the ions

u_r - radial velocity

u_z - velocity in the downward direction

u_s - velocity at the surface of the cone region of the jet

u_t - velocity of the liquid near the sphreical electrode

u_j - velocity of the jet just before the point of break up

v - volume

V_f - volumetric flowrate

V_j - voltage of the jet

V_e - voltage at the end of the jet

V - voltage

V_c - voltage applied to the capillary

V_w - voltage on the outside wall electrode

z - downward direction

Greek letters

$\alpha(t)$ - time dependent amplitude of a disturbance
γ - surface tension
ε - permittivity
ε_o - permittivity of free space
θ_o - semi-cone angle
λ - wavelength
μ - viscosity
μ_m - mobility of ions
ρ - density
σ - charge per unit length
σ_s - surface charge density
τ - relaxation time
ψ - stream function
ω - growth constant of a wave
ω_m - maximum value of the growth constant

ABSTRACT

The formation of the single steady jet issueing from a capillary held at high potential has been studied. Equations were developed to predict the variation of the tangential electrical stress on the surface of the cone region of the jet with the distance from the capillary. The analysis incorporates internal convection. The solutions estimate that the tangential field and tangential stress peak near the tip of the cone. In the cone region, the behaviour of the liquid is similar to that of a conductor. The stress falls in the cylindrical region of the jet, where the liquid behaves like an insulator.

By placing an earthed ring above the capillary, the electric field could be intensified. At high field strengths the single jet is replaced by the formation of several jets at the periphery of the capillary. The numbers of jets drawn out from the liquid surface were found to depend on the voltage applied. The emission of the jets was studied as a function of the electrical conductivity of the liquid, the viscosity and the liquid flowrate. Measurements of the current and dimensions of the jets were used to explain the division of the liquid into an ensemble of jets. New surfaces are formed, so that the increase in surface area is comparable to the increase in the charge carried. The requirement on the surface area was attributed to the value of the conductivity.

The size and charge to mass ratio of the drops produced from the single jet and multiple jets are correlated with the various parameters involved; the flowrate, conductivity and viscosity of the liquid, and the voltage. The drop size was found to be most sensitive to field strength, and the flowrate. The effect of the conductivity was to increase the charge to mass ratio of the drops, while the size remained virtually constant.

CHAPTER ONE

INTRODUCTION

The dispersal of liquids by electrostatic means requires the presence of charges on the surface of the liquid, or on an interface between fluids. Surface charge may be caused in a number of ways. For instance, charge may be induced on the liquid by an externally applied field. If a flat conducting plate, at high potential, is situated above a pool of liquid, a field is established in the gap between the plate and the liquid. The surface acquires charge of opposite polarity to that on the plate in the presence of the field. When the plate is replaced by a sharp metal point, a strong field is established. If the field strength is high enough, ions or electrons are emitted from the conductor. Field strengths high enough to cause electron or ion emission are almost impossible to attain in gaseous environments, because electrical breakdown of the gas occurs at lower field intensities. Therefore it is not a usual method for charging liquids. However, very insulating liquids can be sprayed electrostatically by surrounding a fine point held at high potential with the liquid. In this way, a field is established within the liquid, rather than in a gas.

The liquids that are sprayed electrostatically in industry have finite conductivities (10^{-4}-$10^{-8}(\Omega m)^{-1}$), and are classified as semi-insulators. The conduction method is the most widely used to charge this class of liquids. High potential and a low direct current are applied to the metal electrode, which imparts charge to the liquid by contact.

In the particular application to crop spraying, the liquid issues from an annular gap in the metal electrode. The application of high potential results in the extension of several jets of liquids from the annulus. The jets have finite length and eventually emit drops far from the electrode. An important characteristic of the spraying process is the formation of a charged aerosol.

Electrohrodynamic spraying has several advantages over conventional spray techniques;

1. The production of charged drops leads to more efficient targetting, as the drops are attracted to the earthed target. Since liquids are sprayed at low flowrates, (600-3000 ml/h), the liquid consumption is minimised. Apart from the cost savings, better targeting is also environmentally beneficial.

2. The disintegration of the jets results in a monodisperse size distribution of drops.

3. The drop size can be better controlled by varying the potential applied to the nozzle electrode.

4. Because electrical forces are employed to replace the compressed air and high pressure liquid delivery used in conventional spraying, the energy requirements are lower.

1.1 Factors which influence electrostatic spraying.

If a liquid is allowed to flow through a capillary facing an earthed electrode, the surface tension causes a drop to be transiently formed at the capillary tip. When the liquid mass becomes large, the force of gravity pulls the drop off. Once a potential is applied to the capillary, electrical forces aid gravity forces, so that the dripping becomes more rapid. As the potential is increased, the drop at the tip is elongated before leaving the tip. Further

potential increments lead to pulsation, where the elongation is accentuated until a mass is emitted. The liquid meniscus momentarily relaxes back to the capillary, until the cycle is repeated. Eventually a value of the potential is reached whereby the elongation of the drop is at steady state and a jet is formed.

Clearly, the strength of the field influences the manner of spraying, by determining the magnitude of the electrical forces. These forces operate partly by virtue of the presence of charge on surface of the liquid. The conductivity of the liquid is hence an important factor. Another significant parameter is the surface tension, while the permitivity of the liquid affects the field inside the liquid. In the dynamic situation, the effects of the flowrate and the viscosity of the liquid must also be considered.

1.2 Objectives of the work.

While the externally applied field is the primary factor affecting the spraying regime, the space charge introduces another consideration. In the absence of an applied field, the charge on the liquid establishes its own field. For a curved surface, the value of the field will be highest in the vicinity of the liquid where the electrical forces are operative. Yet surface charge is caused by the application of an external field, so that the overall situation is that of a modification of the field in the region of the liquid surface. Theoretical analyses of the behaviour are further complicated by the free surface of the liquid, the profile of which depends, amongst other forces, on the electrical forces.

The work carried out here applies to a metal capillary facing a flat earthed collector. The capillary

protrudes at right angles from the centre of a flat conducting disc. This arrangement allows assumptions to be made to simplify the theoretical treatment. Much work has been done in the past on predicting the electrical stresses, with different approaches used in different theories. However, many questions about how the current is carried by the jet, and the electrical stress which causes the jet to accelerate remain unanswered. A set of equations has been developed and solved here to predict the distribution of the electrical stress. The estimation of the stress on the surface of the steady jet is presented in the fifth chapter. The stress arises from the motion of the charges under the influence of the field, and from the fields set up due to the convection of charge along with the motion of the liquid. Recent work on the mechanism of the formation of the steady jet is incorporated into the equations (40,41). In the past, the conical portion of the jet, close to the metal electrode, has been assumed to discharge liquid into the cylindrical portion from the bulk of the cone. However observations of internal circulation, made by others, have lead to the conclusion that the material is stripped from the surface of the cone to form the cylindrical geometry. A review of the theories that form the background of the analyses can be found in chapter three. Observations of the break up of the jet are also presented in the first results chapter, along with measurements of the jet at a point prior to break up.

A great many publications refer to the deformation of drops, the ejection of droplets from a parent drop, and the behaviour of the steady jet. However, very little is known about the behaviour of liquid at higher field strengths. In chapter six, another regime of spraying is described. The intensification of the field lead to the formation of more than one jet at the periphery of the capillary. The way in which the field is intensified was

studied, as well as the conditions that determine the numbers of jets that are emitted. Using a telescope, as many as twenty jets were observed.

Although the literature on electrostatic spraying is extensive, there is a lack of knowledge about the aerosol produced. In the case of a static liquid in a container, the application of a field across the liquid results in the conduction of current. The value of the current can be found from the conductivity of the liquid and the cell constant. The constant is determined from the dimensions of the container. The spraying process is a dynamic one, in which the profile of the liquid depends on many factors and is not restricted by solidboundaries. An analogous 'cell constant', i.e. the length and the diameter of the jet, or an ensemble of jets, is difficult to define. Moreover, the charges on the liquid surface are carried, at least partly, by material convection. There is therefore a need to quantify the charge on the resultant drops by direct measurement. The final results chapter contains correlations of the drop size and the charge to mass ratio of the drops, against the parameters that have been investigated. A comprehensuve study was aimed at identifying the factors that have the greatest influence on the numbers of jets formed, and also the characteristics of the spray cloud. Some theories available in the literature are compared with the measured values. An equation was used to confirm the relation, obtained from measurements, between the drop size and the liquid flowrate. The measurements also provide some insight as to why liquids are dispersed in the form of several jets at high field strengths. The ideas concerning the multiple jets were also found to explain the changes occuring to the end of the single jet when the flowrate of the liquid is varied.

The single jet and the ensemble of jets were observed under diferent conditions, where several parameters were varied. Liquids of different conductivity, in the range $2x10^{-6}$-10^{-8} $(\Omega m)^{-1}$, were sprayed. The viscosity of the liquid was varied between 5 and 70mPas, while flowrates in the range 3-300 ml/h were investigated. Different sized capillaries were used in the work on multiple jets. Other electrodes were employed to give high field strengths.

A description of the apparatus and the procedures followed are given in chapter four. The next chapter is a survey of the broad spectrum of publications on the disruption of an electrically charged liquid.

CHAPTER TWO

LITERATURE SURVEY

2.1 Introduction

The electrostatic atomisation of a liquid has applications in a number of areas. Often the spray characteristics vary, for instance in the development of rocket propellants, small highly charged particles are required, whearas crop spraying requires the drops to be within a certain size range and to have moderate levels of charging. Several processes are available for obtaining an aerosol by the imposition of an electric field. The value of the field applied, the flowrate of the liquid, as well as its properties are some of the factors influencing the modes of spraying. Observations reported by authors relating to the different spraying regimes will be discussed in a later section. Also theoretical work presented in the literature concerning the mechanism of formation of a steady jet and the various concepts used to invisage the disruption of a charged liquid are reviewed.

Bose(1) was the first to observe the effect of charge on a liquid, in 1745. The rate at which a liquid drips from a fine needle was seen to increase as the potential was raised so that progressively smaller drops were formed. Later in 1914, Zeleny investigated the stability of a charged drop on the end of a conductor. By raising the voltage he determined the field strengths at which a drop begins to deform (2). Zeleny also studied electrical discharges from pointed conductors and liquids at a time when the mechanisms of corona were little understood(3). During discharge from an apex of liquid, a filament was

formed whose shape broke down far from the electrode into drops (4). Other work involved investigating the onset of currents in the presence of various gases and coating metals with salts and oxides, and testing for the ejection of ions from a surface by impact. He also carried out one of the earliest analyses of the effect of point curvature on electric field intensities.

The behaviour of liquids in a field was explained by the presence of charge at the surface causing electrical forces to counter the cohesive surface tension forces. Rayleigh examined the relative effects to determine when the charge on a conducting drop of specified radius exceeds surface tension so that the spherical form is lost and a fine jet is admitted (5). The criterion depends on the surface tension, radius and permitivity of the surrounding medium. Since then the results have been widely reported and closely related problems have been worked out. However it was not until 1963 that an extensive derivation of the stability of a conducting drop was presented by Hendricks and Schneider to confirm Rayleigh's criterion (6).

Once surface tension has been overcome, a jet is thought to be formed. However the surface tension force comes back into play as it causes instability near the end of the jet, leading to the formation of drops again, though very much smaller than the original drop. Other parameters of the liquid, together with the characteristics of the surroundings, are also important in assessing the circumstances under which a jet disintegrates into drops. Rayleigh showed that the fineness of a jet has a limit; at small enough radii the column of liquid would not support a high charge density. This work applies mainly to a cylindrical shape carrying high charge rather than a jet which would carry a lower level of charge. Earlier (7) he considered the stability of a neutral liquid to gravity and surface tension, using a linear analysis whereby the radius

of the jet is constant prior to the application of a disturbance. The disturbance becomes amplified at a particular wavelength into a drop. One of the most significant outcomes of the analysis is the relation of the drop size to the size of the jet; the drop diameter is 1.9 times that of the jet. Many workers have sprayed semi-insulating liquids from a capillary in such a way that a jet cannot be formed without an external field, (without charging), to find that the ratio of sizes is satisfied despite the charge carried(8,10). This may be due to the insensitivity of the wavelength of disturbance (caused by background noise as opposed to directly imposed) to the amount of charge present. Nevertheless the stability of a jet is affected by charge in so far as it alters the rate of growth of a wave, even though it may leave the characteristic of the wave unaltered. Rayleigh's equations apply to growth in space rather than in time, so they do not apply to discontinuities in flow. Another set of equations were derived to describe this (7). Further work was done on relating the dependancy of the growth rate of a wave on the wavenumber in 1892 (9), when the effects of viscosity were included after observations reported by Plateau on the jet lengths of high viscosity liquids.

Bassett added to Rayleigh's work by carrying out a more general investigation in which the velocity, surface tension, viscosity of the liquid, as well as the influence of the surrounding air were taken into account (11). The jet also carried charge on its surface. He pointed out that if a charged sphere is brought into the vicinity of a jet, the jet is lengthened, but in the case of a more powerful charge, the disintegration proceeds more rapidly. Rayleigh believed that providing the column was not charged to the extent that would cause disruption by the mechanism he had developed, any charge on a liquid jet ought to enhance its stability; colliding charged drops tend to coalesce rather

than rebound. Bassett's results showed that charge tends to produce stability or instability according to the ratio of jet circumferance to the wavelength is less than or greater than 0.6. Thus for small wavelengths, charge will contribute to instability. However Bassett also concludes that at very small wavelengths surface tension stabilises the configuration so that there is a narrow range of wavelengths over which charge acts in concert with surface tension. Nevertheless, a large enough charge will overcome the steadying effects of viscosity and surface tension at the small wavelengths. Some experimental measurements of jet lengths prior to break up are reported by Hendricks (12) who adjusted the charging by varying the conductivity of the liquid. The lengths peaked at a certain conductivity and then decreased as the conductivity was raised further. Neither Hendricks nor Bassett were able to explain the stability due to a slight charge, but the latter's results give a satisfactory explanation of the large charge effect. Melcher (13) has also confirmed Basset's results for a jet and has assesed cases of the influence of differently oreintated fields on the stabilities of liquid sheets.

The tendency for drops to coalesce was studied by Taylor many years later. He supported soap films and drops on two equal coaxial metallic rings and applied a potential difference between them (14). When the drops were placed very close to one another the potential difference for coalescense was found to depend directly on the distance between the drops and indirectly on the square root of their radii.

The analysis on charged jets described above is applicable to cylindrical geometries where the charges residing at the surface are directed outward to air. A more general case of stability of a horizontal interface between a conducting and a non-conducting liquid in an initially vertical field is considered by Taylor and McEwan (15). The

effects of charge relaxation from the bulk and the presence of electrical shear were included for the static case of the horizontal interface subjected to a perpendicular field by Melcher and Smith (16). The inclusion of shear involved the viscosity of the liquid. Anno has analysed the stabilty of a charged viscous jet for the case of flow into another liquid in order to include the effect of shear on a dynamic system (17). The work of Melcher and Schwarz (18) concerns the effect of an ohmic current on waves created by polarization forces on an horizontal interface of a nearly insulating liquid in the prescence of a tangential field. The stability of a dielectric jet in a longitudinal field is evaluated by Nayyar and Murty (19). They examined the effect of introducing a material of different permitivity into a fluid encompassing an electric field. The equations apply to nonconducting inviscid fluids .

2.2 The disintegration of drops

Several workers have considered the formation of a jet from an initially spherical form.

Taylor and Wilson presented photographs of soap bubbles deforming and bursting in a uniform electric field when they placed hemispheres on an earthed disc (20). A second disc was situated at high potential above the first. As the potential was raised, the drop was drawn towards the top plate. Further slight increase resulted in either rapid vibration and the ejection of a jet which emitted drops, or the ejection of drops directly from the liquid meniscus. They determined the field at which a drop just becomes unstable ;

$$E = \sqrt{\gamma r}$$

The equation was verified by experimental results. Macky confirmed the relation for water drops falling through a strong field (21). At the point of instability filaments were formed at both ends and a current was discharged from the drop.

The equation determines the field required to cause deformation, but gives no indication of the mechanics of the process. Taylor analysed the stresses on a drop to show that the assumption made by others of equal internal and external pressures during deformation to be incorrect (22). A drop is shown to become unstable when its length is 1.9 times its equatorial diameter, at which point a cone having a semi-vertical angle of 49.3 is formed. Measurements taken from photograghs of water-oil interfaces and soap films confirmed cone angles close to this value when the required field was applied.

Theoretical analysis of the droplet profiles at lower voltages before a cone is formed from a needle end illustrates successively smaller, longer shapes as the voltage increases. The tendancy for drops to be drawn in the direction of a field has also described mathematically by others (23-26), and the resulting changes in the electrostatic and surface tension energies as the deformation occurs are evaluated for a field of a point charge(27).

A number of authors have studied the increase in the ratio of electrical to surface tension forces by evaporating charged drops suspended in fields. In this way the theoretical Rayleigh limit for disruption into small dropswas approached. Doyle et al (28) used two parallel plates to support drops which had been produced from a needle held at high voltage. It was found that as the drop evaporated, a point was reached whereby the electrical forces caused the drop to be torn apart due to the Rayleigh condition.

Upon disruption, the parent drop lost 30% of its charge and the resulting daughter droplets were estimated to possess more charge than the original drop. For the case of a small parent drop, the daughter droplets were thought to be close to the Rayleigh limit. However, for a larger parent drop, the disruption lead to droplets which possesed charging levels below the limit. Abbas and Latham extended Doyle's technique in order to measure the charge and radius prior to and after disruption (29). The charge per mass lost during disruption was related to the parameters of the original drop. A significant observation was that the drop looses just enough charge so as to maintain the charge below the Rayleigh threashold. As the evaporation proceeds, sucessive emissions occurr within short times from the same drop. They also extended the range of parent drop sizes to determine that 25% of its mass is ejected, and drew attention to the fact that for larger parent drops, (1 mm), charge is lost by corona discharge.

Much smaller drops were investigated by Schweizer and Hanson (30), when they also verified Rayleigh's limit to an accuracy of 4%. Their experiments showed that 23% of charge and only 5% of mass are ejected, whereas the value for mass loss is 25% for the case of a larger parent drop. This could be due to the fact that the maximum charge to mass a drop may withstand increases inversely with the radius. Smaller drops would have to lose smaller amounts of mass in order to lower their size sufficiently.

A theoretical study of the disruption process is based on the idea of minimising the total energy of the system. A single drop of fixed volume is assumed to form equisized droplets by Vonnegut and Neubauer (31). The surface tension and electrical energies of the spray cloud are minimised so that either the final radius or the number of drops produced may be calculated from the known volume and charge of the original liquid. Another interpretation of their work is

that if the resulting drop size is predetermined, then the most probable charge to mass can be estimated. It was pointed out by Ryce (32) that this charge to mass ratio is equal to one half the Rayleigh limit.The energy minimisation theory was one of the first attempts at quantifying the break up of a liquid and stimulated theoretical work on the process, though the theory does not explain the mechanisms of jet formation .

Pfeifer and Hendricks (33) developed relationships between the radius and charge to mass ratio of sprayed particles along the lines of modelling suggested by Vonnegut The exploding parent drop was assumed to be at the Rayleigh limit since it was thought that lower charging would not lead to disruption. The fundamental basis of the work is that an energy sink exists such that during splitting into many particles energy is lost. Distributions of the total surface tension and electrical energies against numbers of particles illustrate the increase in the former relative to the latter. Their equations represent the transference of the energy from electrical to surface tension energy as the number of droplets formed increases. At a particular number of droplets, the sum of the two energies is at a minimum. A lowest limit was placed on the specific charge of a drop by maximising the surface tension energy. Thus the minimum charge to mass was found to be just under a quarter that of the Rayleigh limit. They present evidence that their results for glycerine, metal and Hendricks' results for octoil (52) support the minimum energy concept .

Ryce (32) has questioned the validity of assuming the parent drop to necessarily be at the Rayleigh limit before explosion, since the charging of a liquid at the end of a capillary is dependant on its conductivity and permitivity. Indeed previous work on the field strengths required to deform drops from capillary ends has not indicated the approachment of the limit.

Although many investigators have adopted the minimum energy hypothesis, Krohn (35) presents a number of arguments to demonstrate that it does not apply to electrohydrodynamic spraying, where a jet is formed. He obtained droplet chargings in excess of half the Rayleigh limit for Wood's metal and analysed the work of Vonnegut, Ryce, Hendricks and Doyle to conclude that the minimum energy state is reached by virtue of the comparatively low liquid conductivities.

For very high conductivity liquids the disruption process is accompanied by electrical discharge through the air due to the high field present at the drop tip. Macky and Zeleny had observed this for water (2,21). English (36) studied the behaviour of water drops at the tip of a capillary as both corona and drop emission occured. His observed large differences in positive and negative onset potentials in air. Analyses of point to plane corona and the nature of positive and negative corona are given by Loeb et al (37,38).

2.3 The continuous spraying of liquids.

Experimental results which indicate the possibilty of obtaining a highly dispersed monodisperse aerosol from a jet were first published in 1952 by Vonnegut and Neubauer (31), who atomised a variety of liquids. Both alternating and direct voltages were applied to water, sugar solutions, alcohols and insulating liquids. The drop size and uniformity were assessed from the bright colours present in the higher order Tyndall spectra. They determined that there is an upper conductivity limit for dispersing liquids; at high conductivity uniformity of size is lost and may only be regained at the expense of larger particles. Vonnegut and Neubauer operated at low flowrates and under certain sets of conditions. Later, other authors showed that the formation of a jet and its tendancy to yield monodisperse drops are

linked to various factors. Of these the significance of conductivity is emphasized the most.

Taylor's study on a meniscus deforming and extending to form a continum combines the effects of the voltage applied, the conductivity and the flowrate (39). Non-conducting liquids were seen to emit drops intermitently from the capillary even as the voltage was increased and their coalescence could be acheived by raising the flowrate. The importance of the size of the capillary for producing a jet was reported by Hayati(40). Certain sizes were favourable to conducting, others to less conducting liquids forming a jet. He also reports on the stages of liquid emission from a needle as the voltage is increased. Low values result in rapid dripping, after which a pulsating mode is reached whose frequency increases at higher voltages. An abrupt change to the formation of a steady jet occurs at slightly higher voltage.

Hendricks et al used high speed photography to examine the effects of conductivity and electrode potential on detachment from a needle (42). Drozin (43) describes similar behaviour but adds that when a jet is formed, it separates into several smaller threads at a few centimeters from the capillary tip. At higher voltage the point of division approaches the capillary tip and higher still values lead to a cloud of droplets in addition to three or four threads. The observations were made over long time scales so that it is unclear whether further splitting occurs due to the jet acting as an electrode at high potential or the apparent threads seen were lines of drops at high speed. According to Turnball et al (44) the jet mode is sensitive to the voltage applied. It may be appreciated that the succesive stages observed as the field is raised are accompanied by increases in the current. Thus there is a limit to the current a jet can carry; at high fields the single mode becomes unstable and may be replaced by numbers

of jets formed at the edge of the capillary. The conditions which would favour this behaviour have hardly been commented on in the literature. Hogan et al present pictures of Octoil spraying irregularly around the periphery with almost no liquid flowing along the capillary axis (42).

A monodisperse aerosol was produced via the pulsating regime by Sample and Bollini (45). Sizes in the order of 100 um were produced from very fine capillaries at low flowrates The drop size was found to depend on flowrate as well as geometry of the capillary.

In the interest of using charged drops as collection sites for particle pollutants, Hoburg and Melcher (46) studied current driven water jets. At high flowrate and high field a jet was formed which disintegrated due to the onset of corona. Other work on spraying glycerol doped with salt in vacuum diminished the corona effect(25). However, it should be noted that corona discharges in conditions of reduced pressure occurs at lower field strengths (47). Only below 50 mmHg, is the corona process prevented.

The difficulty of spraying conducting liquids has been tackled by spraying through small points in the pulsating or dripping modes. In their application of spraying conducting viscous liquids such as paints, Sickles and Anestos used a vibrating capillary to avoid the difficulties encountered due to the viscosity (48). The vibration produced drops linked to one another by a jet of liquid. Small drops were then formed from its disintegration in an electric field. This is an interesting deviation from other techniques that utilise vibrations to form drops directly from jets.

Insulating liquids such as nitrogen and freon have been sprayed via the jet mode by the method of charge injection (44,49,50). Liquid was admitted to a glass capillary inside which a sphere of high curvature provides the means of creating high field. The method differs from

the conduction method in that the point charge rather than the capillary sets up the field, so that the characteristics of the resulting jet (and therefore drops) is less dependent on the capillary size. Work on conduction charging has shown that the geometry of the electrodes significantly affect the behaviour of the liquid. A statistical model for spraying by the charge injection mode can be found in ref.51.

Emulsions have been prepared by a number of authors by collecting the disperse phase droplets produced from jets in the continuous phase (53-55). In some cases the disperse phase was sprayed inside the continuous phase (56). Others have measured the drop size of the aerosol by collection in a second immiscible liquid (57), though it was pointed out by Fuhks that the behaviour of a drop in a liquid differs substantially from that in air (58).

The above references to the factors affecting jet formation and the different conditions leading to different modes of spraying from a capillary have highlighted the importance of the field, the electrodes, and the conductivity of the liquid, especially when linked to the flowrate. These are not the only factors; spraying into different gases or straight into different liquids (4,40,56) can result in great deviations from spraying into air. Indeed the conditions in air, for instance humidity (which alters the conductivity) are also important variables. Other parameters of the liquid to be dispersed must also be commented on. The permitivity affects the process because it determines how the liquid responds to the field applied at the capillary. Work on spraying viscous liquids has shown that this parameter influences the behaviour of jets and drops in a field (48,60). Very little comment is available as to the importance of viscosity for the formation of a jet.

Some authors claim that a stage in which a liquid filament extends from the tip of a needle is essential to

the formation of a monodisperse aerosol (8,31,54). Others maintain that a jet is not necessary (52,42) and that fine droplets are sometimes ejected from a liquid apex or a very short cylinder. Analyses of jet stabilty conclude that fine jets are less stable and therefore are more likely to break up rapidly. Thus sprays can result from an apparent "apex", which may be likened to a very short, fine jet. In the case of a thicker jet, the jet could extend further from the electrode before drops appear, though this is also dependent upon the effect of the charge carried.

There is evidence in the literature that applications requiring moderate or high flowrates of liquids to be dispersed (relative to the values reported for single needles) involve the production of jets from points of liquid supply in order to achieve small sizes. Lindblad and Schneider exploited surface tension forces to break up a jet into 25-350 μm drops (61). A piezoelectric transducer was used to apply disturbances of large amplitude at the desired frequency to a jet. Further work on the stability of a jet involved of forming a jet by hydraulic means, the use of an ultrasonic device to create waves on the jet, and then charging the liquid by induction (10). Drops were produced having sizes between the minimum radius and 1.6 times the minimum radius for a particular value of the flowrate. Due to the method of charging, the drops were not accelerated in the field. For a single capillary facing an earthed target, the emitted drops experience a field and so accelerate. Schneider et al (10) developed equations describing the break up into drops and discuss the relative weights of charge on the surefce of the jet and the surface tension. Neukermans (62) later added a correction to the analysis .

Hydrodynamic forces can be combined with charge effects in apparatus for use in industrial or large scale operations (68). Ligaments coming off a spinning disc were charged to obtain more effective aerosols (63); Bell and

Hochberg studied drops sprayed from a rotary atomiser (64). Hines' (65) photographs show paint spraying as ligaments from the edge of a conducting cone. Castle and Inculent (66) sprayed orchards by more conventional means and charged the spray cloud by induction.

In paint and crop spraying optimum sizes are desired but the degree of monodispersity required depends on deposition requirements. The above review of the modes of atomisation considers the parameters affecting spraying. These parameters can also be expected to influence the degree of polydispersity of the drops. Although some work on the pulsating regime (at medium field strengths) indicates the possibility of producing drops of the same size, this mode would be expected to yield two or more sizes as the meniscus forms a throat upon detaching the main drop. In contrast the jet mode ought to lead to more uniform sizes because a jet is considerably finer than a pulsating meniscus. Thong et al (8,67) report that monodispersity occurs for a narrow range of the voltage applied to a capillary, in work relating to the formation of fuel injection particles. Here the mobility, i.e. charging, is important. Others have commented on the disadvantages of over charging; for instance in the case of pertubations of particle trajectories caused by corona (47).

Liquid conductivity was observed to affect the way a jet breaks up (17,39,69); lateral instabilties cause snake type patterns which lead to drop size variation, whearas regular axisymmetric waves tend to favour the formation of single drops. The former appears to be present for conducting liquids and the extent of wavering is influenced by the applied field in the surroundings (69).

The influence of viscosity was briefly discussed in the introduction. Analyses of jet stability conclude that viscosity delays wave growth. Taylor describes other effects namely the reversal of viscous stress on a jet as

aerodynamic drag overcomes the downward force far from the electrode (39). This causes the jet to bend back onto itself. Bailey reports the increase in drop size with increase in viscosity (59).

2.4 Quantifying the process.

A number of authors have connected the charge on the drops with thesize of the drops, but usually for the purposes of comparing measurements with theories, such as the Rayleigh limit or energy minimisation. Hendricks'(52) used a detector consisting of a cathode follower and oscilloscope to obtain charge to mass ratios. The drop sizes were under 10 μm. A stroboscope was employed with a microscope to record the frequency of drop ejection during the pulsating mode (45). The charge was obtained by dividing the current measured on an electrometer by the frequency. This experimental method is applicable for this particular spraying mode, where the frequencies are lower enough for accurate measuremnt. When using a camera to record drop sizes, Carson and Hendricks found that the pulating mode was sensitive to high intensity light (70).

Extensive work on the rotary atomiser lead to correlations of design variables against drop charge and drop size (64).

Hayati presents values for charge to mass ratio of drops produced via the single jet mode under different flowrates from a capillary (40). Drop sizings against conductivity for a spray produced by an annular nozzle illustrate that the size decreases as the conductivity increases until at relatively high conductivity, when the drop size begins to increase. This is an interesting result, since it shows that higher chargings do not reduce the size of the drops indefinately. Jones and Thong's (67) results

for both a horizontal and a vertical jet sprayed from a capillary show the size to be sensitive to flowrate. The dependence of charge to mass on fluid and atomization parameters for various solvents and paints was investigated by Anestos et al (71). They used a conventional atomiser in conjunction with electrostatics. It was found that an optimum value exists for conductivity where the specific charge of the spray exhibits a maximum.

Hogan and Hendricks' (42) tested their analysis of minimum energy and energy sink by measuring the charge of a spray from a thin needle. The theory accounts for the probability of producing various sizes of drops, depending on the balance of the surface tension and the electrical forces, though not for polydispersity observed. In practice absolute uniformity is rarely obtained and charge to mass ratios are averaged for the spray cloud. Some workers have derived specific charge equations applicable to a polydisperse system (72) .

Pfeifer and Hendricks' (34) used a time of flight spectrometer to obtain chargings of glycerol doped with salt. Experiments yielded values which agreed well with a theoretical formula connecting charge to liquid variables. In the derivation they applied a relation for the field at the capillary tip to the drop being formed. The curvature of the latter is much smaller.

Throughout studies on the deformation of liquids in the presence of electric fields, authors have sought to calculate the forces acting on the liquid meniscus (34,39,65,73). Even for the simplest of electrode geometries this has proved to be a formadible task. The presence of space charge around the periphery of a needle, together with the ability of the liquid to maintain afield in the bulk, complicates the situation further. The behaviour of a liquid as it is drawn out into a jet to eventually form drops has been analysed by incorporating the effect of the external

field. The potential distribution around the jet was used by Hendricks to calculate the electrical stresses at the surface of the liquid which cause a jet to accelerate (12). In the case of charge injection, the field established by a small metal sphere inside the jet was used to model the behaviour(44,49). Many others have sought to quantify the distribution of the field in the analyses. Expressions have been used even in predictions of the size of the drops (50). Hines evaluated the equations of momentum and charge to find the electrical stresses acting on a single jet by using an expression for the field (65). Melcher and Warren extended the equations to include all terms and imposed constraints on the outside potentials (60).

Taylor contributed a great deal to the understanding of the physics behind the interaction of the externally applied field and the space charge at the liquid/gas interface (74,75). Isolated charged drops in air were observed to possess internal motion in the bulk due to an electrical shear stress. The internal circulation has also been observed on flat liquid-liquid interfaces stressed by an electric field (74). A very significant finding by Hayati, Bailey and Tadros (41) recently showed that the Taylor cone region of a steady jet also exhibits convection. This observation has implications for the theoretical prediction of electrical stresses as a new mechanism whereby liquid rises in the centre and accelerates most rapidly at the surface.

CHAPTER THREE

THEORY

In this chapter the nature of electrical forces operating on a semi-insulating liquid are briefly reviewed. Previous work concerning the migration of charge and subsequent fluid motion is described. Theoretical analyses of steady jet formation, analysis of jet stability, and the prediction of the resultant drop sizes are also discussed.

3.1 The electric forces operating on a liquid and the relaxation of charge (76,77)

A liquid experiences two distinct forces when a field is applied to the bulk. One of these arises due to the presence of free charge, and its magnitude depends on the field intensity and on the charge per unit volume present within the liquid. The second force is derived from dipole moments of bound charges. The dipole moment of a polarized particle is defined as the product of either of its bound charges, and their distance of separation. The polarisation force set up by virtue of the dipole moments is given by the product of the polarisation and the gradient of the field.

The total force per unit volume of liquid is:

$$F = q_v E + \tfrac{1}{2} (\varepsilon - \varepsilon_o) \text{grad } E$$

where q_v is the charge per unit volume,
ε is the permittivity of the liquid
and E is the electric field applied.

The translational motion of neutral matter caused by polarization effects in an electric field is called dielectrophoresis. It is distinct from motion due to the

presence of free charge within the liquid, which is called electrophoresis. Either of the two components of force will dominate, largely according to the level of free charge in the liquid.

The properties of dielectrophoresis and electrophoresis may be compared to illustrate the distinction:

1. The former produces motion whose direction is independent of the sign of the field. This is not the case for more conducting liquids where the direction of motion depends on the sign of charge and also on that of the field applied.

2. When a uniform tangential field is applied to a dielectric liquid, it is drawn towards lower polarizability. Melcher (18) illustrated this by placing two flat plate electrodes into a dielectric liquid (figure 3.1). The liquid rises towards the air upon application of an electric field to a height depending on the permitivity of the liquid and the field:

$$H = \frac{(\varepsilon - \varepsilon_o)E^2}{2 \rho g}$$

3. Dielectrophoresis usually requires relatively high field strengths and divergent fields. The motion of free charge requires lower fields.

4. The former is a relatively gentle effect which is most easily observed with large particles in low viscosity liquids, whereas the latter is observed with particles of any size, for liquids containing even low quantities of charge. Dielectro-phoresis is a process which depends on the particle size. Electrophoresis depends on the quantity of charge. The degree of free charge present in a liquid is measured by the electrical conductivity;

$$k = nq\mu_m$$

where n is the number of charges, q, per unit volume having mobility μ_m.

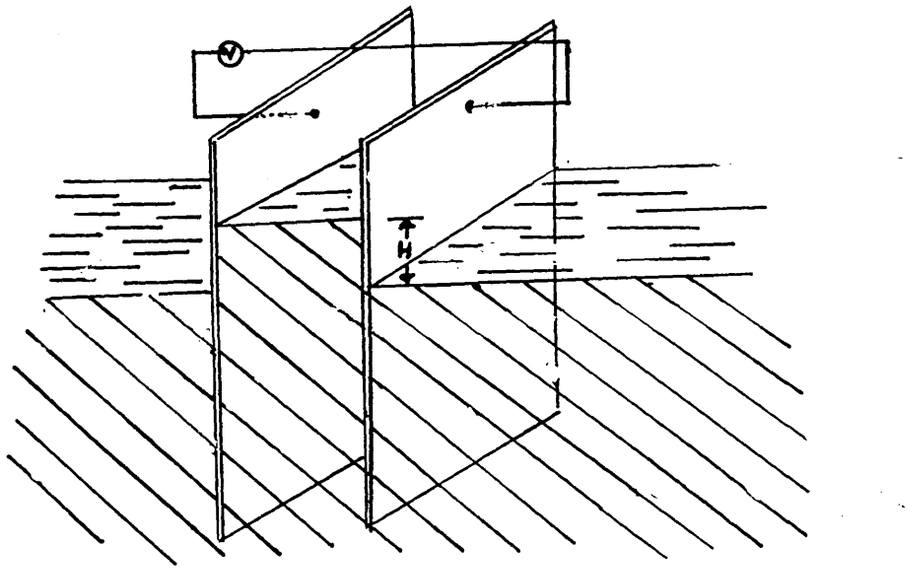

Figure 3.1 An insulating, polar liquid rising towards lower permitivity air under a horizontal field.

The effect of an externally applied electric field is to establish a field within the bulk of the liquid. For conductors, the ions move extremely rapidly to the surface of the liquid and redistribute themselves in such a way as to form an equipotential surface. Under these circumstances a field cannot exist within a conductor. For semi-insulating liquids, the quantity of charge is low enough to maintain a field during the movement of charge from the bulk to the surface. The rate at which charges reach the surface is characterised by the relaxation time of the liquid (47).

Liquids that have relaxation times are also assumed to obey Ohm's law. For static liquids the current density

at any point, at any time, is directly proportional to the local field intensity:

$$J = k\,E$$

An expression for the relaxation time may be found by applying Gauss' law to a small element of volume v containing a charge density q_a. Gauss' law states that the surface integral of the normal component of the dielectric displacement, D, over a surface containing a field is equal to the charge enclosed by the surface.

$$q_a v = \int D\,dA$$

where D is defined as:

$$D = \varepsilon E$$

For a system in which the ohmic current is flowing:

$$-\frac{d(q_a v)}{dt} = \int J\,dA$$

Using Ohm's law and the expression for D in the above equation gives;

$$\frac{dq_a}{dt} = \frac{-q_a}{\varepsilon/k}$$

τ is defined by,

$$\tau = \varepsilon/k$$

The differential equation may be integrated to give the charge in the bulk;

$$q_a = q_o \exp(-t/\tau)$$

The charge relaxation time is an important factor in determining the characteristics of a surface as it is being formed, where dynamic flow times are compared with times for charge decay. The behaviour of charges at interfaces affects the behaviour of the liquid, since it is the interaction of these charges with the surroundings and their spacial distribution that give rise to acceleration forces.

3.2 Stresses operating at an interface.

The presence of charge on the surface of a drop or at an interface between a liquid and a gas is a source of outward force due to the repulsion of like charges. An electric field acting normal to the interface is established by virtue of the space charge, which usually is unable to cross the interface, and by virtue of the permitivity of the gas. The normal stress is expressed as (75):

$$T_n = \tfrac{1}{2}\ \varepsilon_o E_n^2$$

In addition, a surface may be subjected to a tangential stress. This is caused by the presence of both a tangential field and surface charge. The tangential field is established due to the distribution of charges.

$$T_t = \varepsilon_o E_n E_t$$

where ${}_oE_n$ is the charge on the surface and E_t the field acting on it to produce a force on the interface.

Perfect insulators contain bound charges so that the only forces acting on a surface are those derived from polarsation in a field. Conductors also cannot sustain an initial tangential stress.

The requirement of a tangential field as well as surface charge in order that a tangential stress may be present was illustrated by Taylor and Melcher (75). They filled a shallow insulated container with a semi-insulating liquid and applied a horizontal field by placing electrodes at both ends. Surface charge was effected by contacting one of the electrodes with a third positioned at an angle so as to induce even charge. The presence of tangential stress was verified by the observation of convection currents within the liquid bulk. This behaviour also occurs at liquid/liquid interfaces and for spherical geometries when a tangential force is established (74). The velocity distributions for

the cases of a flat air/liquid interface and a drop suspended in another liquid were derived. For the former, it was assumed that the system was stationary, but the motion of the drop necessitated a solution for creep flow.

The concepts outlined above relating to the forces acting on a liquid are applicable to liquids exhibiting slow motion. These concepts are also used to explain the behaviour in systems complicated by overall motion, where the liquid interfaces are not free in the sense that stresses cause them to accelerate, but are free from solid boundaries. During dynamic spraying of a semi-insulating liquid via a capillary held at high potential, Hayati et al (41) observed that a Taylor cone is formed near the tip. The injection of minute quantities of fine lycopodium particles into the liquid illustrated the existence of currents within the cone. This proved the presence of a tangential stress. Earlier work by Hayati (40) suggested that this stress would have to be established for a single jet to be formed; perfectly insulating liquids and conductors did not spray from the needle. Thus a potential gradient present for liquids in the range between the two extremes was required to produce the stress. The velocity profiles for the dynamic spraying case were derived by assuming creep flow and superimposing the inertial flow. The implications for modelling electrohydrodynamic spraying will be discussed in the next section, where the previous theoretical studies are reviewed.

3.3 The mechanisms of jet formation.

The importance of surface charge and charge distribution were discussed above. Almost always the externally applied field is responsible for both of these. Yet the presence of charge itself exerts fields in the vicinity of the fluid interface, thus modifying the fields responsible for setting

up stresses. The overall picture is complicated by the convection of the jet which results from the stresses. So charge may be considered to be carried by two processes; the potential distributions along the surface causing ohmic current, and the bulk motion of the jet.

Some authors have included expressions for the fields at the surface and in the region enclosed by the electrodes in the estimation of the electric forces. One of these analyses considers the jet from a capillary to be steady so the problem becomes a quasi-static electric field problem .

Variable line charge calculation.

Horning and Hendricks' (12) calculations are for a jet extending from a capillary attached to a top plate, with a second plate below (figure 3.2). The potential was broken into two parts, a uniform electric field plus the effects of the capillary and jet. This approach was used by Taylor (73) to solve for the force along a slender cylinder. The analysis involves the method of images where the capillary and jet is replaced by a variable line charge and its image in the ground plane.

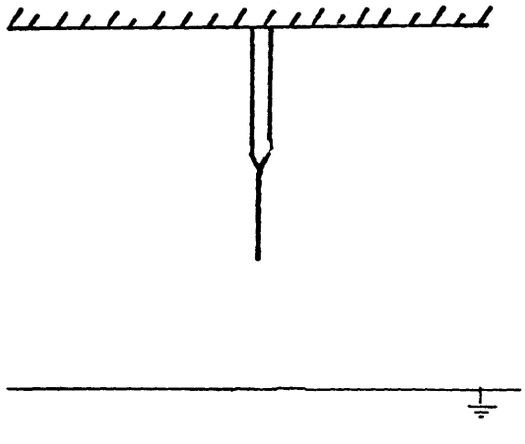

Figure 3.2 Schematic of the top disc, capillary and jet used for the semi-infinite approximation

The potential outside the capillary and jet is given by;

$$V(r,z) = -Ez + \frac{1}{4\pi\varepsilon}\int_0^L \sigma(\zeta)\, x\left[\frac{1}{[(z-\zeta)^2 + r^2]^{\frac{1}{2}}} - \frac{1}{[(z+\zeta)^2 + r^2]^{\frac{1}{2}}}\right]d\zeta \qquad \text{Eqn. 3.1}$$

where $\sigma(\zeta)$ is the line charge per unit length

L is the length of the capillary and jet

and E_z is the applied electric field

The top plate is at ground so that the boundary condition is

$$V(r_t,0) = 0$$

The other boundary conditions on the capillary and jet are res-pectively ,

$$V(r_c,z) = 0$$

$$V(r_j,z) = V_j(z)$$

where r_c is the capillary radius

r_j is the jet radius

$V_j(z)$ is the jet potential

Application of the two boundary conditions to eqn. 3.1 enabled the line charge to be determined as a function of z. In order to calculate the line charge the capillary and jet length are divided into n segments. The integral in the equation then becomes a summation of n unknown points of the line charge function by the use of the trapezoidal rule of integration. The potential was evaluated at n points, resulting in n equations with n unknowns. However further information was required about the distribution of $V_j(z)$. This came from the concept of the two currents ;

$$I_t = I_o + I_c$$

where the convection current is

$$\sigma(z)\, u(z)$$

and the surface charge is assumed to equal the line charge. The potential on the jet was found by integrating the Ohmic current;

$$V_j(r_j,z) = \frac{1}{(\pi k)} \int_{z_c}^{z} \frac{I_o}{r^2} \, d\zeta$$

where z_c is the co-ordinate at the capillary tip
k is the conductivity of the liquid.

The boundary condition for the jet is transformed to :

$$V(r_j,z) = \frac{1}{\pi k} \times \int_{z_c}^{z} \frac{I_t}{r^2} \, d\zeta - \frac{1}{\pi k} \times \int_{z_c}^{z} \frac{\sigma(\zeta)u(z)}{r^2} \, d\zeta$$

Eqn. 3.2

Eqn. 3.2 was incorporated along with the boundary condition on the capillary into eqn. 3.1. Experimental values of the total current carried and the radius of the jet as it varies with z were also required. The n equations were solved on a computer using the Gauss-Seidle method.

The line charge distribution was translated into the normal and tangential stresses operating down the jet. These in turn were integrated over the length of the jet so that the total electric force was compared with the surface tension, inertial and viscous forces. However the balance of forces did not include terms for the curvature of the jet.

Other workers have made use of a variety of expressions for the field, usually depending on their particular experimental apparatus. In all the cases a form of energy or force balance was employed to provide further information about the steady jet of an incompressible liquid. The following section presents a different treatment

in that the purpose of the analysis is the prediction of the final radius reached by the jet as it accelerates away from the main electrode. The general approach of considering the form of the field and the different forces acting on the liquid remains the same.

Jet radius prediction.

The apparatus of Turnball et al (44,49) was constructed to spray insulating liquids. To this end a method of injecting charge was necessary and this was accomplished by placing a small sphere in the centre of a glass capillary orders of magnitude greater than the sphere for field emission (figure 3.3). The field was bounded by a distant ground plane. Thus the situation differs from the previous one since the field is now considered to be established inside the jet as the charges move away from the sphere, whearas before the potential over the jet cross-section was assumed to be constant.

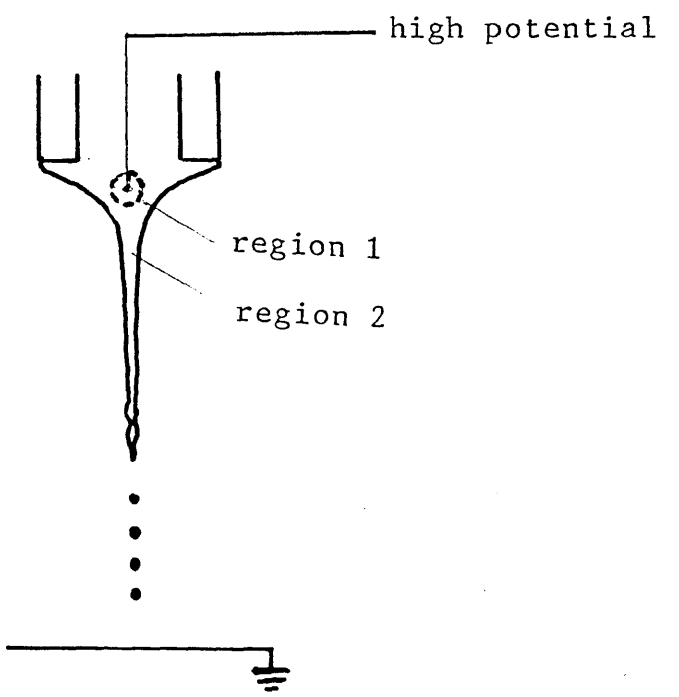

Figure 3.3 Schematic of the jet produced by the charge injection electrode.

The equations of Gauss's law, Ohm's law and charge conservation were solved to give the field. The jet was divided into three regions. In the first, near the sphere, the motion of charge was assumed to be due to the Ohmic current, so that:

$$\mu_m E >> u$$

where μ_m is the mobility
and u is the velocity

The field E was assumed to be spherically symmetrical, which is supported by the large distance set to the earth. In region 2 the condition is:

$$\mu_m E << u$$

and the area of transition between the two is neglected. The charges reach the surface in region 2, where they travel along the surface with the liquid.

The jet radius has reached its final value in the third region. Here the fields were assumed to be purely cylindrical. In order to calculate the final radius, the voltage drop over region 2 was required. Once this was known, energy equations could be utilised to determine the effect of the voltage loss on reducing the jet size.

Rather than attempting to calculate directly the potential difference in region 2, it was found from the potential losses in the other two regions. The boundary between regions 1 and 2 was considered to occur at r_{12}, where this is measured from the centre of curvature of the tip of the sphere. At r_{12}, the charge velocity equals u_t, the liquid velocity at the sphere tip. Assuming space charge effects to be negligible in region 1, the field is:

$$E = \frac{E_o \, r_o^2}{r^2}$$

where r_o is the radius of the sphere
and E_o is the field at the sphere

Since

$$r_{12} = (\mu_m E_o/u_t)^{\frac{1}{2}} r_o$$

the potential drop across region 1 is

$$V_1 = E_o r_o(1-(u_t/\mu_m E_o)^{\frac{1}{2}})$$

The potential drop over region 3 is found from Gauss's law evaluated from the jet radius to the radius of the earth;

$$V_3 = \frac{I}{2\pi\varepsilon_o u_j} \ln \left[\frac{r_g}{r_j} \right]$$

where r_g is the radius of the earthed plate

r_j is the jet radius

u_j is the jet velocity

and I_c is the convection current, equal to the total current. V_2 can then be found from the total drop, V_1 and V_3.

$$V_2 = V_c - V_1 - V_3$$

An energy balance equating the pressure and kinetic energies at the capillary to those at the final radius takes into account the accelerational energy due to the potential loss. When V_2 is substituted into the balance, an equation predicting the radius in terms of the current, flowrate, sphere radius, voltage and liquid properties is obtained. However one variable, the velocity at the sphere, remains unknown. An iterative technique whereby the velocity lies within a certain range was used to overcome this problem.

This approach is specific to the case of a small sphere. Another approach seeks to describe the stresses acting by employing the conservation equations.

Momentum equation calculations.

Hines (65) evaluated a general form of the hydrodynamic equation in his application of paint spraying. He neglected the effects of gravity, viscous and pressure dissipation, as a first approximation to the actual

conditions in the jet. The true values of the field, charge to mass ratio on the liquid surface, and the liquid velocity at a given point were replaced by the values averaged over the jet cross-section. Hence the rate of change of kinetic energy with distance down the jet was expressed as;

$$\tfrac{1}{2} \frac{du_z^2}{dz} = E_t \, c_m \qquad \text{Eqn. 3.3}$$

where u_z is the velocity

z is the vertical distance

c_m is the charge per unit mass

and E_t is the tangential field along the jet

Averaged values were considered to be appropriate if the following condition was satisfied:

$$\frac{du_z}{dr} < \frac{u_z}{r_j}$$

The field and charge were determined from eqn. 3.3, and the equation for charge conservation of;

$$I_t = \pi k r^2 E_t + \rho c_m u_z \pi r_j^2$$

and the continuity equation for incompressible fluids;

$$V_f = \pi r_j^2 u_z$$

Solutions obtained depended on whether the jet was accelerating or slowing down.

Like Turnball et al, Hines made use of measurements of the current and the jet profile. Based on his own experimental results, Hines concluded that the field is low, indicating that at the capillary tip the liquid behaves as a conductor. As the radius becomes smaller, the field rises until at constant radius the field approaches the external value, where the behaviour resembles an insulator. This conclusion was qualified however, by the observation that conditions at the capillary as the fluid is admitted,

depended upon flowrate and the radius. He made use of the relaxation time to determine the point at which a conducting liquid begins to act as an insulator. When the charge relaxation time is equated to the time spent by an element of liquid in the jet;

$$\frac{\varepsilon}{4\pi k} = \frac{r_j}{u_z}$$

since

$$u_z = \frac{V_f}{\pi r_j^2}$$

the final radius of the jet is;

$$r_j = \left(\frac{\varepsilon_o V_f}{4\pi^2 k}\right)^{1/3}$$

At this point on the jet, the potential distribution along the jet becomes significant. Assumung the conduction and convection currents are equal gives;

$$\frac{I_t}{2} = k\pi r_j^2 E_t$$

Combining these two equations which describe the point, yields an expression for the charge to mass ratio, which was assumed to remain constant until break up into drops;

$$c_m = E_t \left(\frac{\varepsilon^2 k}{2\pi\rho^3 V_f}\right)^{1/3}$$

The purpose of Melcher and Warren's (60) work was also to calculate the stresses and using the values, deduce the jet profile. The momentum equation included the terms left out by Hines. Also their treatment did not involve evaluating the field applied to the capillary tip. Instead, Gauss's law was applied to describe the potential variations outside the jet.The outside potentials close to the jet interface were constrained by ring electrodes to acheive

linear variation over the length of the jet. The outside wall potentials were required to calculate the potential distribution at the interface. The potential over a cross-section was assumed to be constant.

Gauss's law shows that there is a radial field outside the jet given by;

$$E_r = \frac{V_j - V_w}{r_j \ln(s/r_j)}$$

where V_j is the jet voltage
V_w is the wall voltage
and s is the radius of the outside electrode
The field in the downward direction is

$$E_t = \frac{dV_j}{dz}$$

so that the tangential stress is

$$T_t = - \frac{\varepsilon_o (V_j - V_w)}{r_j \ln(s/r_j)} \frac{dV_j}{dz}$$

and the normal stress :

$$T_n = \tfrac{1}{2} \varepsilon_o \frac{(V_j - V_w)^2}{r_j^2 \ln^2(s/r_j)}$$

It was assumed that the electrical shear stresses are transmitted to the bulk by the internal viscous stresses so that radial velocity distributions may be discounted. It was also recognised that the free charge travels only on the surface while conduction occurs in the volume. With these assumptions, the equations for charge balance and momentum are (figure 3.4);

$$r_j^2\, u\, \frac{d}{dz}\left[\frac{V_j - V_w}{r_j^2 \ln(s/r_j)}\right] - \frac{k}{2\varepsilon_o}\frac{d}{dz}\left[r_j^2 \frac{dV_j}{dz}\right] = 0$$

and

$$\Delta\left[\rho u^2 \pi r_j^2\right] = -\Delta\left[p\pi r_j^2\right] + p\frac{dr_j}{dz} 2\pi r_j \Delta z + \rho g \pi r_j^2 \Delta z + T_t(2\pi r_j \Delta z) + 2\mu\pi\Delta\left[r_j^2 \frac{du}{dz}\right] - 2\mu\pi \frac{du}{dz}(2\pi r_j \Delta z)\frac{dr_j}{dz}$$

Eqn. 3.4

The first term on the RHS is the downward pressure on the almost vertical surface, the second is the pressure loss due to the curvature. The last two terms are the normal viscous stresses acting over the jet cross sections and over the surface next to the interface respectively.

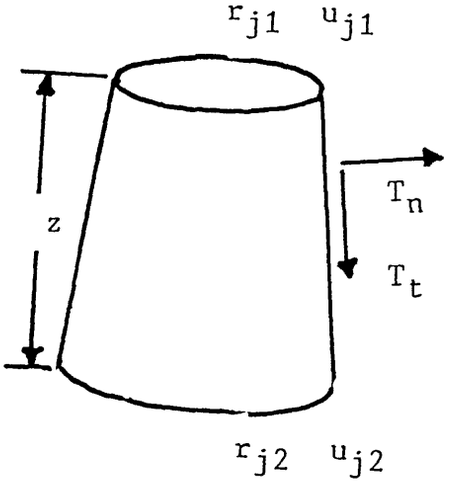

Figure 3.4 Control volume for deriving the momemtum balance in cylindrical co-ordinates.

Information about the pressure in the jet may be obtained from a pressure balance over the interface in terms of the Maxwell stresses:

$$P_a - P = \tfrac{1}{2}\varepsilon_o E_r^2 - \frac{(\varepsilon_o - \varepsilon)}{2} E_t^2 - \frac{\gamma}{r_j}$$

Substituting for the pressure, fields and taking the limit as $\Delta z \longrightarrow 0$, the momentum equation becomes

$$\rho u \frac{du}{dz} = \frac{d}{dz}\left[\frac{\varepsilon_o (V_j - V_w)^2}{2r^2 \ln^2(s/r)}\right] + \frac{(\varepsilon - \varepsilon_o)}{2}\frac{dV_j}{dz}^2 - \frac{\gamma}{r}$$

$$+ \rho g - \frac{2\varepsilon_o (V_j - V_w)}{r^2 \ln (s/r)} \frac{dV_j}{dz} + 2\mu \frac{d^2u}{dz^2}$$

Solutions to the continuity, momentum and charge equations were found by assuming that the surface charge may be neglected so that the conduction current equals the total current, and by neglecting the viscous disipation term in the momentum equation. These assumptions allowed the equations to be solved as ordinary differential equations.

The solutions obtained from the experimental results show the tangential field increasing down the jet. This result is similar to that of Hines, who concluded that the jet behaves like a conductor near the tip of the capillary. In Melcher's work the viscosity was assumed to be high enough to negate radial velocity profiles, and yet low enough to justify the exclusion of viscosity from the equation.

Without exception all the analyses have assumed that the velocity within the jet is unidirectional and that the profile across a cross-section is negligible. If a radial profile were to be present, then continuity for steady,

incompressible flow states that a radial component of the velocity must also be present. A jet which is seen to change its size rapidly with distance suggests that radial flow is occuring. Work by Hayati et al on the formation of Taylor cones from capillary ends has provided a very significant insight into the flow patterns inside the jet (41).

Internal convection (40).

Tracer particles introduced into an insulating liquid proved the presence of closed cells, each inside another, with the liquid rising at the centre of the cone, while downward motion was most rapid at the surface (figure 3.5). The following is an outline of the derivation of the velocities.

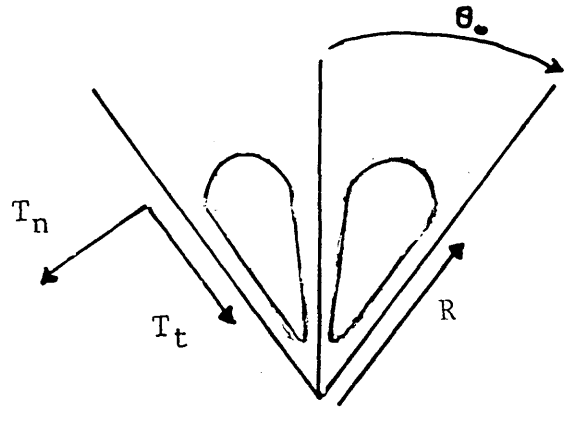

Figure 3.5 Circulation inside the cone

The equations of momentum and continuity were solved using the stream function, ψ . Spherical co-ordinates were appropriate to the cone region. The cone is characterised by the semi-vertical angle Θ_o, with the R co-ordinate in the direction of the capillary, and zero at the cone tip. Since the nature of the process is such that the flow is irrotational, velocity components in the R and directions were sought;

$$u_r = - \frac{1}{R^2 \sin\Theta} \frac{\delta\psi}{\delta\Theta}$$

$$u_\theta = \frac{1}{R\sin\Theta} \frac{\delta\psi}{\delta\Theta}$$

For Reynold's numbers <0.1, the equation of motion for creeping flow is

$$\Xi^4 \psi = 0$$

i.e. $$\left[\frac{\delta^2}{\delta R^2} + \frac{\sin\Theta}{R^2} \frac{\delta}{\delta\Theta}\left(\frac{1}{\sin\Theta} \frac{\delta}{\delta\Theta}\right)\right]^4 \psi = 0 \qquad \text{Eqn. 3.5}$$

Hence four boundary conditions are required;

1. The flow is axisymmetric so that $u_\theta = 0$ at $\Theta = 0$

2. Stress on the centre line is zero, $\frac{\delta u_r}{\delta\Theta} = 0$ at $\Theta = 0$

3. At the surface where Θ_o is the semi-vertical angle, the velocity is in the R direction alone, $u_\theta = 0$ at $\Theta_o = 0$

4. At the surface the tangential electric stress is

$$T_t = - \mu \frac{1}{R} \frac{\delta u_r}{\delta\Theta}$$

The tangential stress was assumed to be proportional to R^2. The solution to eqn.3.5 was obtained in two stages. In the first stage, the discharge from the cone into the

cylindrical region was ignored and a solution was sought such that

$$\psi = Rf(\theta)$$

Substituiting for in eqn. 3.5, and solving for $f(\theta)$ using the boundary conditions gives the components of the velocity;

$$u_\theta = \frac{1}{R}\left(A\,\frac{1}{\sin\theta} + B\,\frac{\cos\theta}{\sin\theta} + C\sin\theta\right)$$

and

$$u_r = -\frac{1}{R}\left(-B + 2C\cos\theta\right) \qquad \text{Eqn. 3.6}$$

the constants are

$$A = -M\,\frac{\sin\theta_o}{1-\cos\theta_o}$$

$$B = M\,\frac{\sin\theta_o}{1-\cos\theta_o}$$

$$C = \frac{M}{\sin\theta_o}$$

$$M = \frac{\varepsilon_o E_n I_o}{4\pi\mu k\,(1-\cos\theta_o)} \qquad \text{Eqns. 3.7}$$

The Ohmic current along the cone was assumed to remain constant. In the second part of the derivation the discharge form the cone is included in the velocity. This was done by superimposing the inertial flow

$$u_r = \frac{V_f}{2\pi(1-\cos\theta_o)R} = \frac{K}{R^2}$$

onto the radial velocity. Adding this to eqn. 3.6;

$$u_r = -\frac{1}{R}\left(-B + 2C\cos\theta\right) + \frac{K}{R^2} \qquad \text{Eqn. 3.8}$$

3.4 The instability of jets (11,13,17).

The break up of a jet is considered to occur at the point where the electric tangential stress goes to zero (12). However break up must also involve stability considerations. Early theory excluding charge effects showed that the finer the jet, the more unstable it is to symmetric disturbances, where surface tension acts to accentuate the growth of sausage type waves. The analysis of stability is based on infinitesimal disturbance analyses. The theories are applicable to situations where a range of disturbances, characterised by wavelength, are available from background noise, though they may also be applied to cases of particular waves induced by large amplitude.

The jet is considered by Basset (11) to be a straight cylinder, having unidirectional velocity (figure 3.6). Taking z as the direction of motion, the equation describing the radius as it is disturbed from the equilibrium is:

$$r_a = r_j + \alpha(t)\cos k_w z$$

where r_j is the radius of the unperturbed cylinder, (t) is a small time-dependent amplitude of disturbance, and $k_w = 2\pi/\lambda$ is the wavenumber, being the wavelength. The solution of the momentum equation gives the velocities which result from the growth of the disturbance;

$$\left(\frac{\mu}{\rho} D - \frac{d}{dt}\right) D\Psi = \left(u_r \frac{d}{dr} + u_z \frac{d}{dz} - \frac{2u_r}{r}\right) D\Psi$$

the operator D is $\frac{d^2}{dz^2} + \frac{d^2}{dr^2} - \frac{1}{r}\frac{d}{dr}$

and the components of the perturbed velocity are :

$$u_r = -\frac{1}{r}\frac{d\Psi}{dz} \quad , \quad u_z = \frac{1}{r}\frac{d\Psi}{dr}$$

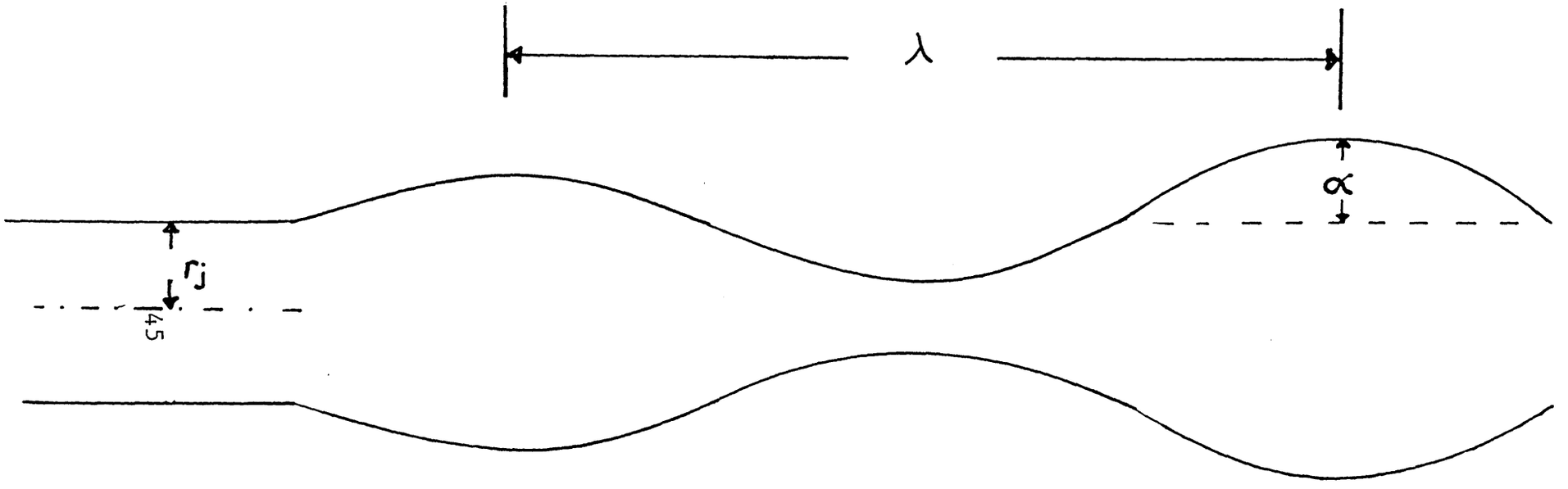

Figure 3.6 The growth of axially symmetric waves on a cylinder travelling at constant velocity when at equilibrium

The stream function was divided into two parts, one representing steady state, and the other representing the disturbance. At equilibrium, $u_z = u$ and $\Psi = \frac{1}{2} u r^2$,

$$\Psi = \tfrac{1}{2} u r^2 + \Psi'$$

The concept of the growth constant comes from the expression of the growth of amplitude, α , with time ;

$$\alpha = \alpha_o \exp(\omega t)$$

Hence if ω is positive, the amplitude of disturbance will grow, but if negative the jet is stable. It is important to find an equation for ω so that the conditions which give rise to instability may be determined. This was obtained from the pressure equation for a perturbed cylinder, and the solved stream function. When the hydrodynamic equations for the pressure are evaluated, and Ψ included together with the boundary conditions of zero tangential stress at the interface, ω is given by ;

$$\omega^2 + \frac{2\mu k_m^2}{\rho}\omega - \frac{\gamma}{2\rho r_j^3}(1-k_m^2 r_j^2) k_m^2 r_j^2 + \frac{I^2 k_m^2 r_j^2}{8\varepsilon_o \rho V_f^2} = 0 \qquad \text{Eqn. 3.9}$$

Terms of order higher than 2 have been neglected in the Bessel functions, and the last term was modified by Taylor (22). The equation is in agreement with Anno's derivation using conservation of mechanical energy (17).

The second term accounts for the viscosity which acts to make ω negative. The third is the surface tension and produces instability, providing $k_m r_j < 1$. The stabilising effect of the current carried is represented by the final term.

It can be seen from eqn. 3.9 that a range of the growth constant is available for a range of possible wave-numbers (present as background noise). Rayleigh's work for

an uncharged jet showed that a maximum value for the growth constant exists. At the maximum, $k_m=1/2r_j$, which gives theratio of jet radius to drop radius equal to 1.89.

3.5 Drop size prediction .

The growth of a wavelength on the end of the jet, with amplitude equal to the jet radius is considered to be emitted as a drop, so that the volume of the growth becomes the volume of the drop. In the case of an electrostatic jet, the profile of the accelerating jet differs significantly from a uniform cylinder. However for long jets, the radius comes to a constant value for a distance before drops are formed. So once the final radius of the jet is known, the drop size can be estimated. One theory predicting radius was described in section 3.3, but it applied to a spherical field established within the liquid by a charge injection electrode. The geometry of the jet produced by conduction charging may be obtained from the electric stresses that drive it. However, various theories, outlined in section 3.3, require knowledge of the profile in order to predict the acceleration forces. This is due partly to the lack of solid boundaries which would normally provide additional information. Other approaches have been used to predict the size of the drops.

Jones and Thong (67) used information about the field between the capillary and the earth plate beneath it, for a single jet at relatively low flowrate. The drop size was predicted from the charge on the liquid emerging from the capillary, which was obtained from the charge on the capillary. The capillary voltage was found from an expression for the field, derived by the method of images;

$$V_c = \frac{\sigma}{4\pi\varepsilon_o} \ln\left[\frac{(r_c^2+4z_o)^{\frac{1}{2}} + 2z_o}{r_c}\right]$$

where σ is the charge per unit length, r_c is the capillary radius and z_o the distance to the earth. For $z_o >> r_c$,

$$\sigma = \frac{4\pi\varepsilon_o V_c}{\ln(4z_o/r_c)} \qquad \text{Eqn. 3.10}$$

The values of the radial and the tangential fields at the capillary tip were assumed to be equal, so that the resultant field is given by;

$$E_c = \frac{2\ V_c}{r_c \ln(4z_o/r_c)} \qquad \text{Eqn. 3.11}$$

The surface charge density σ_s is related to the charge per unit length by;

$$\sigma_s = \frac{\sigma}{2\pi r_c}$$

Substituting for σ and V_c from eqns. 3.10 and 3.11 ,

$$\sigma_s = \sqrt{2}\ \varepsilon_o\ E_c$$

The jet was assumed to act as a conductor, so that that all the charge from the capillary is imparted to the jet. Further, it was assumed that the voltage remains constant over the length of the jet.

A drop forms from both a cylindrical portion, the jet surface and a planar portion, the jet cross-section. Allowance is made for the change in surface areas, by noting that a sphere resulting from a plane carries three times the charge of the plane. From a cylinder the figure is 1.5.

An average of the values proved the best prediction,

$$q = 2.25\ \sigma_s\ 4\pi r_p^{\,2}$$
$$= 9\sqrt{2}\ \pi\ \varepsilon_o r_p^{\,2} E_o$$

where q is the charge on a drop of radius r_p

The equation can be rearranged to give the charge to mass ratio;

$$c_m = \frac{27\sqrt{2}\ \varepsilon_o E_o}{4\rho r_p} \qquad \text{Eqn 3.12}$$

The following analyses predict size from the knowledge of the current carried by the drops, though some do not include the value of the applied field.

Vonnegut and Neubauer (31) considered the surface tension and electrical energies of system of drops produced from a given volume of liquid. The surface tension energy is

$$e_s = \frac{q^2}{8\pi\epsilon_o r_p}$$

and the electrical ,

$$e_e = 4\pi\gamma r_p^2$$

The conservation equations for the volume and charge allow elimination of q. The total energy of the system is then,

$$e_t = \frac{3\gamma v}{r_p} + \frac{Q^2 r_p^2}{6\epsilon_o v}$$

where v is the initial volume of liquid, Q the initial charge.

The total energy was minimised by equating the partial derivative of e_t with respect to r_p to zero. The factors v and Q are fixed, while the charge on the resultant drops and the number of drops are allowed to vary. The most probable charge to mass was derived to be,

$$c_m = \frac{3(\epsilon_o\gamma)^{\frac{1}{2}}}{r_p^{3/2}} \qquad \text{Eqn. 3.13}$$

This analysis does not take into account the means by which drops are produced, and therefore could be applicable to a range of spraying modes.

Pfeifer and Hendricks (33) assumed that the parent drop is at the Rayleigh limit, twice the value of eqn. 3.13, when it disrupts. They allowed for an energy sink such that as the number of droplets increases, the total energy of the system passes through a minimum. As the number of droplets increases, the surface tension energy also increases. Because the total energy cannot exceed the value of initial energy, the electrical energy term falls as the surface tension term rises. The charge on each droplet is at its lowest possible value when the number of droplets is at the maximum. Thus the concept of minimal rather than

minimisation of energy was developed. The analysis proceeds as follows;

The total energy of the parent drop is

$$e_p = 4\pi\gamma R_p^2 + \frac{Q^2}{8\pi\varepsilon_o R_p}$$

Hence from the Rayleigh limit,

$$e_p = 12\pi R_p^2 \qquad \text{Eqn. 3.14}$$

When the Rayleigh limit is substituited into the energy relations for the droplets, the energies are expressed in terms of the droplet number;

$$e_s = 4\pi N^{-2/3}\gamma R_p^2$$

$$e_e = 8\pi N^{1/3} R_p^2$$

Therefore from eqn. 3.14 the total droplet energy is:

$$e_t = f(N)\, e_p$$

where the function f includes the electrical and surface tension terms respectively,

$$f(N) = \frac{2}{3} N^{-2/3} + \frac{1}{3} N^{1/3}$$

N is the number of droplets. For N = 20, and N = 1, the energy of the droplets is at maximum. Expansion of e_t and the relation between R_p and N gives the charge on the drops as a function of the droplet number;

$$\frac{q^2}{8\pi\varepsilon_o r_p} = \frac{8\pi\gamma r_p^2}{N}$$

At N = 20, the electrical energy is at the minimum possible value,

$$c_m = 1.34 \frac{(\gamma\varepsilon_o)^{\frac{1}{2}}}{r_p^{3/2}} \qquad \text{Eqn . 3.15}$$

A model which incorporates the energy minimasation theme into the mode of drop formation was developed by Pfeifer and Hendricks (34). In the pulsating mode drops leaving the liquid meniscus shield the surface from the field for a sufficient time such that the surface charge relaxes back to zero before the liquid begins to recharge (figure 3.7). During the charging process the surface charge density accumulates according to;

$$\sigma_s(t) = \int_0^t k\, E_1\, dt$$

and the field within the liquid is ,

$$E_1 = \frac{\varepsilon_o E_c}{\varepsilon}$$

A pertubation growing on the meniscus is assumed to result in a drop before the surface accumulates enough charge to form an equipotential and therefore cancel the field. Under the assumption that the pertubation area is equal to that of the drop, drop charge is approximated by,

$$q = 4\pi r_p^2 \sigma_s(t)$$

at time $t = t_1$. t_1 is the drop formation time:

$$t_1 = m_d/M$$

The four equations yield the specific charge when combined;

$$c_m = 4\pi r_p^2 k \varepsilon_o E_c / M$$

Based on energy minimisation,eqn. 3.14,

$$c_m = \left(\frac{4\pi}{\varepsilon}\right)^3 \left(9\gamma\right)^2 \left(\frac{\varepsilon_o^5}{\rho^4}\right)^{1/7} \left(\frac{kE_c}{M}\right)^{3/7}$$

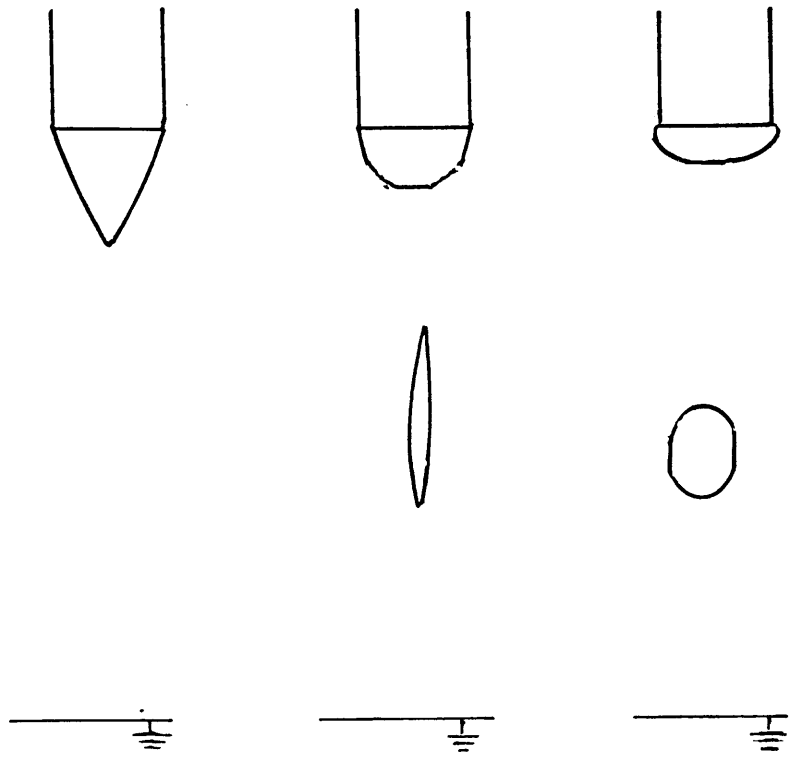

charge at the surface is attracted to earth

liquid is ejected when the electrical and gravity forces overcome surface tension

meniscus is shielded from the field

Figure 3.7 The pulsating mode

CHAPTER FOUR

EXPERIMENTS AND MEASUREMENTS

The apparatus was arranged so that the formation of steady jets from the end of a capillary could be studied. Allowance for changes in electrode geometry were made, in order to observe the behaviour of liquids at various field strengths, when the voltage is varied. Initially, the work concentrated on the single steady jet. Measurements of the dimensions of the jet and the resultant drops were taken by the use of photography and a microscope. Computer programs were employed to solve systems of equations to describe the variation of the electrical shear stress along the jet.

The effect of the application of higher fields was evaluated using a telescope. This enabled the configuration of the liquid meniscus at the tip of the capillary to be observed. Different liquids were sprayed throughout the experiments. The methods used to measure the parameters of the liquid are also presented.

A detailed study of the drop size as it changes with the variables was carried out by other equipment using a laser. The study was supported by the simultaneous measurement of the average drop charge.

4.1 Equipment.

The apparatus consists of a top disc that serves to impart high voltage by contact to a capillary. The disc also provives the support for the capillary. An earthed cup is situated directly below to complete the electric field and collect the liquid drops (figure 4.1). Liquid is delivered to the electrode from a syringe by a pump.

An electric field is applied to the capillary from a high voltage power supply. The high voltage is delivered at low values of direst current. Since the voltages cannot be measured accurately from the power supply unit, a high voltage probe is positioned on the line from the supply to the capillary. Connections from the probe to a voltmeter allow accurate digital display of the values.

The top disc is held in place by means of a rod attached to a support. The support is held on a graduated stand by two screws positioned at a right angle. A second support is similarly positioned below the first for another rod attached to an extra earthed plate.

The high voltage is supplied from a Brandenburg, Alpha II series power supply, model 2807. The power supply is capable of delivering 0-30 kV on the output line and operates from the mains.

Liquid is delivered by a Braun Perfusor pump, series VI. The dial settings permit flowrates of 1.2 , 6, 12, 30, 60, 120, 300, and 600 ml/h .

Two light sources are employed as for visual observations. A sodium lamp is used with the telescope to give a magnified silhouette of the liquid surface. When using the lamp, a cylindrical guard is placed around the capillary, top disc and earthed collector. The inside walls of the guard are earthed in order to eliminate stray currents which may interfere with the behaviour of the liquid, especially at high field intensity. Slits were made in the cylinder to permit observation and adjustment inside the experimental area of the apparatus. A second, white light source with a diaphragm is used with a bellows camera. Again the effect is to produce a shadow outline of the jet. The arrangement was changed for other experiments where a second, slr camera is at right angles to the first camera.

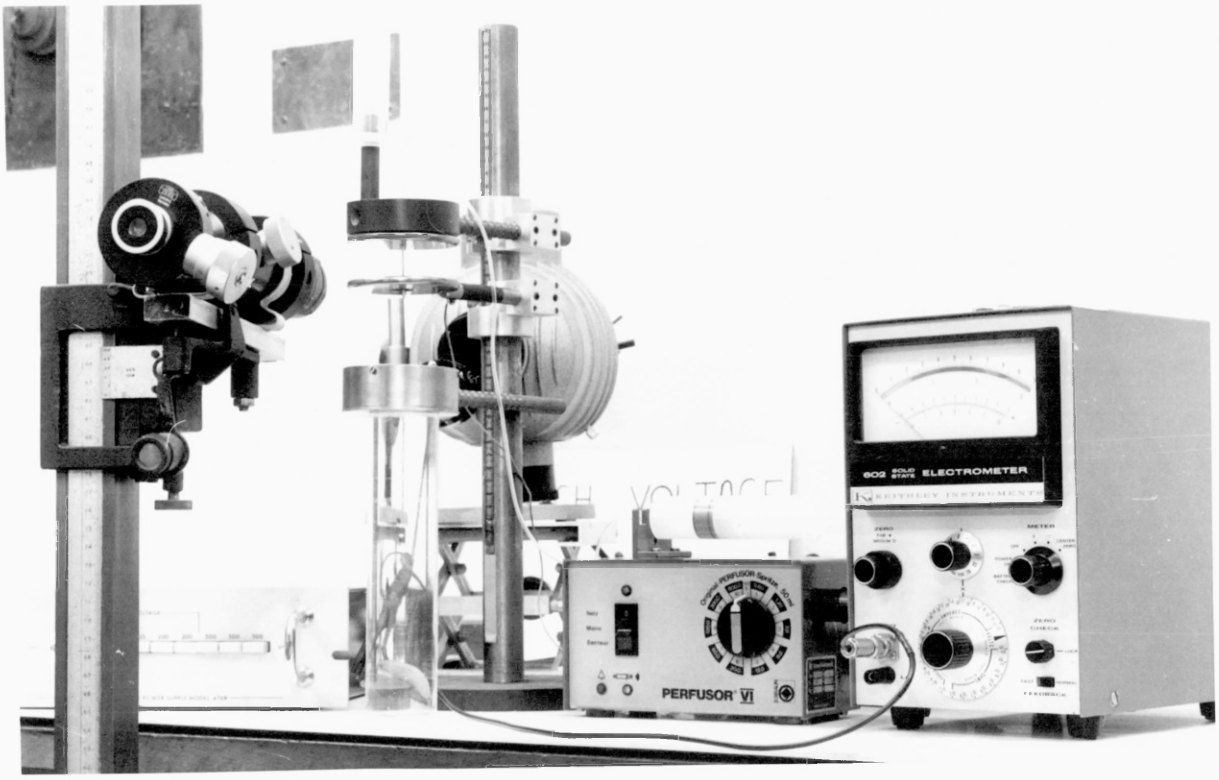

General View

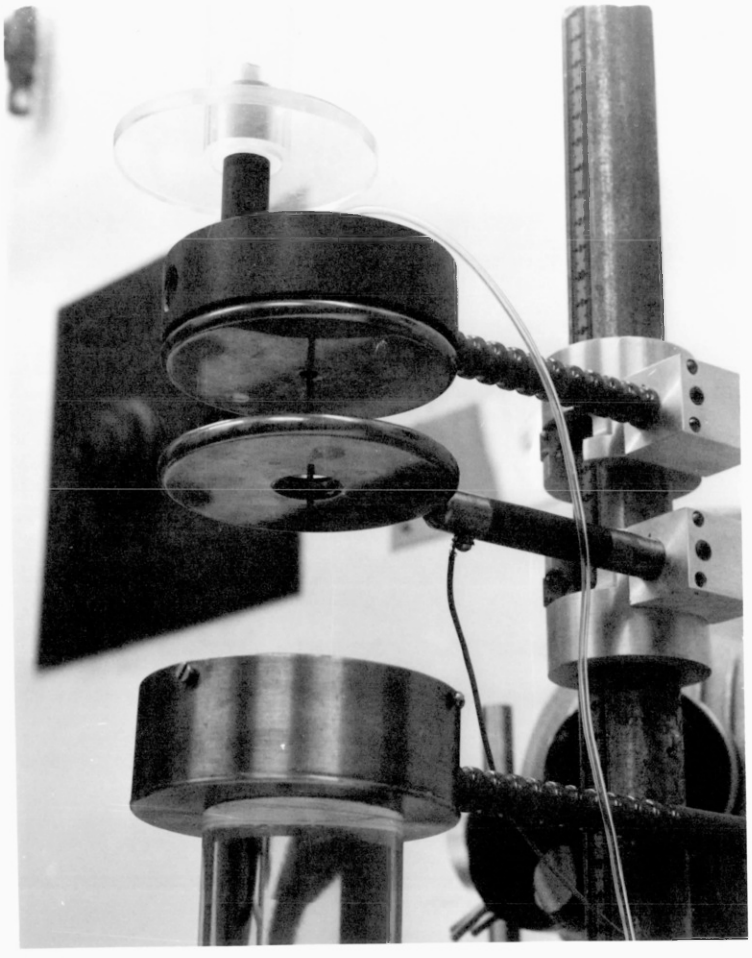

Close up showing the capillary passing through the earthed plate

Figure 4.1 The apparatus.

The slr camera was used to photograph the whole of the single jet and the drops. A sharp image of individual drops was taken by positioning a flash unit, having duration of 1 ms directly, behind the tip of the capillary.

Observations of the multiple jets.

Figure 4.2a is a schematic of the set up. The top disc (at high potential) is insulated by a tufnol disc of slightly larger diameter. The two are connected by a pressure fitting of a vertical copper rod soldered onto the copper disc. This rod pertrudes from the tufnol insulater to make contact with high voltage line. The end of the output line consists of a brass rod surrounded in perspex. The disc and tufnol cover are held onto the support stand by another rod horizontally screwed into the side of the tufnol.

The brass earthed collector below was machined as was the top disc to a diameter of 80 mm. Equal sized electrodes simplifies theoretical by setting one boundary condition at the outside edges. The depth of the collector was set at 25 mm and a guaze covers the cup to allow for spraying over a length of time. An alternative collector was made of brass in case of guaze blockage by viscous liquids. A cup containing a vertical screw at the centre was covered by dome shaped brass. Liquid flows through an annular gap between the edges of the cup and the edges of the dome.

Drozin (43) has commented on the need for high electric fields to observe several streams of liquid from a capillary end. Also, Hayati's (40) work on a capillary showed that the voltages available may not extend this study to the upper limits of the field. Therefore it was decided to make the system of electrodes more accessible to the high fields. A modification was made along the lines of

Hendricks' work (52), where he exploded a liquid meniscus directly into drops without the formation of a jet.

Figure 4.2a Schematic of the set up for multiple jets

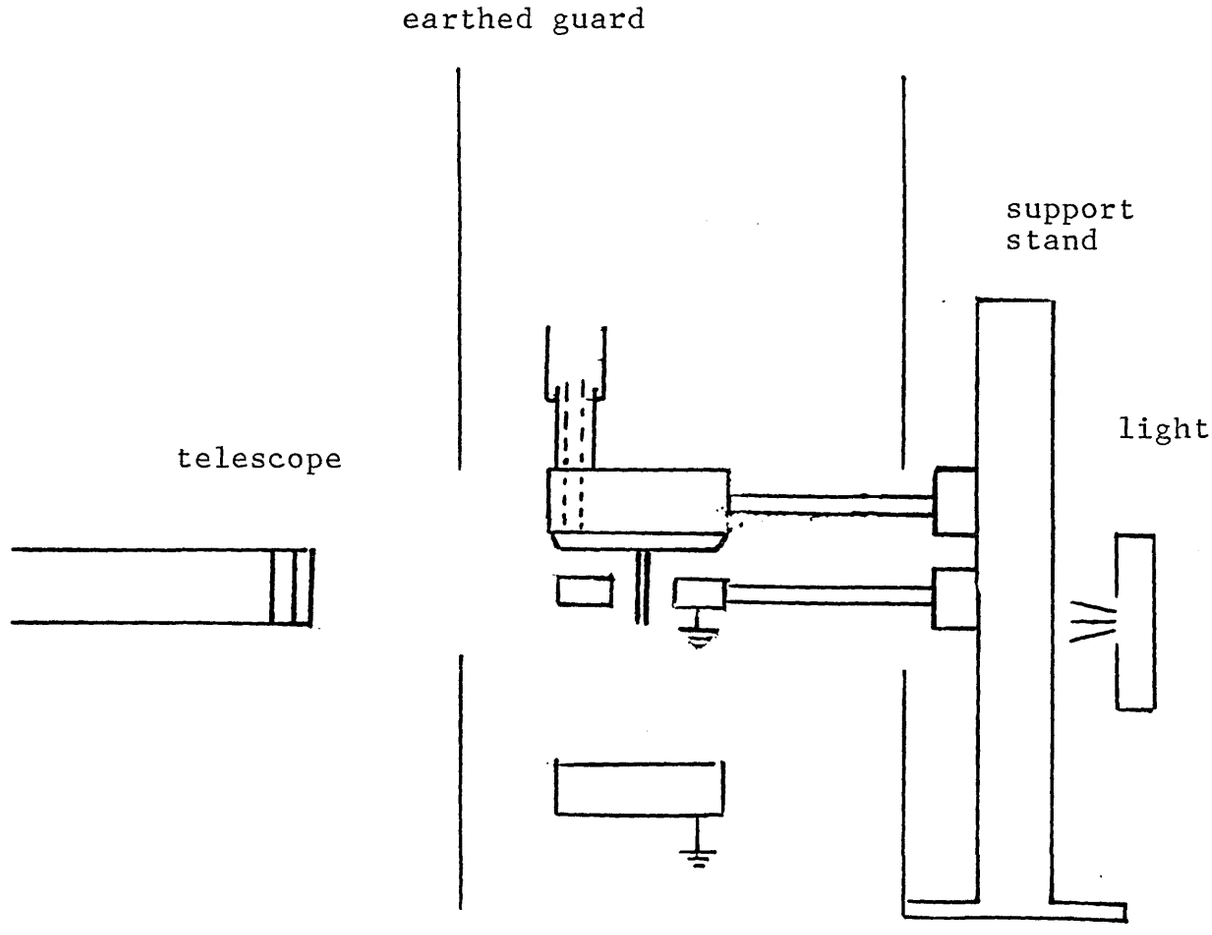

Intensification of the field was achieved by installing an earthed electrode behind a horizontal capillary (52). In order to establish the high fields, two discs were machined to 6mm width and 80mm outer diameter. Two inside diameters, of 15mm and 60mm size were bored at the centre of the discs. In this work, it was important to asses the effect of the hole diameter, and the effect of moving the plate away from the capillary, on the fields at the capillary tip. The support on the graduated stand was adjusted in the vertical direction to set different distances between the capillary and the earthed plate.

Other alterations to the set up were available; the capillary was easily replaced to investigate the effects of the outside diameter and wall thickness. The former has the alters the value of the field and also the value of the average liquid velocity.

At the start of an experiment the liquid was fed to the syringe from a funnel, and the air in the syringe and line to the capillary was slowly expelled. The earthed plate support was adjusted by two screws perpendicular to one another on the stand to ensure that at a set height the capillary passed symmetrically through the hole in the plate. A minimum vertical distance between the underside of the earthed plate and the end of the capillary was set to avoid the accumulation of charged drops attracted towards the earth. After setting the value of the flowrate, the dripping in the absence of voltage was observed through the telescope. The sodium lamp opposite the telescope illuminates the region around the capillary. The magnification was such that the capillary tip occupied over half the area of the eye piece. Positive polarity voltage was slowly applied until a number of jets could be observed to form from the capillary tip. It was found that the accuracy could be read to 0.5 kV. When at a particular number of jets formed, the voltage was lowered by 1 kV, the jets did not change in

number for a few seconds. When the power supply was switched off and on again, to apply a step jump in voltage, the same numbers were observed at the same value of the voltage after a short time lag. For liquids that displayed unsteady jets, either moving in one direction around the edge or switching in number, the unstable behaviour became more pronounced when the voltage was suddenly applied.

The following variables were investigated;

- liquid flowrate
- average velocity at the end of the capillary
- capillary outside diameter
- thickness of the capillary walls
- distance between the earthed plate and the capillary tip
- diameter of the earthed plate
- conductivity of the liquid
- viscosity of the liquid

Observations of the single jet.

The apparatus used is the same as outlined above with a few changes (see fig. 4.2b). The guard was removed from around the experimental area for photography. A camera, held steady on a tripod was placed in front of the capillary with a flash unit behind synchronized with the shutter. The magnification is high enough to see the steadiness of the jet, while low enough to photogragh the entire jet length and drops over a distance. Experimental procedure follows as above with the voltage, flowrate and parameters of the liquid being changed. The negatives were viewed under a microscope to take measurements of the diameter and the length of the jet as well as the drop diameters. For liquids of high conductivity, the resulting highly charged drops accelerated in the field to reach a velocity at which the flash unit was unable to provide a clear image. Also for flowrates below 12 ml/h the jet was too thin for accurate

measurements to be taken from the badly focused low magnification negatives.

Another set of experiments at higher magnification were performed to obtain information about the cone region of the jet. During these experiments the extra earthed plate was absent. The data from the high magnification negatives was used in computer programs to estimate the stresses driving the jet. In this case the bellows camera was used with the white light source and the distances adjusted to prevent fringes of light on the back screen of the camera. Again values were taken on the microscope.

The current carried by the drops was measured by placing an electrometer in the line between the collector and earthed connection. The support stand was earthed to preclude currents from the tufnol insulation. The Keithley electrometer when zeroed is capable of measuring currents as low as 10^{-12} A.

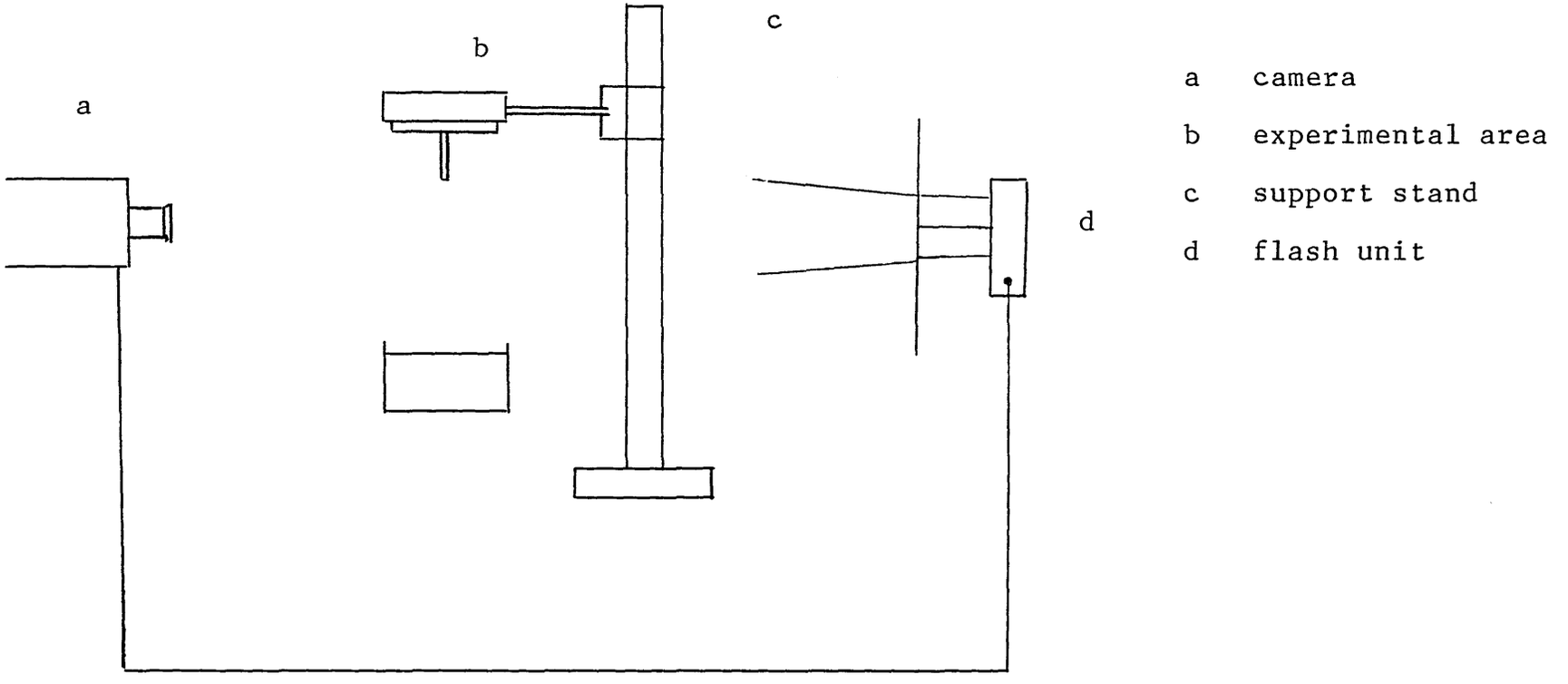

Figure 4.2b Schematic of the set up for the observations of the single jet

Photography

A pentax camera provided the negatives of the single jet. Two extensions were fixed onto a 50 mm lens to give sufficient magnification. Ahu film (equivalent to 25 ASA) was chosen to give good contrast. Since the film is very slow the aperture had to be almost fully opened to admit enough light from the relatively low intensity flash unit. The shutter speed was set at 1/60 s. The negatives were processed using Ilford universal film developer. Magnifica-tion was determined under the microscope from the known out side diameter of the capillary, to be x1.9.

The bellows camera gave images of the cone region with another 50 mm lens. The image clarity could be observed through the screen at the end of the camera. Five seconds shutter time was found to be optimal for Kodalith film, which has the characteristic of forming and losing the image rapidly during development. Monocromatic light bulbs provided enough light to control development time. Magnification for this camera was x12.8.

A travelling microscope, with x-y variation, was employed for the measurements. The lenses were inter-changeble to provide 10x, 20x, and 30x magnification. The lengths and diameters measured were accurate to 10 μm.

4.2 Drop size measurements.

It was originally intended to use a Malvern laser light diffraction unit to obtain the size inflight. The equipment has limitations to the number of particles it measures within the sample area. At a high concentration of particles the conversion of the collected data into a size distribution is inaccurate. Similarly, low concentrations result in suspect distributions, or no values at all. It was found that the spray from a single jet or ensemble of jets was too sparse for measurement, perhaps due to the low

flowrate. A number of attempts were made to overcome the limitations of the equipment. Three capillaries were placed in series in the path of the beam. Even near the point of jet break up the particle density was too low to provide a reading. In the second attempt, the drops were collected in liquid N_2 and placed in an optical container designed for the equipment. However, the heat losses could not be lowered sufficiently to stop vaporisation and the bubbling. The collection of the particles on optical glass was also unsuccessful.

Another device overcame the limitation on the concentration of drops. A probe at ICI, ppd, admits a laser ribbon across two mirrors facing one another. The degree of shadowing produced from a drop passing through the ribbon is relayed to a computer, which gives information about sizes, distributions, velocities of the spray and number of drops counted.

The Particle Measuring System comprises the OAP-2D-GA2 probe containing the He-Ne laser, and the microprocessor. A 64-element linear array of photodiodes detects the shadows of the drops. Three levels of darkness are sensed by each element in the array. The conditions in the array are stored at one instant to comprise one image slice. Further slices are stored at time intervals determined by the velocity of passage of the drops. In this way a complete two dimensional image containing scales of grey is stored on RAM chips.

The spraying apparatus is the same as in the case of the single jet observations, but because the full range of spraying was investigated, the earth plate with the smallest hole was placed above the capillary. The probe was position ed under the jet and commands were typed into the computer. An images command shows the drops passing across the ribbon (figure 4.3). In this way it was ensured that drops rather than the jet was sampled. Readings of the size

were taken at various heights from the tip of the capillary. Providing the centre of the spray cloud was sampled, the size was found to be independent of the sample distance from the capillary. However, the average size at the centre differed from that at the edges of the cloud by a maximum of 20 μm, for a jet at flowrates above 30 ml/h. For lower values of the flowrate, the size was uniform across the cross-section. Therefore, it was decided to slide the probe across the diameter of the cloud when taking measurements. The presence of the earthed probe in the experimental area affected the jet; when all the conditions had been set, adding the probe caused the tip of the jet cone to approach the capillary. The former position of the cone was re-established by decreasing the voltage. Use of the extra earthed plate with the probe positioned just above the collector, diminished this effect. The earthed plate causes the potentials on the outer boundary between the underside of the plate and the collector to be reduced to zero. The probe was stationary during sampling of several numbers of jets, and was placed in such a way that the drops from at least two jets could be recorded. Previous measurements showed the average drop size from each of the jets to be the same.

For conditions leading to average sizes above 200 μm the accuracy of measurement was ± 20 μm. At lower values the accuracy increased; for an average of 100 μm, the accuracy was ± 10 μm and for < 100 μm, ± 5 um. The current was simultaneously monitored by the Keithley electrometer. Current readings were accurate to 5%.

The average size of the drops and the current were measured against the following parameters;

- flowrate
- voltage
- conductivity of the liquid
- viscosity of the liquid

A matrix of experiments was designed to investigate the effect of varying one parameter on the effects produced on the spraying by another parameter.

Some measurements of the drop size in a spray cloud produced from the ICI electrodyn nozzle (78,79) were taken in a humidity and temperature controlled booth. An important feature of the metal electrode is the annular gap of 250 μm, from which several liquid jets issue.

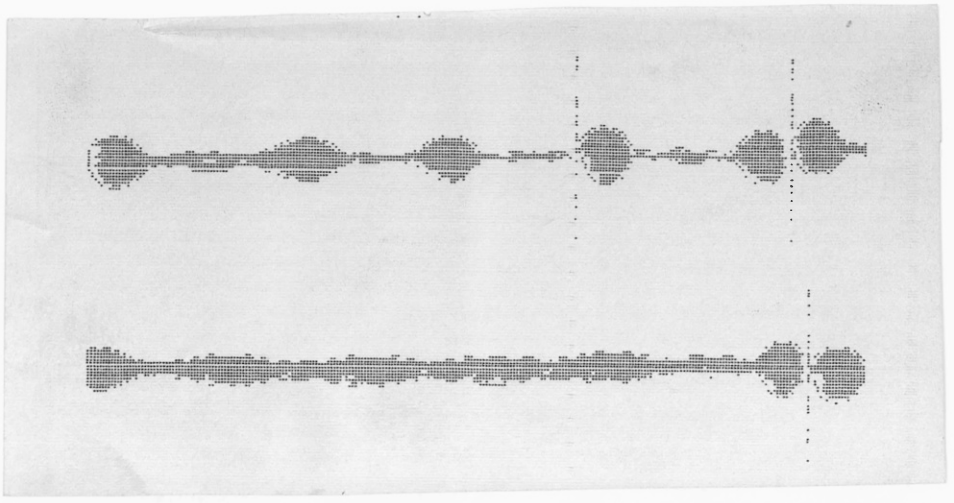

a jet passing through the ribbon

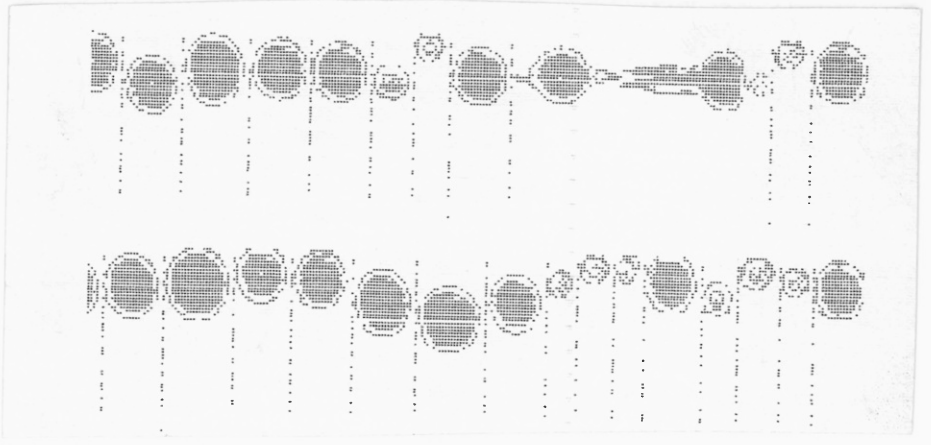

drops passing through the ribbon

Figure 4.3 The shadow image of the sample

4.3 Measurement of liquid properties .

Electrical conductivity at low fields .

An illustration is given in figure 4.4. The cell consists of two circular electrodes, one of which is earthed, separated by a cylindrical container made of acetal. Leads attached to the electrodes have terminals connected to the Keithley electrometer. The electrometer measures the current resulting from the application of a constant field intensity between the electrodes. About 25 mls of liquid are required to fill the cell upto the top electrode. Cleanliness was essential to avoid contamination by very small amounts of conducting liquids. The cell is placed in a Faraday cage to isolate the electrodes from stray currents in the surroundings. Once the current is known, the conductivity is obtained from the current and the known cell constant of 10 mm.

Conductivities in the range 1×10^{-8} to 2×10^{-6} $(\Omega m)^{-1}$ were measured to an accuracy of 2 %.

In practice the field at the capillary tip is higher than the fields applied across the cell. Furthermore, the value of the field depends on the value of the voltage applied to the capillary. The conductivity of a liquidat high field can vary from the value measured at low field strengths, due to the variation of the mobility of the ions. One author who conducted a theoretical analysis of the process derived an equation to predict the conductivity but estimates that the value never more than doubles (65) at high field strengths. The present method was not accessible to measuring the conductivity at high field intensities, so another set up was used for this purpose.

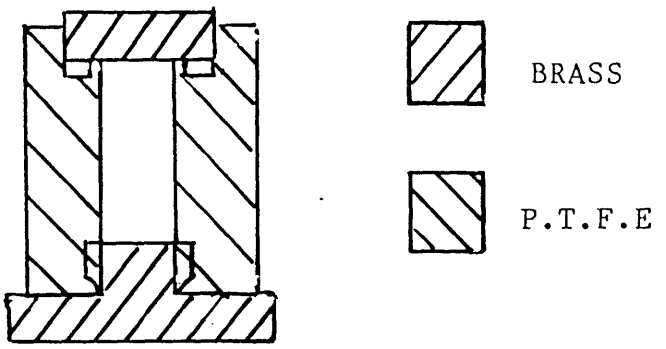

Figure 4.4 Cell used for conductivity measurements at low field.

Conductivity at high field.

The important feature of this technique is the cell, shown in figure 4.5. A 50 μm melanex spacer sets the length over which a voltage difference is applied from the control unit. The phosphor bronze electrodes are insulated by the p.t.f.e. packing. A predetermined voltage is applied at first to calculate the capacitance of the cell. Although this is known, the equipment must be zeroed before taking the readings. The cell is placed in a metal cage and a voltage difference, selected on the control unit, is applied across the electrodes. A reference capacitor on the output line charges over a peroid of time. The output signal is amplified across a resistor and the output voltage is

measured as a function of time. When the capacitor is fully charged the resistance of the liquid is obtained from the gradient of the linear portion of the voltage time curve. Values of the conductivity were taken as a function of the field applied .

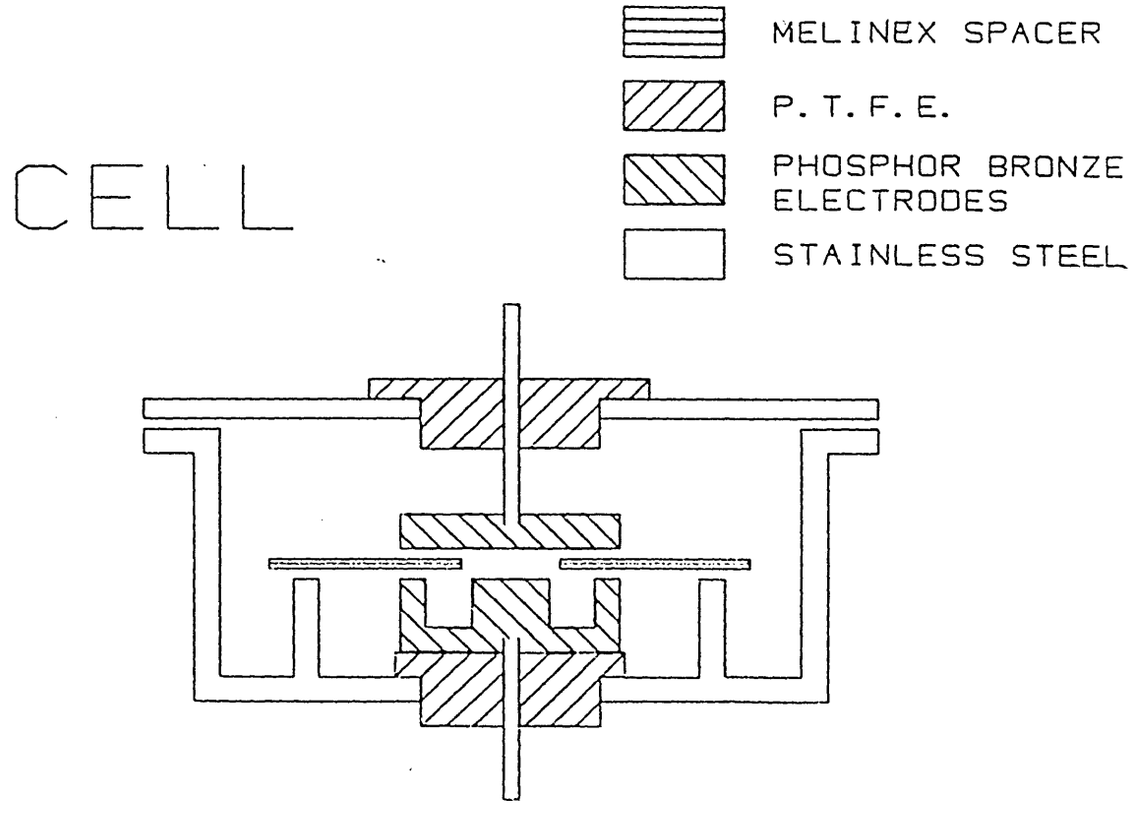

Figure 4.5 Cell used to obtain conductivity values at high field

Permittivity.

Another cell is employed to measure the permittivity of the liquids. This method of measurement is limited to values of the dielectric constant below 5. A known volume of liquid was placed in a test tube containing electrodes wired to a Wayne Kerr autobalance bridge. The tube is concentric with a polyester casing to eliminate outside effects. The permitivity of the liquid is found from knowledge of its capacitance and also the capacitances of air and mercury. First the tube was cleaned to measure the value for air. Then the capacitance of fresh mercury was measured. Finally, the test liquid replaced the mercury. The measured dielectric constant is calculated from the equation;

$$\varepsilon_m = \frac{C_{Hg}/C_{air} - 1}{C_{Hg}/C_s - 1}$$

The true dielectric constant is related to the measured value by the known cell constant (a function of the area and the distance between the electrodes);

$$\varepsilon = \frac{\varepsilon_m}{k_c}$$

Viscosity.

Viscosity was measured on a Rotovisco unit made by Haake. The liquid sample is placed inside a fine annulus between the outer metal cylinder and a central solid lightweight cylinder. The cylinder on the inside is rotated by a shaft operated by a motor to apply shear to the liquid. The motors may be interchanged so as to vary the order of magnitude of shear, though in most cases the lowest power motor was used. The liquid temperature, controled by a thermostat, was always held constant at 25 ° C. A chart recorder provides the variation of viscosity with time, for different values of sensitivity. Both the measurement duration time and the chart sensitivity are selected by the operator on the controls.

The viscosity is determined from the S_t line, recorded against time, by the relation;

$$\mu = \frac{\%T \; S_t \; A}{D \; M}$$

where %T is the sensitivity, and A, M, D are constants for the motor. Since the liquids sprayed were Newtonian, the variable S_t was found to be constant over time.

Initial readings to assess the accuracy of the procedure indicated a value of 3% at both ends of the viscosity range investigated. The viscosity was varied from 5 mPas to 70 mPas.

Surface tension

The surface tension measurements were taken using a Kruss digital tensiometer (model K10). The measuring body used is a horizontally suspended wire ring of known circumference (figure 4.6). Values of the surface tension are recorded as the immersed ring is raised from the liquid-air interface to the point at which the neck of the liquid hanging below tears away. As the ring is raised, the contact angle of the liquid on the ring increases, leading to an increase in the surface tension force. When the tangent to the ring is vertical, the force has reached the maximum value. Further rise of the measuring ring breaks contact with the liquid, and the force on the ring falls sharply. The surface tension is determined from the maximum value of the force and the dimension of the ring;

$$\gamma = \frac{F_{max}}{2 \times \text{ring circumference}} \times \text{correction factor}$$

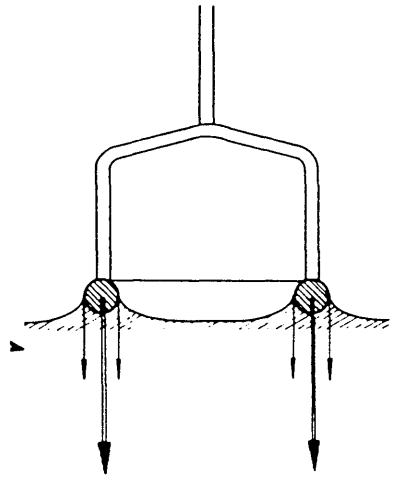

Figure 4.6 Schematic of the tensiometer ring.

4.4 Liquids.

Throughout much of the work mixtures of liquids had to be prepared in order to assess the effect of the properties of the liquid on the spraying process and also to investigate the interdependency of the factors. Work reported by others has shown that the conductivity of the liquid to be an important parameter for the formation of a steady jet. It was reasonable to look to the conductivity for effects on the profile of a steady jet, the disintegration of the jet, and the resultant drop size. It was also likely that conductivity could determine the charge on the drops. Isopar M, an isoparaffinic oil, was used as the low viscosity base liquid to which Aerosol ot was added to modify the conductivity. As the Aot concentration was increased, the conductivity rose sharply, but above 40 % w/w Aot, it remained constant. At higher concentrations further addition of Aot resulted only in an increase in the viscosity. During experiments requiring constant viscosity, mixtures with concentrations in the lower region were sprayed. Conversely, the upper concentration region was used in experiments where the viscosity was varied, though at a high value of the conductivity. Although aot acts as a surfactant, once small quantities have been added the surface tension of the mixture is constant. It was possible to replace Aot with n-butanol to affect a change in the conductivity. The latter was rarely used in a two component mixture.

Since the effect of the viscosity on jet formation and the size of the drops produced was to be investigated, it was necessary to vary the parameter over a range of the conductivity, in order to avoid one factor outweighing the other. The addition of a third component, heavy paraffin oil changed the viscosity but also lowered the conductivity of the mixture. Graphs of conductivity versus concentration of paraffin, with %Aot in isopar M in the original mixture as

the parameter, allowed the sample liquids to be chosen at the required conductivity. The viscosity was selected from a similar graph of viscosity against concentration of paraffin, again with the original concentration of Aot as a parameter. If the full viscosity range required could not be reached, the conductivity was reselected to give new mixtures. Higher conductivities were reached at higher Aot fractions, leading to higher values of the viscosity.

For the experiments in which the viscosity was varied, two further systems were used. The introduction of n-butanol meant that the species of conductivity additive could be changed, though in some cases Aot was also present in the paraffin mixture. N-butanol had the effect of countering the viscosity rise associated with Aot, to reach the lower viscosities at high conductivity. One system was the four components: Aot, isopar M, heavy paraffin, butanol. The other system of liquids excluded the viscosity modifier, heavy paraffin.

CHAPTER FIVE

STUDIES ON THE SINGLE JET.

The way in which electrostatic energy is imparted to a liquid has been known to affect its behaviour in the electric field. At low voltage, a drop is pulled away from the capillary and accelerates towards the earthed target. An increase in the voltage results in an increase in the rate of drop detachment. This process is time dependent; as the drop leaves the tip, the remaining liquid meniscus is sheilded from the electric field. Once the ejected drop is far away, the liquid responds to the field and charge is able to build up again at the surface (figure 3.7). The drops produced in this mode are relatively large and have low charge. Higher voltages produce pulsating spraying, where the meniscus is extended and then relaxex back to,the tip at higher frequencies. Still higher voltages stabilise the extension of the liquid so as to form a steady jet.

The photography of the jet profile enabled observations to be made about how the liquid reacts when the voltage, flowrate and the parameters of the liquid are varied. Measurements of the diameter and the length of the jet were taken. Under certain conditions, the drops could also be observed. Of particular interest was the relation between the diameter of the jet and the diameter of the drops that it emits. Other experimental work on the single jet was concerned with the conical region. Readings were taken from high magnification negatives of the cone and used as data to estimate the electric tangential stress operating at the jet surface.

5.1 Jet sizes.

A portion of the jet far from the capillary was found to have constant diameter before breaking up into drops (figure 5.10). It is in this region that the measurements of the diameter were taken. The values were obtained from negatives under a microscope at x 30 magnification. A flash unit was employed behind the capillary to expose the jet for 1 ms. The flowrate, conductivity, voltage and viscosity were varied to assess their effect on the length of the jet upto the point of break up and on its diameter. Figure 5.1 plots the sizes against average inlet velocity when the flowrate is varied at a conductivity of 2.9×10^{-8} $(\Omega m)^{-1}$. The voltage applied to the capillary is held constant. Both the diameter and the length can be seen to increase non-linearly with the velocity, until at large values of the velocity, where the effect is reduced.

The tendency for the two sizes to decrease as the voltage at the capillary rises, is illustrated by figures 5.2 and 5.3a. Raising the voltage causes the jet to accelerate more and break up at a shorter distance. Referring to the flowrate of 30 ml/h, for both values of the conductivity, the diameter changes more rapidly at the lower voltage values. When higher voltages are applied, the electrical energy influences the current carried on surface of the jet rather than reducing its diameter. However at 120ml/h (figure 5.3b) the change in the diameter is linear for the slightly higher conductivity liquid. The lower flowrate curves also show a greater change in the length of the jet as a percentage of the highest value (28%), compared with the 120 ml/h experiments where the length is only reduced by 10%. Apart from increasing the lengths, the effect of the flowrate counteracts the effect of the voltage. In contrast, the diameter decreases by the same percentage at both flowrates.

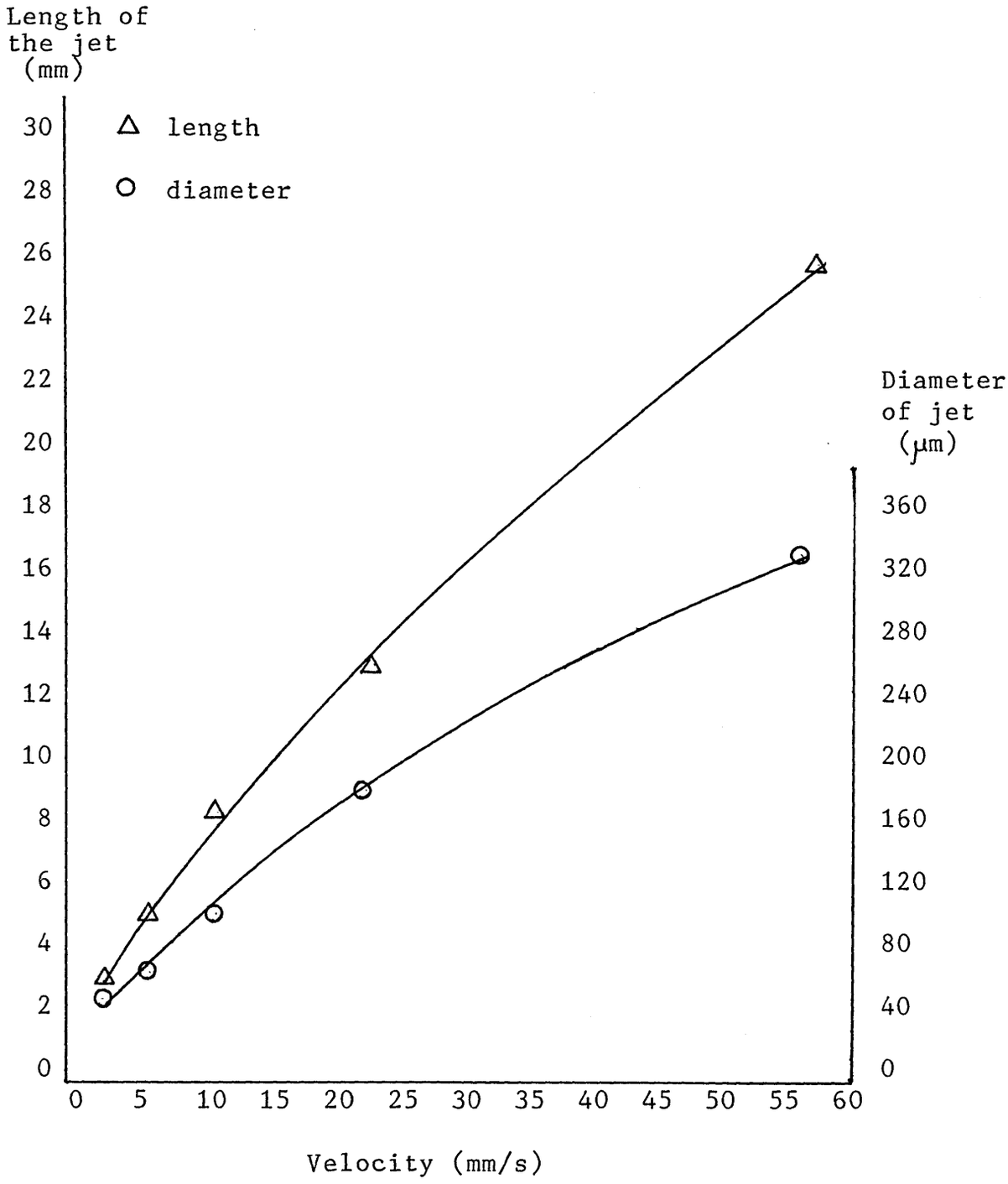

Figure 5.1 Variation of the length and final diameter of the single jet with the average velocity inside the capillary. $k=2.9\times10^{-8}$ $(\Omega m)^{-1}$. Capillary inside diameter=1.35mm.

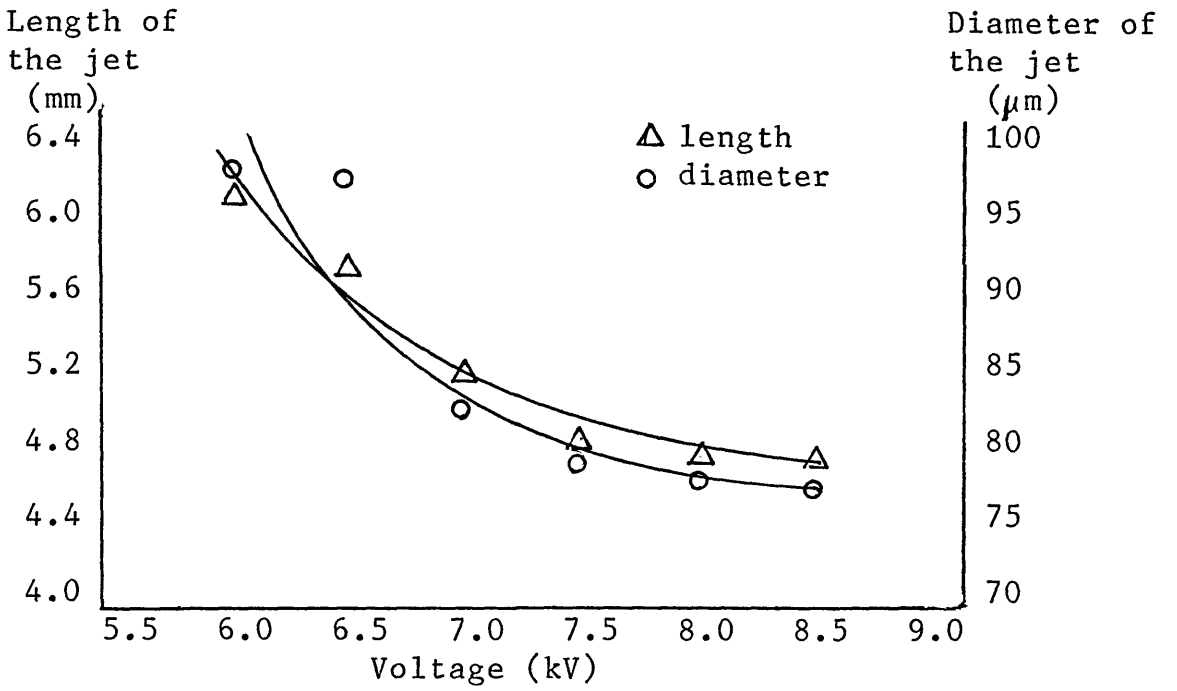

Figure 5.2 Variation of the length and diameter of the single jet with the voltage applied to the capillary. $k=10^{-8}$ $(\Omega m)^{-1}$. V_f=30ml/h.

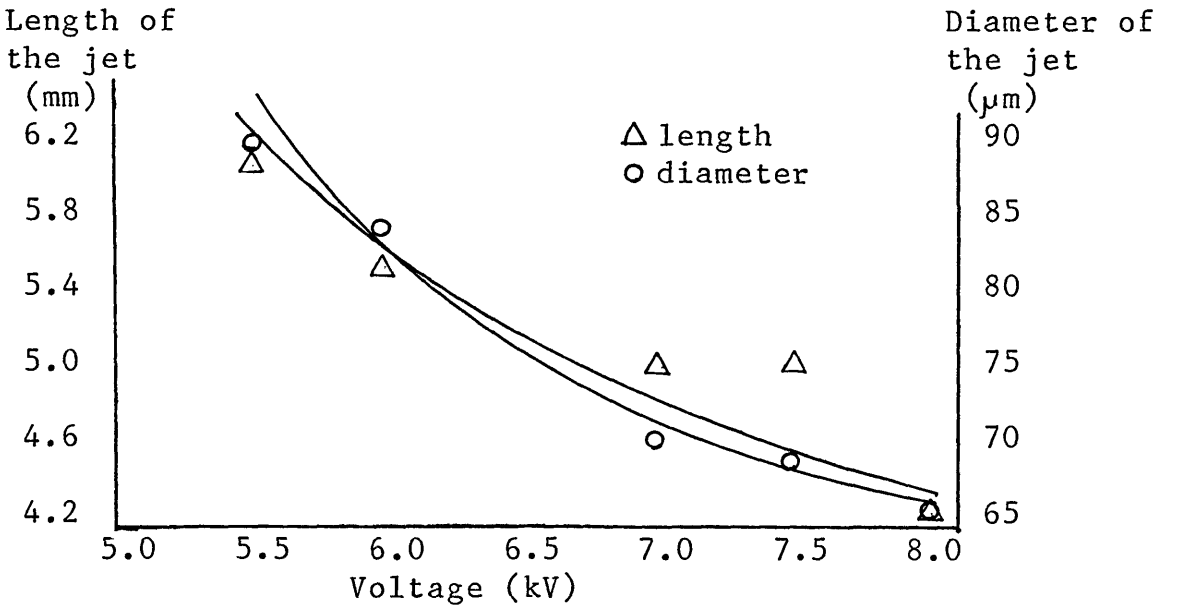

Figure 5.3a Variation of the length and diameter of the single jet with the voltage applied to the capillary. $k=2.86\times10^{-8}(\Omega m)^{-1}$. V_f=30ml/h.

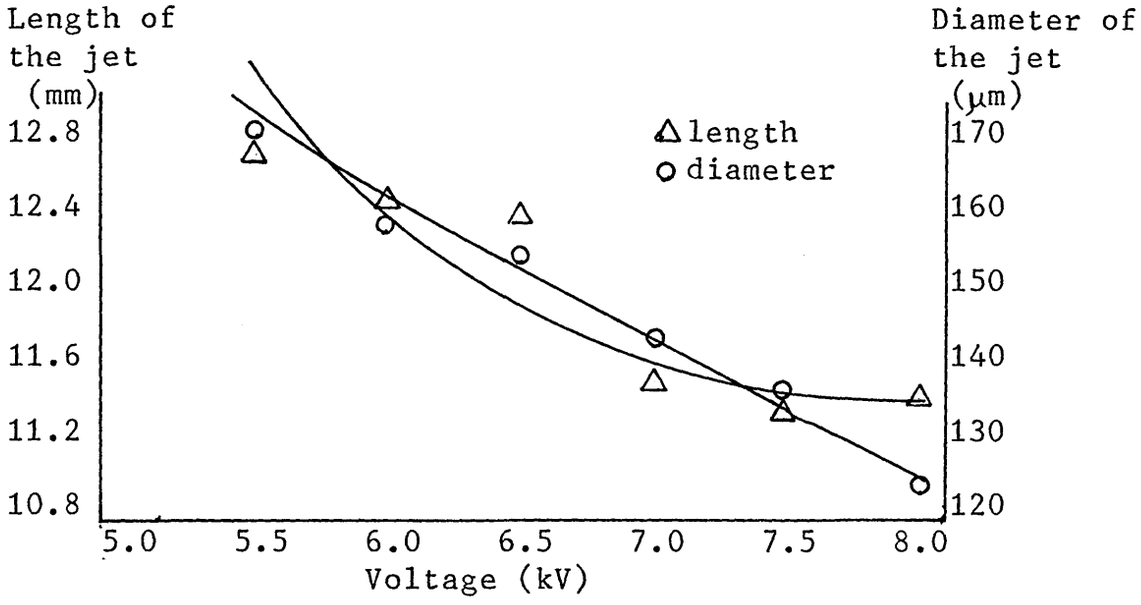

Figure 5.3b Variation of the length and diameter of the single jet with the voltage applied to the capillary. $k=2.86\times10^{-8}$ $(\Omega m)^{-1}$. V_f=120ml/h.

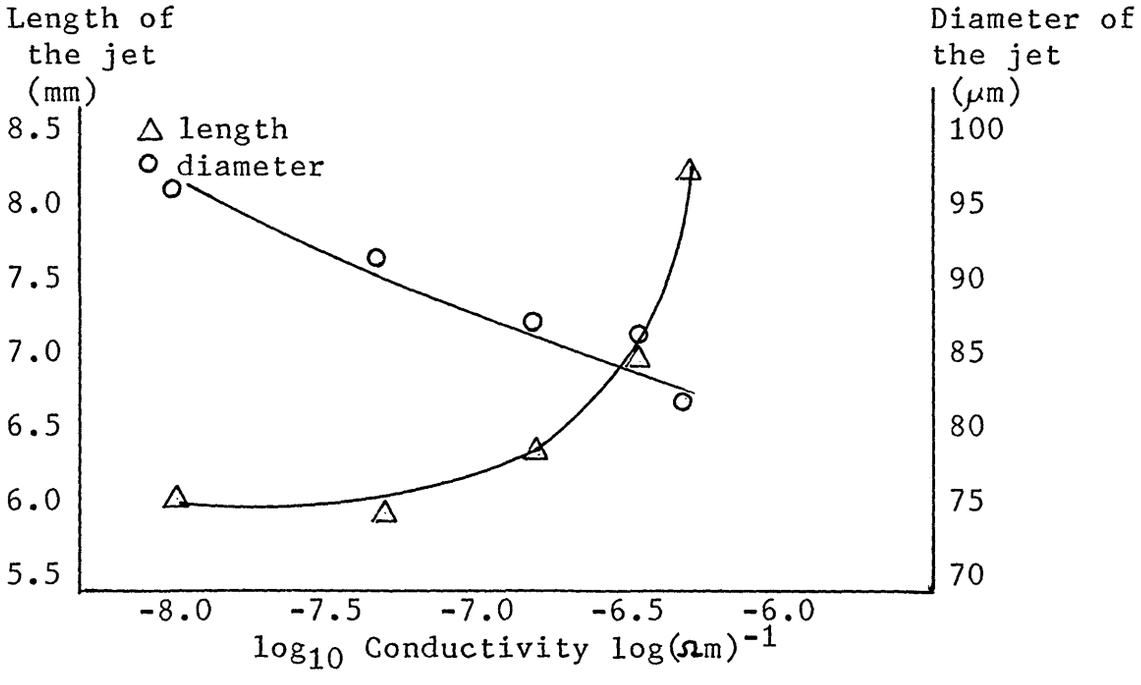

Figure 5.4a Variation of the length and diameter of the jet with the liquid conductivity. V_f=30ml/h. Voltage=6kV

The results outlined above link the trends of the diameter and length, so that a fine jet is apparently less stable to the forces that cause it to break up. However the results shown in figure 5.4 a are not in agreement with this hypothesis. An increase in the conductivity of the liquid is accompanied by sharp increase in the length and a reduction in the diameter. Figures 5.4 b and 5.5 confirm the behaviour at different voltage and flowrate. Increasing the conductivity and the capillary voltage both have the effect of imparting more charge to the jet and hence more energy is available for the acceleration that leads to smaller diameters. However the contrasting trends for the lengths obtained when the voltage and conductivity are varied, suggests that the current carried causes the jet to be extended further, before disintegrating into drops, only under certain conditions.

The importance of the electrical forces acting on the surface of a jet for its stability has been considered by various authors (13,17,60). For an axisymmetric wave growing due to surface tension, the electric force normal to the jet interface tends to stress the liquid radially, preventing curvature.

The electrical forces responsible for promoting longer jets in this way originate from two sources. Considering the first source; the dielectric property of the liquid ensures that polarization forces are operative in the presence of a tangential electric field. For a cylindrical column of liquid carrying charge on the surface, the current at any cross section is constant. A constriction at a point on the jet results in an increase in the charge density and the presence of a local tangential stress. This produces the outward polarization force that restores the jet to its original diameter.

In an attempt to explain the lengthening of the jet at the higher conductivities, attention was drawn to the

possibility that the dielectric constant could be increasing with the addition of Aot. The measurements of the dielectric constant, taken in a cell connected to a Wayne Kerr bridge, were found to be independent of Aot concentration (table 5.1).

Table 5.1 Dielectric constants of Aot/Isopar M mixtures.

% w/w Aot in Isopar M	5	10	15	20	30
Dielectric Constant	1.5	1.9	1.6	1.8	1.8

The second source of an outward force is the convection of charge on the surface of the jet. The normal electric stress is the product of the charge density and the normal field. Raising either the voltage at the capillary or the conductivity of the liquid is expected to have the effect of raising the current carried. However, the effects the variables produce on the density of charge is not immediately obvious. Measurements of the currents for each condition of the voltage and conductivity were used with the final diameter of the jet to calculate the charge density. Since the jet maintains a constant diameter over a distance before breaking up, the electrical acceleration force can be assumed to be negligible. By this reasoning, the Ohmic current is zero, so that all the current is carried at the surface of the jet;

$$I_t = 2\pi r_j u_j \varepsilon_o E_n$$

Rearranging for the charge density and expressing the velocity in terms of the volumetric flowrate gives,

$$\varepsilon_o E_n = \frac{I_t r_j}{2V_f}$$

The variation of the charge density on the surface of the jet with the conductivity and the voltage are given in table 5.2 and plotted in figures 5.6 and 5.7 respectively. As the voltage is raised, the final value of the radius reached by the jet falls in proportion to the increase in the current carried on the jet. The charge density remains virtually constant. When the conductivity is varied, only a portion of the increase in the electrical energy is translated into the acceleration of the jet. The formation of constricted areas on the jet is therefore prevented more effectively by a higher value for the charge density.

However this conclusion is limited to the range of conductivity investigated here ($1x10^{-8}$ - $2x10^{-6}$ $(\Omega m)^{-1}$). Some measurements of the length of a more conducting jet are available from the literature. Conductivity was adjusted by doping glycerol with sodium chloride. The length of the jet is shown in figure 5.8 to increase with the conductivity until a plateau is reached. At high conductivity, $8x10^{-5}$ $(\Omega m)^{-1}$ the jet becomes shortened.

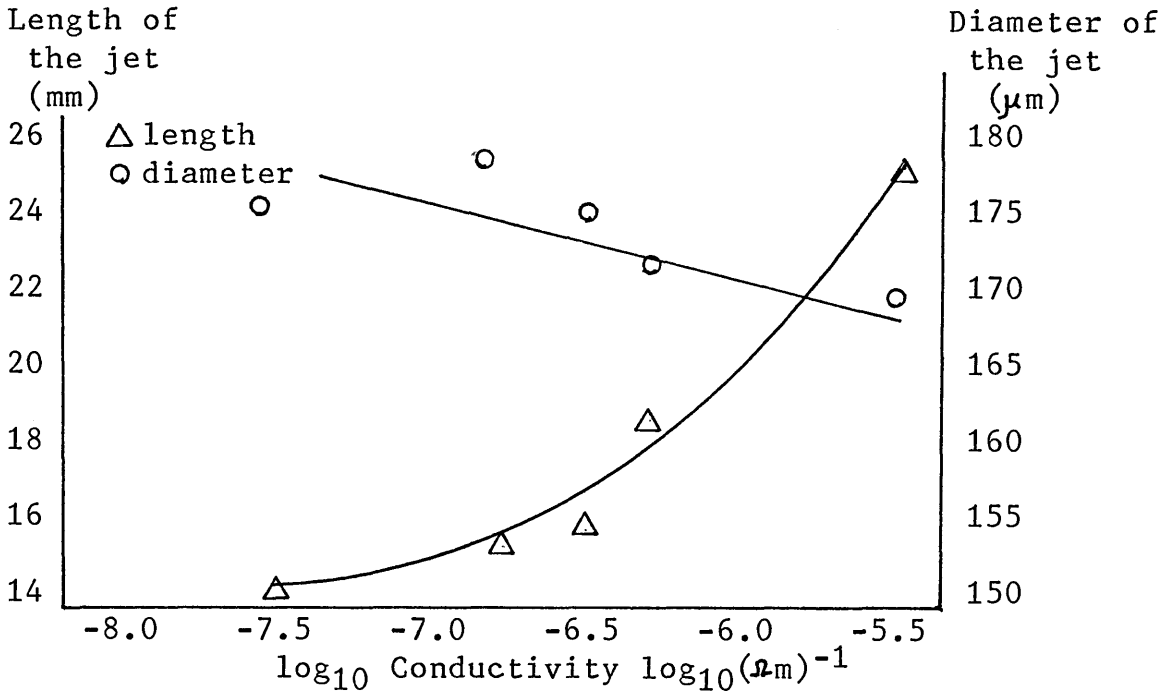

Figure 5.4b Variation of the length and diameter of the jet with the conductivity. V_f=120ml/h. Voltage=6kV

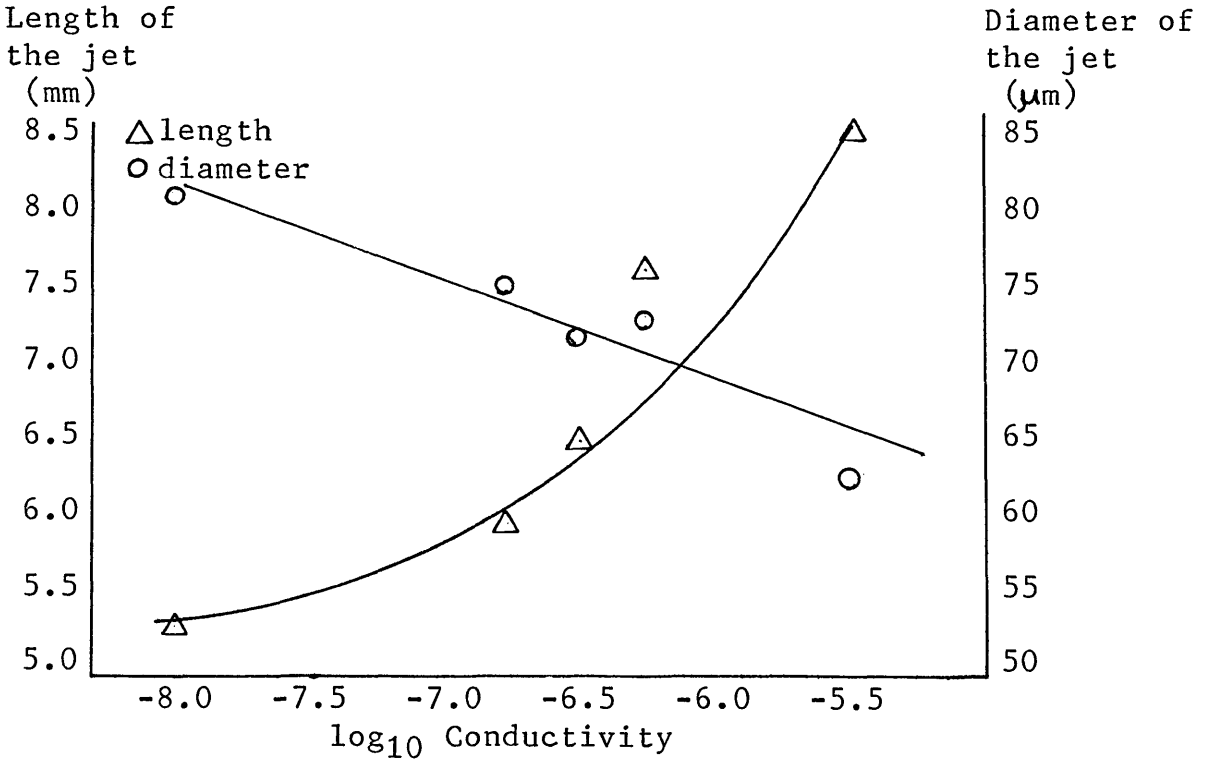

Figure 5.5 Variation of the length and diameter of the jet with the conductivity. V_f=30ml/h. V=7kV.

Table 5.2a The variation of the charge density on the surface of the jet with increase in the capillary voltage.

Conductivity = 10^{-8} $(\Omega m)^{-1}$
Flowrate = 30 ml/h

Voltage (kV)	Jet diameter (μm)	Current (A)	Charge density (C/m^2)
6.5	95	$1.0x10^{-8}$	$2.85x10^{-5}$
7.0	82	$1.0x10^{-8}$	$2.46x10^{-5}$
7.5	80	$1.1x10^{-8}$	$2.64x10^{-5}$
8.0	77	$1.2x10^{-8}$	$2.77x10^{-5}$
8.5	75	$1.3x10^{-8}$	$2.93x10^{-5}$

Conductivity = $3.0x10^{-8}$ $(\Omega m)^{-1}$
Flowrate = 30 ml/h

Voltage (kV)	Jet diameter (μm)	Current (A)	Charge density (C/m^2)
5.5	91	$1.3x10^{-8}$	$3.55x10^{-5}$
6.0	84	$1.4x10^{-8}$	$3.53x10^{-5}$
7.0	70	$1.5x10^{-8}$	$3.15x10^{-5}$
7.5	68	$1.55x10^{-8}$	$3.15x10^{-5}$
8.0	65	$1.6x10^{-8}$	$3.12x10^{-5}$

Conductivity = $3.0x10^{-8}$ $(\Omega m)^{-1}$
Flowrate = 120 ml/h

Voltage (kV)	Jet diameter (μm)	Current (A)	Charge density (C/m^2)
5.5	171	$1.7x10^{-8}$	$2.13x10^{-5}$
6.0	157	$2.0x10^{-8}$	$2.36x10^{-5}$
6.5	153	$2.2x10^{-8}$	$2.50x10^{-5}$
7.0	143	$2.4x10^{-8}$	$2.58x10^{-5}$
8.0	123	$2.6x10^{-8}$	$2.40x10^{-5}$

Table 5.2 b The variation of the charge density on the jet with increase in the conductivity.

Flowrate = 30 ml/h

Conductivity $(\Omega m)^{-1}$	Jet diameter (μm)	Current (A)	Charge density (C/m^2)
1.0×10^{-8}	82	1.0×10^{-8}	2.46×10^{-5}
1.7×10^{-7}	74	1.3×10^{-8}	2.89×10^{-5}
3.0×10^{-7}	72	1.5×10^{-8}	3.24×10^{-5}
5.0×10^{-7}	70	3.0×10^{-8}	6.30×10^{-5}
2.0×10^{-6}	65	4.0×10^{-8}	7.45×10^{-5}

Flowrate = 120 ml/h

Conductivity $(\Omega m)^{-1}$	Jet diameter (μm)	Current (A)	Charge density (C/m^2)
1.0×10^{-8}	178	1.3×10^{-8}	1.74×10^{-5}
1.7×10^{-7}	179	1.7×10^{-8}	2.29×10^{-5}
3.0×10^{-7}	174	2.6×10^{-8}	3.40×10^{-5}
5.0×10^{-7}	172	3.9×10^{-8}	5.05×10^{-4}
2.0×10^{-6}	171	6.4×10^{-8}	8.20×10^{-4}

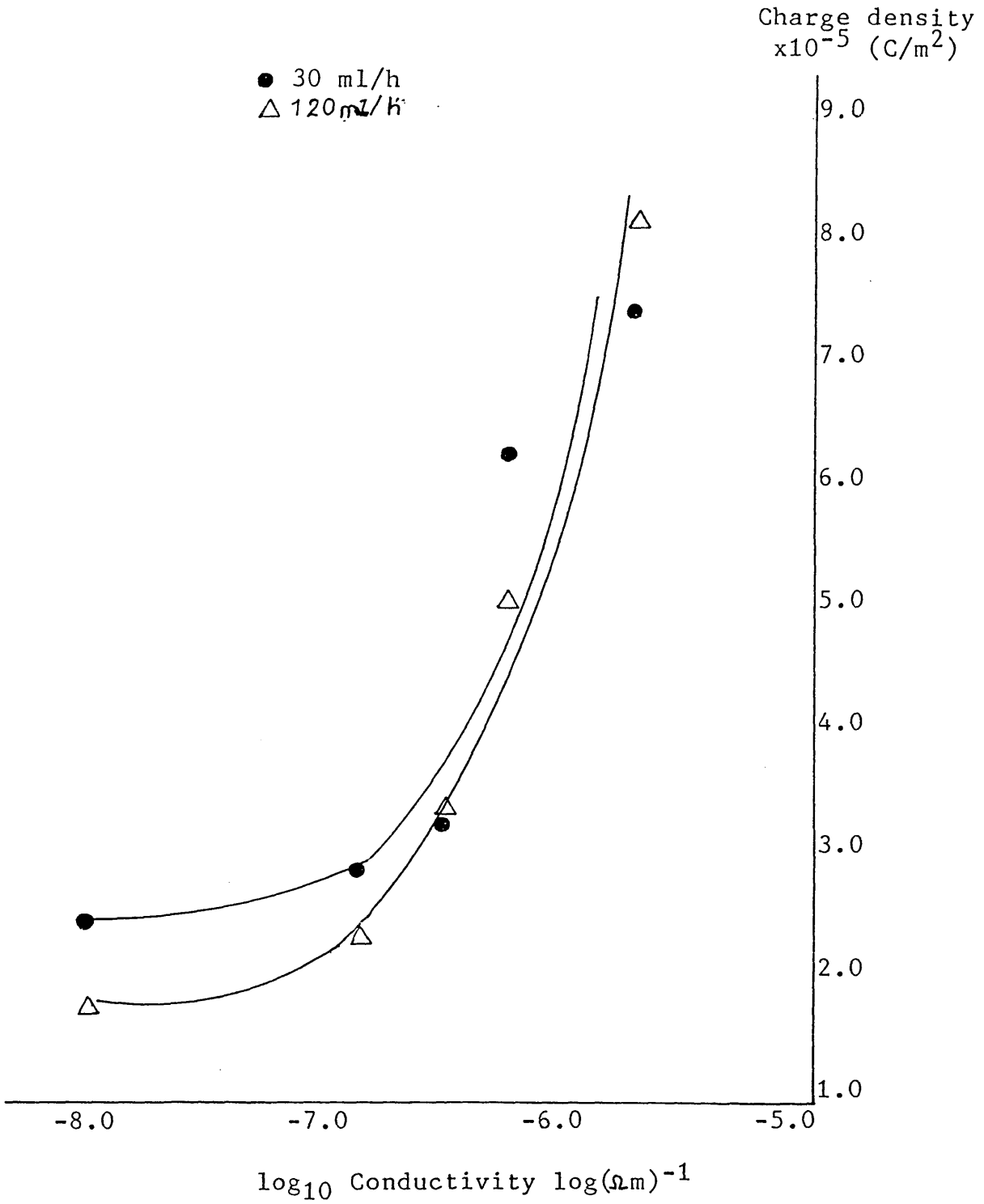

Figure 5.6 The charge density on the surface of the jet, just before the point of break up, increases with the conductivity of the liquid.

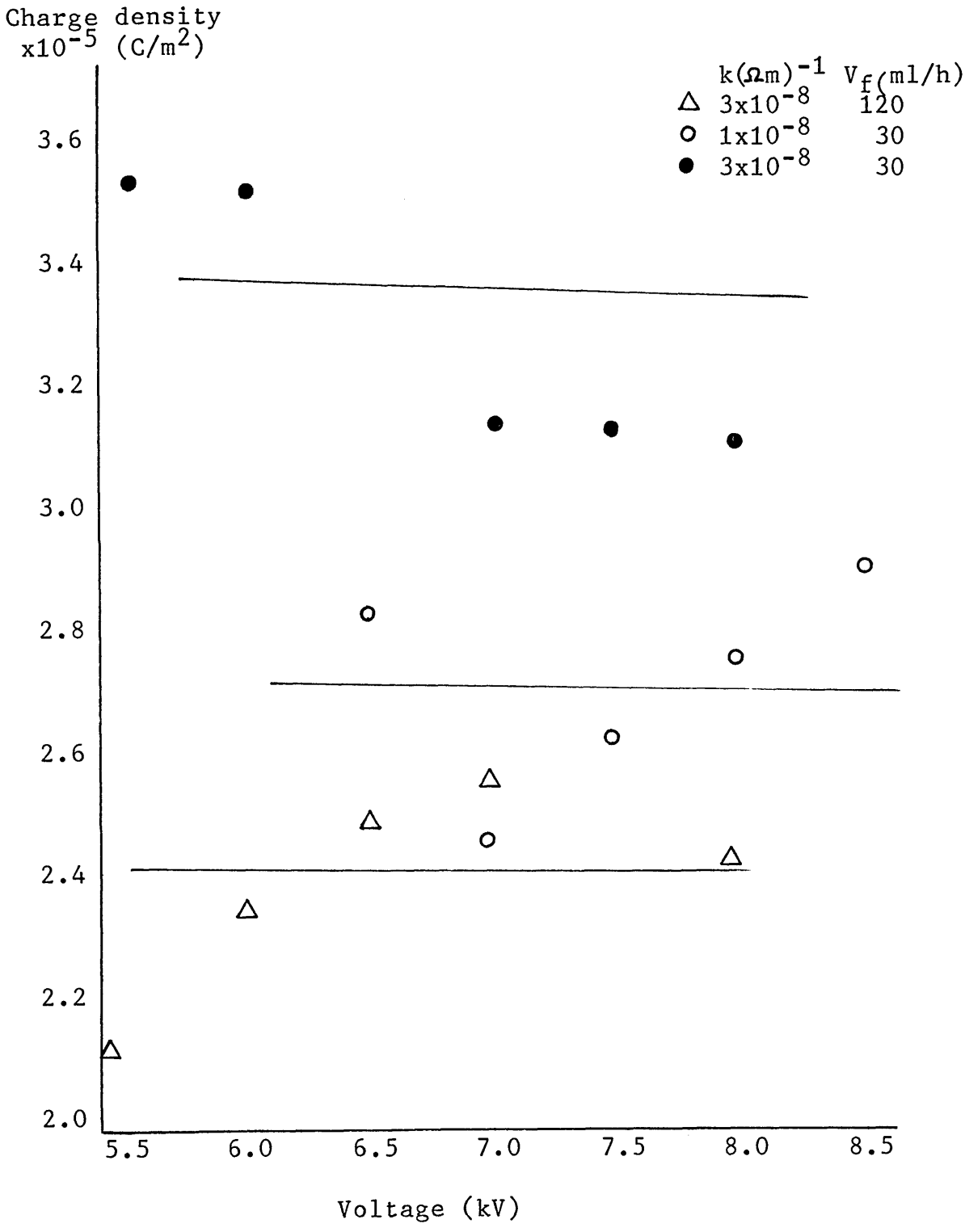

Figure 5.7 The charge density on the surface of the jet, just before the point of break up, is virtually independent of the voltage applied to the capillary.

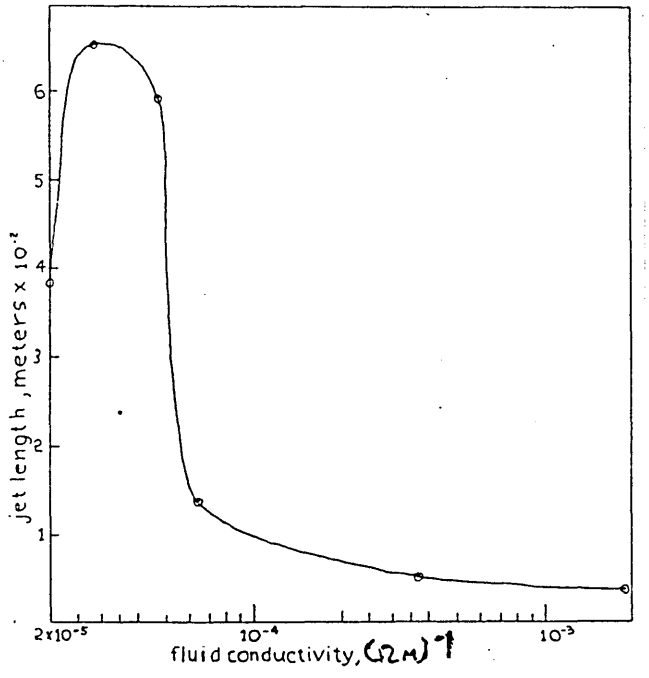

Figure 5.8 The length of the jet against conductivity for mixtures of glycerol and sodium chloride (12).

The effect of the viscosity on the diameter and length of the jet for mixtures of Aot, isopar M and paraffin, is illustrated in figure 5.9. The viscosity curves are the only results which can be considered independently of the charging levels. The other effects have been discussed in view of the charge imparted to the liquid. Again the trends for the sizes are reversed, with the length increasing and the diameter decreasing as the viscosity rises. Below 25 mPas the length is relatively unaffected, but above that value, the viscosity has the greatest effect on the length, with a twofold increase in viscosity resulting in almost a threefold increase in the length. Figure 5.1 shows that an order of ten increase in flowrate causes the jet to extend to five times its initial value. Similarly a conductivity rise of 100 times only results in a doubling of the values. So of the factors considered in this study, the length of the jet has been found to be the most sensitive to viscosity. The extension of the jet to form smaller diameters is a consequence of the gravity force and viscosity.

5.2 The break up of the jet.

Two methods of break up are reported in the literature. The first concerns axisymetric waves which are amplified by surface tension and are growths in space. The second is the result of angular disturbances which also grow due to surface tension, but the motion is dependent on time, and the pattern of the jet is snake like. The second mode of break up is a consequence of high charge on the jet and the trajectory followed by the liquid is influenced by the applied field. The growth of axisymetric waves is believed to result in monodisperse size distributions, whereas polydisperse drops are produced from the angular wave.

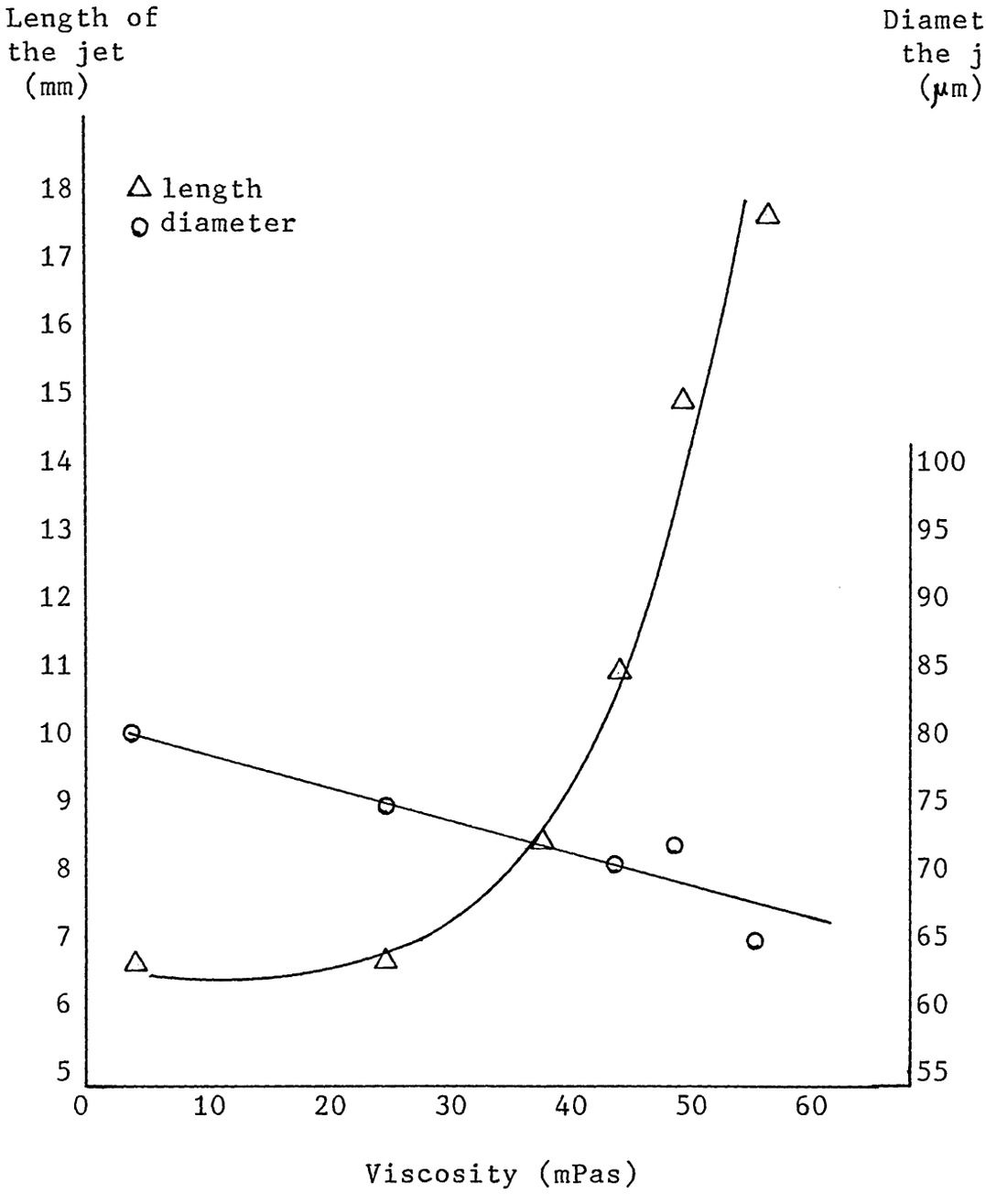

Figure 5.9 Variation of the length and final diameter of the jet with the viscosity.
$k=1.47\times10^{-7}(\Omega m)^{-1}$. $V_f=30ml/h$

Photographs taken using a 50 mm lens and a 1 ms flash positioned directly opposite the camera, showed a straight jet under all conditions. Axisymmetric waves were always apparent. When liquids of intermediate conductivity, $k > 2x10^{-7}$ $(\Omega m)^{-1}$ were sprayed, the flash was unable to freeze the drops travelling at high velocity.

Figure 5.10 shows jets breaking up at conductivity $2x10^{-8}$ $(\Omega m)^{-1}$ for different flowrates and capillary voltages.

Figure 5.11 illustrates that the form of the jet is not constant with time, the jet sometimes being extended while at other times the wave growth is present. The theory of the development of waves considers a drop to be emitted when the amplitude of the wave reaches the value of the radius of the jet. Deviation from this behaviour is a consequence of the exterior field, which forces the growth at the end of the jet to be pulled off. Theoretical treatment of charged jets includes the normal stress only and does not allow for the acceleration of the drops away from the jet. The disintegration of viscous jets is shown in figure 5.12. Two or three wavelengths may be emitted at the same time as the region between the emitted mass and the remaining liquid is drawn out.

Measurements of the drops were made using a high quality microscope at 30x magnification. Ratios of the drop diameter to the jet diameter are given in table 5.3, for mixtures of (a) Aot and isopar M and (b) mixtures of Aot, isopar M and paraffin. The average value is 1.87 within an accuracy of 9 %. Rayleigh's analysis for the disintegration of a cylindrical uncharged jet predicts a ratio of 1.89.

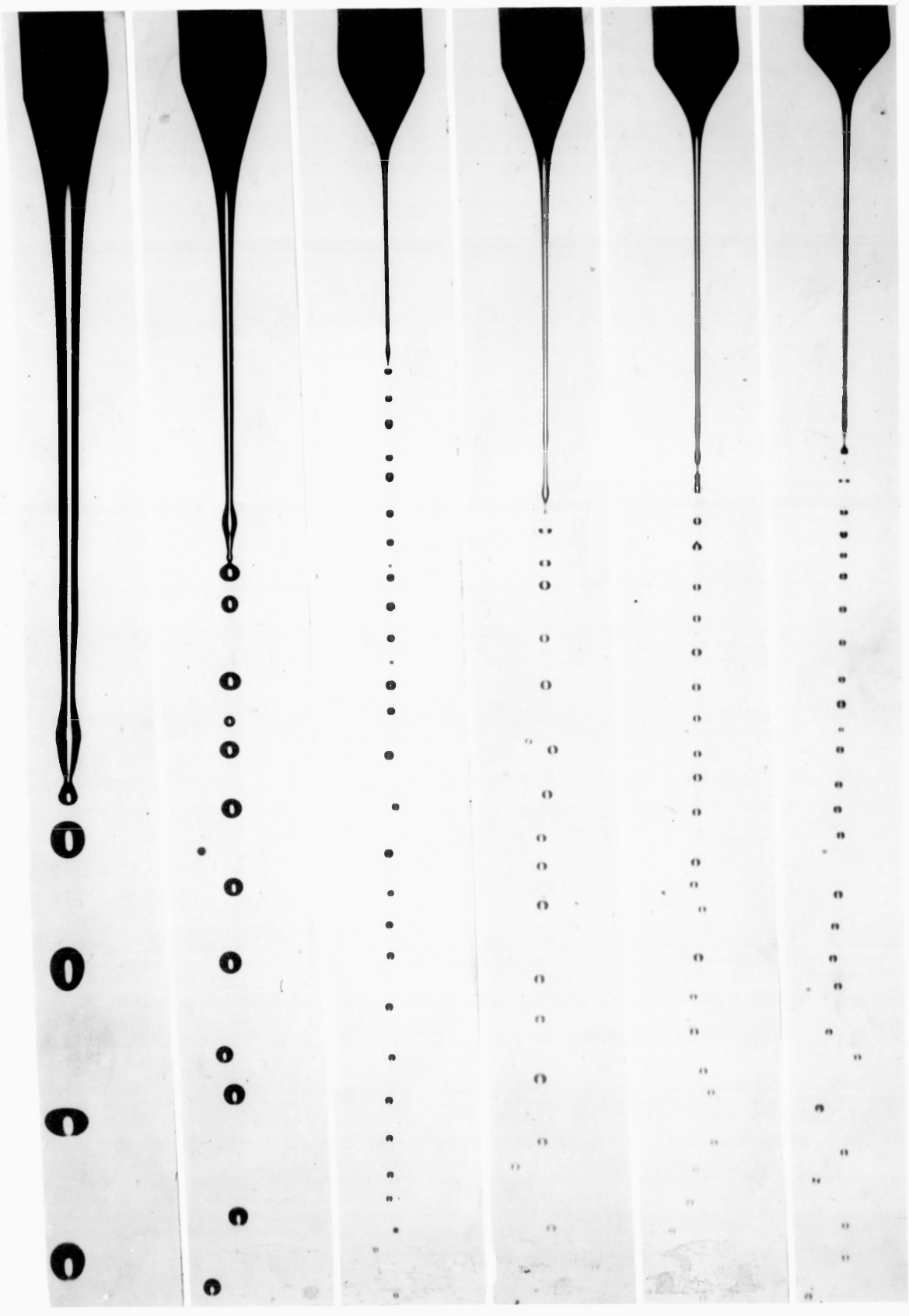

a b c d e f

Figure 5.10 The disintegration of the jet into drops. (a) V_f=300 ml/h. (b) V_f=120 ml/h. (c) V_f=30 ml/h. (d) V_f=60 ml/h, at 5kV. (e) V_f=60 ml/h, at 6 kV. (f) V_f=60 ml/h, at 7 kV.

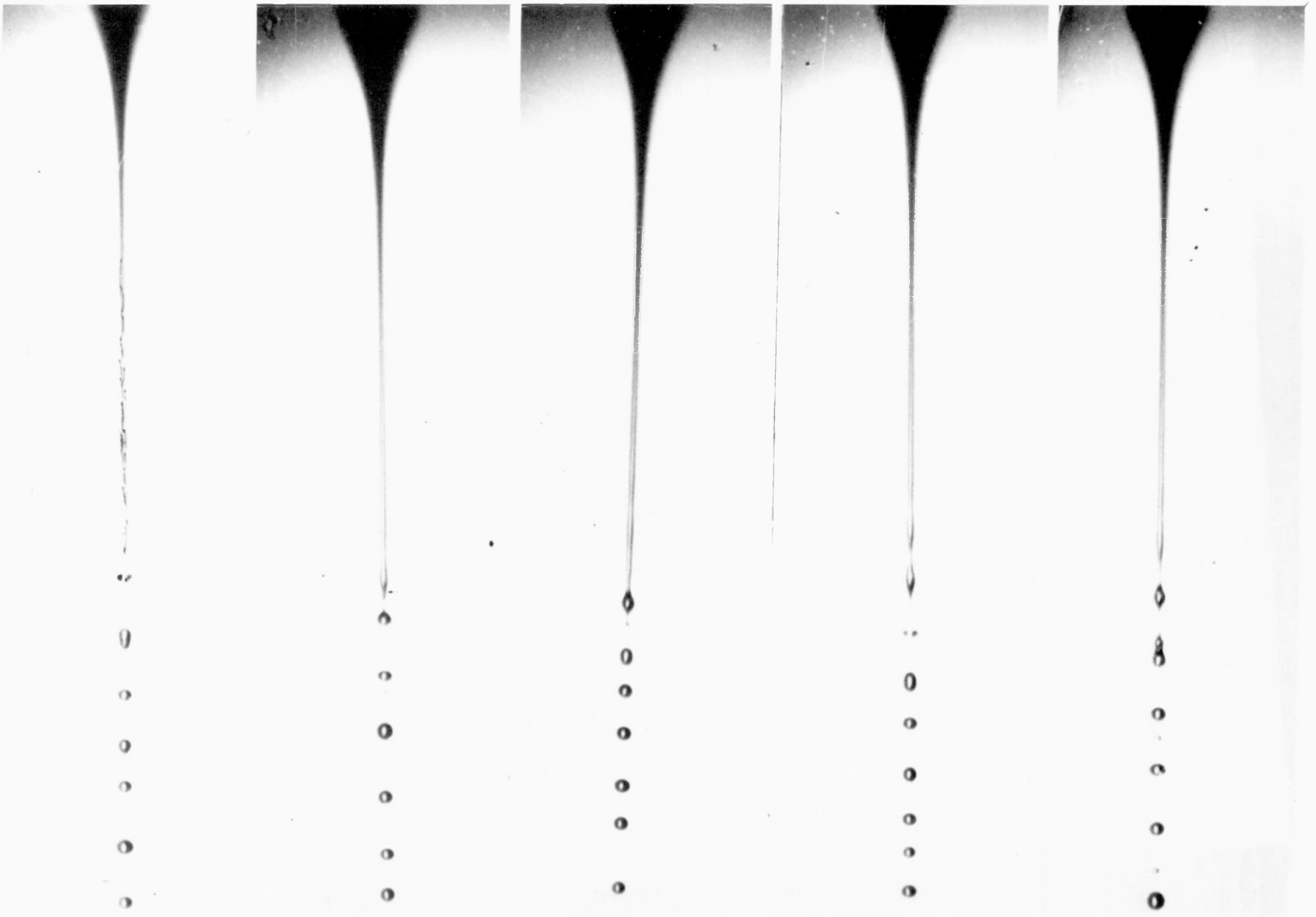

Figure 5.11 The disintegration of the jet at different times

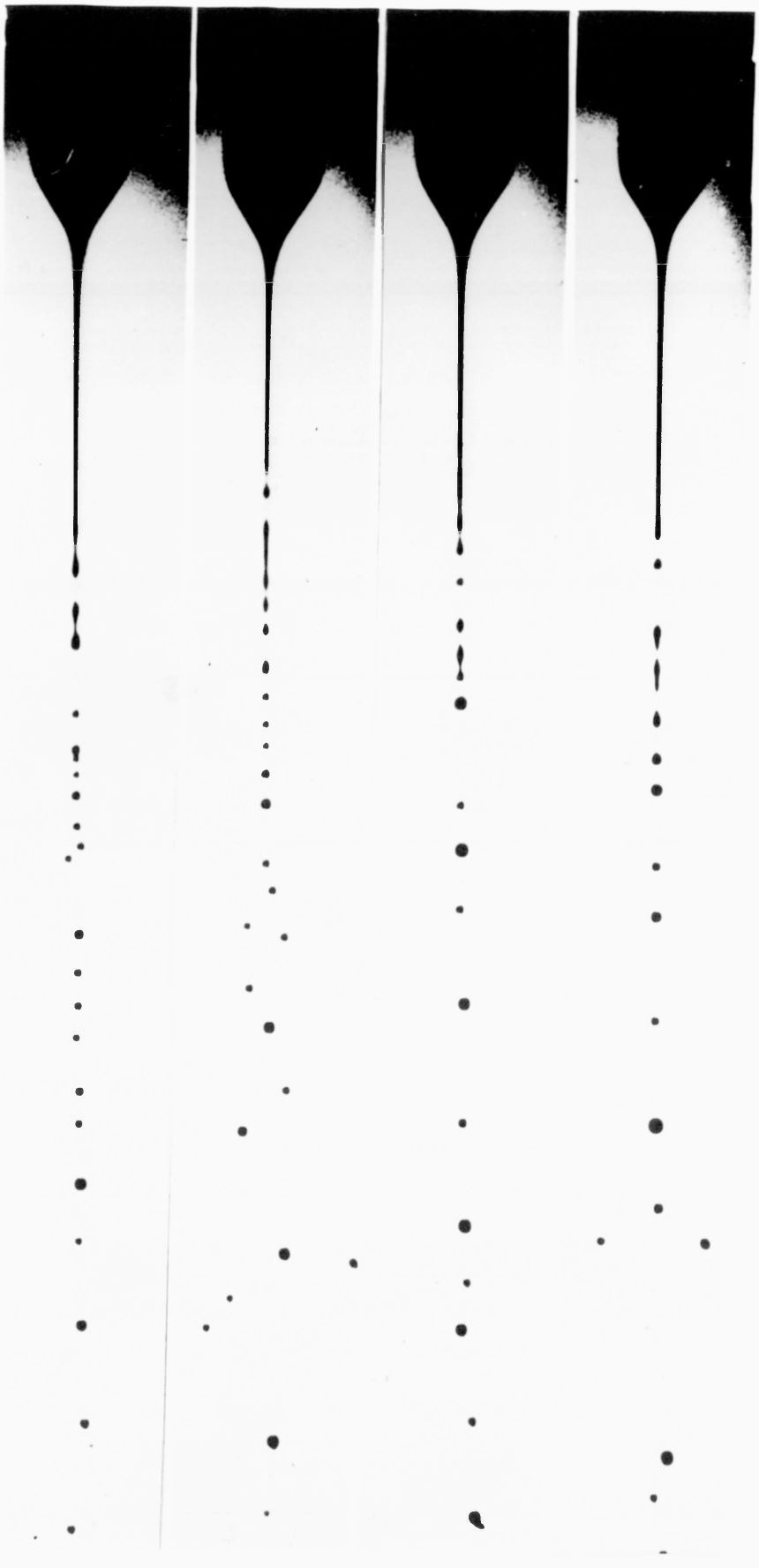

Figure 5.12 A viscous jet emits two or more wavelengths from its end. 40 mPas

Table 5.3 Ratios of drop diameter to drop diameter at different viscosity, conductivity, for two flowrates.

Flowrate (ml/h)	Conductivity $(\Omega m)^{-1}$	Viscosity (mPas)	Drop diameter / Jet diameter
60	3.0×10^{-8}	5.0	1.93
120	3.0×10^{-8}	5.0	1.70
30	1.5×10^{-7}	25.0	1.88
30	1.5×10^{-7}	45.0	1.95

Despite the agreement between the values, the case of a jet being subject to a tangential stress and therefore experiencing accelerating force is different to the case of the straight cylinder used to model break up. In addition the mechanism of jet formation has been shown to depend on a tangential field as well as surface charge. At the capillary tip convection inside the jet cone causes the liquid at the surface to accelerate in the direction of the field and the discharge from the cone surface forms the rest of the jet. Even at the discharge point and lower, the liquid jet may be seen to be changing shape significantly, indicating that two components of velocity, in the radial and longitudinal directions still exist. None of these factors are included in the classic linear stabilty analyses. In fact the form of the electrical stresses as they vary down the jet has been the subject of research for several authors. The inclusion of these facors into stability analysis is complicated by potential distributions on the jet surface and in the regions surrounding it.

Nevertheless, the study of the growth of waves on the jet has shown the theory to correctly predict the

wavelength that causes disintegration. Other predictions are available, one of which is the length of the jet up to the point of drop emission. Although the assumptions implicit in the equations are not applicable to these jets, the trends for the jet lengths may be compared. The theory was briefly discussed in chapter 3, section 3.4. The constant radius r_j is perturbed by a wave of wavenumber k_m, and the radius of the jet is given by,

$$r_a = r_j + \alpha(t)\cos k_m z$$

where $\alpha(t)$ is the time dependent amplitude growing according to the growth constant ω, such that

$$\alpha(t) = \alpha_o \exp(\omega t)$$

The initial amplitude of the disturbance has been found experimentally to be equal to $r_j \exp(-12)$ (17). The growth constant can be calculated from equation 3.9, which takes into account the viscosity and surface tension of the liquid and the uniform surface charge. The prediction of the jet lengths is carried out by noting that for an unperturbed jet having unidirectional velocity ,

$$\underline{1}_j = ut \qquad \text{Eqn. 5.1}$$

the time t is found from the equation for the amplitude. Assuming that at time t the amplitude has reached the value of the jet radius, equation 5.1 becomes,

$$\underline{1}_j = \frac{u}{\omega} \ln \frac{r_j}{\alpha_o}$$

A computer program was written to predict $\underline{1}_j$ as the flowrate is increased. A listing of program waves is given in appendix 1. The value for the growth constant was calculated using eqn.3.9, neglecting the viscosity. Since a range of wavelengths is available from background noise, the disturbance leading to the greatest growth rate must first be found. When eqn. 3.9 is differentiated to find the maximum value of the growth constant, the wavenumber becomes

$$k_m^2 = \frac{I_t^2 r_j}{4\varepsilon_o \gamma V_f^2}$$

Substituiting into the relation for the growth rate ,

$$\omega_m^2 = \frac{\rho r_j^3}{2\gamma}\left[\frac{\gamma}{2\rho r_j^3} - \frac{I_t^2}{8\varepsilon_o \rho V_f^2}\right]^2 \qquad \text{Eqn. 5.2}$$

The entire jet was assumed to be of radius r_j. Evaluation of equation 5.2, which is concerned with linear analysis, to include the profile of the jet where the radius is changing, is meaningless because the wavelength is ill-defined. Measurements of the current and radius were used in the predictions of the jet length. Figure 5.13 compares the length of the jets as predicted by the theory with experimental values when the flowrate is varied. At low flowrates the prediction is close to the actual values, but above 60 ml/h the prediction deviates. Thus although the basis for the stability theory is not applicable to a nonlinear jet, the flowrate effect on lengthening jets can be explained in terms of the longer time taken for the amplitude of a wave to reach the value of the radius.

The prediction did not compare well with experiments in which the viscosity was varied. The measured values increased sharply with viscosity, while calculations suggested a more gradual lengthening of the jets.

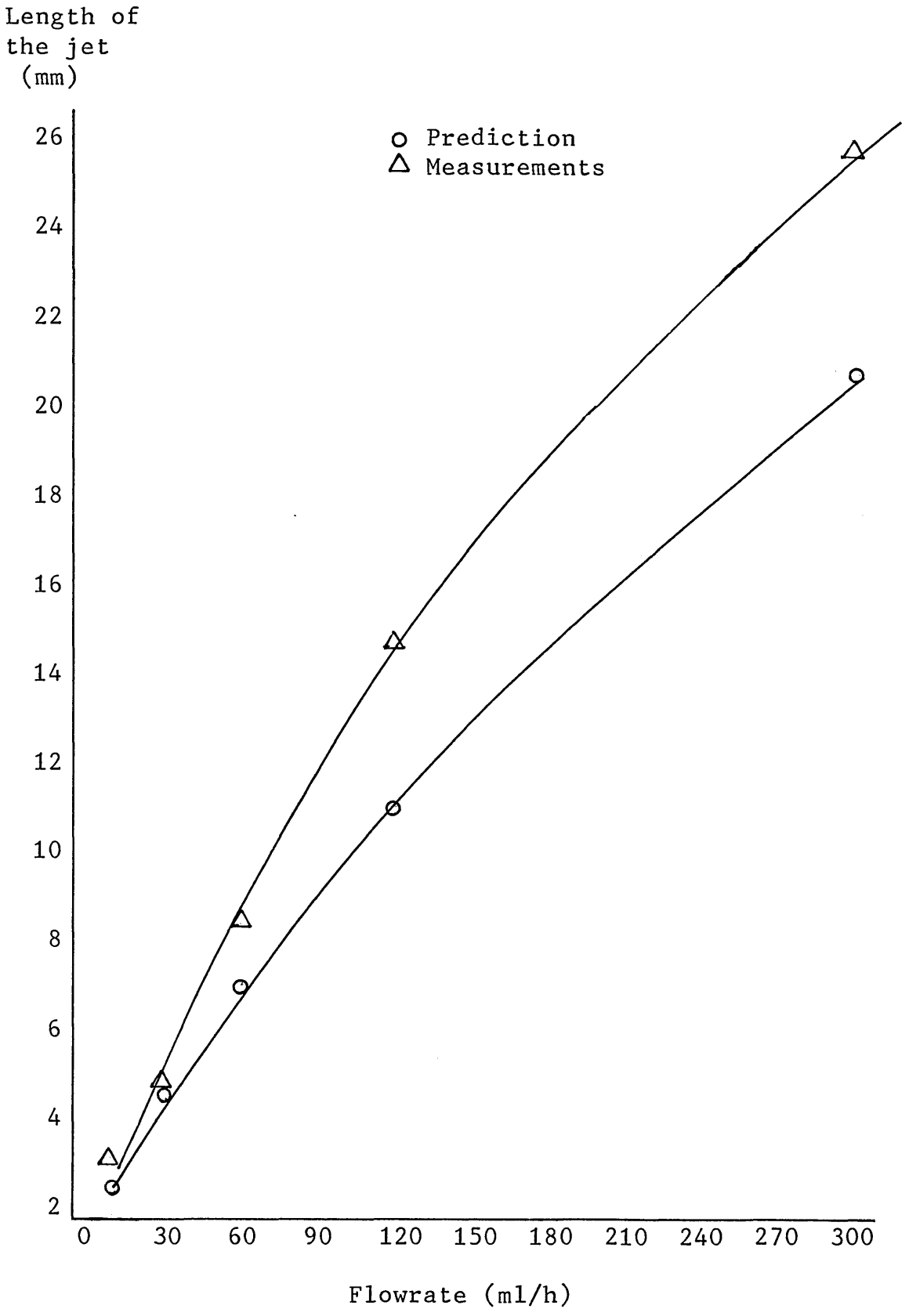

Figure 5.13 Comparison of the predicted values for the jet length, as a function of flowrate, with the measured values

5.3 Calculation of the tangential electric stress

Previous workers have used various approaches to predict the stresses that drive a jet. Hendrick's theory involved the applied field outside the liquid with allowances for the space charge on the jet. The distribution of potentials was employed together with a charge balance that assumes constant velocity over a cross section of the jet. Other work on solving the equations of motion has also involved the assumption of a single velocity. However recently it has been observed that the cone of a jet is a region of internal circulation, with liquid rising at the centre and accelerating at the surface. The velocity is very different from the unidirectional velocity assumed in the past. In this section two approaches to solving for the shear stress are presented when the velocity distribution in the cone (40,41) is used. Both the analyses require the jet profile, found from experiments and are therefore applicable to the experimental arrangement described in chapter 4. The first of these uses a computer program written by Dr.I. Hayati at Imperial College for predicting the stresses when the circulating pattern is incorporated into the analysis.

5.3.1 Conservation of potential energy.

The stresses at points along the jet surface are estimated from the fields operating on the jet. These in turn depend upon the local values of the voltage. The field applied outside the jet must be modified to allow for the space charge. Thus the approach is to conserve potential energy at the liquid interface and in the region between the electrodes. Because electrostatic spraying is irrotational in nature, axisymmetry is assumed. Laplace's equation is solved in the radial and axial co-ordinates (47),

$$\frac{\delta^2 V}{\delta z^2} + \frac{1}{r}\frac{\delta V}{\delta r} + \frac{\delta^2 V}{\delta r^2} = 0$$

The top disc held at the applied potential forms one boundary (figure 5.14). Similarly the capillary is at this potential over its length;

$$V(r,0) = V_c \qquad r_c<r<d_d$$
$$V(r_c,z) = V_c \qquad 0<z<c_l$$

where r_c is the capillary radius, d_d is the disc radius, and c_l is the length of the capillary. The earthed collector positioned at a distance l below the top disc is the other boundary electrode,

$$V(r,l) = 0 \qquad 0<r<d$$

In addition, the potential variation on the jet in the axial direction must be known. This is dependent on the potentials in the region of the interface as well as on the Ohmic current carried by the liquid, the conductivity and radius of the jet. The jet is divided into two parts; a cone region and a cylindrical portion. Spherical co-ordinates are used for the cone region. A charge balance for the cone equates the Ohmic and convection currents to the total current;

$$2\pi R^2(1-\cos\theta_o)kE_t + 2\pi R\sin\theta_o u_s \varepsilon_o E_n = I_t \qquad \text{Eqn. 5.3}$$

where R is in the radial direction of the cone and is zero at the cone tip. θ_o is the cone semi-angle and u_s is the velocity at the surface of the cone. The steridian area of the cone is expressed as,

$$2\pi R^2(1-\cos\theta_o)$$

The first term in eqn. 5.3 is the Ohmic and the second is the convection current. Similarly the charge balance for the cylindrical portion below the cone is ,

$$\pi r_j^2 kE_t + 2\pi r_j u \varepsilon_o E_n = I_t \qquad \text{Eqn. 5.4}$$

For the cylindrical part, the velocity u is assumed to be constant over any cross section.

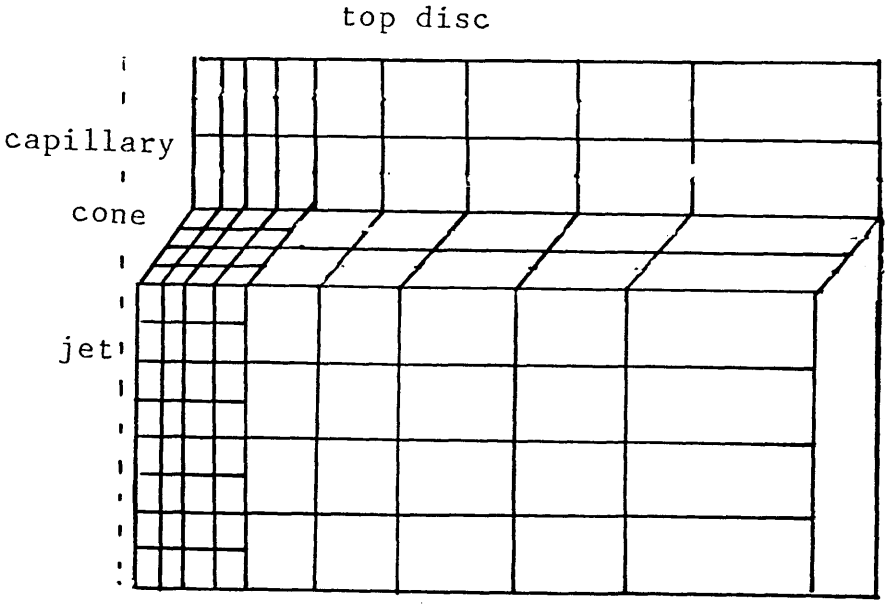

Figure 5.14 The solution of Laplace's equation at points.

A listing of program "PDE" is given in appendix 1. The program accesses a library subroutine to solve Laplace's equation by using finite difference equations. Before the subroutine is called, the potentials at the jet surface must be estimated, since these form one set of boundary conditions. The procedure is iterative. At time t = 0 all the current is assumed to be equal to the Ohmic current. The potentials along the cone surface are found from,

$$V_1 - V_2 = \frac{I_t}{2\pi(1-\cos\theta_o)k}\left(\frac{1}{R_2} - \frac{1}{R_1}\right)$$

The subscripts denote consecutive intervals. The cone and cylinder comprise 6 and 26 intervals respectively. In the

cylindrical region the potentials are found from,

$$\Delta V = \frac{I_t \, \Delta z}{\pi r_j^2 k}$$

The normal fields are calculated from the output of the subroutine. At any interval, the normal field is found by subtracting the potential at an adjacent point normal to the jet from the potential at the jet surface, and dividing the value by the distance between the points. The program also calculates the convection currents at each interval. The new values for the Ohmic currents at each interval are then given by the charge balances so that the jet potentials can be recalculated. The process is repeated until the potentials converge.

Measurements of the cone semi-angle and the jet profile were obtained from high magnification photographs. The total current of the jet was also measured. These values were used as data for the program. The results of the analysis are given in the next section where the two methods of prediction are compared.

5.3.2 Conservation of momentum.

Initial work on predicting the tangential electric stress made use of the general hydrodynamic equation (eqn 3.3), which equates the inertial force to the stress. Hines' (65) solution of the continuity, charge balance and hyrodynamic equations involves measurements of the profile of the jet. The expression for the tangential electrical field contains a term in the rate of change of jet velocity with distance along the jet axis. Application of his equations to this work was unsuccessful because the acceleration of the jet was higher than allowed for in the solutions. Further work was carried out to include all terms in the momentum equation.

The work of Melcher and Warren (60) includes viscous forces, the pressure inside the jet and gravity. They developed the momentum equation (eqn. 3.4) in cylindrical co-ordinates for the case of a steady jet that can be regarded as nearly cylindrical. The theory was reviewed in chapter 3, section 3.3. They also made use of the knowledge of the field external to the jet. This was controlled by placing a number of electrode rings around the jet to produce a linear potential. The momentum equation was solved together with a charge balance and the external field to predict the electrical stresses.

Their momentum equation was applied in the integral form to this work in order to check the balance of electrical and hydrodynamic forces over segments of the cone region of a jet. The electrical forces were taken from the results of computer program PDE, which conserves potential energy. It was found that the electrical forces did not balance the viscous, surface tension, gravity and inertial forces. Although the momentum equation contains terms which account for the changing radius, the nearly cylindrical approximation may not be suitable for this work. The cone of the jet is better described by using spherical co-ordinates. The present analysis also differs from the previous work because it incorporates the velocity at the surface of the cone into the charge balance. The velocity distribution which describes the circulation inside the cone was derived in spherical co-ordinates (40).

The velocity inside the cone has a component in the direction and a component in the R direction. In order to simplify the momentum equation it is assumed that a single velocity exists in the R direction, with u_θ conserved. The R component of the velocity was averaged over the semi-cone angle θ_o. However, inclusion of the convection components of the average velocity complicated the analysis. When these are ignored the velocity is expressed as the

inertial component only (eqn.3.37),

$$u = \frac{V_f}{2\pi R^2(1-\cos\theta_o)} \qquad \text{Eqn. 5.5}$$

where V_f is the volumetric flowrate, and R is the distance along the cone. The cone of semi angle θ_o is shown in figure 5.15.

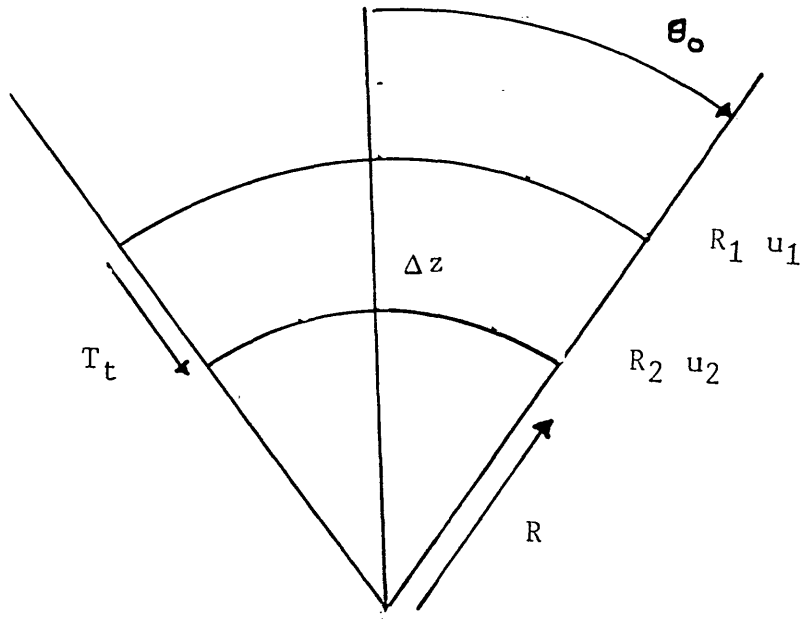

Figure 5.15 The jet cone in spherical co-ordinates

The force balance for steady state over the surface of an element of the cone in the axial direction is,

inertial forces = pressure force + shear force at surface + + gravity force

so that,

$$\rho 2\pi(1-\cos\theta_o)(u_1^2R_1^2-u_2^2R_2^2) = -2\pi(1-\cos\theta_o)(p_1R_1^2-p_2R_2^2) + 4\pi R(1-\cos\theta_o)\Delta Rp + 4\pi R(1-\cos\theta_o)\Delta RT_t + 2\pi R^2(1-\cos\theta_o)\Delta R\rho g \qquad \text{Eqn. 5.6}$$

where T_t is the electrical shear stress and p is the pressure inside the jet. The first and second terms on the right hand side of eqn. 5.6 are the pressures acting over cross-sections of the element and over the surface respectively. The third term is the electrical shear force at the surface, which is assumed to be completely transmitted to the bulk of the liquid by the internal viscous stresses. The fourth term is the gravity force. The longitudinal viscous forces were evaluated over segments of the cone using the integral equation developed by Melcher and Warren (eqn.3.4). The viscous force was found to be insignificant compared to the other terms and have been ignored here. Taking the limit, as $\Delta R \longrightarrow 0$, and using the equation of conservation for incompressible flow,

$$V_f = 2\pi R^2(1-\cos\theta_o)u$$

eqn. 5.6 becomes,

$$\rho V_f \frac{du}{dR} = -2\pi(1-\cos\theta_o)\frac{d(pR^2)}{dR} + 4\pi R(1-\cos\theta_o)p + 4\pi R(1-\cos\theta_o)T_t + 2\pi R^2(1-\cos\theta_o)\, g \qquad \text{Eqn. 5.7}$$

The tangential shear stress is

$$T_t = \varepsilon_o E_n E_t$$

A pressure balance over the interface gives more information about p. In terms of the Maxwell stresses,

$$p_a - p = \tfrac{1}{2}\varepsilon_o E_n^2 - \frac{\gamma\cos\theta_o}{R\sin\theta_o}$$

where p_a is the pressure outside the jet, $R\sin\theta_o$ is equivalent to the radius of the jet, and $\gamma\cos\theta_o$ is the component of the surface tension normal to the jet interface. The first term on the right hand side is the electrical normal stress. Differentiating the pressure equation with respect to R,

$$-\frac{dp}{dR} = \varepsilon_o E_n \frac{dE_n}{dR} + \frac{\gamma\cos\theta_o}{R^2\sin\theta_o} \qquad \text{Eqn. 5.8}$$

By substituiting the electrical tangential stress and eqn.5.8 into eqn.5.7, the momentum equation is expressed in terms of the electric fields,

$$\rho V_f \frac{du}{dR} = 2\pi R^2(1-\cos\theta_o)\varepsilon_o E_n \frac{dE_n}{dR} + \frac{\gamma\cos\theta_o}{R^2\sin\theta_o} + 4\pi R(1-\cos\theta_o)\varepsilon_o E_n E_t + 2\pi R^2(1-\cos\theta_o)\rho g$$

Rearranging to give the rate of change of the normal field with R, gives

$$\frac{dE_n}{dR} = \frac{\rho V_f}{2\pi R^2(1-\cos\theta_o)\varepsilon_o E_n}\frac{du}{dR} + \frac{2E_t}{R} - \frac{\rho g}{\varepsilon_o E_n} - \frac{\gamma\cos\theta_o}{R^2\sin\theta_o\varepsilon_o E_n}$$

The average velocity inside the cone can now be substituted into the above equation. Eqn. 5.5 when differentiated gives,

$$\frac{du}{dR} = \frac{-V_f}{\pi R^3(1-\cos\theta_o)}$$

so that,

$$\frac{dE_n}{dR} = \frac{-\rho V_f^2}{2\pi^2 R^5 (1-\cos\theta_o)^2 \varepsilon_o E_n} - \frac{2E_t}{R} - \frac{\rho g}{\varepsilon_o E_n} - \frac{\gamma \cos\theta_o}{R^2 \sin\theta_o \varepsilon_o E_n}$$

Eqn. 5.9

Everything is known in eqn. 5.9 apart from the variation of E_t with R. In order to calculate the distribution of the fields an expression for E_t is required. The conservation of charge equation provides the link between the fields,

$$2\pi R^2 k(1-\cos\theta_o)E_t + 2\pi R \sin\theta_o u_s \varepsilon_o E_n = I_t \qquad \text{Eqn. 5.10}$$

where u_s is the velocity at the surface of the cone. Differentiating with respect to R,

$$CR^2\frac{dE_t}{dR} + 2CRE_t + u_s E_n + Ru_s\frac{dE_n}{dR} + RE_n\frac{du_s}{dR} = 0 \qquad \text{Eqn. 5.11}$$

where the constant C is

$$C = \frac{k(1-\cos\theta_o)}{\sin\theta_o \varepsilon_o}$$

The velocity at the surface of the cone is,

$$u_s = -\frac{1}{R}\left[-\frac{M\sin\theta_o}{1-\cos\theta_o} + \frac{2M\cos\theta_o}{\sin\theta_o}\right] + \frac{K}{R^2}$$

The constant M contains the terms in the Ohmic current and the normal field;

$$M = \frac{\varepsilon_o E_n I_o}{4\pi k(1-\cos\varepsilon_o)\mu}$$

Using M the velocity becomes,

$$u_s = \frac{-1}{R}\left[\frac{-\varepsilon_o E_n I_o \sin\theta_o}{4\pi k(1-\cos\theta_o)^2\mu} + \frac{\varepsilon_o E_n I_o \cos\theta_o}{2\pi k(1-\cos\varepsilon_o)\sin\theta_o\mu}\right] + \frac{V_f}{2\pi(1-\cos\theta_o)R^2}$$

Eqn. 5.12

The Ohmic current is the first term in the charge balance, eqn. 5.10. Substituiting for the current gives,

$$u_s = \frac{-1}{R}\left[\frac{\varepsilon_o E_n \sin\theta_o}{4\pi k(1-\cos\theta_o)^2\mu} \times 2\pi R^2 k(1-\cos\theta_o)E_t + \frac{\varepsilon_o E_n \cos\theta_o}{2\pi k(1-\cos\theta_o)\sin\theta_o\mu} \times 2\pi R^2 k(1-\cos\theta_o)E_t\right] + \frac{V_f}{2\pi(1-\cos\theta_o)R^2}$$

Using the constants,

$$a = \frac{\varepsilon_o \sin\theta_o}{2\mu(1-\cos\theta_o)}$$

$$b = \frac{\varepsilon_o \cos\theta_o}{\mu\sin\theta_o}$$

$$K = \frac{V_f}{2\pi(1-\cos\theta_o)}$$

the velocity at the surface of the cone is simplified to,

$$u_s = (a-b)E_nE_tR + \frac{K}{R^2}$$

The derivative of the velocity is,

$$\frac{du_s}{dR} = (a-b)E_nE_t + (a-b)R\frac{dE_nE_t}{dR} - \frac{2K}{R^3} \qquad \text{Eqn. 5.13}$$

Substituiting for the velocity and eqn. 5.13 into eqn. 5.11,

$$CR^2\frac{dE_t}{dR} = -RE_n\left[(a-b)E_nE_t + (a-b)R\frac{dE_nE_t}{dR} - \frac{2K}{R^3}\right] - 2CRE_t$$

$$- \left[(a-b)E_nE_tR + \frac{K}{R^2}\right]\left[E_n + R\frac{dE_n}{dR}\right]$$

Rearranging to find an expression for the derivative of E_t;

$$CR^2\frac{dE_t}{dR} - (a-b)RE_n^2\frac{dE_t}{dR} = -RE_n^2(a-b)E_t - (a-b)R^2E_nE_t\frac{dE_n}{dR}$$

$$+ \frac{2KE_n}{R^2} - 2CRE_t - (a-b)E_n^2E_tR$$

$$- (a-b)E_nE_tR^2\frac{dE_n}{dR} - \frac{KE_n}{R^2} - \frac{K}{R}\frac{dE_n}{dR}$$

and

$$\frac{dE_t}{dR} R^2 \left[C + (a-b)E_n^2\right] = -2E_tR \left[C + (a-b)E_n^2\right] - R\frac{dE_n}{dR}\left[2(a-b)RE_nE_t + \frac{K}{R^2}\right] + \frac{KE_n}{R^2}$$

so that finally,

$$\frac{dE_t}{dR} = -\frac{2E_t}{R} + \left[\frac{\frac{KE_n}{R^2} - R\frac{dE_n}{dR}\left[2(a-b)RE_nE_t + \frac{K}{R^2}\right]}{R^2(C + (a-b)E_n^2)}\right]$$

Eqn. 5.14

Eqn. 5.14 was solved simultaneously with the momentum equation, eqn. 5.9. A computer program was written to access a library subroutine which integrates systems of ordinary differential equations using a fourth order variable step Gear method. At a particular value of R, the values for E_t and E_n are determined from the equations. The step size to the next value of R is selected by the subroutine so that the value for E_t at the previous R may be used in eqn. 5.9. The integration allows for commands to set the accuracy of computation. A different set of equations had to be written for each set of experimental conditions to include the constants a,b,and C, which change according to the data. The subroutine does not have a facility for reading the constants in the equations. A listing of program fields for one set of conditions is given in appendix 1. The integration of the equations from the tip of the capillary to the bottom of the cone region involved the

initial values of E_t and E_n. These values were taken from the output of computer program PDE, which was described in the previous section. As in the case of using program PDE, the solution of equations 5.14 and 5.9 depended on the actual geometry of the cone region. The measurements of the jet which had been used to conserve potential energy were also used as data to integrate the equations of momentum and charge conservation.

5.3.3 Predictions using potential energy conservation and the conservation of momentum.

The output from both computer programs give predictions of the fields tangential to the jet surface and normal to it, the velocity at the surface, and the convection current along the surface. The results are presented here in terms of the variation of the tangential stress and the Ohmic current along the jet. The tangential stress is important because it is the acceleration force which causes an otherwise spherical mass of liquid to be drawn from the tip of the capillary. The stress is dependent on the presence of the tangential field, a consequence of the Ohmic current. A large value for the Ohmic current reflects that the current is carried predominately by conduction and the jet behaves as a conductor, whereas a low value means that the charges have reached the surface of the jet.

Table 5.4 lists the variation of the Ohmic current, the tangential field and the tangential stress down the jet, for both methods of calculation. The results are applicable to one set of experimental conditions where the flowrate is 60 ml/h, for a liquid of conductivity $8 \times 10^{-7} (\Omega m)^{-1}$ and viscosity 12.5 mPas. Figure 5.16 is a graph illustrating the variation of $\log_{10}$ of the tangential stress with distance from the tip of the capillary for these conditions. Both the

predictions show the stress increasing with distance along the cone of the jet, until a peak is reached, after which the stress falls. The upper curve is calculated from the results of the integration of the momentum equation. The values for the stress are 10% higher, near the tip of the capillary, than those predicted using the conservation of potential energy.

At a distance of 1.75 mm from the tip of the capillary the upper curve reaches the maximum value of the tangential field. Here the deviation from the other solution is closer to 15%. This point had been identified on the negative of the jet as the transition from the cone region to the rest of the jet. A straight line of angle $_{o}$ to the vertical, the semi-cone angle, was drawn along the surface of the jet. Further down the jet, where the jet began to deviate from the line, a second line of smaller angle to the vertical was drawn along the surface. However the jet was found to deviate from the second line over a short distance. From this point on, the jet could not be characterised as being conical in shape. According to the momentum equation, the stress goes very rapidly to zero after the peak due to the decrease in the tangential field. Therefore, upon discharge from the cone region, the liquid continues to fall under the force of gravity.

The lower curve peaks at 2.4 mm from the capillary tip and the stress approaches zero further down the jet, at 3.6mm, compared to the upper curve. The length of the jet was measured from low magnification negatives to be 12.5 mm. Despite the disagreement of the curves on the point of vanishing tangential stress, both methods predict that the jet is free from the shear stress for the majority of its length, during which the its shape is cylindrical.

The very rapid growth of the stress on the cone is confirmed in figure 5.17, which is a similar plot as in figure 5.16, and under the same conditions for the lower

flowrate of 30 ml/h. The values of the Ohmic current, the tangential field and tangential stress are given in table 5.5. Again the trend of the predictions obtained from the momentum equation are similar to those obtained from Laplace's equation. For this flowrate the peaks in the stress occur at about the same point, but the value from the latter equation is 25 % lower than the value from the momentum equation. The jet experiences maximum tangential stress at the tip of the cone, an observation also made from figure 5.16. According to the results of the momentum equation, the stress vanishes very near to the discharge from the cone, but the lower curve shows the stress continuing further from this point. It is interesting to note that the tengential field increases along with the tangential stress, figure 5.18.

The variation of the Ohmic current with the jet distance is shown in figure 5.19 for the case of the higher flowrate. Both sets of results are consistent up to the tip of the cone. Above a distance of 2mm, the conservation of potential gives higher values for the Ohmic current.

Table 5.4 The variation of the Ohmic current, tangential field and tangential stress along the jet.

Flowrate = 60 ml/h
Conductivity = 8×10^{-7} $(\Omega m)^{-1}$
Viscosity = 12.5 mPas

Results from the integration of the momentum equation.

Distance (mm)	Ohmic current (A)	Tangential field (V/m)	Tangential stress (N/m^2)
0.00	2.80×10^{-8}	1.24×10^{4}	0.1436
0.15	2.75×10^{-8}	1.69×10^{4}	0.2659
0.43	2.70×10^{-8}	2.42×10^{4}	0.4806
0.71	2.60×10^{-8}	3.75×10^{4}	0.9158
1.00	2.50×10^{-8}	6.52×10^{4}	1.9841
1.35	2.16×10^{-8}	1.37×10^{5}	5.4989
1.75	1.50×10^{-8}	2.35×10^{5}	12.314
2.00	0.00	5.6×10^{3}	0.4610

Results from the integration of Laplace's equation.

Distance (mm)	Ohmic current (A)	Tangential field (V/m)	Tangential stress (N/m^2)
0.00	2.81×10^{-8}	1.448×10^{4}	0.1656
0.28	2.80×10^{-8}	2.057×10^{4}	0.2538
0.56	2.78×10^{-8}	3.095×10^{4}	0.4183
0.84	2.75×10^{-8}	5.286×10^{4}	0.7972
1.12	2.68×10^{-8}	1.085×10^{5}	1.8436
1.75	2.36×10^{-8}	3.770×10^{5}	9.4107
2.37	1.56×10^{-8}	9.127×10^{5}	17.385
3.61	4.10×10^{-10}	2.931×10^{4}	0.7190

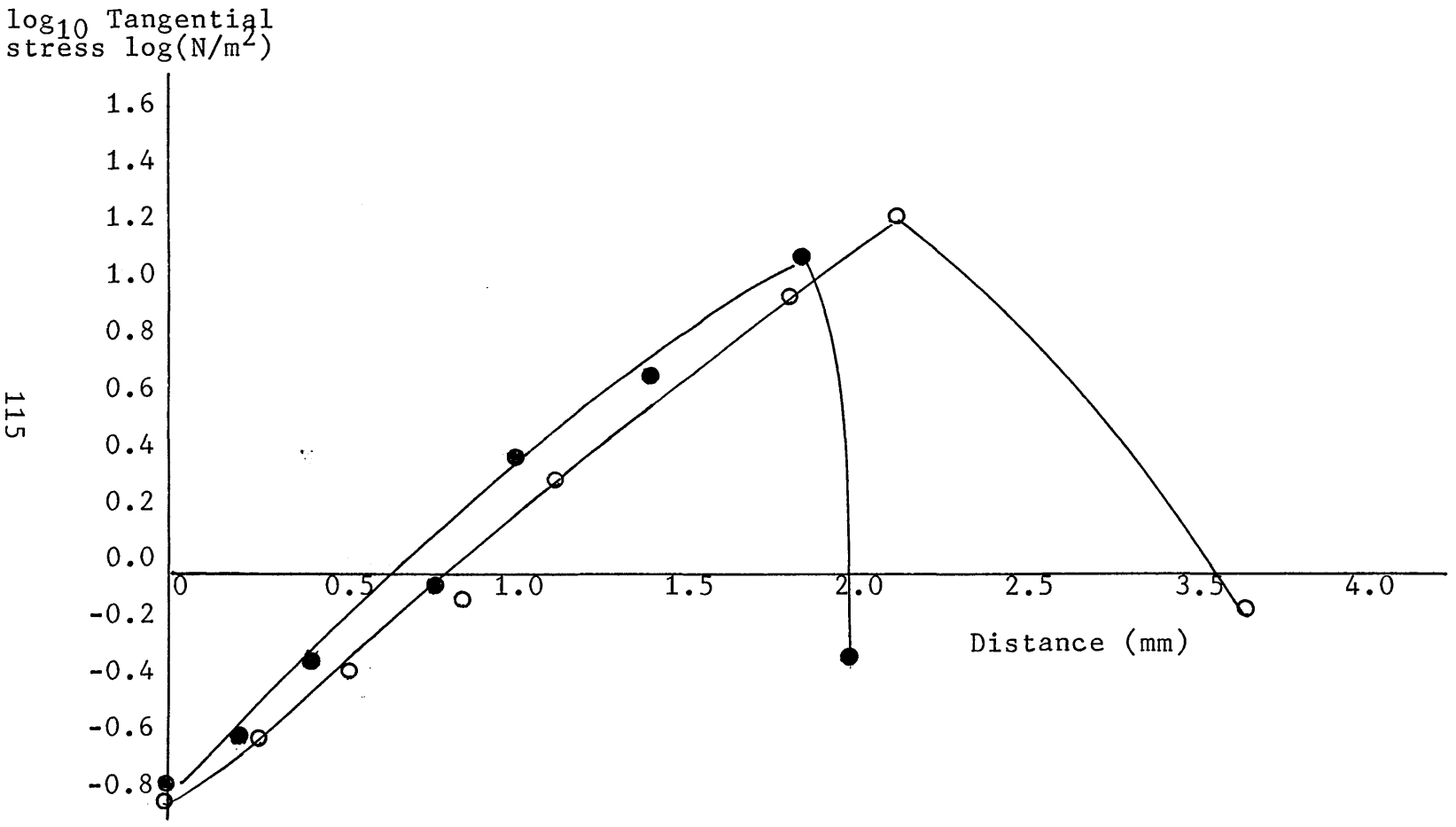

Figure 5.16 Variation of $\log_{10}$ of the tangential stress with the distance from the tip of the capillary. V_f=60 ml/h. Viscosity=12.5 mPas.
● Results of momentum eqn. ○ Results of Laplace's eqn.

Table 5.5 The variation of the Ohmic current, the tangential stress and tangential field along the jet.

Flowrate = 30 ml/h

Conductivity = 8×10^{-7} $(\Omega m)^{-1}$

Viscosity = 12.5 mPas

Results from the integration of the momentum equation.

Distance (mm)	Ohmic current (A)	Tangential field (V/m)	Tangential stress (N/m^2)
0.00	2.46×10^{-8}	1.071×10^{4}	0.1297
0.24	2.42×10^{-8}	1.731×10^{4}	0.3065
0.50	2.38×10^{-8}	2.730×10^{4}	0.6082
0.76	2.31×10^{-8}	4.923×10^{4}	1.3760
1.02	2.14×10^{-8}	1.129×10^{5}	4.1880
1.13	2.02×10^{-8}	1.630×10^{5}	6.8521
1.21	1.81×10^{-8}	2.508×10^{5}	12.3852
1.26	1.59×10^{-8}	3.320×10^{5}	18.5250
1.32	1.29×10^{-8}	4.069×10^{5}	26.2860
1.67	7.62×10^{-9}	4.058×10^{5}	31.9449
1.98	0.0	0.0	0.0

Results from the integration of Laplace's equation.

Distance (mm)	Ohmic current (A)	Tangential field (V/m)	Tangential stress (N/m^2)
0.00	2.33×10^{-8}	1.071×10^{4}	0.1417
0.26	2.32×10^{-8}	1.713×10^{4}	0.2245
0.52	2.31×10^{-8}	2.761×10^{4}	0.4007
0.78	2.28×10^{-8}	5.166×10^{4}	0.8458
1.04	2.27×10^{-8}	1.290×10^{5}	2.4431
1.36	1.97×10^{-8}	5.250×10^{5}	15.100
1.98	1.06×10^{-8}	6.320×10^{5}	18.740
3.22	7.30×10^{-9}	4.350×10^{5}	13.590
4.47	3.50×10^{-9}	2.090×10^{5}	8.0090

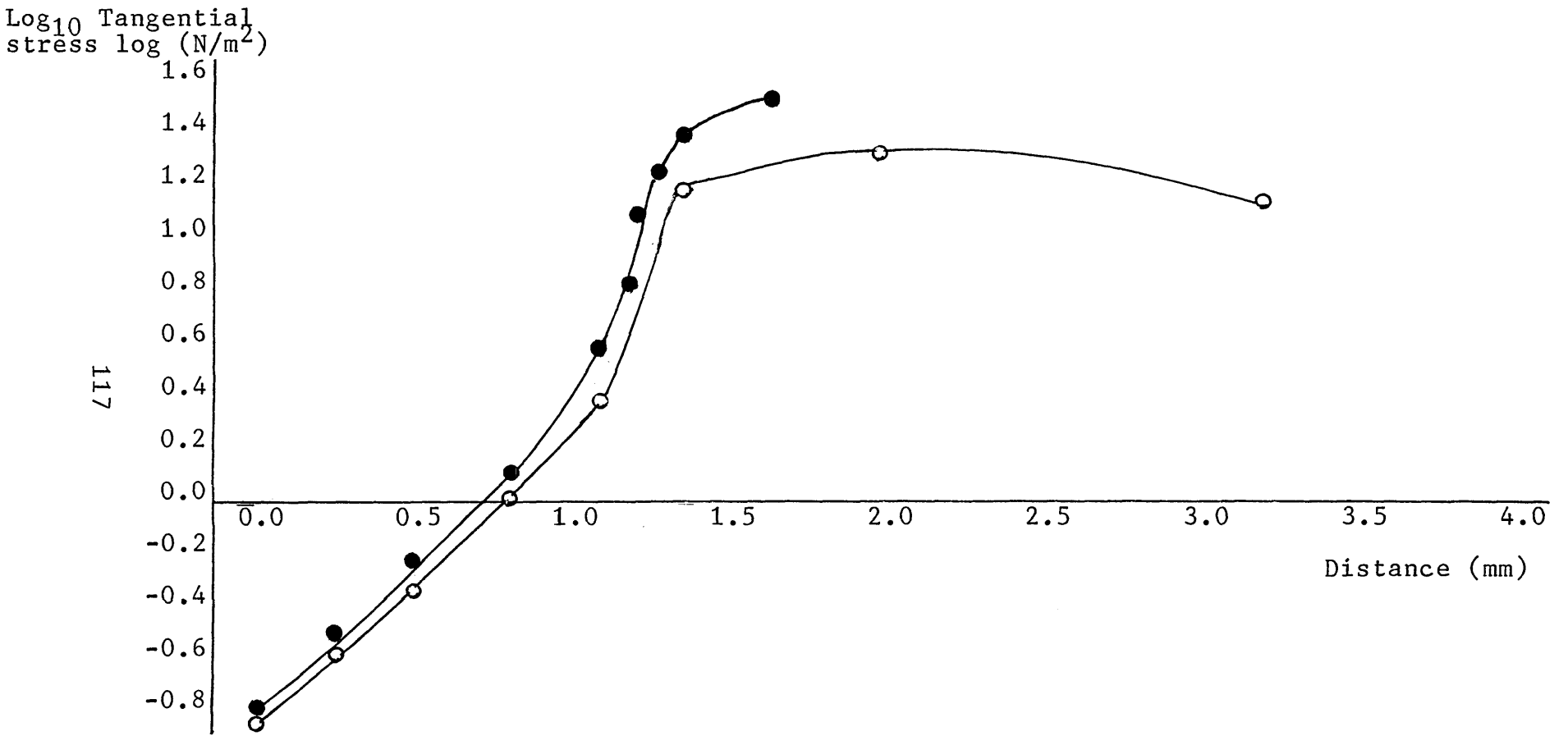

Figure 5.17 Variation of $\log_{10}$ of the tangential stress with the distance from the tip of the capillary. $k = 8 \times 10^{-7}$ $(\Omega m)^{-1}$. V_f = 30 ml/h. Viscosity = 12.5 mPas.

● Results of momentum eqn. ○ Results of Laplace's eqn.

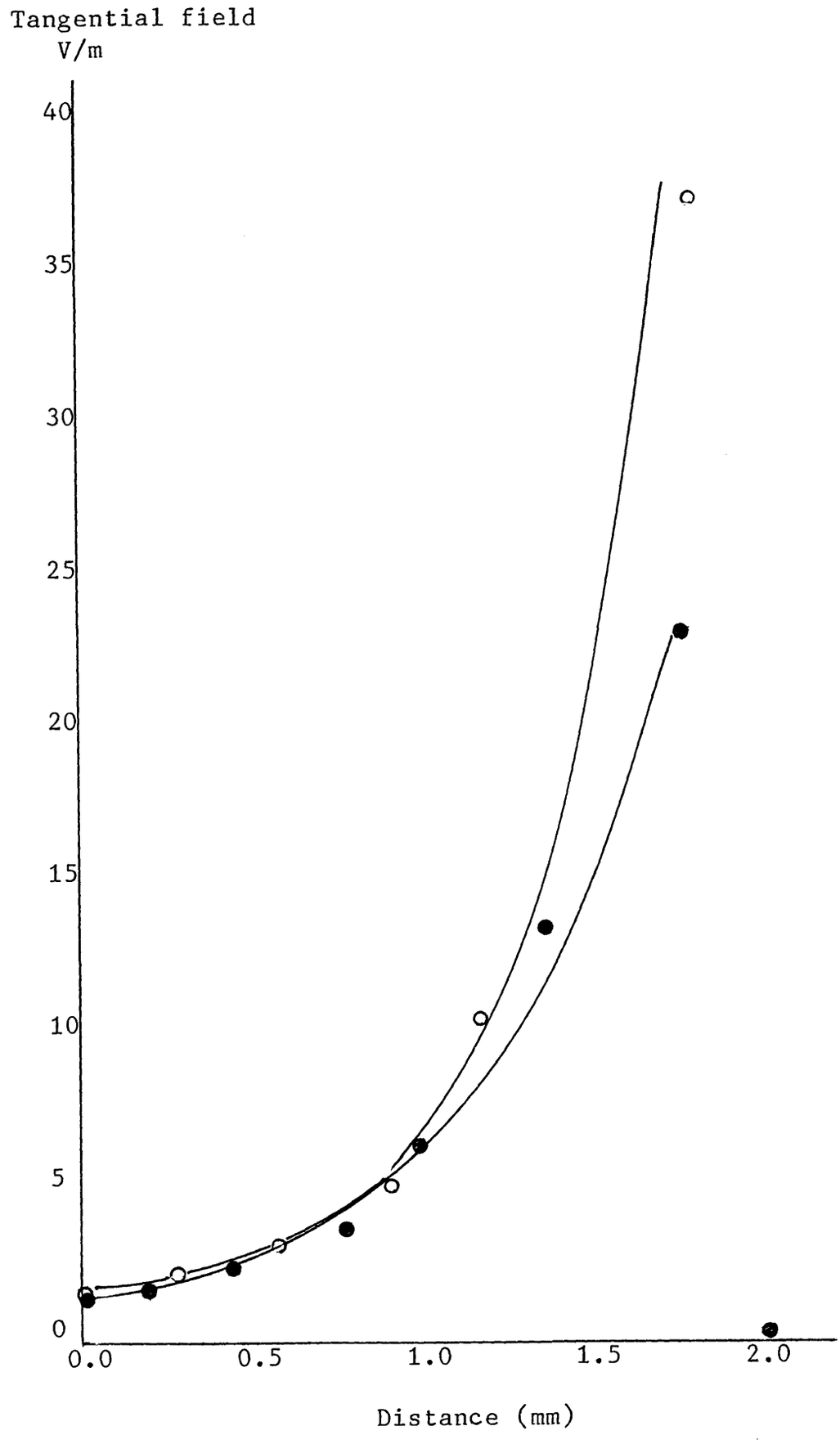

Figure 5.18 Variation of the tangential field with the distance from the tip of the capillary.
$k = 8 \times 10^{-7}$ $(\Omega m)^{-1}$. V_f = 60 ml/h. Viscosity 12.5 mPas
● Results of momentum eqn. ○ Results of Laplace's eqn

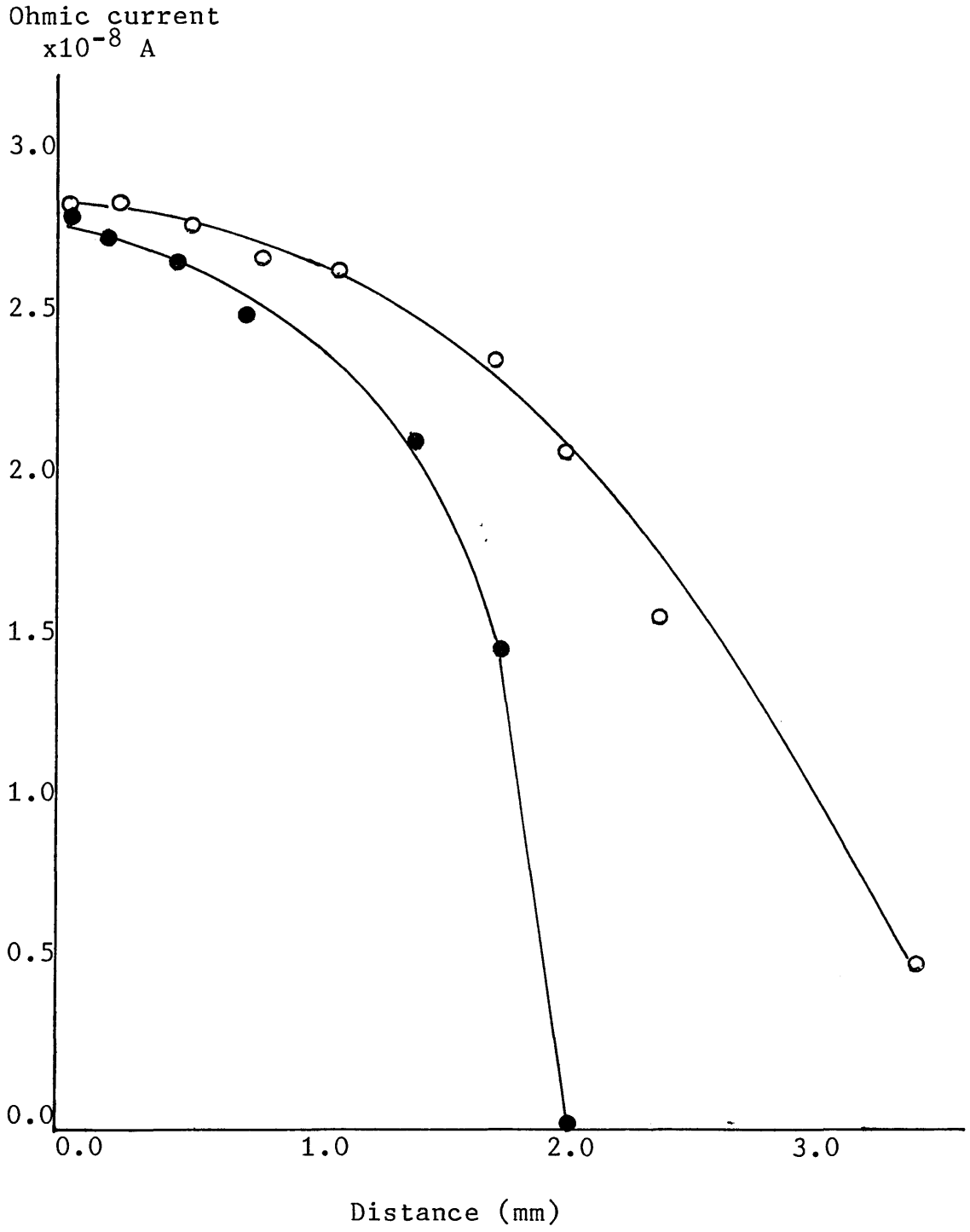

Figure 5.19 Variation of the Ohmic current with the distance from the tip of the capillary. V_f = 60 ml/h. k = 8×10^{-7} $(\Omega m)^{-1}$. Viscosity = 12.5 mPas.
● Results momentum eqn. ○ Results Laplace's eqn.

The discrepancy between the results can be traced to the numerical methods used to solve the equations. Potential energy is conserved by using finite difference equations evaluated at a set number of intervals along the cone surface and the cylindrical portion of the jet. In contrast, the solution of the momentum and charge equations is carried out as a continuous integration. The step size is calculated in the subroutine to minimise the error. During computation different values for the step size were used to check the accuracy. The results were found to be independent of the step size, within a certain range, indicating that the solutions had converged.

Values of the normal field from the two solutions diverge near the tip of the cone (figure 5.20). Various terms are taken into account in the momentum equation which were not included in the other analysis. The normal field integrated from the momentum equation is dependent on terms whose denominators contain high powers of the jet radius (eqn. 5.9). Near the cone tip, where the radius is small, the inertial and surface tension terms in the momentum equation contribute to a large gradient for the normal field. The normal field therefore increases very rapidly towards the discharge region of the cone.

Potential energy conservation evaluates the normal field over a small distance between a point on the jet surface and an adjacent point in the surroundings. It is possible that the field increases as the jet is approached. Only a few intervals could be allocated below the tip of the cone, in order to take into account the potentials in the relatively large region between the top disc, earthed collector and capillary. An overestimation of E_n by the momentum equation and an underestimation by Laplace's equation cause the values of the Ohmic current to deviate.

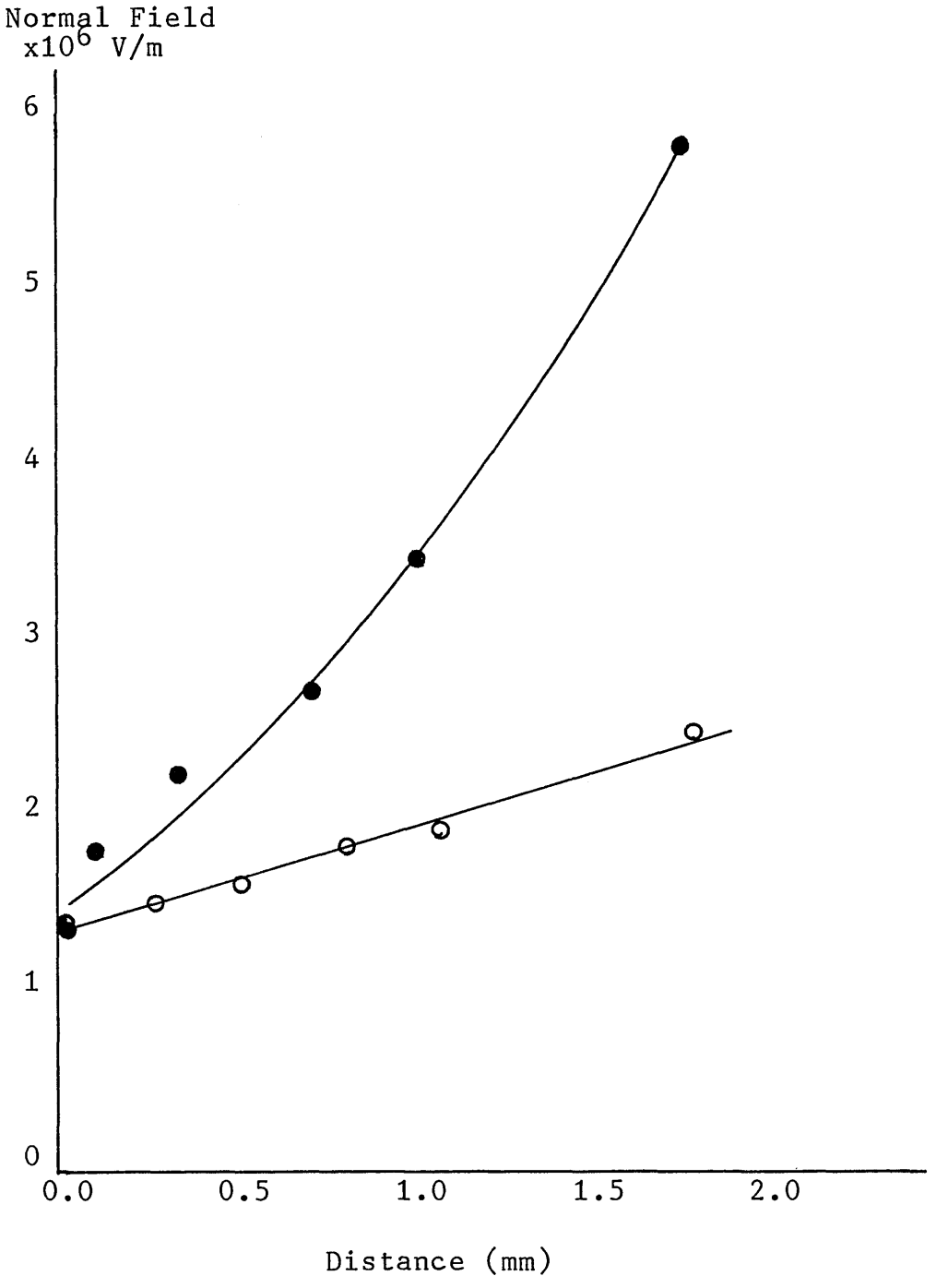

Figure 5.20 The normal field increases more sharply, along the cone, according to the results from the momentum equation.
● Results momentum eqn. ○ Results Laplace's eqn

The solutions give sharply increasing tangential field and tangential stress over the cone region, with the peak in the stress occuring as the liquid is discharged from the cone. The liquid behaves as a conductor at the beginning of the cone where the Ohmic current is high. The charges reach the surface of the liquid towards the tip. The Ohmic current was calculated to approached zero at different points along the cone, according to the two methods. Nevertheless all the charge has reached the surface before the jet disintegrates into drops. Just before the point of break up the liquid acts as an insulator, and a tangential field is absent.

The tangential field was evaluated for the case of two liquids of different conductivity. In table 5.6 the field along the cone is of the order of 10^4 V/m at a conductivity of 3.85×10^{-8} $(\Omega m)^{-1}$, from the results of program fields. At the higher conductivity of 7.94×10^{-7} $(\Omega m)^{-1}$ the fields are reduced by two to three times. It may be seen that the lower conductivity liquid sustains higher potential drop in the upper regions of the cone.

Table 5.6 The tangential field on the cone at two values of the conductivity.

Results form the integration of the momentum equation.
Conductivity = 3.85×10^{-8} $(\Omega m)^{-1}$

Distance(mm)	0.0	0.58	0.87	1.16	1.46
E_t (V/m)$\times 10^4$	6.682	7.233	7.903	8.871	10.07

Conductivity = 7.94×10^{-7} $(\Omega m)^{-1}$

Distance(mm)	0.0	0.43	0.71	1.00	1.35
E_t (V/m)$\times 10^4$	1.248	2.420	3.745	6.523	23.54

CHAPTER SIX

STUDIES ON MULTIPLE JETS.

In the last chapter, predictions of the tangential field within the steady jet showed that the value is highest near the tip of the cone region, from which the liquid is discharged to form a cylindrical jet. The tangential field is established within the liquid as a response to the field at the end of the capillary. For a particular arrangement of electrodes, the field at the capillary tip is controlled by the application of voltage. The positioning of the electrodes is also an important factor in determining the field at the end of the capillary. When for instance, the earthed collector is brought closer to the capillary, the field rises without requiring an increase in the voltage. If the capillary is attached to the centre of a disc, so that it passes through it, the disc acts to raise the voltages in the regions near the capillary, thereby altering the field.

Not only has previous work shown that the position of the electrodes combined with voltage influences the way a liquid is sprayed, but the liquid must have the appropriate properties to be sprayed in a steady way. Among the properties of the liquid, the conductivity has been cited as being particularly significant. Once the requirements on the conductivity are met, the steady jet is present only over a certain range of voltages. With lower values intermittent drops are produced and at the other extreme, the high voltage interferes with the steadiness of the jet.

In view of the sensitivity of the spraying process to field variations, it was decided to investigate the behaviour of liquids at high field strengths. Since the ultimate objective is to control the drop size, emphasis

was given to attaining more than one jet. The viscosity and conductivity of the liquid were varied to assess the relative importance of hydrodynamic and electrostatic forces for determining the conditions under which multiple jets are established.

6.1 The formation of multiple jets.

The apparatus used in the study is described in chapter 4, section 4.1 and shown in figure 4.2a. The capillary electrode is in contact with and passes through the centre of the top disc. The earthed collector is positioned below the capillary and the disc, and completes the field. In addition to the collector, a second earthed electrode ring is held above the end of the capillary and is concentric with it.

Initial work on the single jet showed that as the capillary voltage is raised, a point is reached in which the steady jet mode is disturbed. The subsequent behaviour was observed to depend on the voltage applied, for a particular set of conditions. During the steady single jet mode, the form of the electrical stresses on the liquid/air interface changes as the field at the capillary is increased. The variation of the stresses is reflected in the changes that occur to the size of the cone. The rise in voltage causes the semi-cone angle to increase and the tip of the cone approaches the tip of the capillary, (figure 6.1). For constant liquid flowrate, the decreasing size of the cone means that the liquid is being accelerated to a greater extent. This suggests that the electrical accelerational force is increasing with the applied voltage. However there is a limit to the degree a single jet may be accelerated.

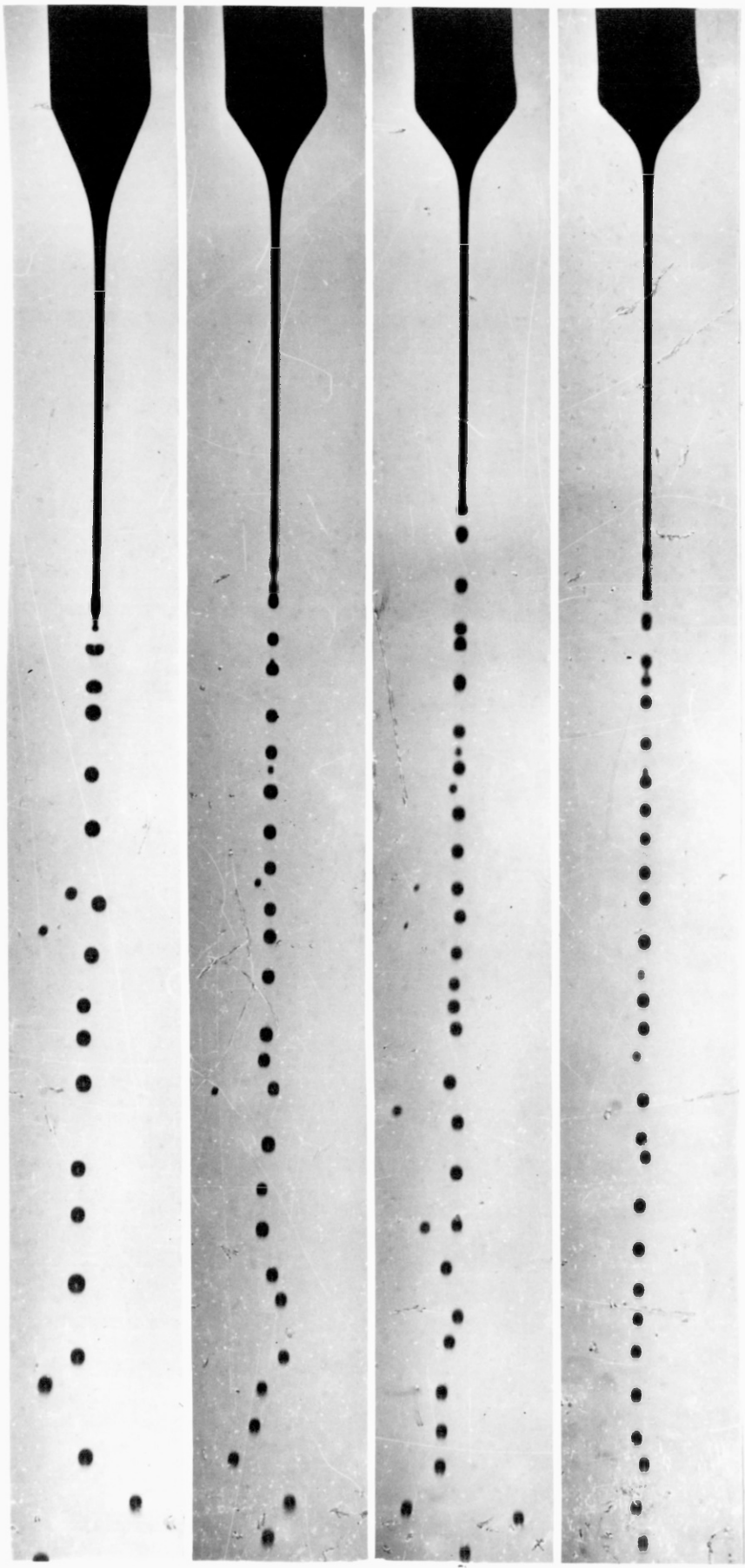

Figure 6.1 The tip of the cone approaches the capillary as the voltage is raised. V_f = 60 ml/h.

On the application of higher voltages the jet was observed by eye to split. The intermediate stage between a single jet and several stable jets is unsteady. The external potentials close to the interface as well as those at the interface determine the motion of the liquid in the field. Moreover, the potentials on the liquid affect those in the surroundings, and vice versa. Apparently the state of the potentials at one instant causes the single steady jet to become unsteady, over times long compared with the time taken for the ions in the liquid to react to the field.

With the imposition of still higher voltages, the liquid reacts more quickly to set up the electrical stresses that stabilise the configuration. At this point more than one jet has been established at the periphery of the capillary, figure 6.2. It is significant that at the first stage of the formation of multiple jets, the liquid has approached the tip of the capillary.

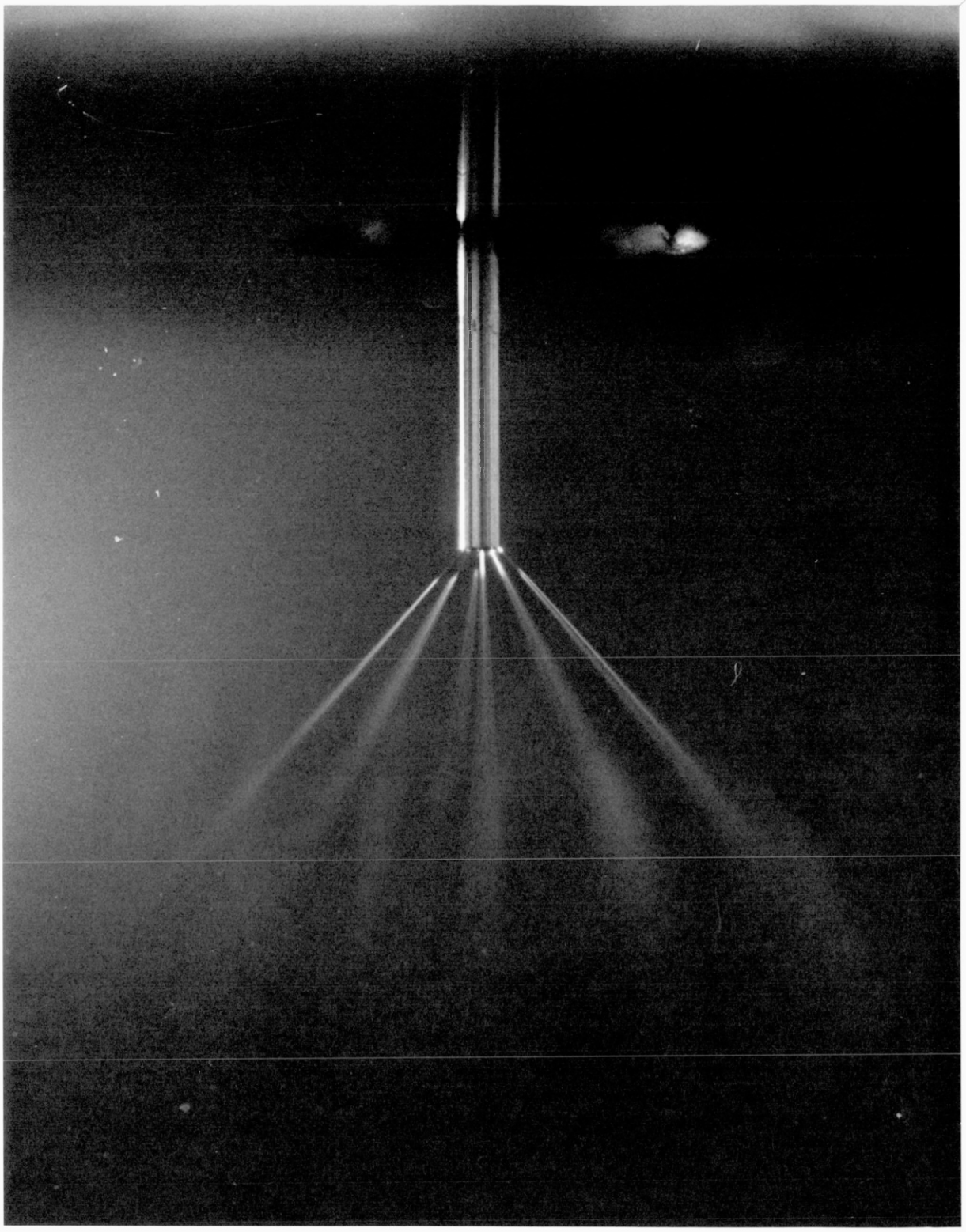

Figure 6.2 Spraying from the edges of the capillary.

6.1.1 The transition from a single jet to multiple jets.

Observations made during experiments to study the effect of the conductivity have shed light on the transition from a single jet to multiple jets. The experiments are coupled with the presence of the earthed ring plate placed above the end of the capillary (figure 4.2a). The effect of the plate on the equipotential lines on the region enclosed by the electrodes is illustrated schematically in figure 6.3. In the absence of the plate, the equipotentials near the top disc follow roughly the contours of the top disc and the capillary. The extension of the capillary from the top disc results in a higher field at its tip than would be present if the capillary tip were to be placed in line with the top disc. In the latter case the tip forms part of the disc and the field everywhere between the disc and the earthed collector is linear.

The addition of the earthed plate imposes a linear vertical field between the plate and the top disc. A second, radially dependent field is established in the gap between the capillary and the inside edge of the earthed plate. The equipotential lines pass through the gap and are thus tightened around the end of the capillary. In this way the field becomes intensified at the tip of the capillary as well as in the region below it.

When a liquid of conductivity 10^{-6} $(\Omega m)^{-1}$ was sprayed in the presence of the earthed plate, a single jet could not be formed, despite the application of a range of voltages. Instead a pulsating jet was observed at lower values of the voltage. A steady jet was only formed when the earthed plate was removed. The plate may be considered to narrow the voltage range over which the steady jet is established to almost zero. Thus the spraying progresses from a pulsating jet to the unsteady mode without passing through the single jet mode. This behaviour may be explained by comparing the

field that would be set up on the liquid surface, for the case of a steady jet, with the field in the immediate surroundings. The intensification of the field around the capillary imposes high fields outside the cone region of the jet; the drop in potential along a line adjacent to the cone surface is high. In contrast, the situation of the potentials along the surface of the cone is different. For a jet carrying ohmic current I_o, the voltage falls according to,

$$-\frac{dV}{dz} = \frac{I_o}{2\pi r_j^2(1-\cos\Theta_o)k} \qquad \text{Eqn. 6.1}$$

It may be seen that the more conducting the liquid, the lower the tangential field along the cone. The charges in the liquid act to maintain high potential, whereas the potentials in the surroundings fall more rapidly. Thus the result of the application of high field is an increase in the field normal to the cone. It is known that the formation of the steady jet depends on charges reaching the surface in such a way as to establish the tangential field. The increased potential difference between a point on the cone surface and an adjacent point may provide enough force to distribute the charges evenly on the surface, thereby negating the tangential field.

For less conducting liquids, the presence of the earth plate did not preclude the formation of the steady single jet. The greater drop in potential over the length of the cone at the lower conductivity results in a reduction of the field normal to the liquid surface. Hence it may be inferred that the potential drop over the interface must be low enough to maintain the jet.

Initially it was thought that in the intermediate stage between steady spraying regimes the liquid flickers between one jet and two jets at low values of the flowrate. However, photography using the 1ms flash revealed the jet to be wavering rapidly from one side of the capillary to the other (figure 6.4). The snake like motion, though unsteady, is similar to that observed by others for the case of a steady jet carrying high charge on its surface. However the shape of the liquid does not resemble the conical form that is observed when the jet is steady. The lack of a distinct cone suggests that the electrical forces acting on the liquid surface differ form those operating when the jet is steady. The photographs show one side of the jet to be stretched more than the other.

At higher voltages the charges are accelerated more quickly away from the capillary, and several steady jets are formed at the periphery, figure 6.2. It may be inferred from this that the reduction in cross-sectional area of the jets is linked with the stabilisation of the jets. The liquid meniscus is now close to the capillary tip where the field intensity is very high.

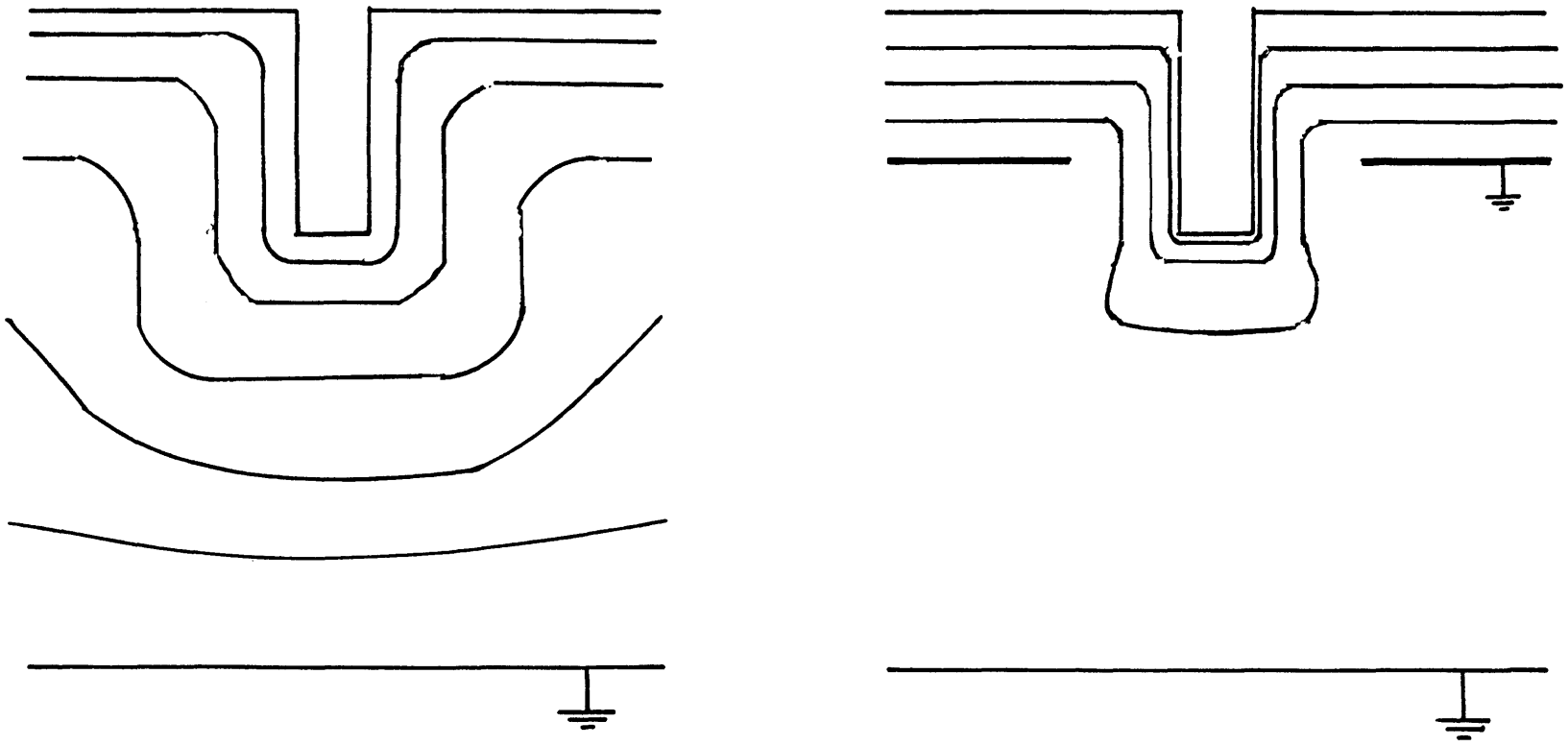

Figure 6.3 The effect of the earthed plate on the equipotentials in the region of the tip of the capillary.

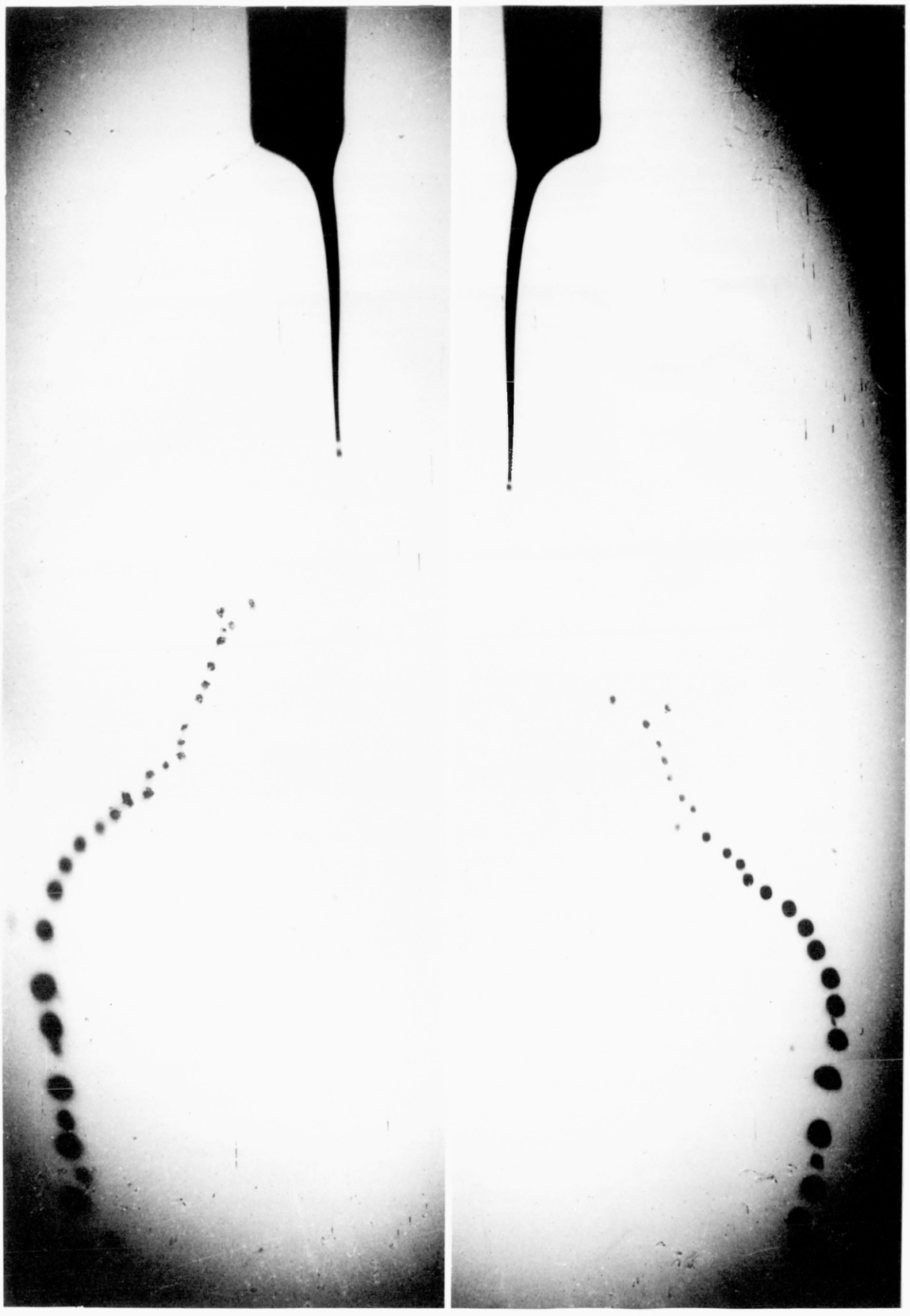

Figure 6.4 At high voltage the jet becomes unstable and wavers from side to side.

6.1.2 Spraying from the edges of the capillary.

When a conducting liquid is sprayed as a single jet, the potential drop along much of the surface of the cone is low. The highest field in the liquid is found at the tip of the cone, from which the cylindrical portion of the jet issues. As the single jet becomes unsteady at high fields, the effect of the capillary electrode becomes more significant.

At high field intensity the velocity of the ions is increased according to the relation,

$$u_i = \mu_m E \qquad \text{Eqn. 6.2}$$

The rapid removal of the liquid from the capillary decreases the amount of material residing at the end of the electrode. When the liquid meniscus is small, the tip of the capillary is shielded to a lesser extent by the ions in the liquid. The effect of the sharp outside edges of the metal, where the radius of curvature is high, becomes accentuated as the space charge surrounding the edges is reduced. Thus the increased ionic velocity augments the effect of the voltage to establish higher fields. Liquid emerging from the capillary flows to the point of highest field intensity and subsequent spraying depends, among other parameters, on the fields set up at the metal edges.

During spraying from the outside edges of the capillary, the formation of many jets so that the liquid occupies a small proportion of the volume around the capillary, suggests that the equipotential lines follow closely the contours of the capillary. In the case of spraying via the single jet mode, the cone region comprises a relatively large volume. Together with the tendency of a conducting cone to support a high voltage, this large volume

of space would cause the equipotentials to be modified to a greater extent by the liquid.

Other authors have reported that the conductivity of a liquid may depend on the value of the field applied. More particularly, the mobility of the ions is thought to be raised at the high fields. If this were to be the case, a large value for E in equation 6.2 together with an increase in mobility would result in greater ionic velocity. In order to investigate a possible secondary effect of the field on the process of forming multiple jets, the conductivity was measured at different field intensities, ranging from 1.8×10^4 to 110×10^4 V/m. The values were obtained by placing a small volume of the liquid between two horizontal electrodes positioned 50 μm apart (chapter 4, section 4.3), and measuring the conductivity for different applied voltages. Table 6.1 shows values of the conductivity of a mixture of Aot/isopar M to be independent of the field.

Table 6.1 Conductivity at high field for 17% w/w Aot in Isopar M

Field $\times 10^4$ V/m	1.8	10.9	26.0	32.3	60.0	74.4	10.0
Conductivity $\times 10^{-7}$ $(\Omega m)^{-1}$	1.7	1.4	1.6	1.3	1.6	1.5	1.5

A significant observation of the effect of the high field was the change in the shape of the liquid meniscus at the metal edges, where the electrical force on the liquid counters the surface tension and gravity forces and the inertial force at the outlet from the capillary. The surfaces from which several jets are emitted are very different from a drop being elongated to form a single jet. Liquid emerging from the capillary flows outwards to the periphery, where the configuration of the liquid may be considered to be an annular plane, with jets issuing from distinct points on the surface.

The flow to the periphery is likely to be nonuniform to some degree. For instance, a very small gravity force would result in an extension of the liquid perpendicular to the surface. The field normal to the surface at such a point would be higher, by virtue of its curvature, than at an adjacent point where the surface is comparatively straight. A slight, localised increase in the field would then cause the charges on the liquid surface to move towards the extended point. In this way a local potential gradient may be established along the surface that, together with surface charge, results in a downward electrical force. Thus the extension of the liquid at the point becomes amplified to yield a jet.

Greater numbers of points along the surface become extended as the voltage is increased. At a particular number of jets, the spraying was observed to be unaffected by voltage increase until a value of the voltage at which more jets were emitted from the surface. The behaviour is interpreted in terms of the charge density on the surface of the liquid. The charge per unit area residing at the surface of the liquid increases with the field according to $\varepsilon_o E_n$. The electrical pressure acting on the surface increases with the field and the charge density;

$$1/2\varepsilon_o E_n^2$$

Following the reasoning that the surface is subjected to a tangential stress due to the migration of charge towards an extended point, the convection of the liquid carries more charge as the charge density on the surface is increased. This establishes an even higher field at the extended point. An increase in the pressure differential between a region which is slightly curved and another region which is planar, results in a finer extension of the liquid to form a jet.

When the charge density on the surface is high, the pressure differentials between the straight portions and the slightly curved portions are increased. A tangential field is established with more ease at more points along the surface, which leads to the emission of higher numbers of jets.

6.2 Effect of the earth plate.

The intensification of the field that results from placing an additional earthed plate above the end of the capillary is illustrated in figure 6.3. Part of the investigation was concerned with the effectiveness of the plate for creating the high fields necessary to establish multiple jets, when the distance between the underside of the plate and the end of the capillary is varied. Another aspect that was studied was the importance of the gap between the inside edge of the plate and the outside of the capillary for forming the jets.

Two copper discs were machined to a diameter of 80mm so that their size is the same as that of the top conducting disc and the earthed collector. The discs were drilled and bored at the centre to two different diameters, 15 mm and 60 mm. Both the inner and outer edges were given high radius of

curvature to avoid corona and sparking. The positioning of the plates above the end of the capillary was limited by the deposition of liquid drops on the undersides. When the earthed plate was very close to the tip of the capillary, the charged drops accumulated on the earth, leading to intermittent dripping from the underside of the plate.

Figure 6.5 is a plot of the voltage required to form particular numbers of jets. As the applied voltage rises, the number of jets increases. The two lower lines were obtained using the plate with the smaller hole, at two values of the liquid flowrate. It may be seen that lower voltages are needed to form any given number of jets, at both flowrates, in the presence of the plate with the smaller hole. At a constant voltage, the radial field between the inside edge of the plate and the capillary rises as the hole size decreases, approaching that of the capillary. The higher value of the radial field imposed by the plate with the smaller hole leads to higher fields being established at the tip of the capillary.

At the higher flowrate of 60 ml/h, a greater rise in voltage is required to maintain a set number of jets when the hole size increases. The main effect of the smaller diameter is to produce higher fields, while all values of the jet number can be obtained by adjusting the voltage.

Figure 6.6 is a graph of applied voltage against the distance of the earthed plate from the tip of the capillary. The two curves are measurements taken for the case of the formation of five and nine jets. The requirements on the voltage in order to maintain constant jet number increase as the plate is moved away from the capillary. So increasing the distance results in a reduction of the fields at the capillary tip. The action of raising the plate lessens the influence of the radial field in the gap between the capillary and the inside edge of the earthed plate on the

field experienced by the liquid as it emerges from the capillary. Effectively, the equipotential lines passing through the gap diverge from the outline of the capillary. The relation between voltage and distance is linear, so that the field at the capillary tip is directly proportional to the distance. However the effect is reduced when the plate is very close to the top disc.

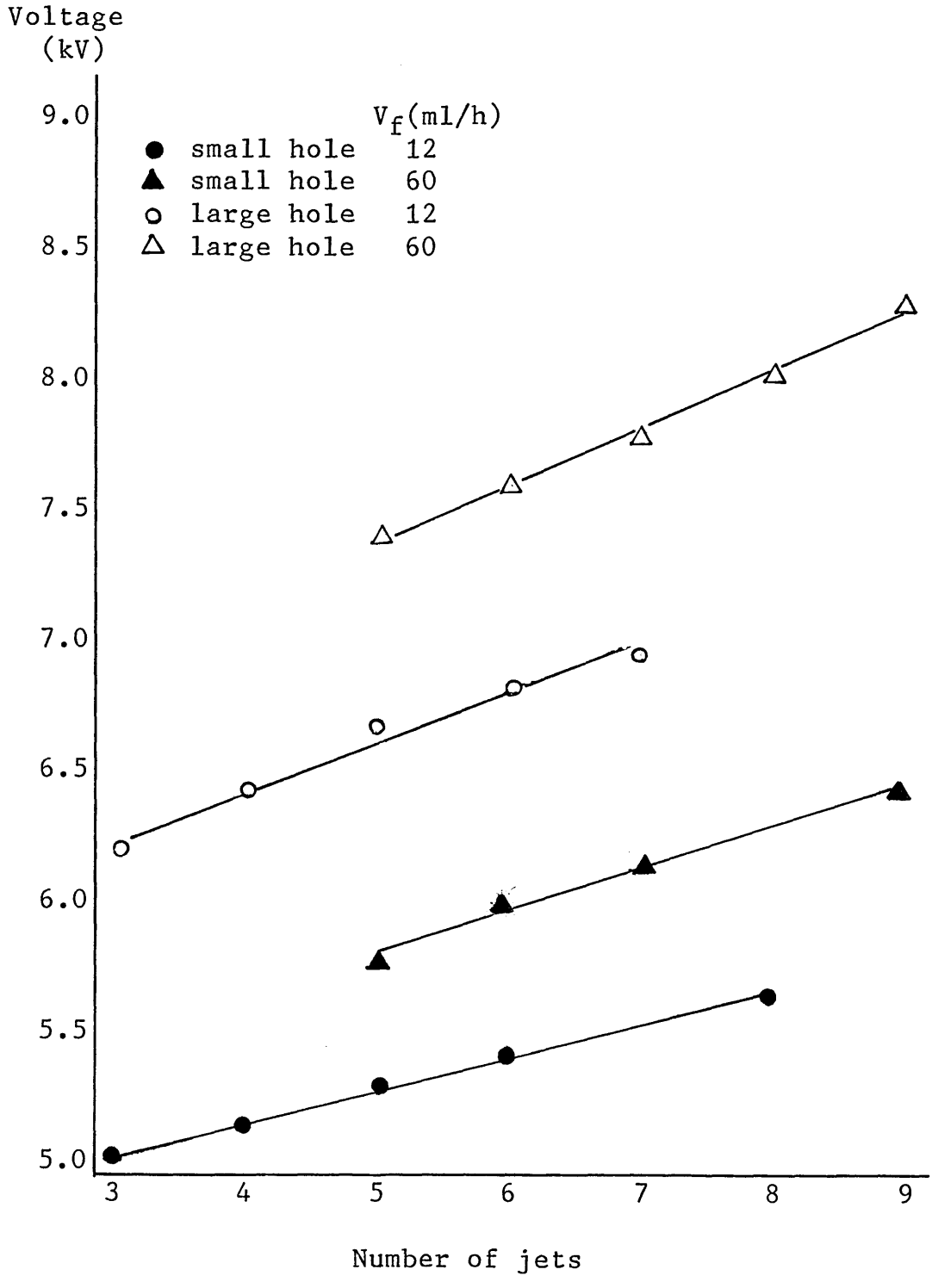

Figure 6.5 The minimum voltages required to form several numbers of jets in the presence of the earthed plate. Capillary i.d.=1.35mm.
$k = 1.54 \times 10^{-6} (\Omega m)^{-1}$

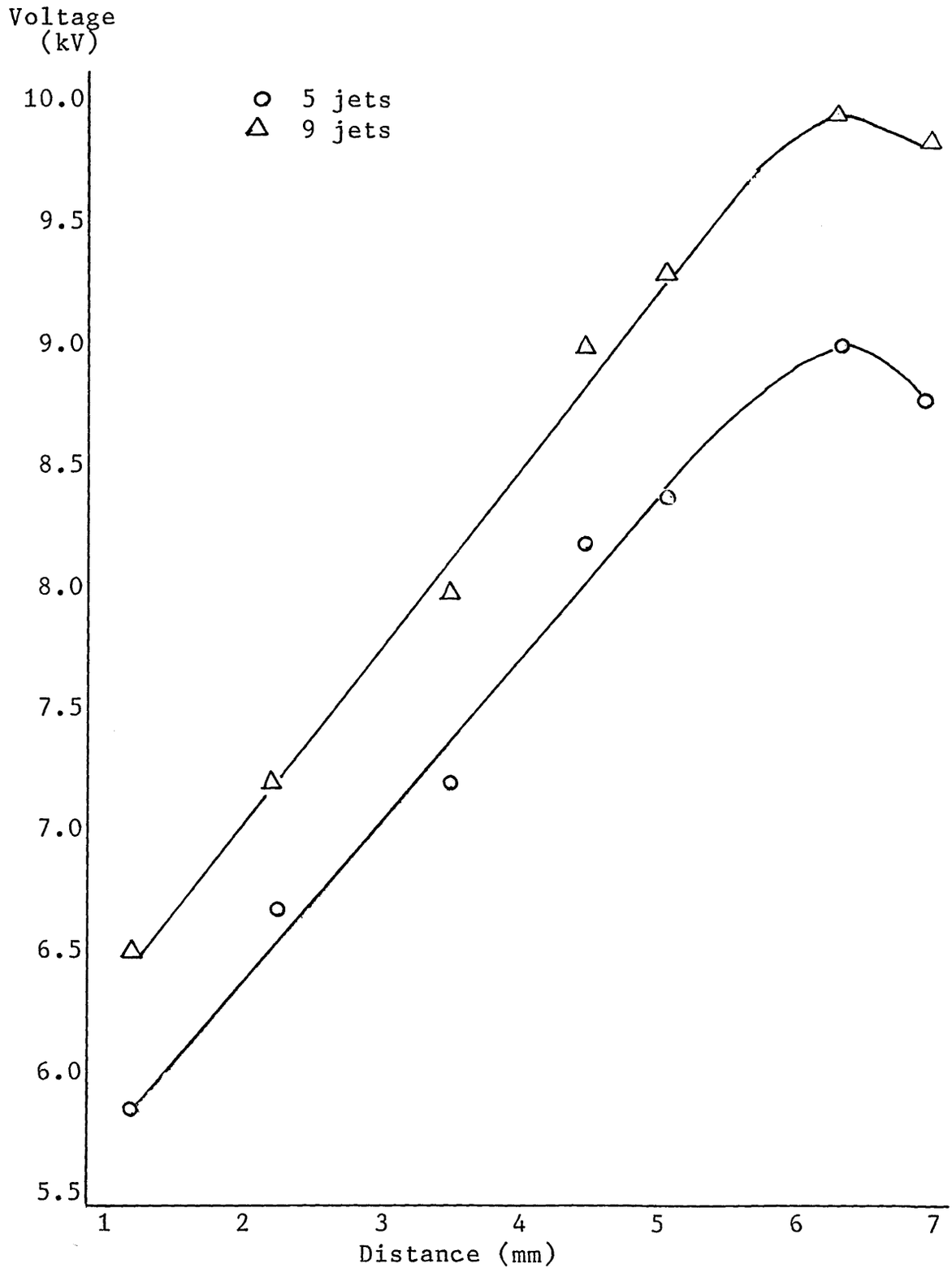

Figure 6.6 The voltages required to form 5 and 9 jets, when the distance between the earthed plate and the capillary tip is varied. $k = 1.54 \times 10^{-6}\ (\Omega m)^{-1}$. V_f = 30 ml/h. Capillary i.d. = 1.35 mm.

6.3 Effect of capillary size and flowrate.

Figure 6.7a and b are plots of the voltage at which several numbers of jets are formed. The internal diameter of the capillary is the parameter at two different average inlet velocities of an aerosol ot (Aot) isopar M mixture of conductivity 1.54×10^{-6} $(\Omega m)^{-1}$. It may be seen that the higher voltages lead to increased numbers of jets. The lower velocity set indicates that the gradients are the same for all diameters. At both velocities the narrower capillaries are found to form the jets at lower values of the voltage.

The flowrate of the liquid and its velocity inside the capillary are unavoidably linked since changing the diameter of the capillary alters one or the other. An important factor to consider is the inertial force at the liquid delivery point. High inertial forces aid in single jet formation but hinder the flow of liquid sideways. The kinetic energy at the capillary tip is decreasing as the diameter decreases, since lower flowrates maintain the constant velocity. However, the decrease in the inertial forces at smaller diameters is not responsible for the lower requirements on the voltage. Figure 6.8 can be used to demonstrate this argument. Now the flowrate is held constant and the inertial forces increase with a decrease in the diameter. The plot confirms the trend of lower voltages required at smaller diameters for a particular number of jets, despite the fact that the inertial forces are higher at the tips of the finer capillaries. The tendency for smaller sizes to yield jets more readily can be attributed to the higher fields imposed at constant voltage by the capillaries of smaller radius.

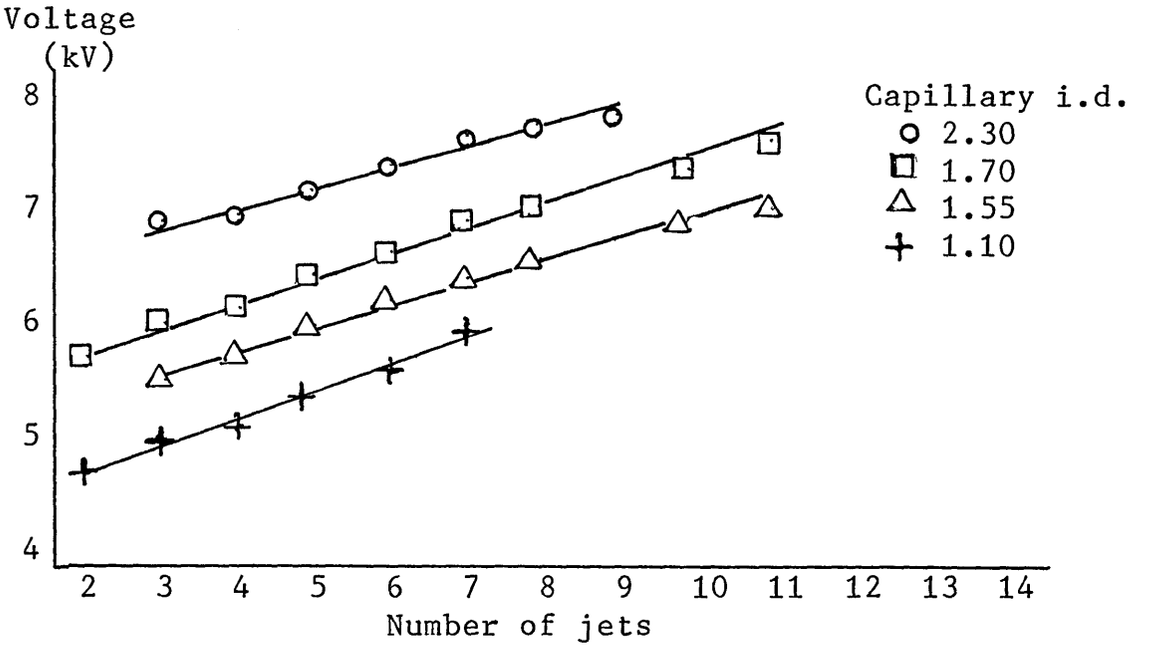

Figure 6.7a Minimum voltage required to form several numbers of jets. Capillary i.d. is the parameter. Average velocity inside the capillary = 2mm/s. $k=1.54\times10(\Omega m)^{-1}$.

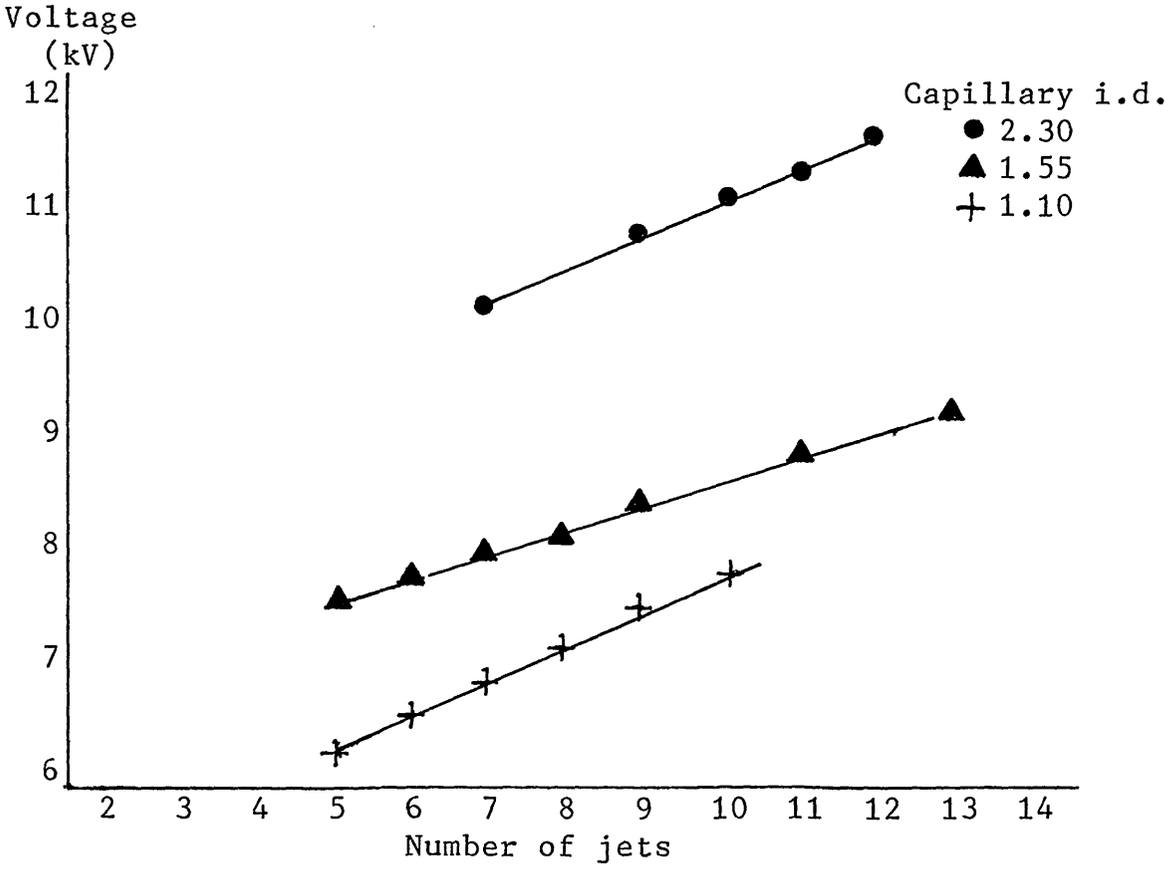

Figure 6.7b The minimum voltage required to form several jets with different capillaries. Velocity = 18 mm/s.

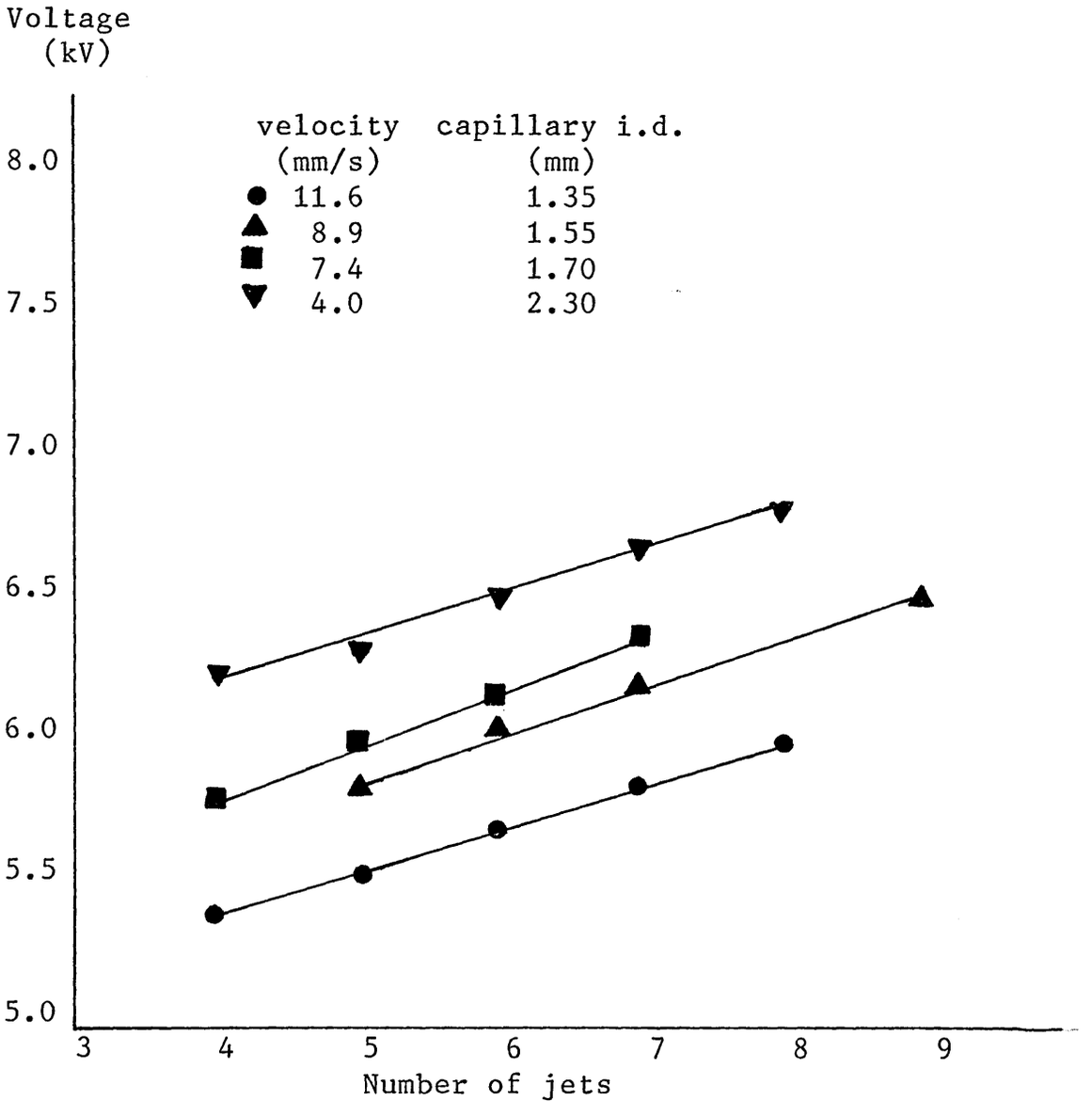

Figure 6.8 The minimum voltages required to form multiple jets. The capillary inside diameter is the parameter. The flowrate is held constant at 60 ml/h. k = 1.54×10^{-6} $(\Omega m)^{-1}$.

Refering to figure 6.7b, the trend at a higher velocity is similar, with higher voltages being applied. It was found that the value of the voltage at which a single jet becomes unsteady increases with the flowrate. The application of progressively higher voltages has the effect of thinning the jet until the point at which it is destabilised. Thus the voltage at which spraying from the edges of the capillary commences is raised with flowrate.

A significant observation was the tendancy for a minimum of five or six jets to form at higher flowrate, while numbers of two or three are present only at lower rates. This pattern was reproducible for different size capillaries. At the value of the field corresponding to the first number of jets formed, the surface of the liquid is drawn out to a specific radius of curvature. It was argued above that the increase in the field causes an increase in charge at the surface, which in turn leads to a reduction in the flowrate of each jet. The surface reacts to emit more jets in order to spray the increased amount of liquid.

The graphs also indicate that the gradient of voltage against jet number is greater at the higher velocity. Increasing the flowrate lowers the residence time of the liquid at the tip of the capillary. Charges do not reach the surface over the reduced times. By raising the voltage at the capillary, higher fields increase the velocity of the ions so that enough charge can build up.

6.4 Effect of capillary wall thickness.

The importance of the capillary edges in imparting the high fields necessary for multiple jets has been emphasized. Figure 6.9 is a plot of voltage against jet number with wall thickness and flowrate as the parameters.

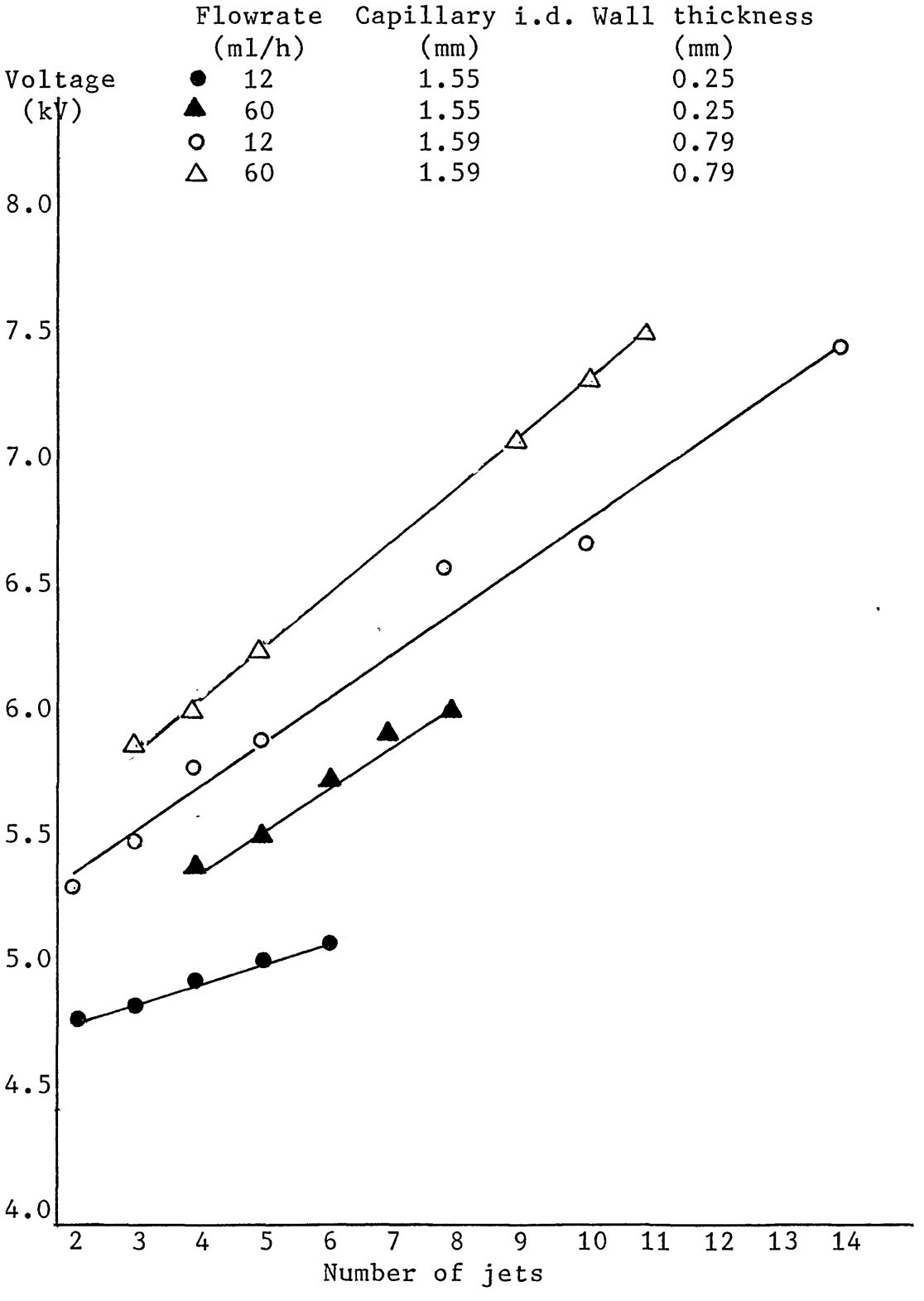

Figure 6.9 The minimum voltages required to form multiple jets at two values of the capillary wall thickness. k = 1.54×10^{-6} $(\Omega m)^{-1}$.

Capillaries of comparable internal diameter were chosen to keep the inlet velocity constant. The capillary with thicker walls requires higher voltages to achieve the same number of jets and this trend is accentuated as more jets are formed. The larger size may be expected to require the higher values, regardless of thickness, due to the larger outside diameter which lowers the field. However, the gradients in figure 6.9 are greater at the larger thickness, suggesting an independent thickness effect. The requirement of high fields is associated with the wetting of the capillary end. Jets were clearly seen to issue from the outer edge. A liquid which wets the whole area would move to the point of highest field with more ease if the thickness is reduced. Both sets of results show the same trend.

A second observation is the higher numbers of jets attained for the thicker walls. If this effect is a continuous function of thickness, then very large numbers should be produced from large sized tubes, provided the higher fields required do not lead to the electrical breakdown of air. It was hoped to investigate this effect further, but accurately bored, smooth ended capillaries were not available from the manufacturer.

6.5 Effect of conductivity.

The measurements of conductivity against concentration of Aot in isopar M are shown in figure 6.10. Figure 6.11 is a plot of the voltages required to form two jets vs conductivity at three values of the flowrate. The two lower curves indicate that more conducting liquids form the jets at lower voltages. The results are explained by making the distinction between the field imposed at the end of the capillary and the field experienced by the surface of the liquid.

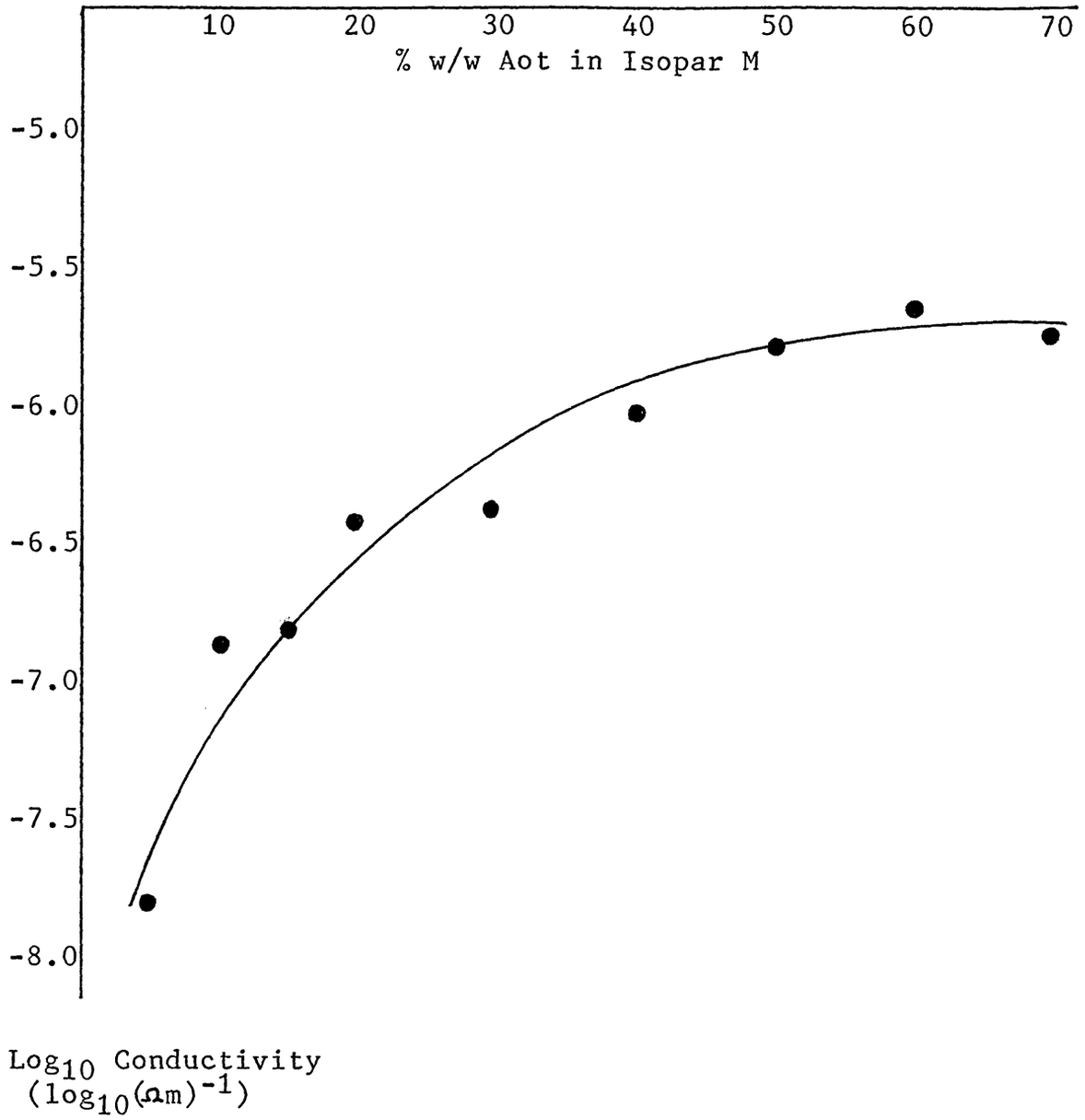

Figure 6.10 Conductivity of the Aot/Isopar M mixtures as a function of the concentration of Aot. The Measurements were taken at low values of field strength.

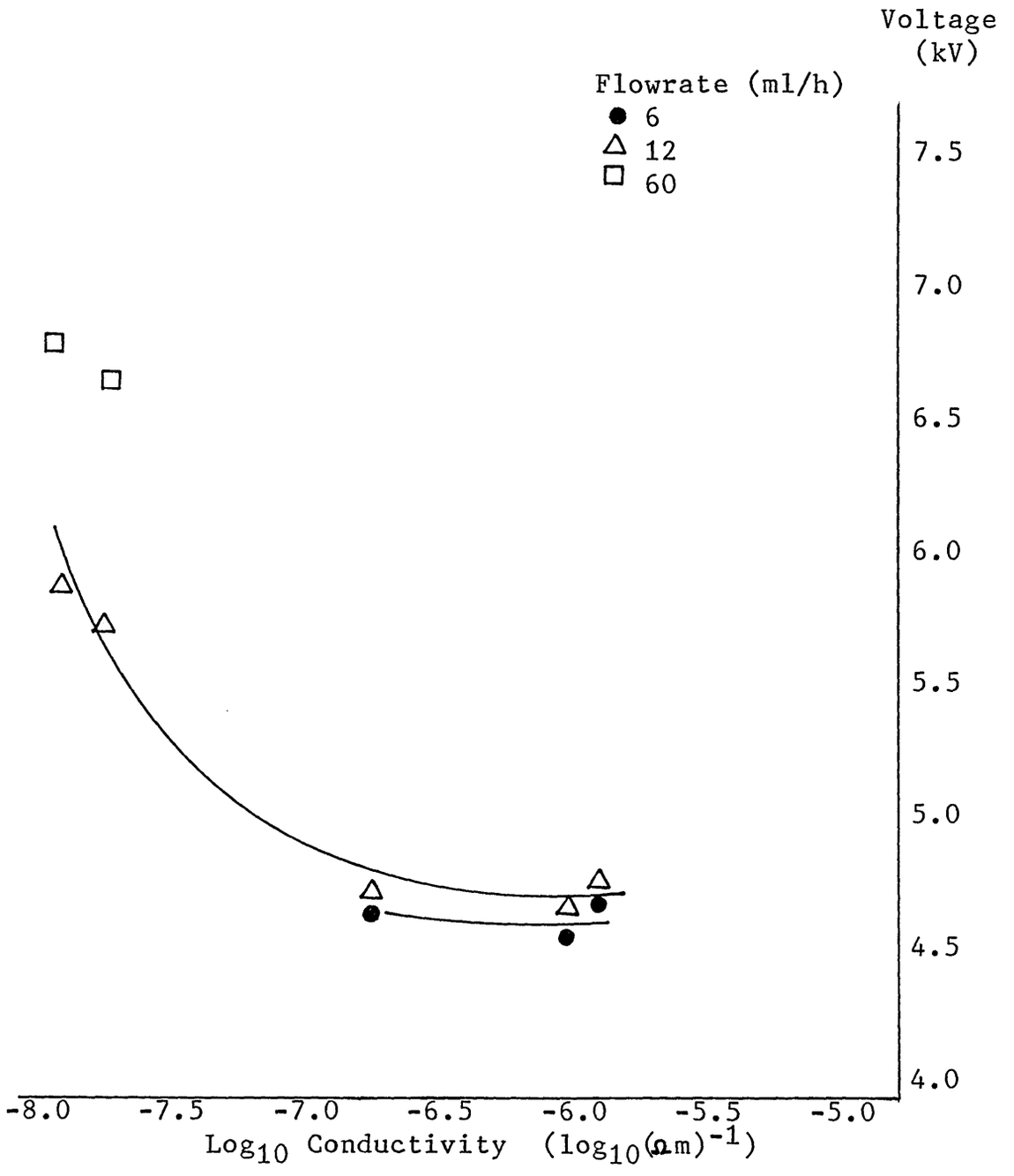

Figure 6.11 The minimum voltages required to form two jets at the periphery of the capillary, when the conductivity of the liquid is varied. The flowrate is the parameter.

The ability to maintain a field within the liquid characterises semi-insulating liquids. Liquid adjacent to the capillary is at the applied voltage, but the value of the voltage on the surface is lower due to the field established within the liquid. The curve shows the voltage required is proportional to 1/k, a relation predicted by eqn. 6.1, for the drop in voltage with conductivity when the current and the geometry of the jet are constant. A higher conductivity liquid allows the voltage to be transmitted more effectively to the liquid surface. Therefore a lower value of the applied voltage establishes the value of the field normal to the surface that gives rise to two jets. The trend of conductivity with voltage is confirmed in figures 6.12 and 6.13, where three and four jets are formed respectively.

When the voltage at the capillary is kept constant, more jets are formed at higher conductivities. It has become clear from these results that the charge density on the surface of the liquid controls the manner in which the liquid is emitted from the surface. For constant volumetric flowrate, the increase in jet number reflects that a higher surface charge density leads to the formation of higher numbers of jets, each of lower flowrate.

It is interesting to note from figure 6.11 that the attainability of two jets depends on the value of the flowrate. At 60 ml/h or higher, two jets are not formed at increased conductivity. Figure 6.12 also shows that three jets cannot be established for the more conducting liquids when the flowrate is raised to 60 ml/h. However in figure 6.13, the restriction on the conductivity is different. Four jets are formed at the high flowrate at higher conductivities. The less conducting liquids on the other hand are unable to yield four jets. The condition of low flowrate overcomes the limitation of the lower

conductivities to form four jets. Similarly the low flowrates enable the more conducting liquids to yield two and three jets.

The restriction to low flowrates allows effective control over jet number. This has implications for controlling the size of drops produced. Jet diameter is known to affect the size of the drops emitted from a single jet. If the relation is the same for the case of finer jets, higher numbers of jets are expected to result in smaller drops. Apparently, regardless of the voltage applied, high rates restrict the system to producing larger drops when spraying less conducting liquids. Conversely, the transition from a single jet to many jets for more conducting liquids at high flowrate results in a greater change in the drop size. The relations between size and factors such as the field, flowrate and liquid parameters will be discussed in the next chapter.

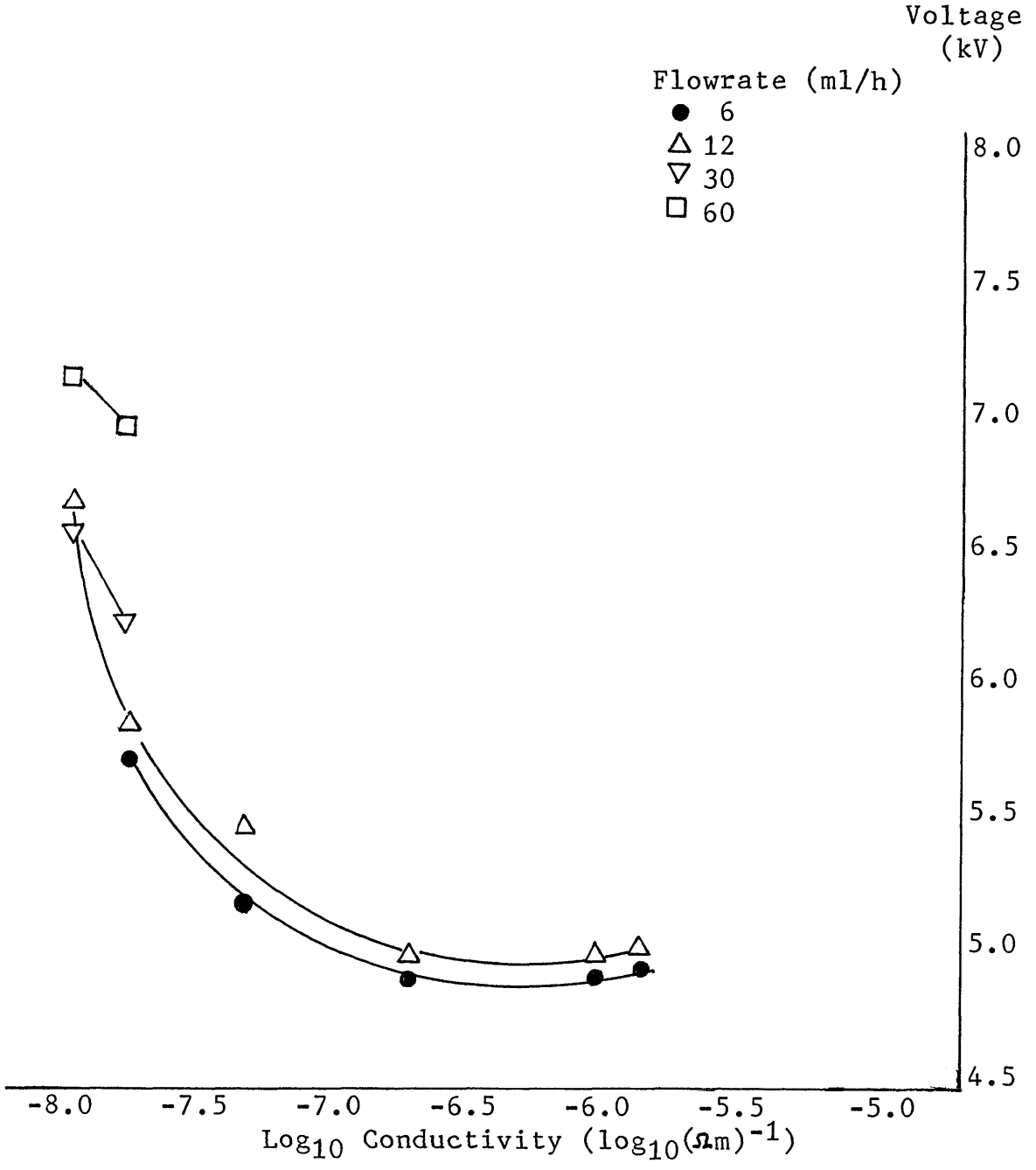

Figure 6.12 The minimum voltages required to form three jets when the conductivity of the liquid is varied. The flowrate is the parameter.

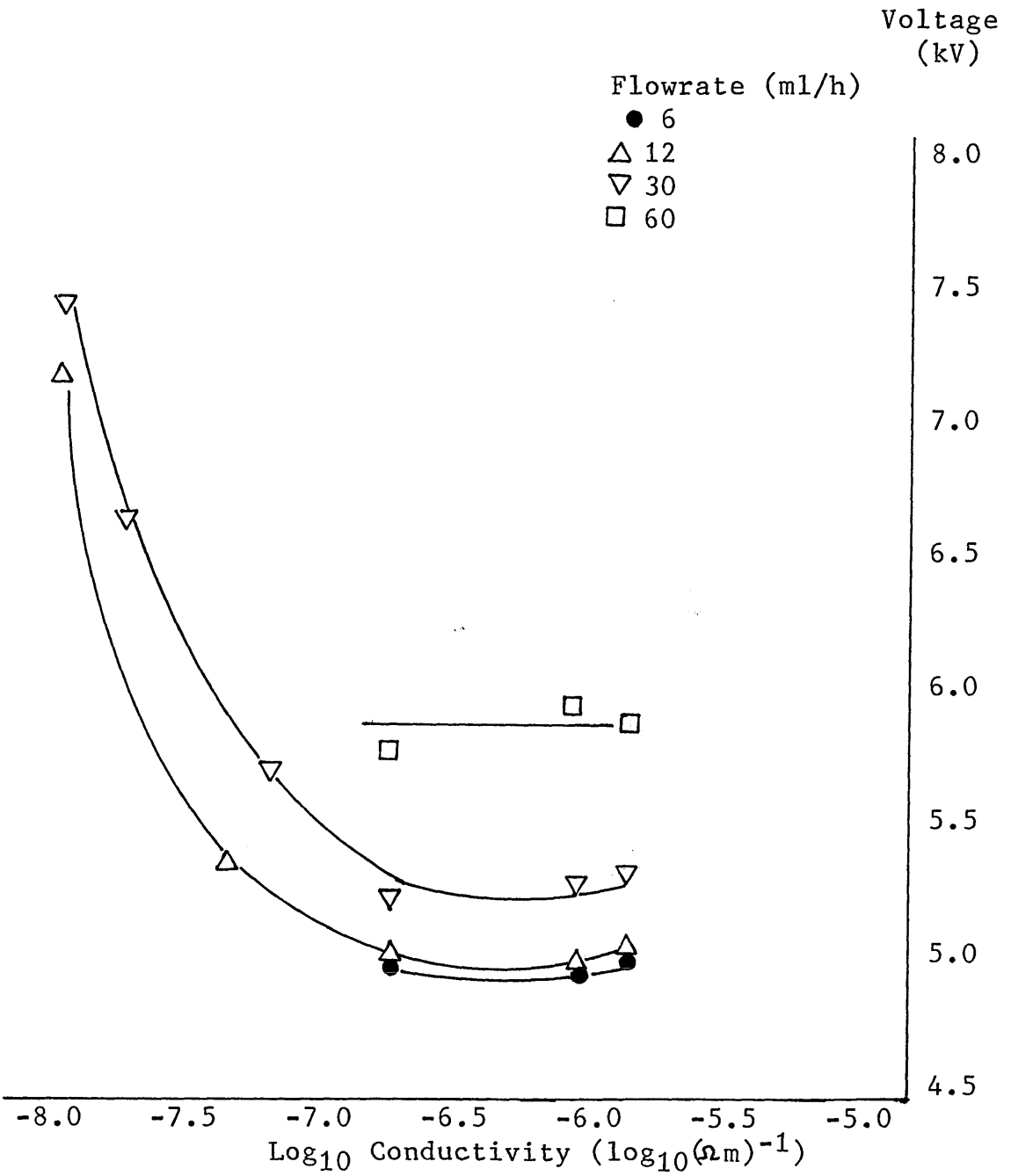

Figure 6.13 The minimum voltages required to form four jets when the conductivity of the liquid is varied. The flowrate is the parameter.

6.6 Effect of viscosity.

Four systems of mixtures of liquids were used to vary the viscosity. In the first of these, the amount of Aot in isopar M was varied. Figure 6.14 shows the relation between viscosity and concentration of Aot. During these observations, the conductivity could be held constant because the conductivity-concentration curve reaches a plateau above 35% Aot.Values of the applied voltage against viscosity are plotted in figure 6.15. The number of jets is the parameter for a conductivity 1.79×10^{-6} $(\Omega m)^{-1}$. The viscosity has a significant effect in lowering the field for the single jet, while the increase in the required voltage for the formation of many jets is slight, with the gradients increasing at the higher numbers.

In order to confirm the trend, it was decided to extend the results to include lower viscosities. The Aot isopar M mixture was not accessible to a wider viscosity range, so the system was changed to one of three components. The second system is a mixture of Aot, isopar M and paraffin. Plots of the conductivity and viscosity variations for the three component mixtures are given in figures 6.16 and 6.17. The parameter in both the figures is the percentage of Aot in isopar M in the two component system before the paraffin is added. Figure 6.18 is the graph of voltage against viscosity, in which the viscosity range extends from 7 to 61 mPas, at the same flowrate as in figure 6.15. Hiwever, the conductivity of the solution has been decreased by a factor of ten. The trend for the single jet does not show as great a dependence on viscosity as for the case of the higher conductivity. The measurements taken with the three component system show that viscosity has virtually no effect on the fields required, which contradicts earlier results.

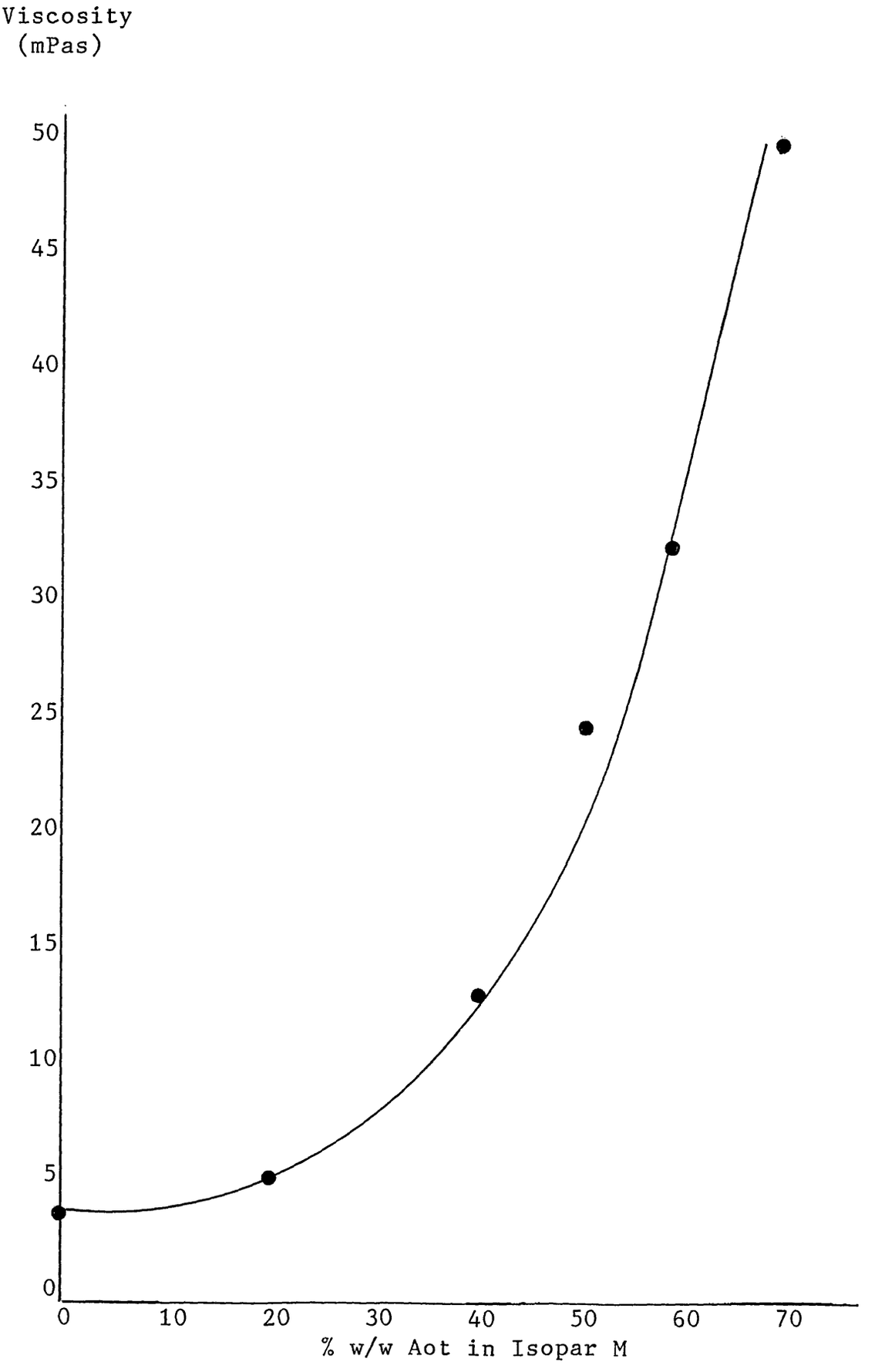

Figure 6.14 The viscosity of Aot/Isopar M mixtures as a function of the concentration of Aot.

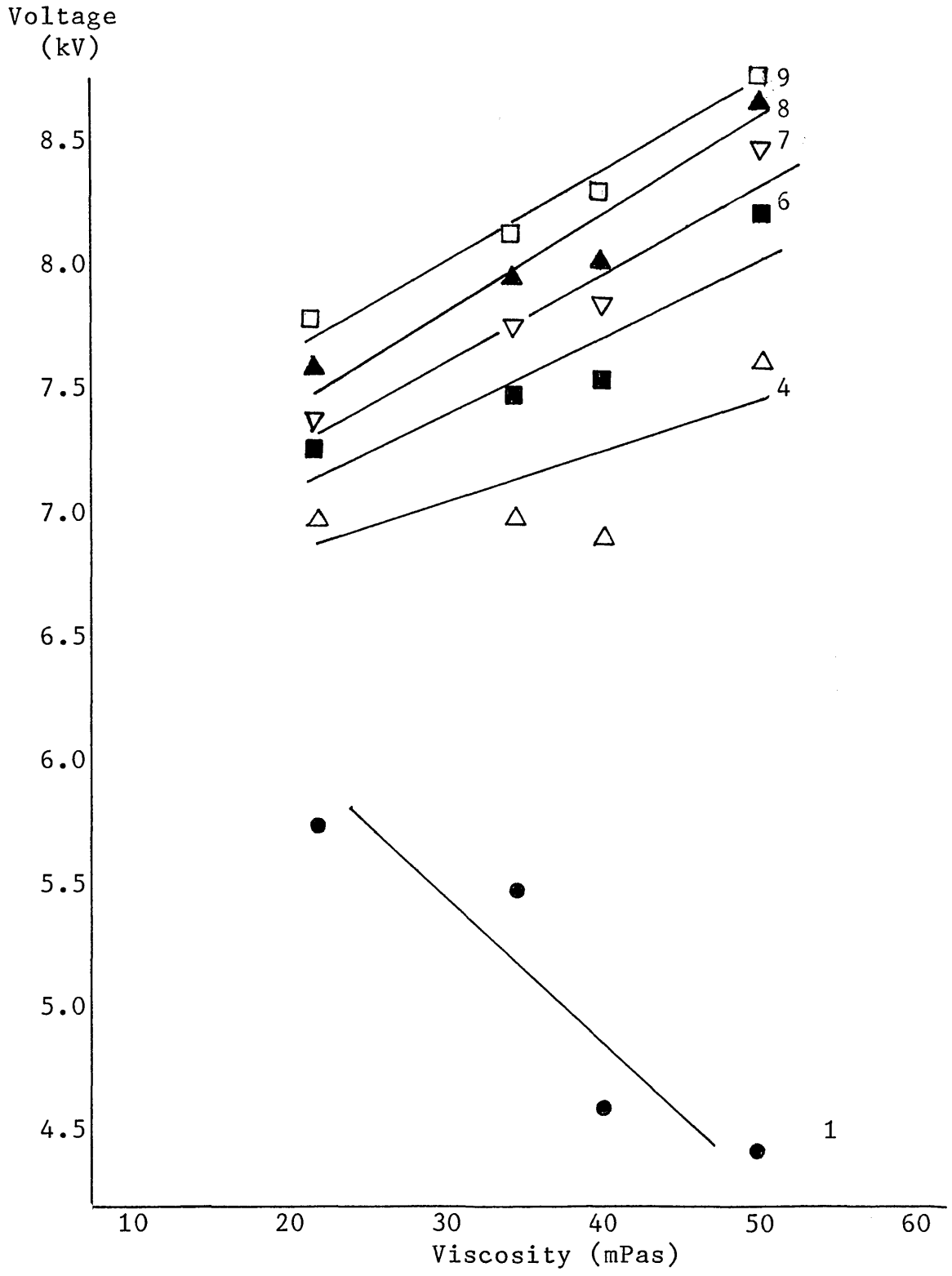

Figure 6.15 The minimum voltages required to form the multiple jets and the single jet when the viscosity is varied. Aot/IsoparM mixtures. $k = 1.79 \times 10^{-6}\ (\Omega m)^{-1}$. V_f = 60 ml/h. The numbers of the parameters signify the numbers of jets.

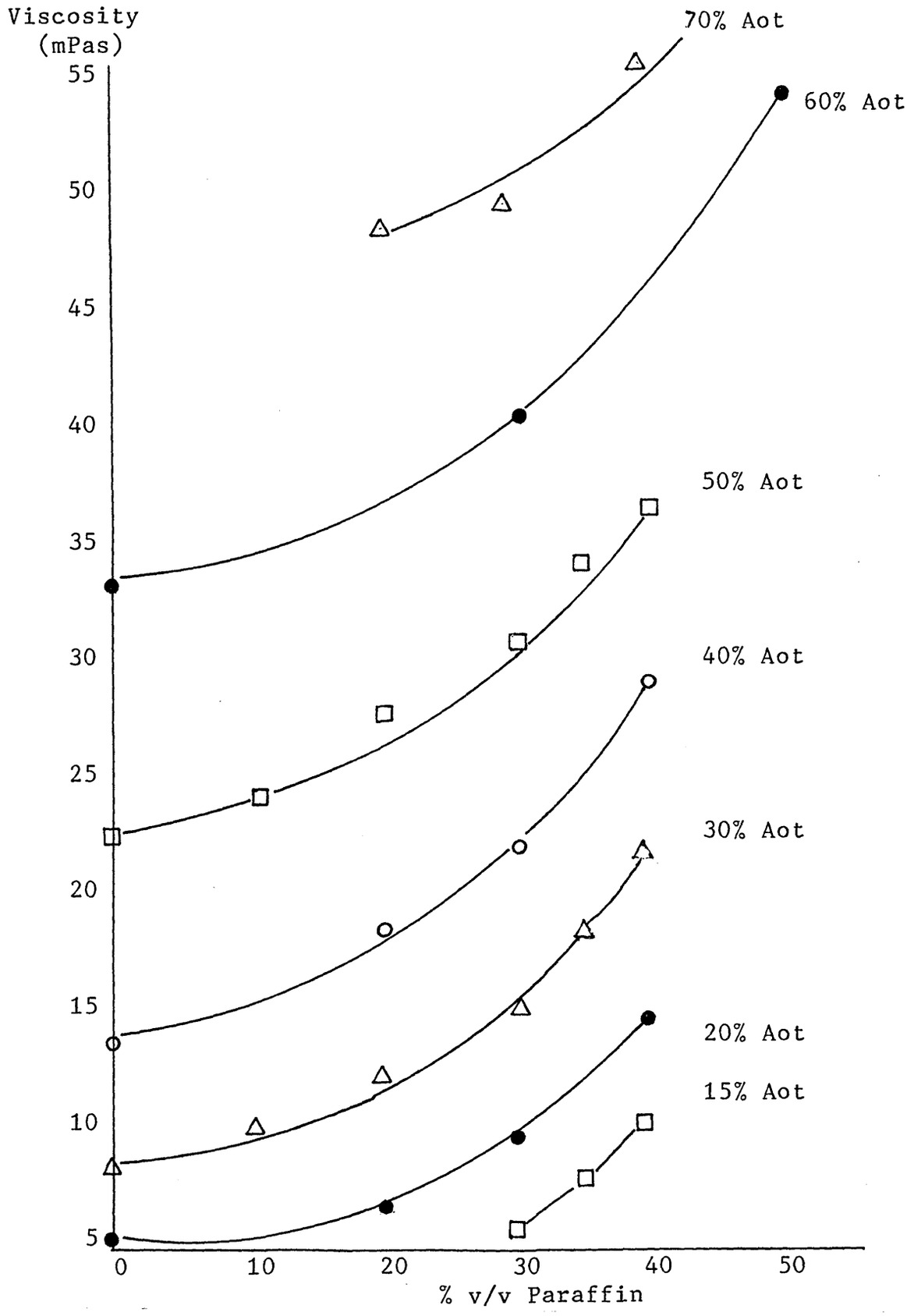

Figure 6.16 The viscosity of Aot/Isopar M/paraffin mixtures as a function of the concentration of paraffin. The numbers for the parameter signify %Aot in isopar M in the original solution.

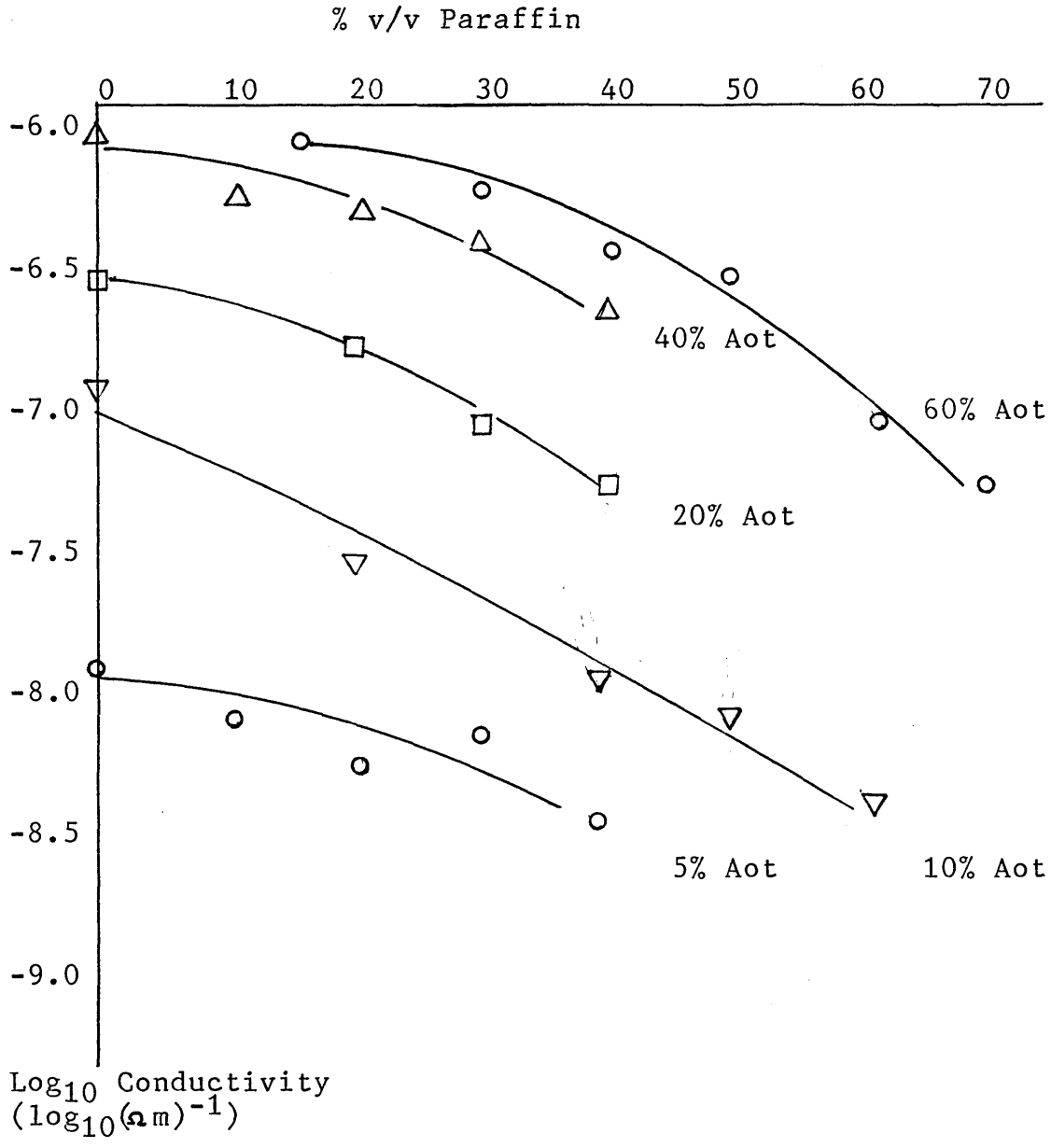

Figure 6.17 The conductivity of Aot/Isopar M/paraffin mixtures as a function of the concentration of paraffin. The parameter is the concentration of Aot in Isopar M , in the original solution, before adding the paraffin.

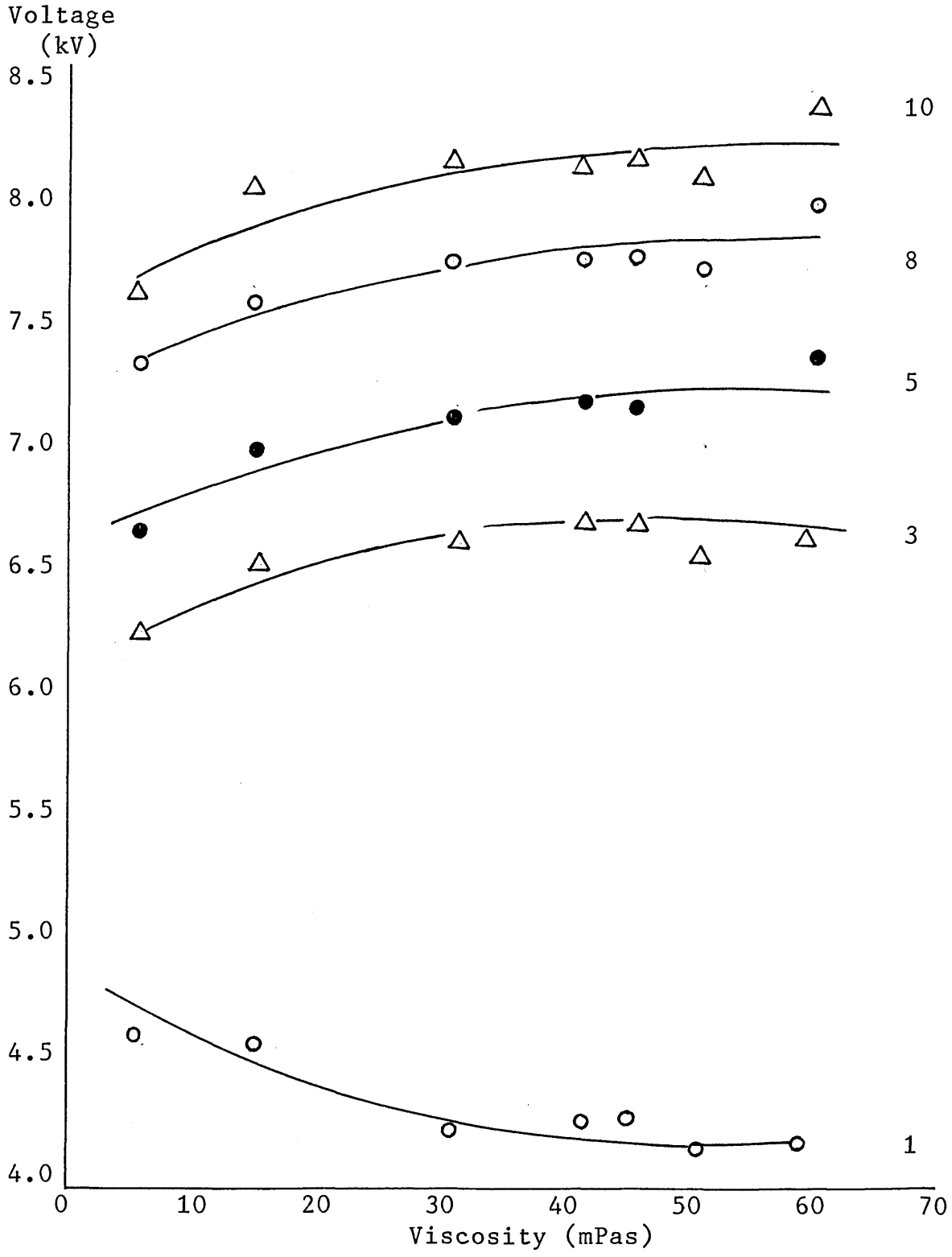

Figure 6.18 The minimum voltages required to form multiple jets and a single jet when the viscosity is varied. Aot/Isopar M/paraffin mixtures. The numbers on the parameter signify the numbers of jets. V_f = 60 ml/h. k = 1.78×10^{-7} $(\Omega m)^{-1}$.

It was thought that the disagreement between the two systems could be due to the difference in conductivity. The relative concentrations of the three components could not be changed to achieve the same viscosity range at the higher conductivity, where a slight dependence on viscosity had been detected. Therefore a third system, consisting of n-butanol, aot, isopar M, and paraffin was chosen. At the same conductivity as in figure 6.15, the viscosity had no effect on voltage requirements for multiple jets (figure 6.19).

Despite the disagreement with the results obtained for the two component system, it is concluded that the voltage requirements are independent of the viscosity. Other observations on the jets were concerned with whether all the systems of mixtures of liquids allow the jets to be formed. While spraying the Aot isopar M mixtures, the jets were reproducible and their stability was not affected by sudden application of voltage. It was observed that not all systems of liquids exhibit stable jets. When the n-butanol was used in the four component system, the behaviour was different. Instead of forming multiple jets instantaneously, the motion of the liquid was unsteady for seconds. Once a certain configuration was established, it was very sensitive to a slight increase in voltage. A sudden rise in the voltage caused the jets to revolve clockwise around the periphery of the capillary. Flickering between different numbers of jets was apparent for all jet numbers and under all conditions of the flowrate. Fine adjustment of the voltage sometimes helped to prevent this, though only transiently. When the fifth system, employing n-butanol, isopar M and paraffin was tested, the absence of the Aot resulted in more erratic behaviour. The importance of the Aot for more stable behaviour was confirmed by comparisons made between the system of (a) n-butanol, Aot, isopar M, paraffin and the system of (b) n-butanol, Aot, isopar M. The latter required larger amounts of Aot in order to increase the viscosity and

resulted in more stable behaviour under all conditions, compared to system (b). The difference in sensitivities of the multiple jets, when Aot and n-butanol are used appears to be due to the difference in the nature of the charge carriers.

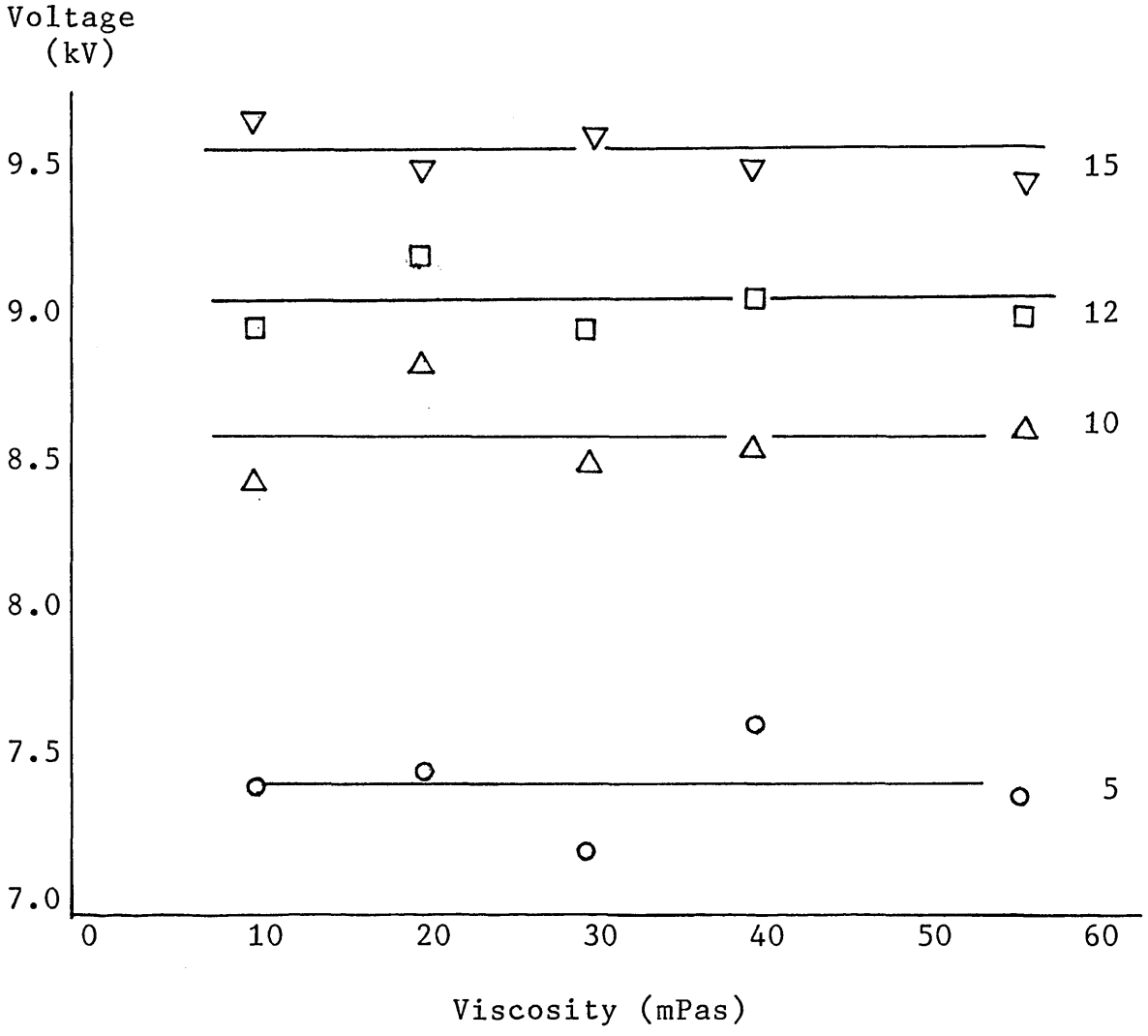

Figure 6.19 The minimum voltages required to form multiple jets when the viscosity is varied. Aot/Isopar M/paraffin/ n-butanol mixtures. V_f = 60 ml/h. k = 1.78×10^{-6} $(\Omega m)^{-1}$. The numbers on the parameter signify the number of jets.

CHAPTER SEVEN

MEASUREMENTS OF DROP SIZE AND DROP CHARGE

In the previous chapter, the process of the formation of several numbers of jets at the edge of the capillary was described. The number of jets established was found to be very sensitive to the applied voltage. When the more conducting liquids were sprayed in this way, less electrical energy was necessary to pull the liquids out into jets. These observations suggest that a high value of surface charge causes small amounts of liquid to be drawn out from the surface. The magnitude of charge was therefore linked to the size of the jet.

Studies conducted on the single jet included measurements of the size of the drops. Data collected in this way was limited by the photographic technique used, and it became apparent that a more accurate method of measurement was needed to study and compare the drop sizes and charges from both single and multiple jets. A suitable method will be described briefly below. Apart from assessing the influence of the various parametrs, the measured values have been used to evaluate the changes occurring to the jets as the parameters are varied. The division of the liquid into increasing numbers of jets at higher voltages can be explained in terms of the magnitude of charge carried by the liquid.

7.1 Factors affecting the drops from a single jet.

The size of the drops issuing from the jets was measured using a probe which emits a laser ribbon. Shadows of the drops passing through the ribbon are reflected by mirrors positioned inside the probe, onto a 64 element array

of photodiodes. A computer collects the signals from the probe at different time intervals and processes the information into an average size as well as a size distribution. The average charge on the drops was obtained by connecting the collector to a Keithley electrometer, which is capable of detecting very low currents.

Several parameters were investigated to determine the relative influence of the design variables (such as the flowrate and applied voltage) and the conductivity and viscosity of the liquid. The majority of the results are plotted as $\log_{10}$ of the measured value against the $\log_{10}$ of the variable. This manner of presentation allows the relation between the measured value and the variable to be determined in terms of power dependancies.

For the case of the formation of a single jet, an increase in the flowrate resulted in larger drops. The flowrate effect was detected in earlier studies on the jet when the diameters of both the jet and the drops were measured from low magnification photographs. The size and the charge to mass ratio of the drops are listed in table 7.1 for varying flowrate at two values of the conductivity. Figure 7.1 is a log-log plot of the drop size, showing similar dependence on the flowrate for three liquids. Values of the power dependance on the flowrate at five different conductivities are shown in table 7.2. When the correlated power dependencies are averaged,

$$d \propto V_f^{0.63}$$

to within an accuracy of 15%.

Measurements of the current carried by the drops are expressed in terms of the average charge to mass ratio;

$$c_m = \frac{I_t}{\rho V_f}$$

Table 7.1 The charge to mass ratio and size of the drops from a single jet as a function of the flowrate at two conductivies.

Conductivity = 5.623×10^{-8} $(\Omega m)^{-1}$

Flowrate (ml/h)	Charge to mass (C/kg)	Volume mean diameter (μm)
3.36	0.01071	31
6.60	5.93×10^{-3}	43
9.00	5.50×10^{-3}	65
12.6	4.64×10^{-3}	81
18.0	3.75×10^{-3}	98
25.2	2.95×10^{-3}	125
35.4	2.35×10^{-3}	151
49.2	1.78×10^{-3}	173
66.0	7.64×10^{-4}	200
96.0	6.31×10^{-4}	267
132.0	4.47×10^{-4}	340
186.0	3.16×10^{-4}	439

Conductivity = 1×10^{-6} $(\Omega m)^{-1}$

Flowrate (ml/h)	Charge to mass (C/kg)	Volume mean diameter (μm)
3.36	0.01540	32
6.60	0.01432	42
9.00	0.01100	52
12.6	8.93×10^{-3}	73
18.0	8.50×10^{-3}	65
25.2	7.08×10^{-3}	82
35.4	5.62×10^{-3}	93
49.2	4.57×10^{-3}	113
66.0	3.55×10^{-3}	150

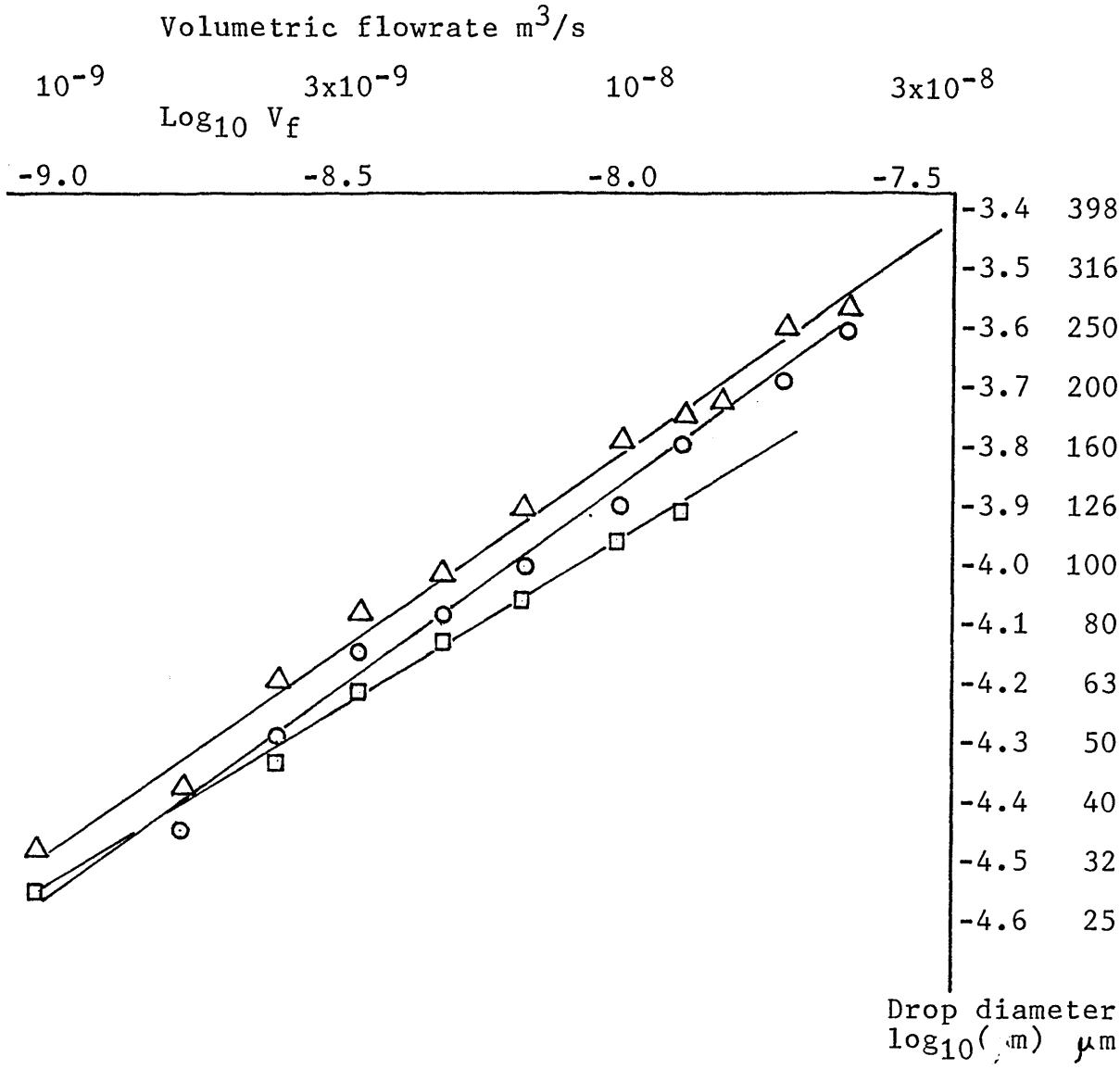

Figure 7.1 Variation of the volume median diameter of the drops from the single jet with the flowrate.

△ $k = 5.62x10^{-8}$ $(\Omega m)^{-1}$.

○ $k = 3.16x10^{-7}$ $(\Omega m)^{-1}$

□ $k = 10^{-6}$ $(\Omega m)^{-1}$

Table 7.2 The dependence of the drop size from a single jet on flowrate for conducting and semi-insulating liquids.

Conductivity$(\Omega m)^{-1}$	5.62×10^{-8}	1.59×10^{-7}	3.16×10^{-7}	1.00×10^{-6}
Power dependence	0.619	0.668	0.689	0.530

The rise in the diameter of the drops at higher flowrates is accompanied by a decrease in the average charge to mass ratio. Figure 7.2 presents correlations of $\log_{10} c_m$ against $\log_{10}$ flowrate for the three liquids. As the conductivity is raised, two regions having different dependence on the flowrate can be identified.
For $k < 3.16\times10^{-7}$ $(\Omega m)^{-1}$,

$$c_m \propto V_f^{-0.78} \qquad \text{at all values of the flowrate}$$

For $k > 3.16\times10^{-7}$ $(\Omega m)^{-1}$,

$$c_m \propto V_f^{-0.49} \qquad \text{in the range } 3.36<V_f<35 \text{ ml/h}$$
$$\text{and} \quad c_m \propto V_f^{-0.75} \qquad \text{in the range } 35<V_f<9.0 \text{ ml/h}$$

The above constants of proportionality imply that at a particular value of the applied voltage, the supply of more liquid causes the current carried by the drops to increase. However the increase in the current is not comparable to the increase in the flowrate, and the charge to mass ratio falls. The degree to which this happens is a

function of the conductivity of the liquid. Within the lower range of flowrate, relatively higher currents are imparted to a more conducting liquid, thus offsetting the decrease in the ratio. In the upper flowrate range, the effect of the flowrate overcomes the effect of the conductivity and all the liquids behave as semi-insulators.

The way in which the conductivity affects the charge to mass ratio is illustrated in figure 7.3. The trends are consistent at four values of the flowrate. The gradients taken from the log-log plots show that the ratio is less sensitive to the conductivity than to the flowrate;

$$c_m \propto k^{0.27}$$

However the influence of the conductivity on the size of the drops was found to be dependent upon the value of flowrate (figure 7.4). At low flowrates, < 12 ml/h, no change in size could be detected by the method of measurement used. At 50 ml/h, semi insulating liquids were found to still have a limited effect, while spraying progressively more conducting liquids resulted in a reduction of the size. On average the diameter of the drops is proportional to the conductivity according to;

$$d \propto k^{-0.11}$$

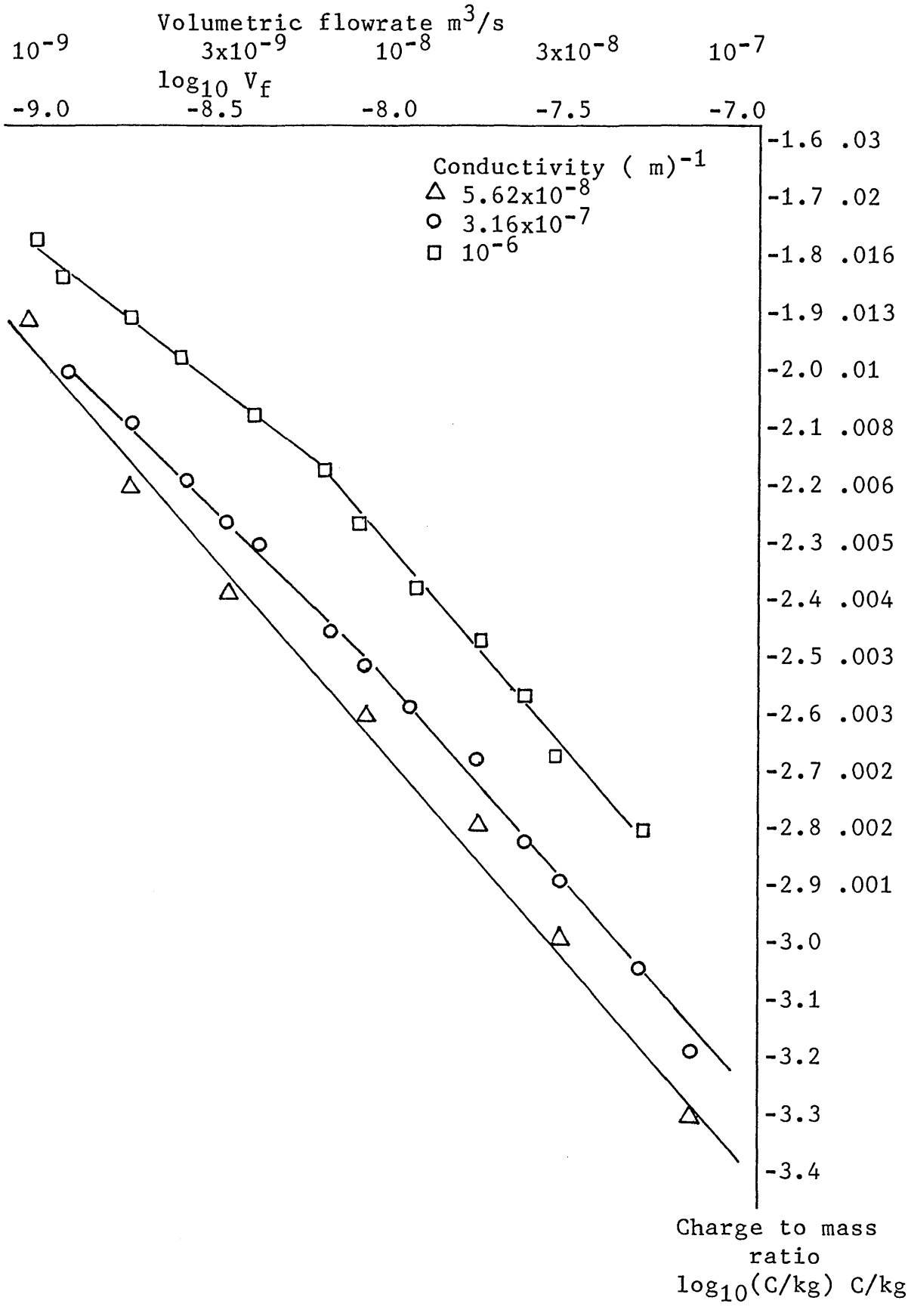

Figure 7.2 Variation of the average charge to mass ratio of the drops from the single jet with the flowrate.

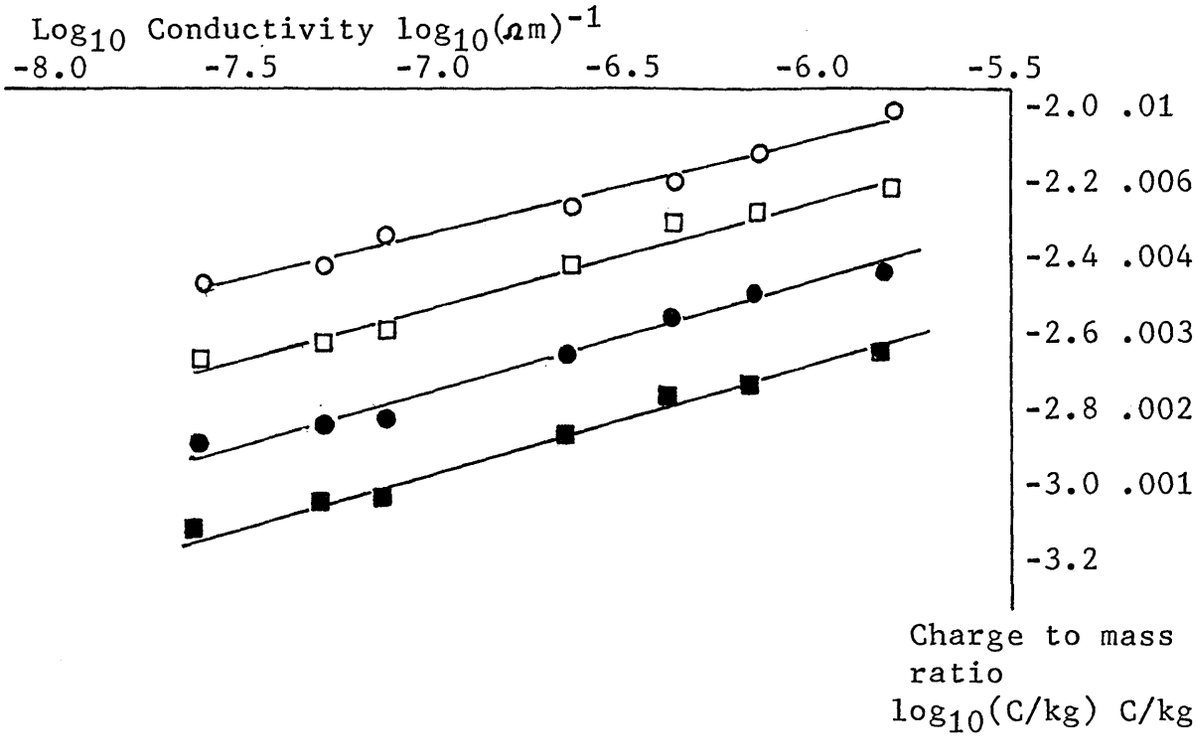

Figure 7.3 Variation of the average charge to mass ratio of the drops from a single jet with the conductivity.
○ 12 ml/h. □ 30 ml/h. ● 60 ml/h. ■ 120 ml/h.

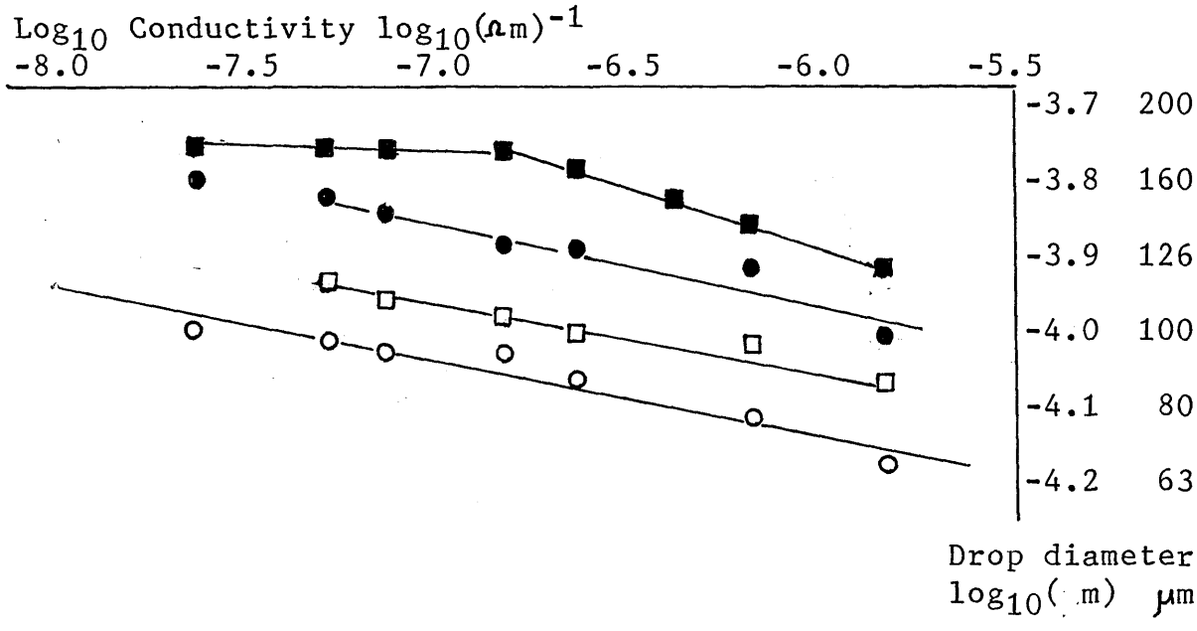

Figure 7.4 Variation of the volume median diameter of the drops from a single jet with the conductivity.
○ 18 ml/h. □ 25 ml/h. ● 35 ml/h. ■ 49 ml/h.

In chapter 5 the measurements of the length of the jet as a function of the conductivity were discussed. The extra electrical energy imparted to the liquid by increasing the number of ions was found to be reflected in the current carried by convection, rather than an increase in the degree of acceleration of the jet. It was concluded that as the conductivity increases, the charge per unit area on the surface of the jet just before the point of break up rises. Further work carried out within a certain flowrate range showed that the drop diameter is always approximately twice the diameter of the jet, irrespective of the conductivity of the liquid. The above correlations are therefore consistent with the earlier results of the effect of conductivity.

The current carried by the drops was also increased by the application of higher voltages at the capillary (figure 7.5),

$$c_m \propto V^{1.3}$$

A linear relation (figure 7.6) with the voltage was found for the drop size,

$$d \propto V^{-1}$$

The above results show that the flowrate, conductivity and voltage affect the charge carried on the drops. However, the viscosity, did not affect the charge, and had only a limited effect on the size of the drops (figure 7.7). The radius is increased by the viscosity according to

$$d \propto \mu^{0.2}$$

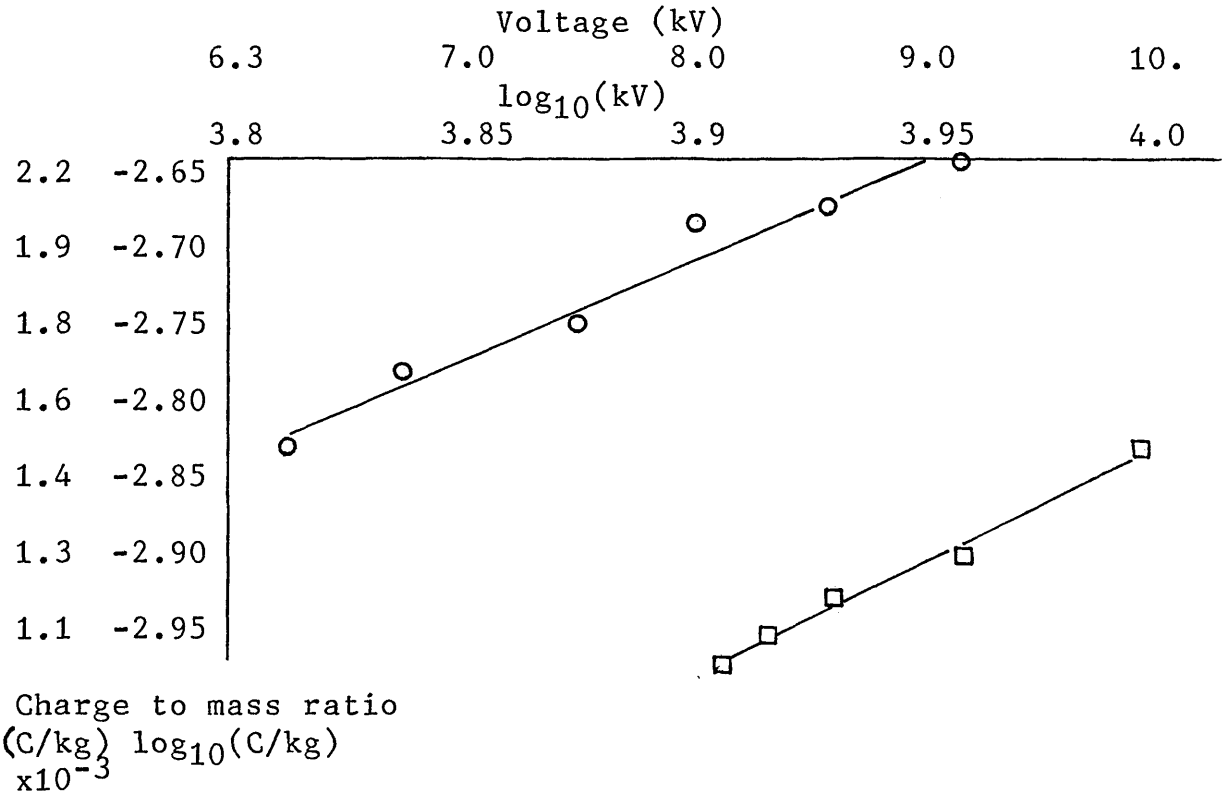

Figure 7.5 Variation of the charge to mass ratio of the drops from the single jet with the voltage.
o V_f=30 ml/h, k=5.3x10^{-8} (Ωm)$^{-1}$. □ V_f=96 ml/h, k=2x10^{-7} (m)$^{-1}$.

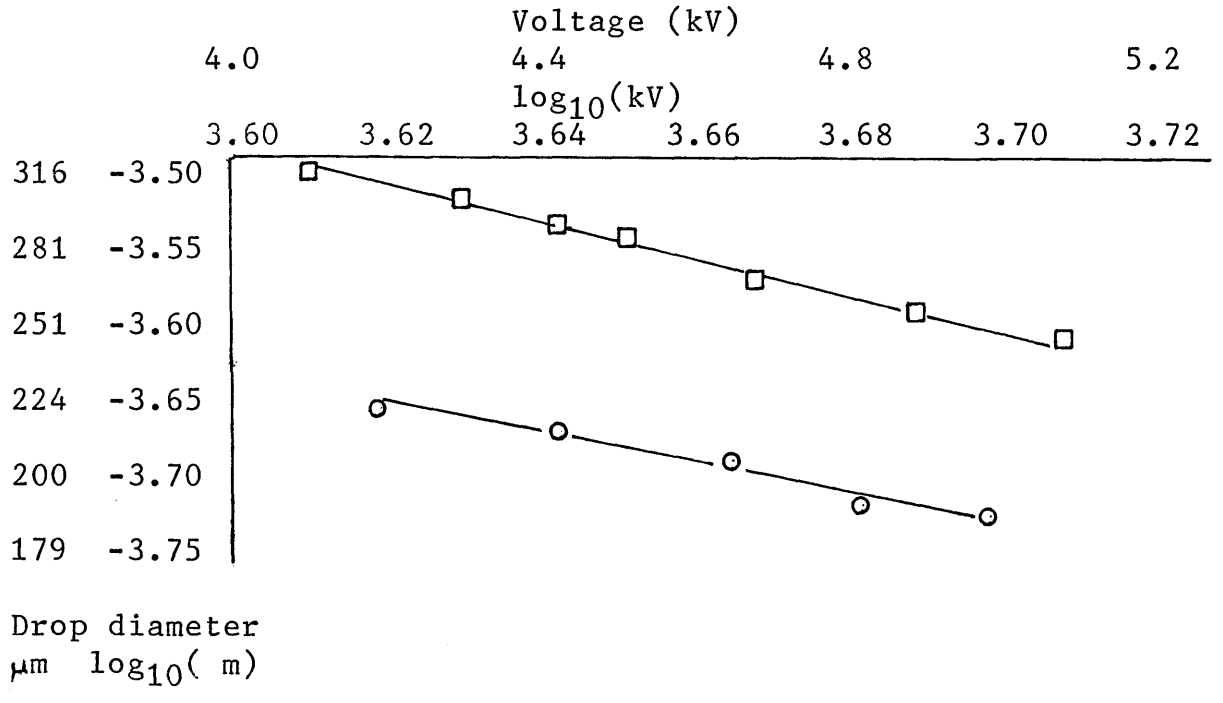

Figure 7.6 Variation of the volume median diameter of the drops from a single jet with the voltage.
o V_f = 66 ml/h. □ V_f = 96 ml/h.

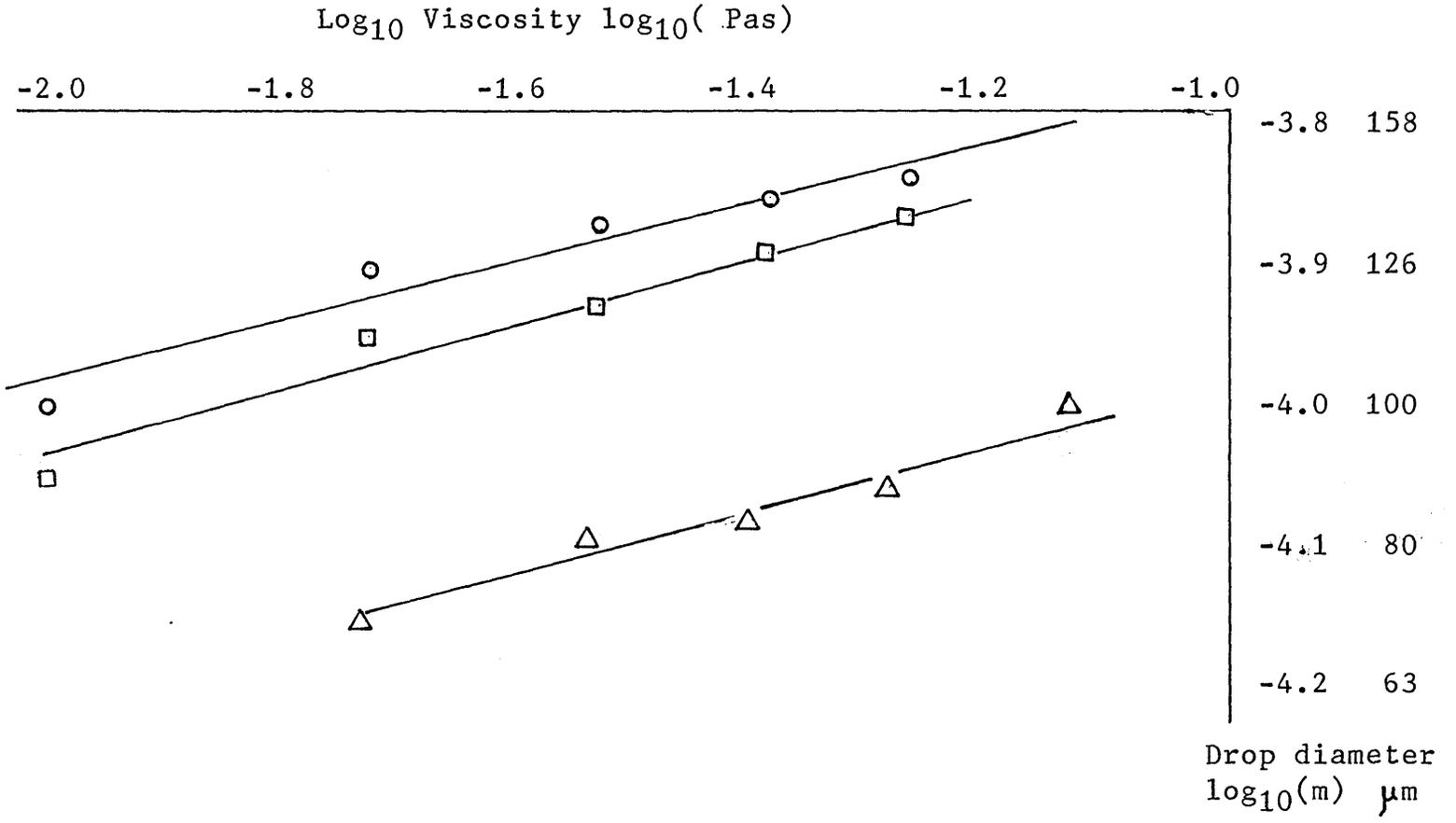

Figure 7.7 Variation of the volume median diameter of the drops from the single jet with the viscosity.
○ 25 ml/h. □ 18 ml/h. △ 6.6 ml/h.

7.2 Factors affecting the drops produced from multiple jets

The relations between the size of the drops produced from many jets and most of the parameters investigated were similar to those determined for the case of a single jet. Figure 7.8 shows the volume median diameter increases with increase in the viscosity. Again the gradient of the log-log curve gives,

$$d \propto \mu^{0.25}$$

When the flowrate supplied to the capillary is increased, the drops issuing from five jets increase in size by the relation (figure 7.9);

$$d \propto V_f^{0.59}$$

while the charge to mass ratio at two values of low conductivity decreases by an amount similar to the case of a single jet of a semi-insulating liquid (figure 7.10);

$$c_m \propto V_f^{-0.56}$$

The conductivity was found to have a limited effect on the size of the drops from a relatively large single jet. The drop size produced from the spraying of four jets at low flowrate is also found to be independent of the conductivity of the liquid (table 7.3), while the increase in the charge to mass ratio with the conductivity is the same as for one jet (figure 7.11).

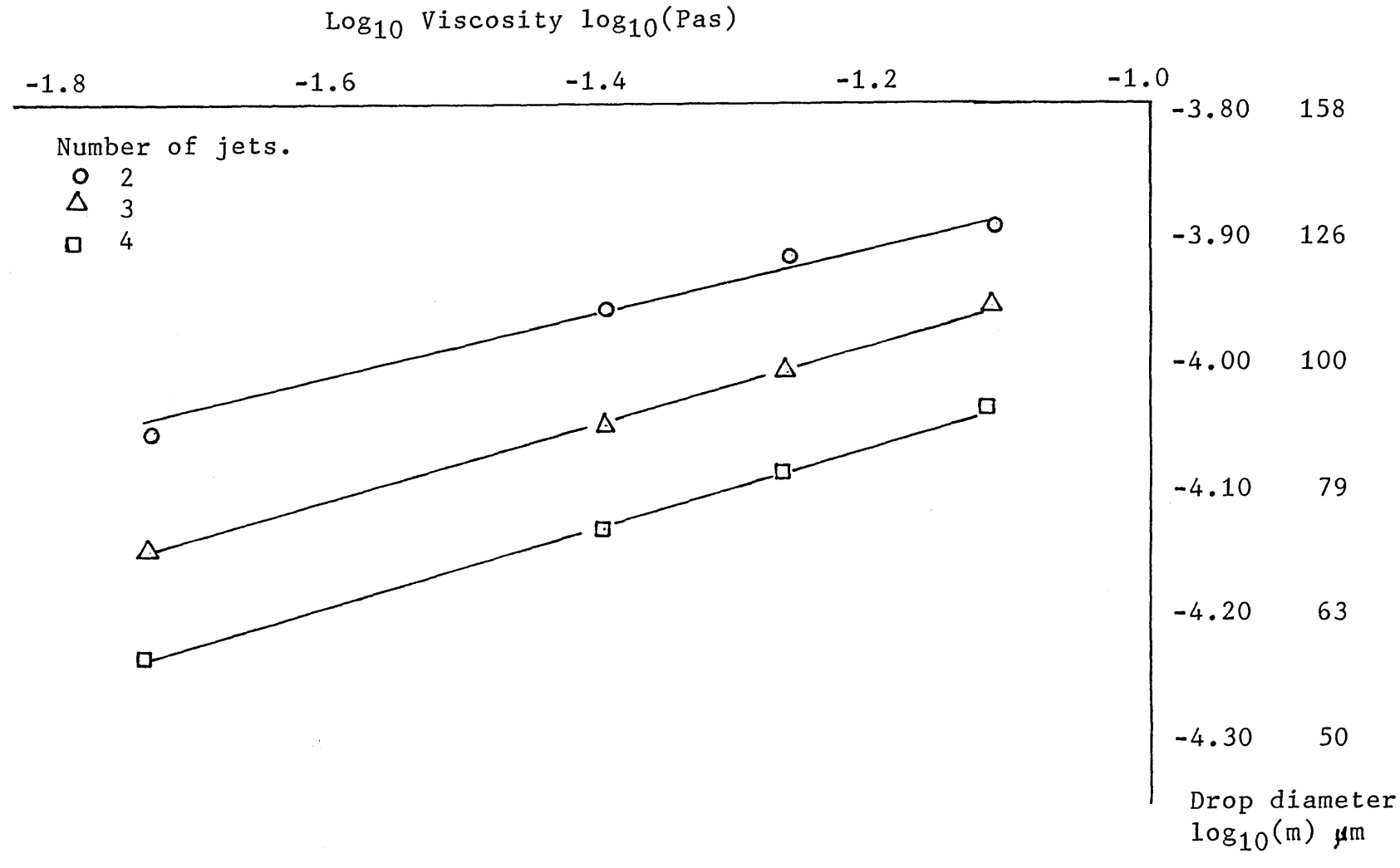

Figure 7.8 Variation of the volume median diameter of the drops from multiple jets with the viscosity. V_f = 25 ml/h. k = 2.5×10^{-8} $(\Omega m)^{-1}$.

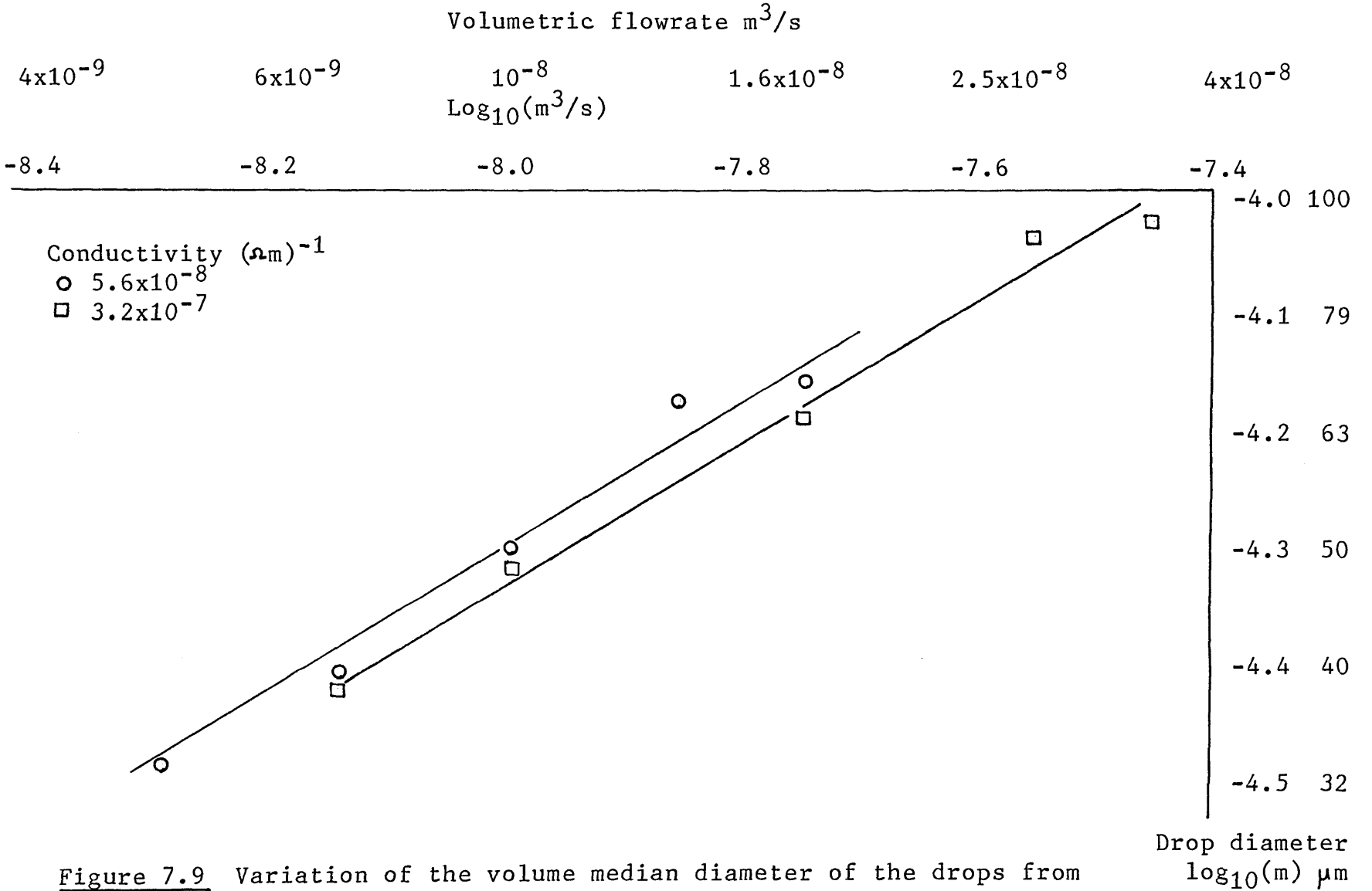

Figure 7.9 Variation of the volume median diameter of the drops from five jets as a function of the flowrate.

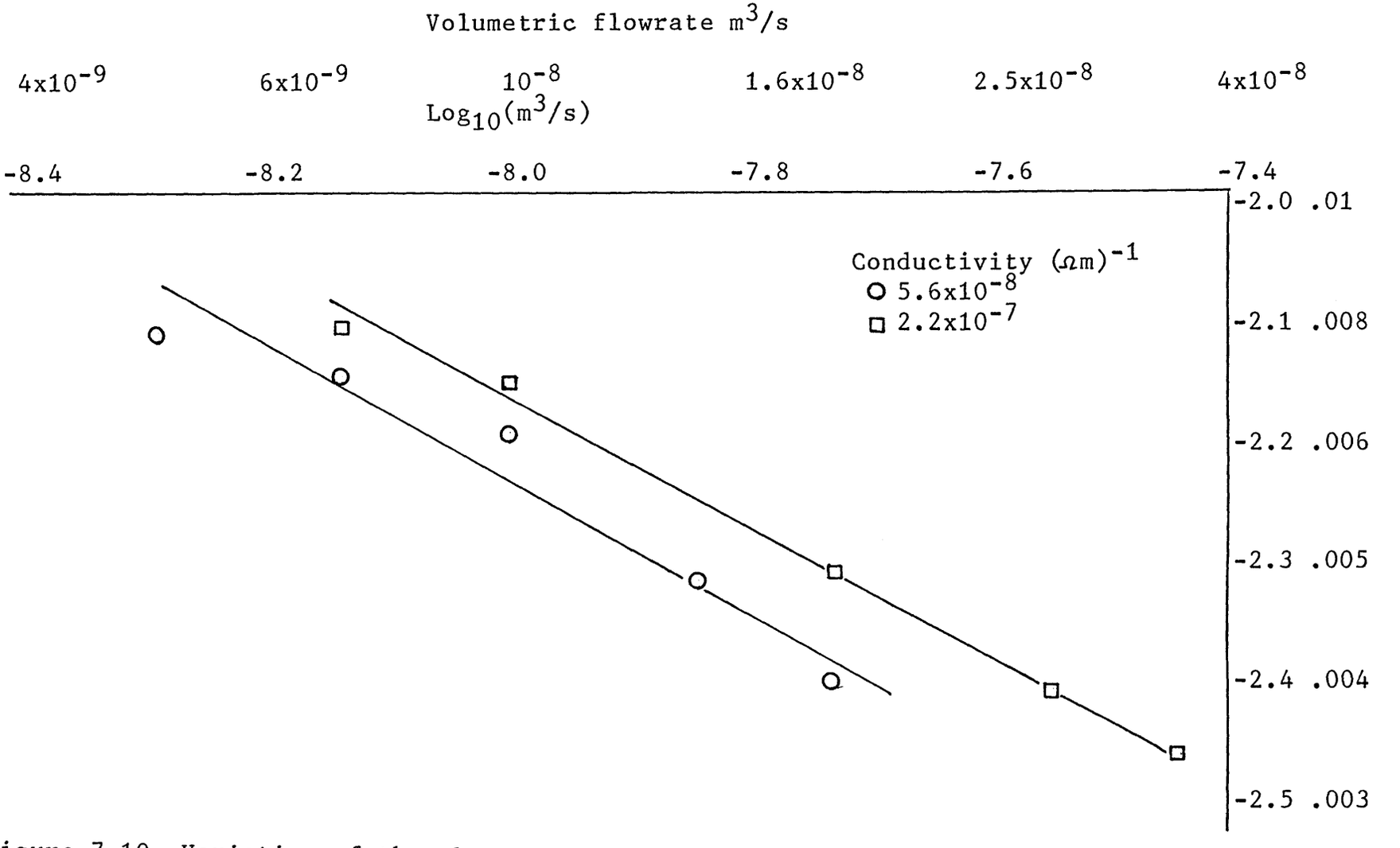

Figure 7.10 Variation of the charge to mass ratio of the drops from five jets as a function of the flowrate.

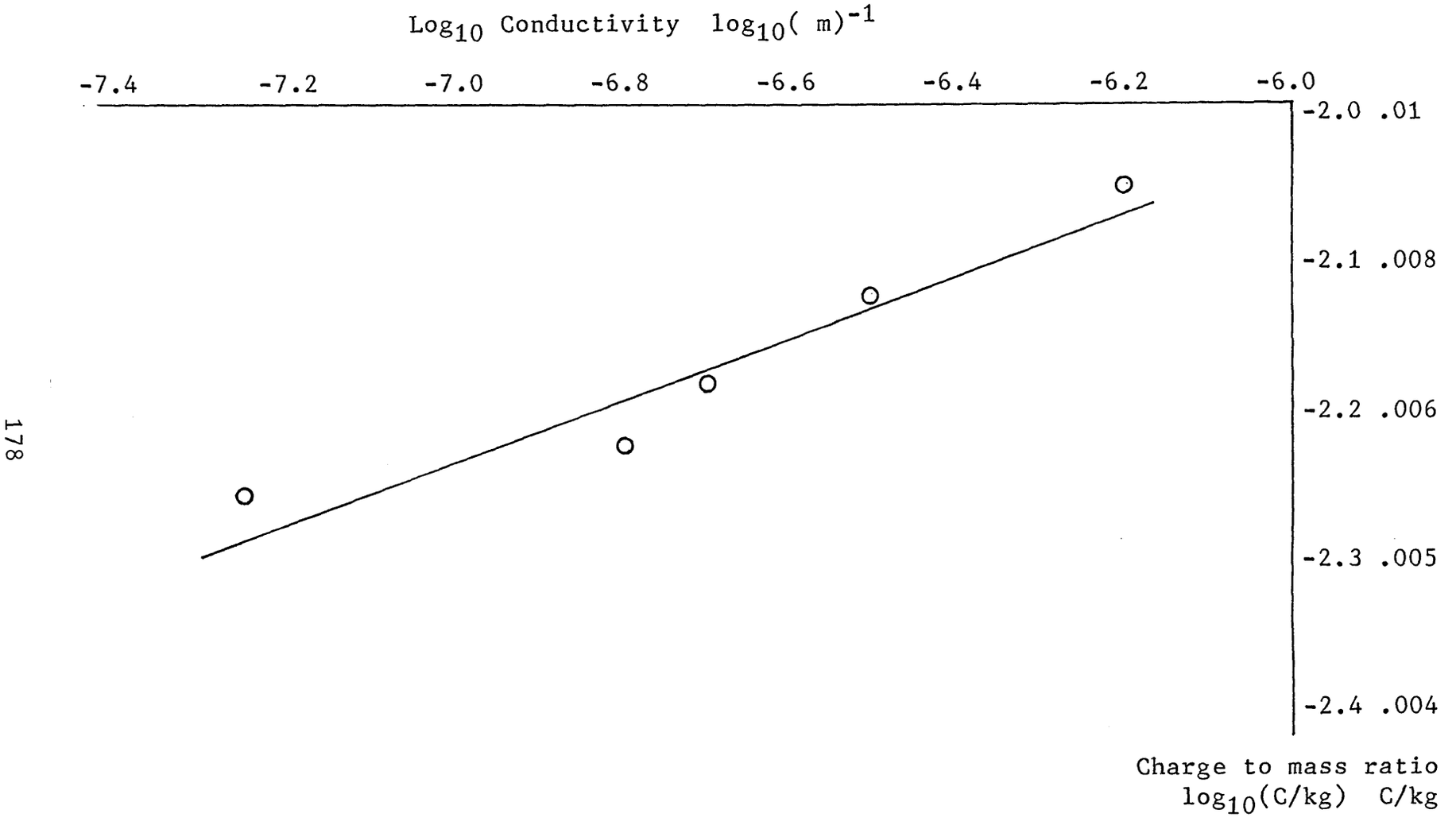

Figure 7.11 Variation of the charge to mass ratio of the drops from four jets as a function of the conductivity. V_f = 35 ml/h.

Table 7.3 The drops from four jets at 0.59 cc/min are independent of the liquid conductivity.

$k\ (\Omega m)^{-1}$	5.6×10^{-8}	1.6×10^{-7}	2.2×10^{-7}	3.2×10^{-7}	6.3×10^{-7}
Drop size (μm)	60	60	57	54	62

It is interesting to compare the factors that influence the charge and drop size from jets sprayed via a capillary with measurements in the literature for jets formed by other means. During the spraying of semi-insulating liquids from a rotary atomiser, the rotational speed causes several jets to form at the periphery of the bell. By using a combination of centrifugal forces and contact charging at high potential, the number of jets can be controlled. Correlations of the drop sizes with the flowrate and viscosity of the liquid, at constant rotational speed, are reported to be similar to those determined here for the case of the formation of multpile jets from the single capillary (64). Even at high viscosity, 2 Pas, the drop size was found to depend on the viscosity to the power 0.2. Values of the charge to mass ratio, as a function of the flowrate and conductivity of the liquid, are consistent with those found above.

Some measurements of the drop size as a function of the viscosity were taken of aerosols that are produced from the electrodyn nozzle (figure 7.12). Liquid issues from an annular gap which is about 250 μm wide. The drop size is controlled by the number of jets formed, which in turn

depends on the value of the applied voltage. Two significant differences may be identified between spraying via the nozzle and spraying from a capillary. Firstly, at the highest flowrate, a rise in the applied voltage results in a significant reduction in the drop size. This result is contrary to that observed for a capillary, where the voltage differential is high to reduce the drop size at the high flowrates. Secondly, a range of drop sizes is produced from the electrodyn nozzle at the high flowrate, which is absent for the case of spraying conducting liquids from the capillary. These differences appear to be due to the large surface area of the nozzle edge available to the liquid, to reduce the density of space charge around each jet, as well as due to the fine size of the annulus, which creates high field strengths.

An important feature of the process of spraying through many jets is the increase in number along the edge of the capillary with the applied voltage. The formation of more jets is accompanied by the production of smaller drops. For a particular number of jets, a slight increase in the voltage did not cause the liquid to form another jet. A change in the drop size could not be detected by the measurement technique used when the voltage was increased slightly at a particular number of jets. Providing the relation between the diameter of the drops and the diameter of the jet remains constant, regardless of the numbers of jets formed, this result can be related to size of the jets. Unlike the relatively larger single jet that is formed at low values of the field, a particular number of jets do not become progressively thinner on the application of higher voltage, until the liquid responds to emit larger numbers of jets.

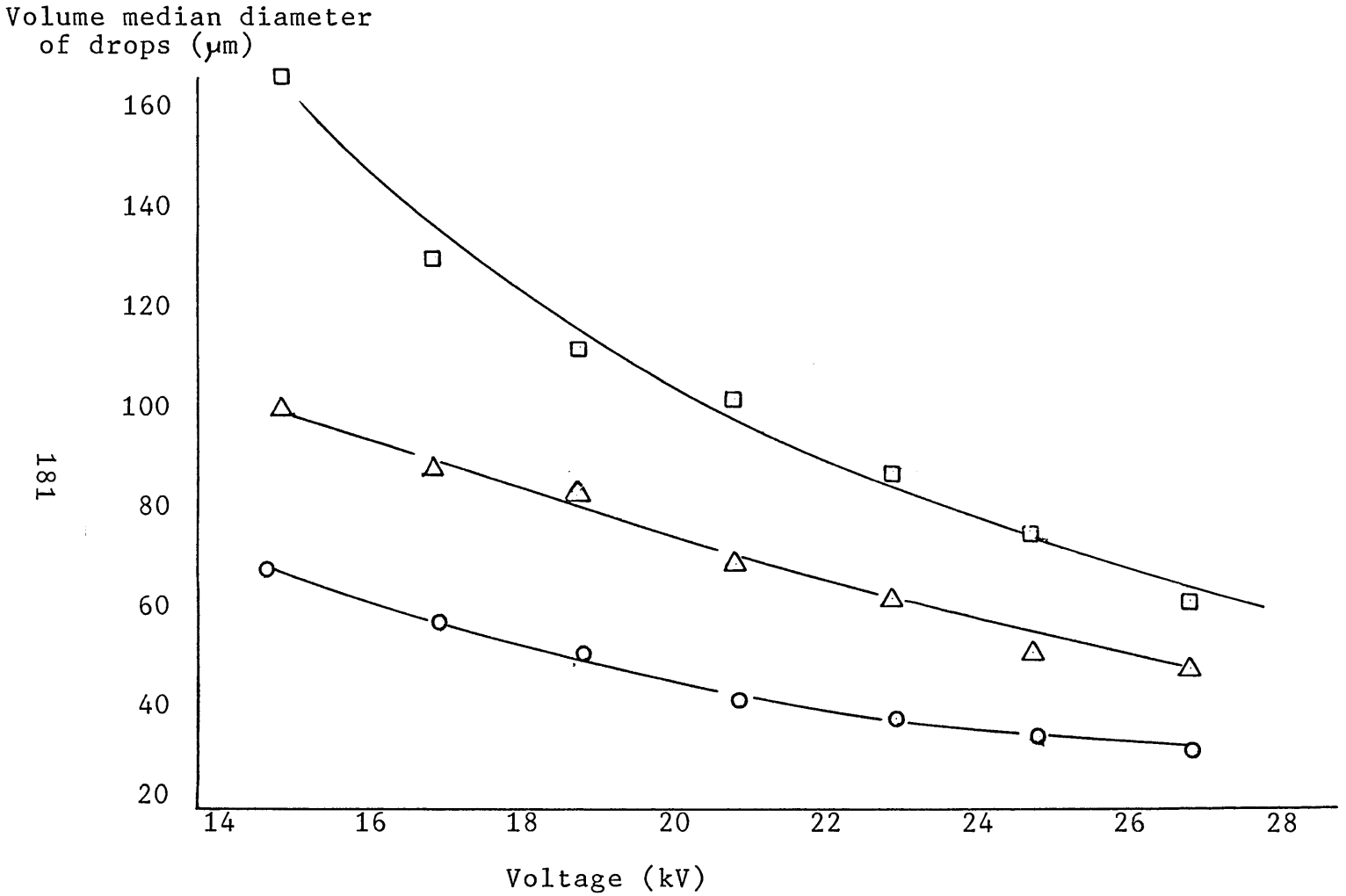

Figure 7.12 The variation of the diameter of the drops from an electrodyn nozzle with the voltage applied. The number of jets issueing from the nozzle increases with the voltage.

○ V_f = 84 ml/h. △ V_f = 180 ml/h. □ V_f = 336 ml/h

Several jets are formed with relative ease, at lower voltages, when the flowrate is low (figure 7.13). However the demands on the electrical energy rise at higher values of the flowrate. Another interesting observation from the plot is the larger drops that result during the first stage of multiple jets when the flowrate is high (the largest drops on each line represent the single jet). At 96 ml/h, when the liquid is sprayed as five jets, the drop size is 95 μm, whereas the formation of three jets at 25 ml/h results in 53 μm drops.

The relation between the drop size and the voltage applied is also affected by the conductivity of the liquid. Figure 7.14 illustrates that smaller drops are produced at a particular voltage for the higher conductivity. The inability of the more conducting liquids to produce large drops at high flowrates can be seen in both figures 7.14 and 7.15. These small drops are emitted from many jets, while the lower jet numbers are not attained under these conditions.

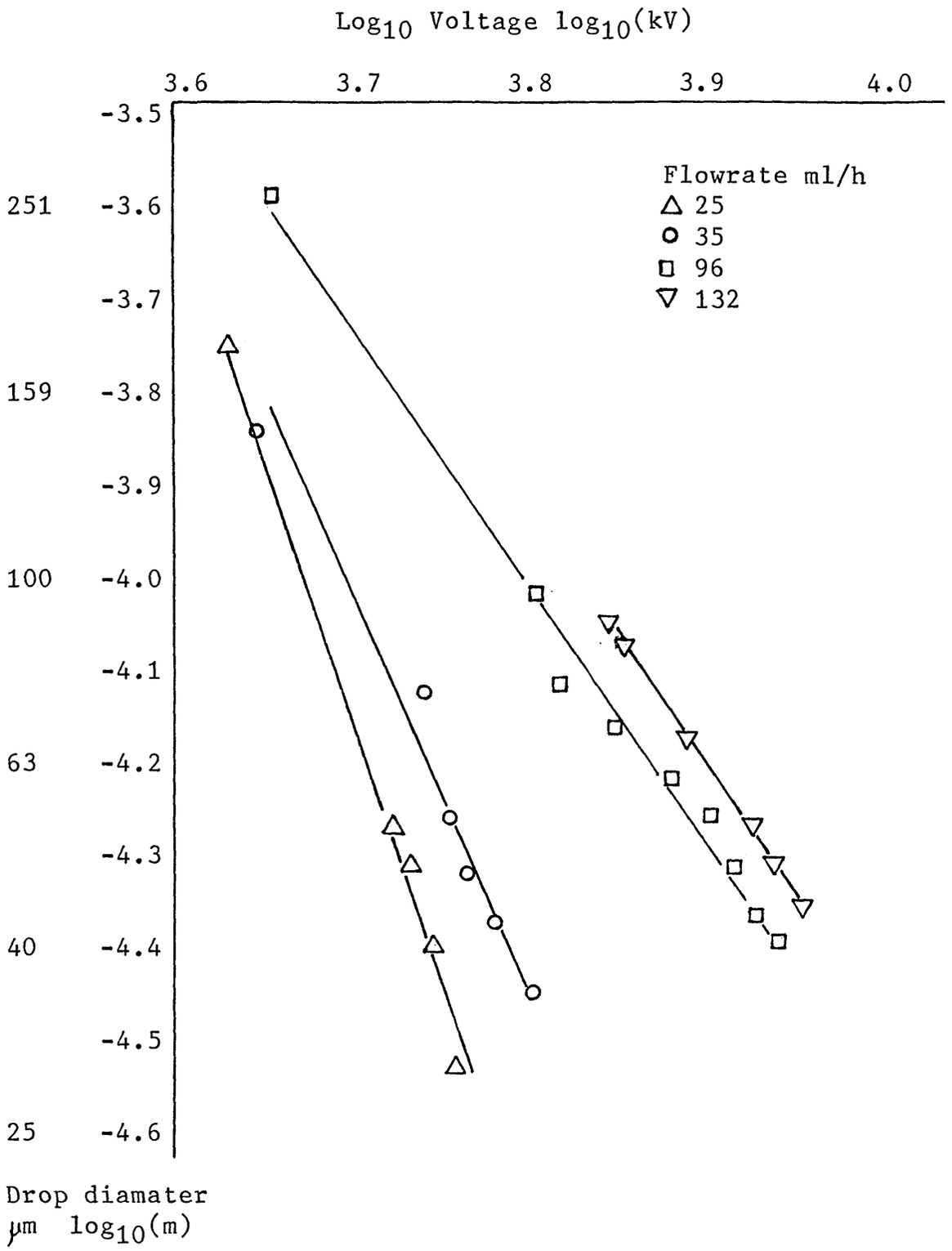

Figure 7.13 Variation of the diameter of the drops from the multiple jets with the voltage applied. The number of jets increases with the voltage. $k = 1.5 \times 10^{-7}\ (\Omega m)^{-1}$.

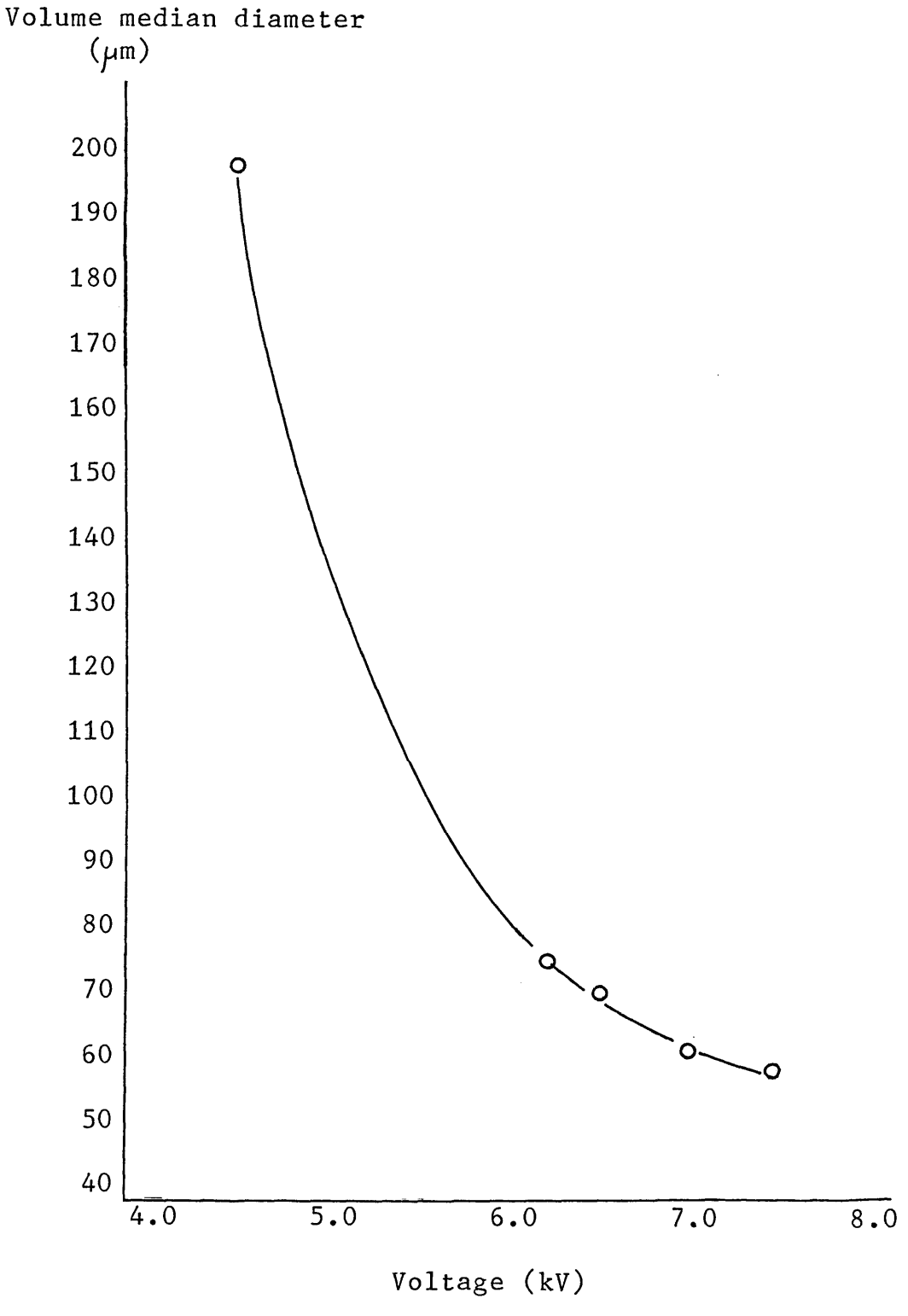

Figure 7.14 The drop size produced from conducting jets as a function of the voltage applied.
$k = 2.7 \times 10^{-7}$ $(\Omega m)^{-1}$. V_f = 66 ml/h.

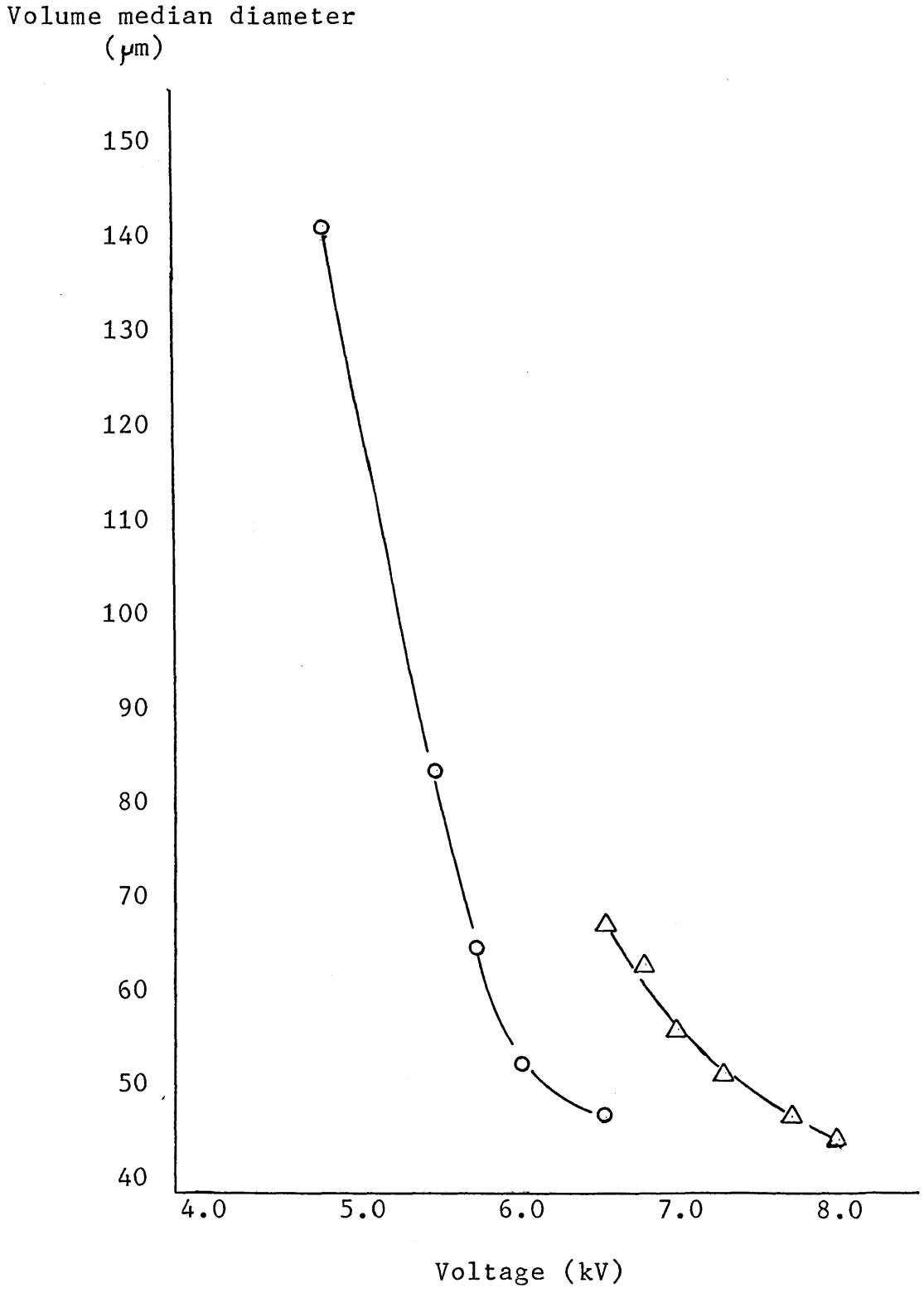

Figure 7.15 The drop size from multiple jets as a function of the voltage applied. $k = 6.46 \times 10^{-7}$ $(\Omega m)^{-1}$
o V_f = 35.4 ml/h. Δ V_f = 96 ml/h.

7.3 Reasoning behind the formation of higher numbers of jets and the changes occuring to the single jet .

A range of average drop sizes can be emitted from the multiple jets, depending on the properties of the liquid, the voltage applied and the flowrate. Conversely, the same drop size can result under different sets of conditions. Where the spray characteristics are similar, the jets which yield the drops, under the different conditions, must also be similar in some way. The diameter of drops has been related to the diameter of the jet for the single jet. Comparative measurements for the formation of multiple jets could not be made due to the fineness of the jets. Nevertheless, the drop size is determined by the number of jets formed, if all other conditions are constant.

Increasing the jet number is equivalent to reducing the volumetric flowrate in each of the jets. Therefore attention was directed to the drop size and charge obtained when different numbers of jets, that are formed at different liquid flowrates, can be characterised as being similar by virtue of the flowrate in each jet. Table 7.4 gives the size and charge to mass ratio at constant flowrate per jet for three values of the conductivity. When the jets carry the same flowrate, the charge to mass ratios and drop sizes produced are virtually the same.

Once it became apparent that the spraying of liquids at high flowrates, through more jets, is a scale up to the situation in which fewer jets are formed at the lower flowrates, the drop sizes and charges were compared for the cases of a single jet and multiple jets. Table 7.5 is a list of the measured values, again with the flowrate per jet kept constant. If the criteria for comparison are the charge to mass ratio and the diameter of the drops, then providing the flowrate carried in each jet is comparable, the behaviour of several jets is similar to the behaviour of a single jet.

This conclusion is supported by the similarity of the trends observed for the drop diameter and the charge to mass ratio when the parameters under investigation are varied. The power dependencies are almost the same for spraying as an ensemble of jets and as a single jet. When the jet number is high and small drops are produced, the conductivity has little effect on the size due to the low flowrate per jet. Similarly, no change in size with conductivity was detected for a single jet at low flowrate.

The extensive study of the average charging levels and average drop sizes has provided an insight into the effect of high field. As the voltage is increased, the liquid is dispersed in progressively thinner jets. The significance of forming several jets is the reduction of the flowrate and a reduction of the current carried by each of the jets. For any conductivity liquid, the charge per unit mass remains constant as long as the flowrate of the jet is constant. However, the charge to mass rise with an increase in the jet number, as the flowrate of each jet is reduced.

Table 7.4 Drop size and charge from several jets when the flowrate per jet is constant.

Conductivity = 1.58×10^{-7} $(\Omega m)^{-1}$

Flowrate (ml/h)	Jet number	Flowrate per jet (ml/h)	Drop size (μm)	Charge to mass (C/kg)
66.0	6	10.8	60	6.14×10^{-3}
49.2	4	12.6	68	6.04×10^{-3}

Conductivity = 2.23×10^{-7} $(\Omega m)^{-1}$

Flowrate (ml/h)	Jet number	Flowrate per jet (ml/h)	Drop size (μm)	Charge to mass (C/kg)
35.4	3	12.0	72	5.09×10^{-3}
66.0	5	13.2	68	5.11×10^{-3}
96.0	7	13.2	70	5.16×10^{-3}
35.4	5	7.2	51	7.12×10^{-3}
66.0	9	7.2	49	6.68×10^{-3}

Conductivity = 3.16×10^{-7} $(\Omega m)^{-1}$

Flowrate (ml/h)	Jet number	Flowrate per jet (ml/h)	Drop size (μm)	Charge to mass (C/kg)
35.4	3	12.0	65	6.36×10^{-3}
49.2	4	12.6	70	6.06×10^{-3}
66.0	5	13.2	70	5.87×10^{-3}
35.4	4	9.0	54	7.50×10^{-3}
66.0	8	8.4	51	6.82×10^{-3}

Table 7.5 Drop size and charge from a single jet compared to the values obtained from several jets.

Conductivity = 5.62×10^{-8} $(\Omega m)^{-1}$

Flowrate (ml/h)	Jet number	Flowrate per jet (ml/h)	Drop size (μm)	Charge to mass (C/kg)
35.4	4	9.0	60	5.59×10^{-3}
9.0	1	9.0	65	5.50×10^{-3}
35.4	5	7.2	50	6.36×10^{-3}
6.6	1	6.6	43	5.93×10^{-3}

Conductivity = 2.24×10^{-7} $(\Omega m)^{-1}$

Flowrate (ml/h)	Jet number	Flowrate per jet (ml/h)	Drop size (μm)	Charge to mass (C/kg)
96.0	5	19.2	95	4.00×10^{-3}
18.0	1	18.0	90	4.25×10^{-3}

Conductivity = 3.16×10^{-7} $(\Omega m)^{-1}$

Flowrate (ml/h)	Jet number	Flowrate per jet (ml/h)	Drop size (μm)	Charge to mass (C/kg)
96.0	4	24.0	90	3.72×10^{-3}
25.2	1	25.2	107	3.57×10^{-3}
96.0	5	19.2	87	4.69×10^{-3}
18.0	1	18.0	83	4.74×10^{-3}
35.4	3	11.8	65	6.36×10^{-3}
12.6	1	12.6	71	5.71×10^{-3}
35.4	5	7.2	45	8.77×10^{-3}
6.6	1	6.6	47	8.86×10^{-3}

The estimation of the charge density at the surface of the jets, just before the point of drop emission, provides an explanation of how higher charge per unit mass is carried by the formation of higher numbers of jets. Close to the capillary, the current is carried by conduction, but as the jets accelerate away from the capillary, the ions reach the surface and all the current is carried by convection. The convection current is imparted to the drops, so that measurements of the current together with the diameter and flowrate of the jets can be used to calculate the surface charge density. All the current is carried by convection through n_j jets, each of equal radius r_j and velocity u_j,

$$n_j 2\pi r_j u_j \varepsilon_o E_n = I_t \qquad \text{Eqn. 7.1}$$

where $\varepsilon_o E_n$ is the charge density on the surface of each of the jets. The total volumetric flowrate supplied to the capillary is constant and is given by,

$$n_j \pi r_j^2 u_j = V_f$$

Substuiting into equation 7.1,

$$\varepsilon_o E_n = \frac{I_t r_j}{2V_f} \qquad \text{Eqn. 7.2}$$

The value of the radius of the jet is assumed to be half the radius of the drops. Values of the charge density on each jet are plotted against the number of jets formed in figure 7.16. The increase in the voltage is implied on the x-axis as the jet number increases. A rise in the voltage causes a rise in the measured current I_t. In order to maintain constant charge per unit area, the liquid forms new surfaces by emitting more jets. The final radii attained by the jets, just before disintegration into drops, is such that the increase in the total area is comparable to the

increase in the total charge.

In figure 7.16, the parameters are the conductivity of the liquid and the flowrate at the tip of the capillary. Although the charge density remains constant for one set of conditions, a particular number of jets can maintain varying charge densities depending on the conductivity.

When a single jet is formed, the flowrate of the jet can only be varied by use of the pump. Calculations of the charge density, using the value of the final radius before drops are emitted from the single jet, are plotted against the flowrate in figure 7.17. As the flowrate increases, the number of ions reaching the capillary per unit time rises. Although the current increases, the charge per unit mass falls. It may be seen that the radius of the single jet increases in order to keep the charge density constant. So the increase in the jet diameter, required to maintain constant charge density on the surface of the jet, leads to the emission of larger drops, having lower charge to mass ratios. The three lines in figure 7.17 correspond to different conductivities, with the value of constant charge density increasing as the conductivity rises.

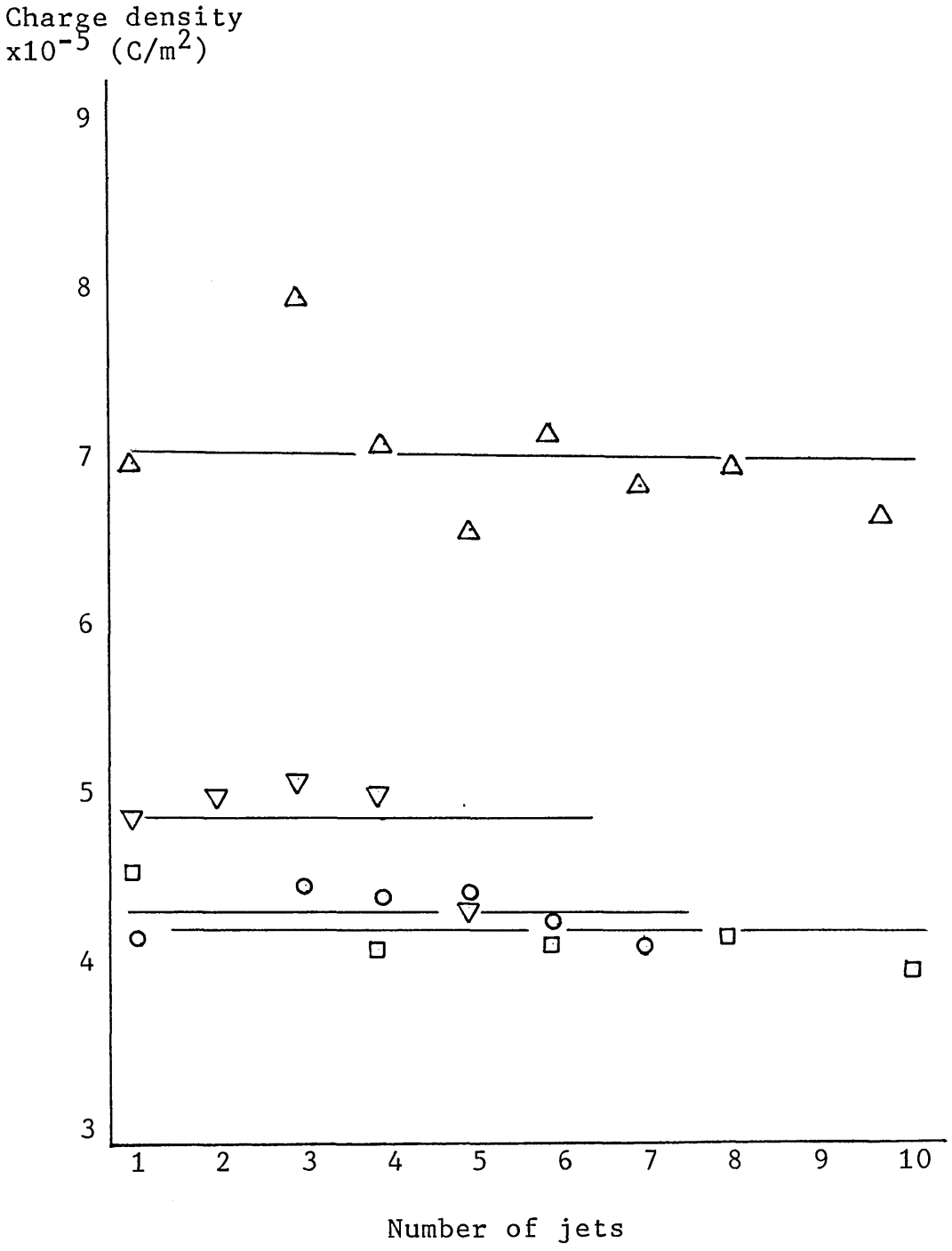

Figure 7.16 The charge density on the surface of the jets against the number of jets formed. The increase in the applied voltage is implied along the x-axis.

○ k = 1.52 x 10^{-7} $(\Omega m)^{-1}$. V_f = 35 ml/h.
▽ k = 2.8 x 10^{-7} $(\Omega m)^{-1}$. V_f = 35 ml/h.
□ k = 2.8 x 10^{-7} $(\Omega m)^{-1}$. V_f = 96 ml/h.
△ k = 6.5 x 10^{-7} $(\Omega m)^{-1}$. V_f = 35 ml/h.

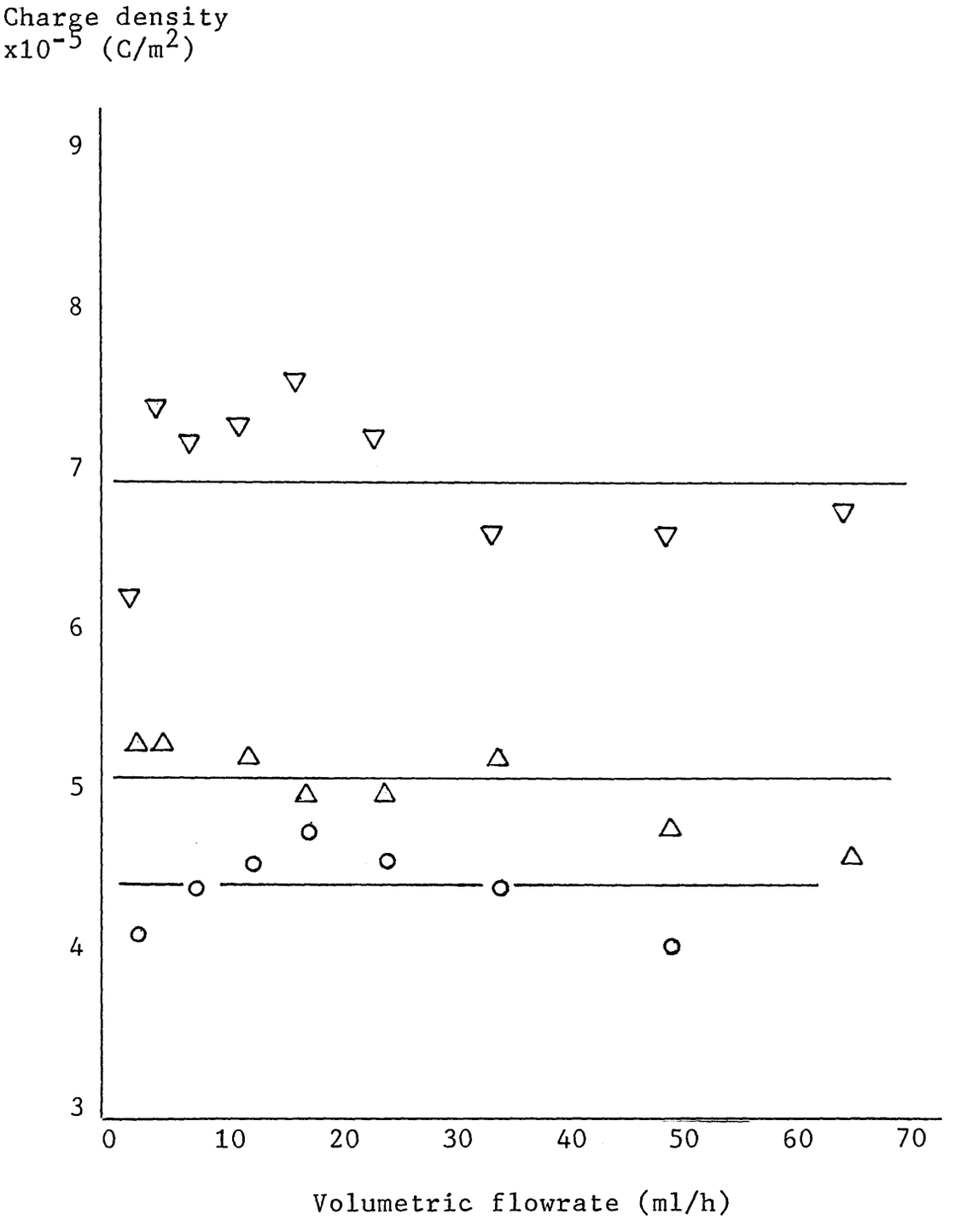

Figure 7.17 The charge density on the surface of the single jet as a function of flowrate.

○ $k = 5.6 \times 10^{-8}\ (\Omega m)^{-1}$
△ $k = 3.2 \times 10^{-7}\ (\Omega m)^{-1}$
▽ $k = 1.0 \times 10^{-6}\ (\Omega m)^{-1}$

Considering the effect of the conductivity of the liquid alone, higher charge densities can be carried by both the single jet and an ensemble of jets when liquids of higher conductivity are sprayed. Measurements of the drop diameter showed that drop size is only dependent on the conductivity to a small extent. In the case of the single jet, the drop size begins to decrease with increasing conductivity, when the flowrate is high. However the correlations of the charge to mass ratios show that the main effect of the conductivity is higher charging of the slightly smaller drops. Since the drop size and jet size are related, it may be concluded that the final radius attained by the single jet remains virtually constant with an increase in the conductivity. Hence it may be assumed that the time spent by the liquid as a jet is constant, (the velocity of the cylindrical portion of the jet is unchanged), so that the times available for charge to reach the surface of the liquid are comparable for jets of different conductivity liquids. However, the times taken for charges to reach the surface of the jets decrease with the conductivity. As a consequence, the jet not only carries more current as the conductivity increases, but also a higher density of charge at the surface. The drops produced from the disintegration of the jet become more charged and therefore approach the Rayleigh limit for a perfectly conducting drop , as the conductivity increases. In figure 7.18 the rise in conductivity is implied on the y-axis, as the charge to mass ratio increases. The theoretical values of charge per unit mass were calculated from the Rayleigh limit using the measurements of the drop diameters.

The drops from several jets are almost always smaller than those produced from the single jet. As more jets are formed, the flowrate carried by each jet decreases, the size of the drops becomes independent of the conductivity. In figure 7.19 the increase in the measured charge to mass

ratio at constant diameter is compared with the charge to mass ratio calculated using the Rayleigh limit. The measurements of the charge to mass ratio increase with the conductivity of the liquid. The plot applies to the formation of four jets from the edge of the capillary, at a flowrate of 36 ml/h. It may be be seen that the effect of the conductivity is the production of drops having charge to mass ratios that approach the Rayleigh limit. When the highest conductivity liquid is sprayed, the charge on the drops is more than half that predicted for a perfectly conducting drop.

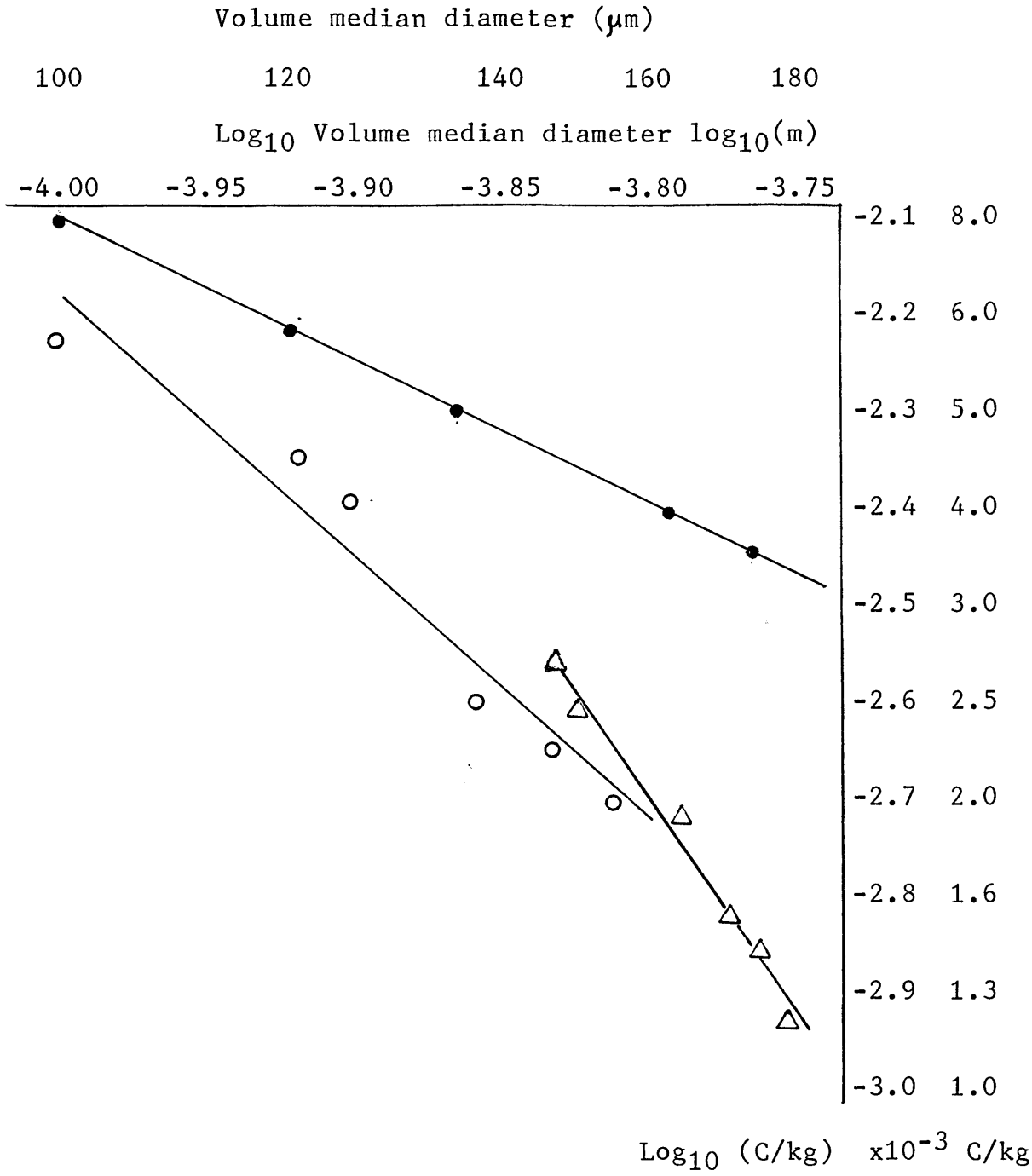

Figure 7.18 The charge to mass ratio of the drops from the single jet against the drop size. The smaller drops are produced from spraying higher conductivity liquids. Measured values of the ratio are compared with the Rayleigh prediction.

Measured values; ○ V_f=35 ml/h, △ V_f=49 ml/h.
● Rayleigh prediction.

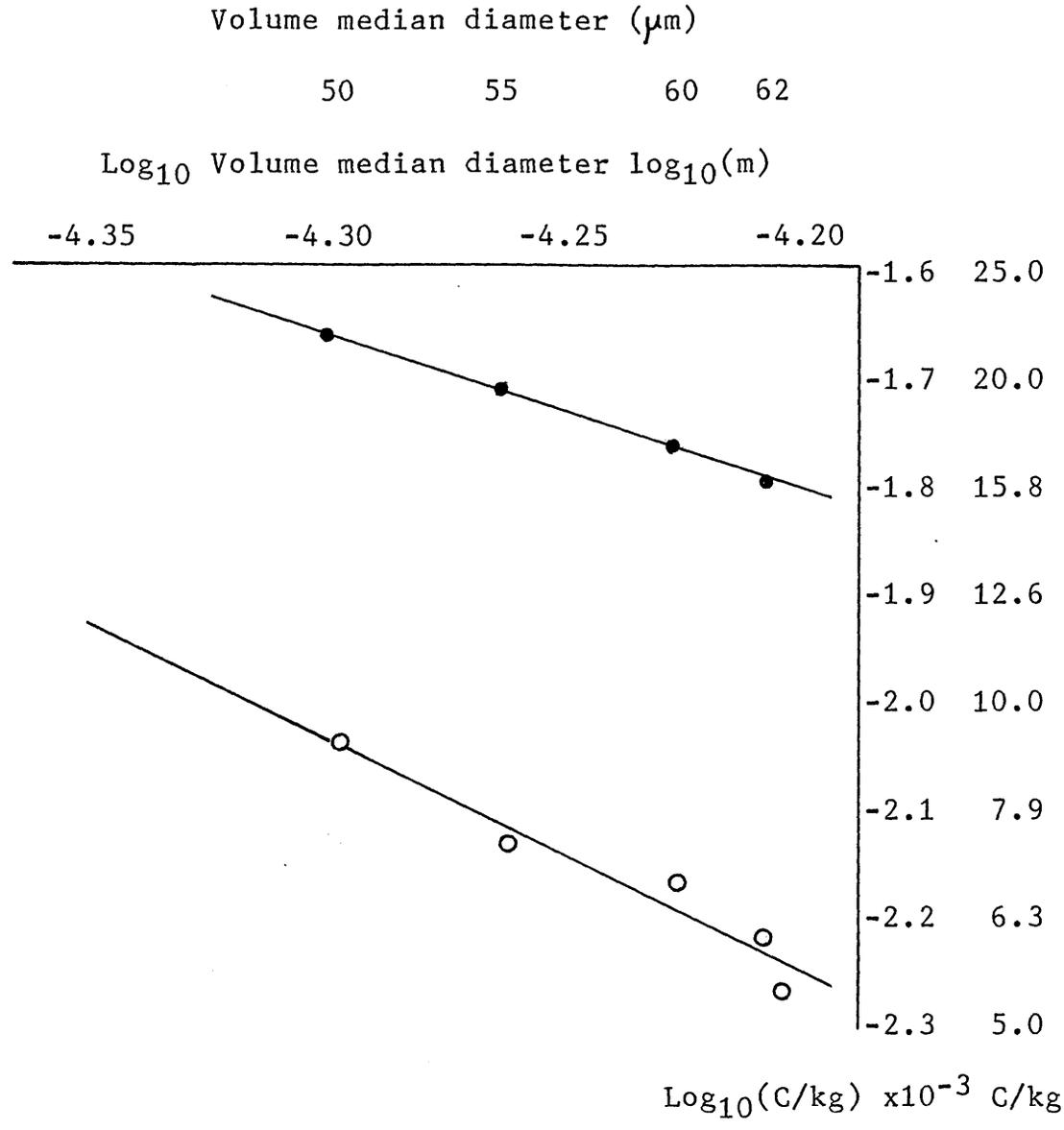

Figure 7.19 The charge to mass ratio of drops from four jets as against the drop size. The conductivity decreases with the drop size. The measured ratios are compared with values from the Rayleigh prediction.

o Measured values V_f = 35 ml/h. • Rayleigh prediction.

7.4 The dependence of diameter on the charge and the prediction of the drop size.

A plot of the average median diameter of the drops against the average charge to mass ratio shows that smaller drops result from the greater charge imparted to the liquid, figure 7.20. A band of points may clearly be seen, due to the different dependencies of the drop size on the charge. The varying dependencies can be identified when the parameters under investigation are considered separately. In the case of the single jet, for a variation of the flowrate, the drop size correlates with the charge to mass ratio according to;

$$d \propto c_m^{-1.0}$$

The correlation for the formation of multiple jets is similar, as the flowrate is varied;

$$d \propto c_m^{-0.9}$$

These dependencies have been explained in terms of the charge density on the surface of the jets before the point of drop emission. It has been shown that the jet attaines its final radius such that the change in surface area corresponds to the change in the charge carried. The above correlations can therefore be interpreted in the light of equation 7.2, which expresses the convection of current by the jets.

When liquids having succesively higher conductivities are sprayed as a single jet, the charge on the jets increases significantly, which has a minor effect on the size;

$$d \propto c_m^{-0.4}$$

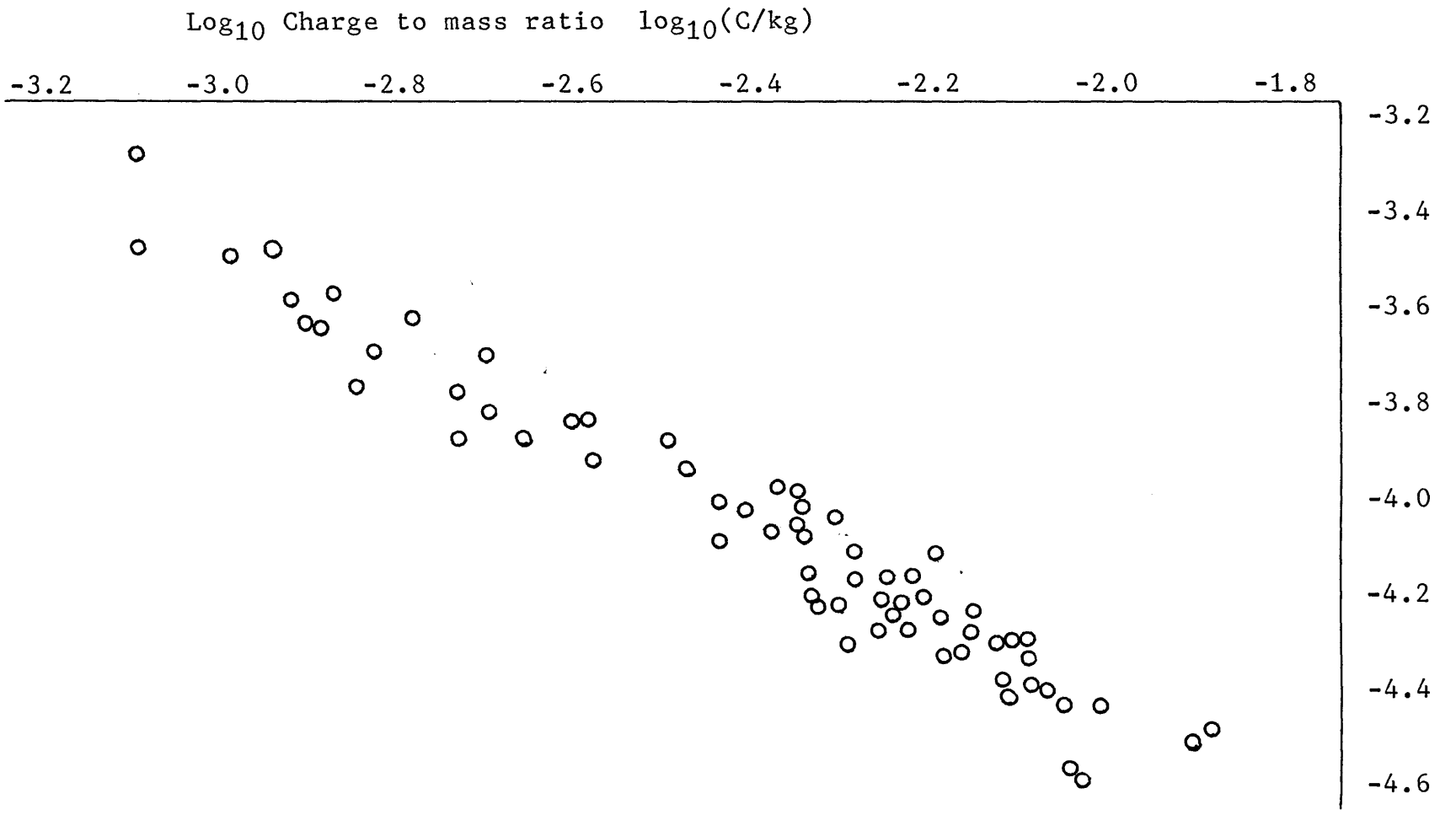

Figure 7.20 The diameter of the drops issuing from both the single jet and multiple jets as a function of the average charge to mass ratio

The above correlation applies to figure 7.18, where it is apparent that the measured values approach the values predicted for a conductor.

Theories that are available for the prediction of the drop size rely on a knowledge of the current carried by the drops. The diameter is usually evaluated from the known charge to mass ratio, but the size is proportional to varying powers of the ratio, depending on the analysis. The method used by Jones and Thong (67) involves estimation of the field intensity at the tip of the capillary, as well as measurements of the volumetric flowrate and current carried by a single jet. The field was derived from the estimation of the charge per unit length along the capillary (eqns. 3.10 and 3.11) using the method of images. The charge density at the metal tip was assumed to be completely imparted to the jet. Moreover, the voltage drop over the length of the jet was considered to be negligible. Once the areas corresponding to the different surfaces, from which a drop is formed, were related to the spherical surface of the drop, an equation was found for the drop size i.e.,

$$d = \frac{27\sqrt{2}\varepsilon_o E_c}{4\rho c_m} \qquad \text{Eqn. 7.3}$$

Equation 7.3 is applicable to the specific situation of a single jet emerging from a metal capillary. Others have developed analyses that are valid for a range of spraying modes. In the work of Vonnegut and Neubauer (31), a liquid of known initial volume and charge is thought to be disrupted into a number of equisized drops, each of uniform charge. The final state of the liquid, as drops, is determined by first summing the energies of the drops. It is assumed that the total energy of the drops is minimised during the disruption process. The most probable drop size

was found to be equal to half the value determined from the Rayleigh criterion,

$$d = \frac{3(\varepsilon_o \gamma)^{1/2}}{\rho c_m^{2/3}} \qquad \text{Eqn. 7.4}$$

Pfeifer and Hendrick's (33) analysis is an extension of the work, with the added assumption that the initial volume of liquid holds the Rayleigh limit of charge at its surface. Further, the sum of the surface tension and electrical energies is held constant. With the total energy constant, the surface tension energy rises as the number of drops formed increases. The analysis minimises the electrical energy, while maximising the surface tension energy of the drops. From eqn. 3.56, the drop size is related to the minimal charge by,

$$d = \frac{1.34(\varepsilon_o \gamma)^{1/2}}{\rho c_m^{2/3}} \qquad \text{Eqn. 7.5}$$

These equations apply to either the case of a jet which is sufficiently conducting that it carries all the charge from the capillary, or to a more general case in which the process by which the liquid is dispersed is not defined, and energy considerations dictate the final state of the liquid mass as drops. In these approaches, the finite conductivity of the liquid is not taken into account. In practice, only liquids with conductivities within a certain range may be sprayed as a steady single jet from the end of a capillary. The range of conductivity is determined by comparing the time taken for the ions to reach the surface of the liquid with the time taken to form a drop at the tip of the capillary. When a jet is formed, all the current is eventually carried by the convection of the jet, near the

point of disintegration into drops. The drop size may be predicted from the radius of the jet by equating the time for drop formation to the charge relaxation time;

$$\frac{r_j}{u_j} = \frac{\varepsilon}{k}$$

The radius and velocity of the jet are linked by continuity, and using the relation $d=1.87r_j$, gives;

$$d = 3.74\left(\frac{\varepsilon V_f}{k}\right)^{1/3} \qquad \text{Eqn. 7.6}$$

Predictions of the drop diameter from eqns. 7.3, 7.5 and 7.6 are compared with experimental values in figure 7.21. Measurements of the drop diameter and the charge to mass ratio of the drops were taken as a function of the flowrate. The analysis for the conducting jet gives the best fit to the measured values, while the equation which expresses energy minimisation predicts a different relation between the diameter and the charge to mass ratio. Similarly, eqn 7.6 gives an underestimate of the dependence of the diameter on the flowrate. Correlations of the measurements have determined that the diameter is proportional to the flowrate to the power 0.63.

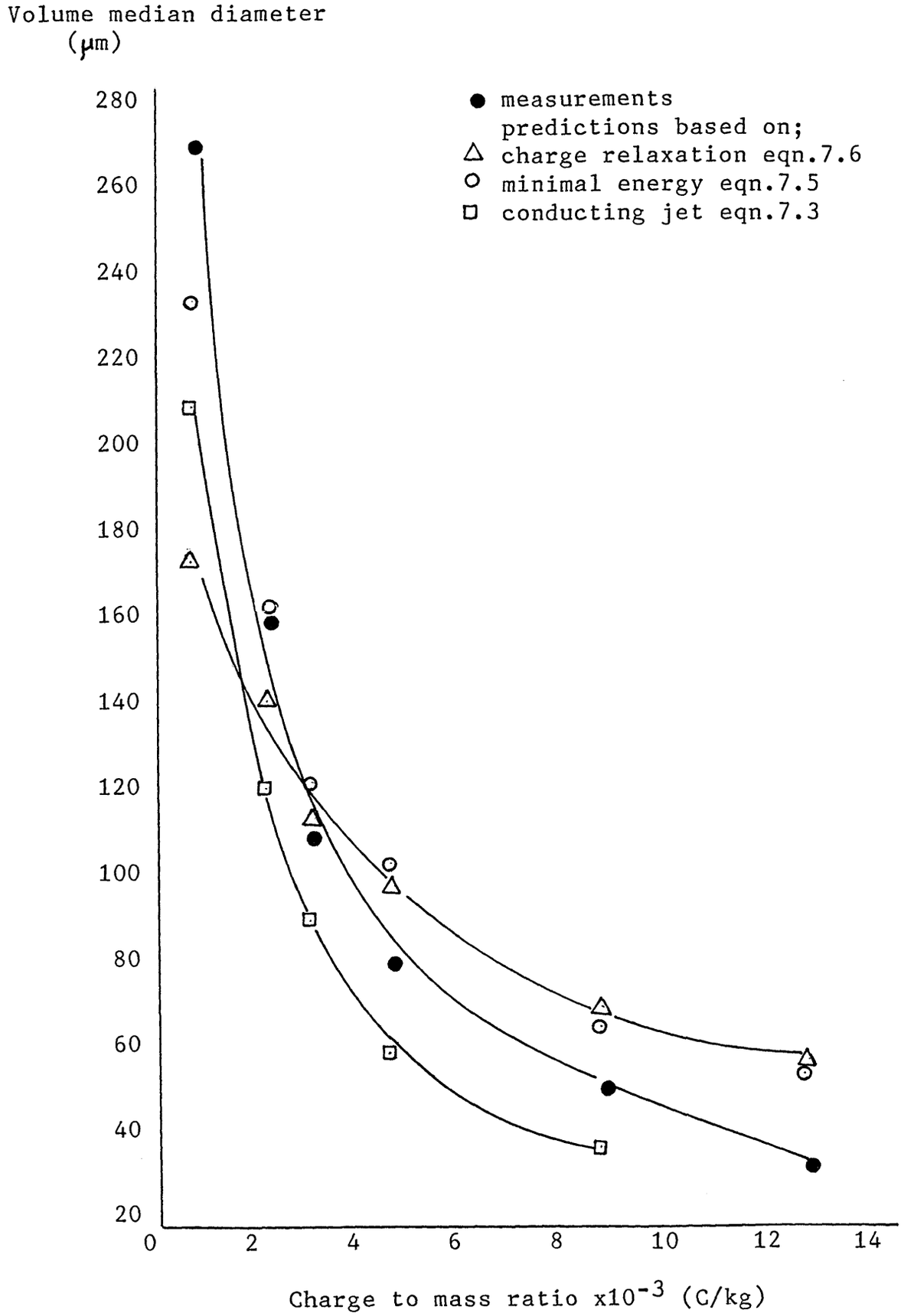

Figure 7.21 The size of the drops from the single jet as a function of the charge to mass ratio. Predicted values are compared with measurements. k = 2.78x10^{-7} $(\Omega m)^{-1}$. The drop size varies as the flowrate is varied.

Another analysis is used here to predict the drop size, which takes into account the voltage drop over the length of the jet. The prediction is based on an overall power balance of the electrical energy given to the jet, and the flow of the jet. A rigorous treatment would include all the forces acting at each horizontal segment of the jet. The estimation of the electrical forces acting over the length of the jet, however, involves prior knowledge of the jet profile. The balance is considerably simplified by making the following assumptions; if the jet is considered to be a straight cylinder, having constant uni-directional velocity, then the electrical power imparted to the liquid is partly converted into the kinetic energy of the jet, and partly used to overcome the surface tension forces that would otherwise cause the jet to form into a drop. The electrical power consumed by the jet, as the voltage falls over the length, is equated to the power used to produce kinetic energy and the power used to overcome the surface tension of the jet;

$$I_t V_c - I_t V_e = \frac{1}{2} \rho V_f u_j^2 + 2\pi r_j u_j \gamma \qquad \text{Eqn. 7.7}$$

where I_t is the total current, V_c and V_e are, respectively, the voltages at the capillary and at the end of the jet where the drops are formed. It is assumed that the jet is long enough for the voltage at the end of the jet to be related to the voltage at the boundary of the earthed electrode. At a radial distance equal to the radius of the earthed collector, the voltage is zero. The final voltage of the jet is found using the normal field on the jet surface.

$$- \frac{dV}{dr} = E_n$$

The field is given by the convection of the current;

$$E_n = \frac{I_t}{\varepsilon_o 2\pi r_j u_j}$$

from which it follows,

$$\int_{V_g}^{V_e} dV = -\int_{r_g}^{r_j} \frac{I_t}{\varepsilon_o 2\pi r u_j} dr$$

where $V_g=0$ and r_g is the radius of the earthed collector.

The voltage at the end of the jet is therefore;

$$V_e = \frac{I_t}{2\pi u_j \varepsilon_o} \ln\left[\frac{r_g}{r_j}\right]$$

Equation 7.7 now becomes,

$$I_t V_c - \frac{I_t^2}{2\pi u_j \varepsilon_o} \ln\left[\frac{r_g}{r_j}\right] = \frac{1}{2}\rho V_f u_j^2 + 2\pi r_j u_j \gamma \qquad \text{Eqn. 7.8}$$

All the parameters in eqn. 7.8 are known, apart from the radius of the jet. The velocity can be expressed in terms of the radius by the use of the continuity equation. Eqn. 7.8 was solved iteratively, by first guessing the value of the radius, and then calcuating the velocity. The value of the radius was then refined until the equation was balanced.

The predicted results are compared with the measured values in figure 7.22, for two liquids of different

conductivity. The former is in all cases an underestimate of the size. The inconsistency between the prediction and the measured values is partly due to the assumption that the jet is cylindrical over all of its length. Photographs of the jet show a cone region near the tip of the capillary, as well as a fall in the diameter over a portion of its length until the final radius is reached. Moreover, equation 7.8 is a balance in which the power due to the normal electrical stress, the surface tension and kinetic energies only are included. The tangential stress and the force of gravity, both factors which cause the jet to accelerate, have not been taken included. Despite the disageement, a log-log plot of the predicted values against the flowrate has shown that the radius of the jet is proportional to the flowrate to the power 0.64. This compares well with the power dependency of 0.63 that was determined empirically.

The volume median diameters plotted in the figures presented in this chapter are the averages for a range of drop sizes in the spray cloud, produced under any one set of conditions. When the conditions are changed so as to vary a parameter, the distribution of drop sizes is also affected.

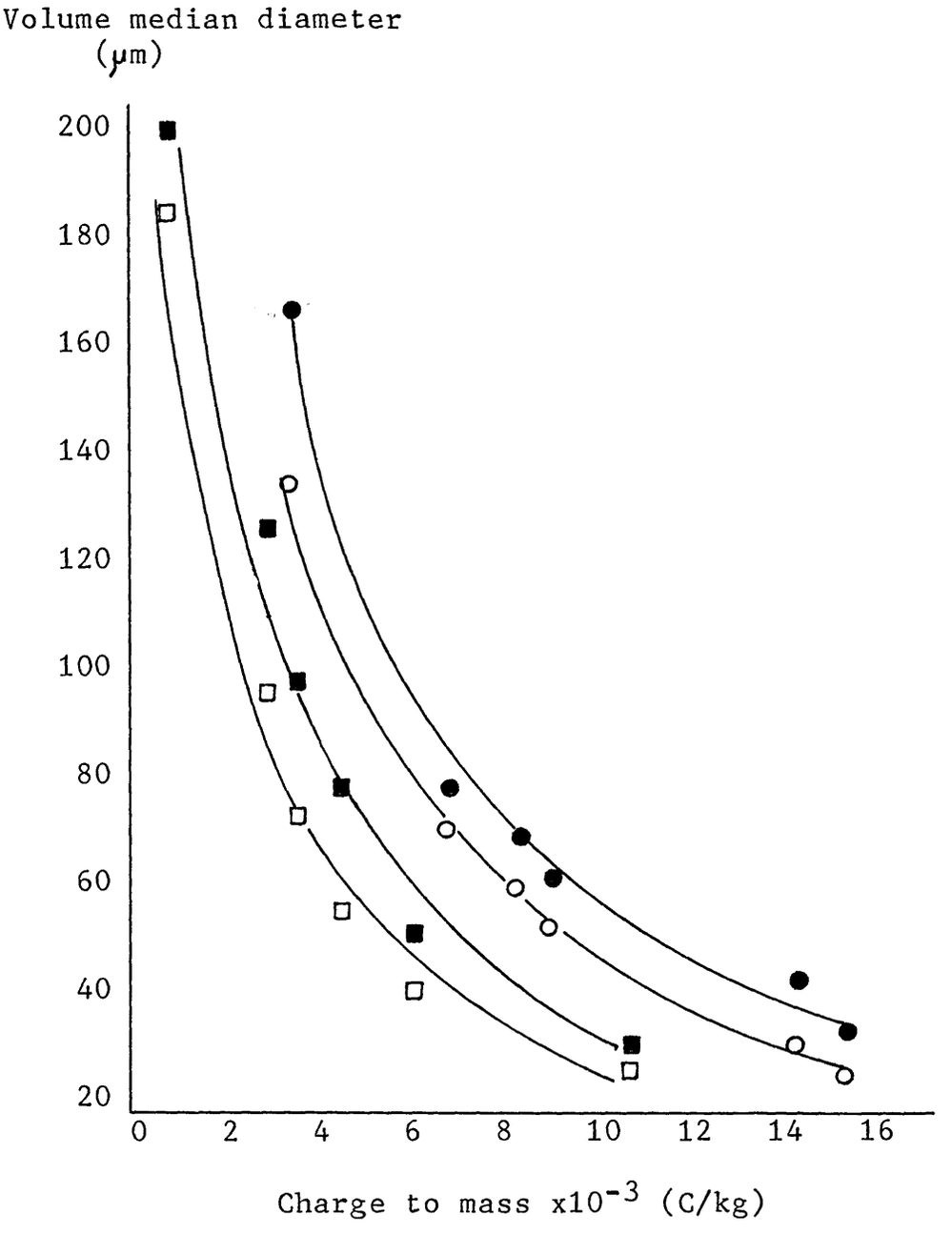

Figure 7.22 The prediction of the drop size from a single jet using the power balance(eqn.7.8). The drop size changes as the flowrate is varied.
Measured values; ■ k = 5.6×10^{-8} $(\Omega m)^{-1}$. ● k = 10^{-6} $(\Omega m)^{-1}$.
Predicted values; □ k = 5.6×10^{-8} $(\Omega m)^{-1}$. ○ k = 10^{-6} $(\Omega m)^{-1}$.

7.5 Size distributions of the drops.

Of the parameters that have been investigated in this study, the flowrate has been found to have the greatest effect on the range of drop sizes emitted. Figure 7.23 shows the bar charts for the case of increasing the flowrate of the single jet of a liquid of conductivity 3.2×10^{-7} $(\Omega m)^{-1}$. As the flowrate rises, the distributions become more polydisperse, until at a value of 49 ml/h, when a bimodal distribution appears. It is significant that jets of larger diameter disintegrate to give a wider range of sizes. The production of several sizes suggests that drops are emitted from the jet before the amplitude of the growth of a wave reaches the value of the jet radius. Liquid in the regions between the growths break off from the jet to form the smaller drops.

It may also be speculated that the velocity of the jet has an influence on the degree of polydispersity. Higher flowrates lead to higher values of the average drop size and lower values of the velocity of the jet. If the velocity of the wave growing on the jet is equal to that of the jet, then the external electric field at the end of the jet may cause liquid to be pulled off before a drop is fully formed.

When the voltage is increased to form more jets at the edge of the capillary, the distribution becomes more monodisperse (figure 7.24). As the number of jets increases from 2 to 4, at a constant value of the total flowrate, the flowrate of each jet is reduced. Thus the monodisperse nature of the sprays from multiple jets can be linked to the flowrate effect. The formation of thinner jets results in the emission of more uniform sizes.

For the case of the single jet, increasing the voltage had little influence on the range of sizes. However, the distribution is narrowed when the current carried by the

jet rises by virtue of the conductivity of the liquid (figure 7.25).

Another parameter of the liquid, the viscosity, was found to lead to polydisperse sprays (figure 7.26). The three bar charts are for liquids of viscosity 17.4, 30, and 57 mPas. Photographs of the break up of viscous jets are presented in chapter 5 (figure 5.9). In the figure, a mass of liquid consisting of several wavelengths can be seen to be emitted from the end of the jet. Not only does the viscosity interfere with "wavelength"emitted from the jet, it also acts to link a mass undergoing detachment from the jet with the end of the jet.

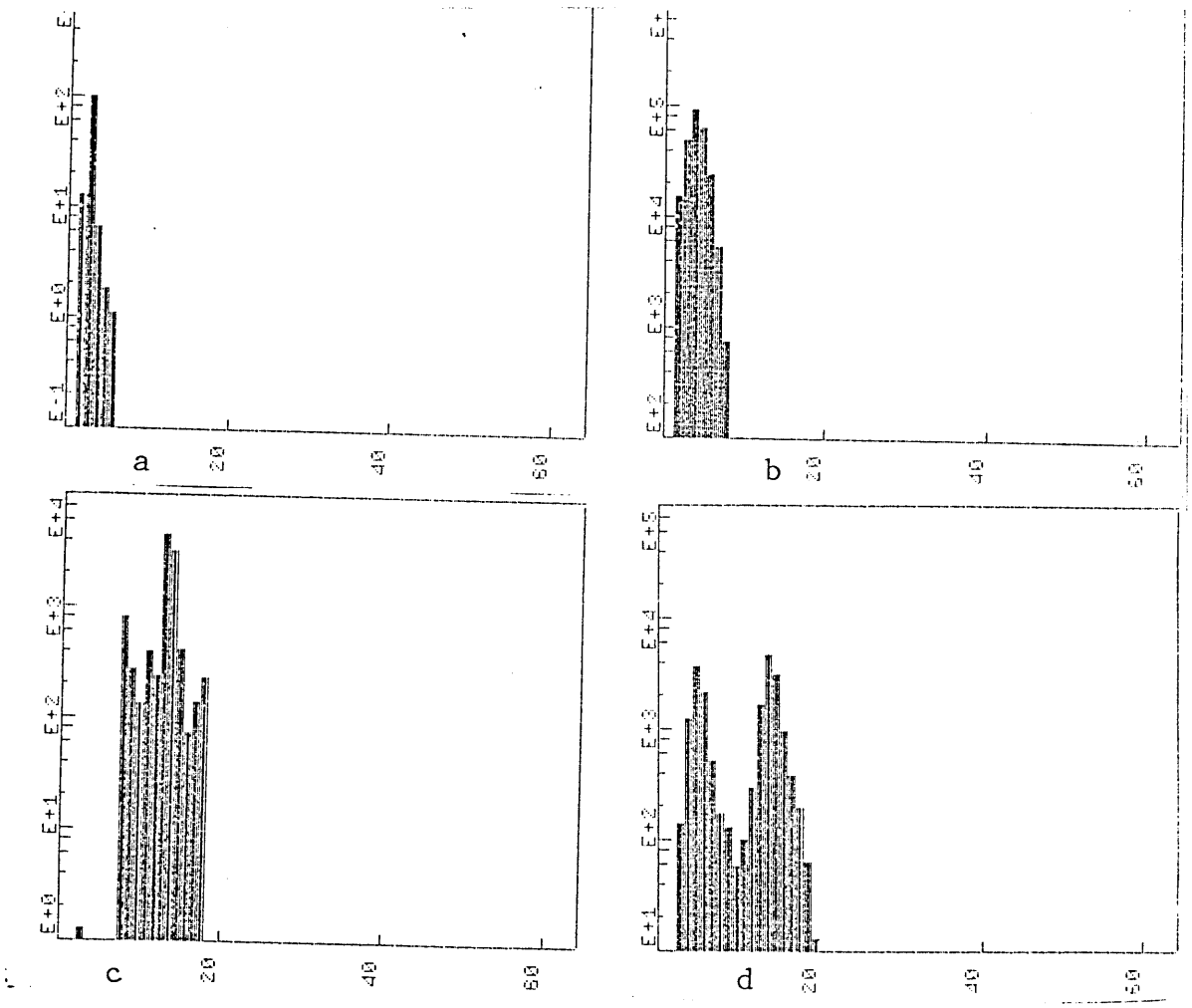

Figure 7.23 Bar charts showing the range of sizes.
(a) 4.5 ml/h. (b) 9.0 ml/h. (c) 35 ml/h. (d) 49 ml/h.

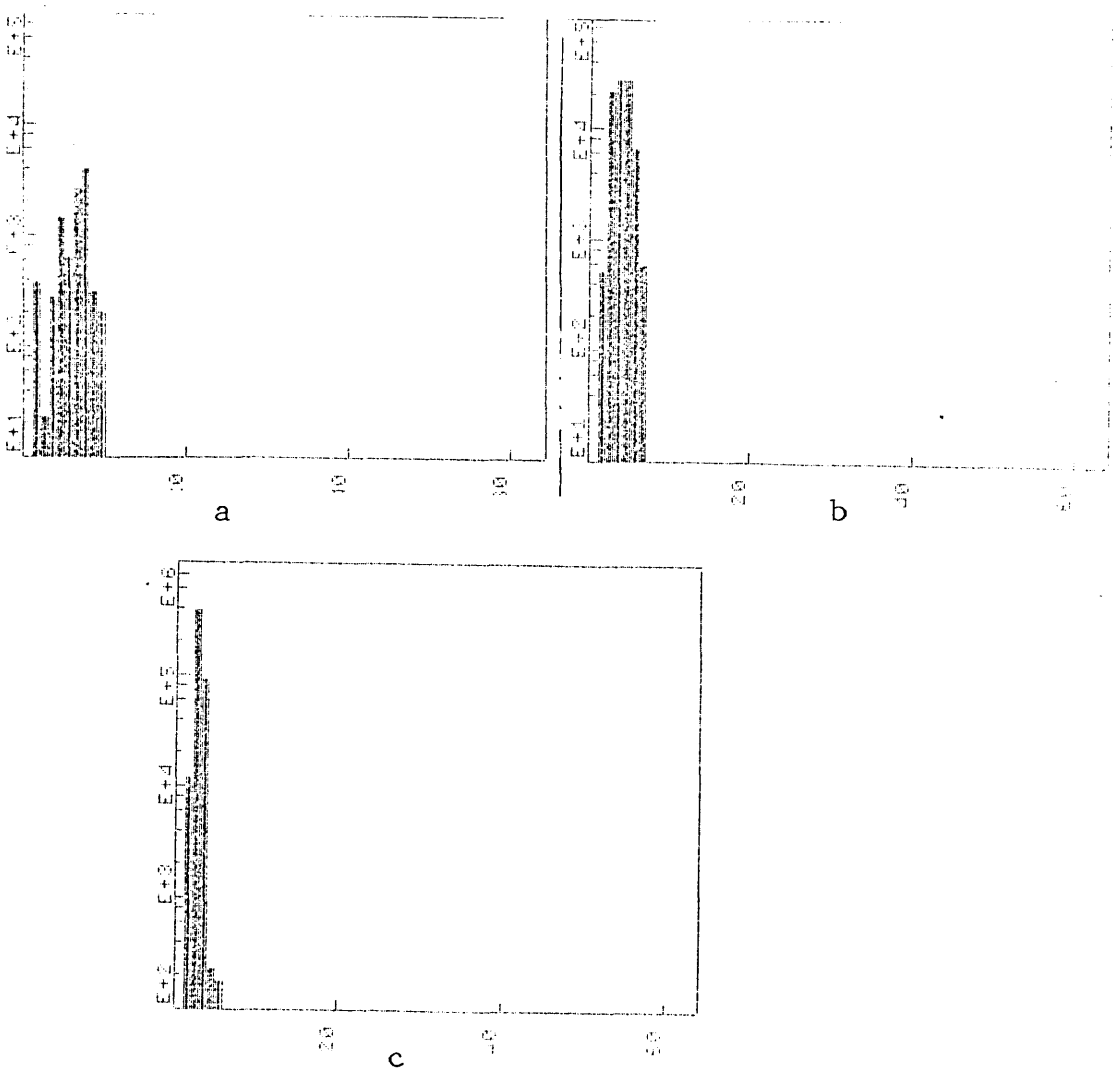

Figure 7.24 The spray becomes more monodisperse as the number of jets formed increases.

V_f = 36 ml/h

(a) 2 jets (b) 3 jets (c) 4 jets

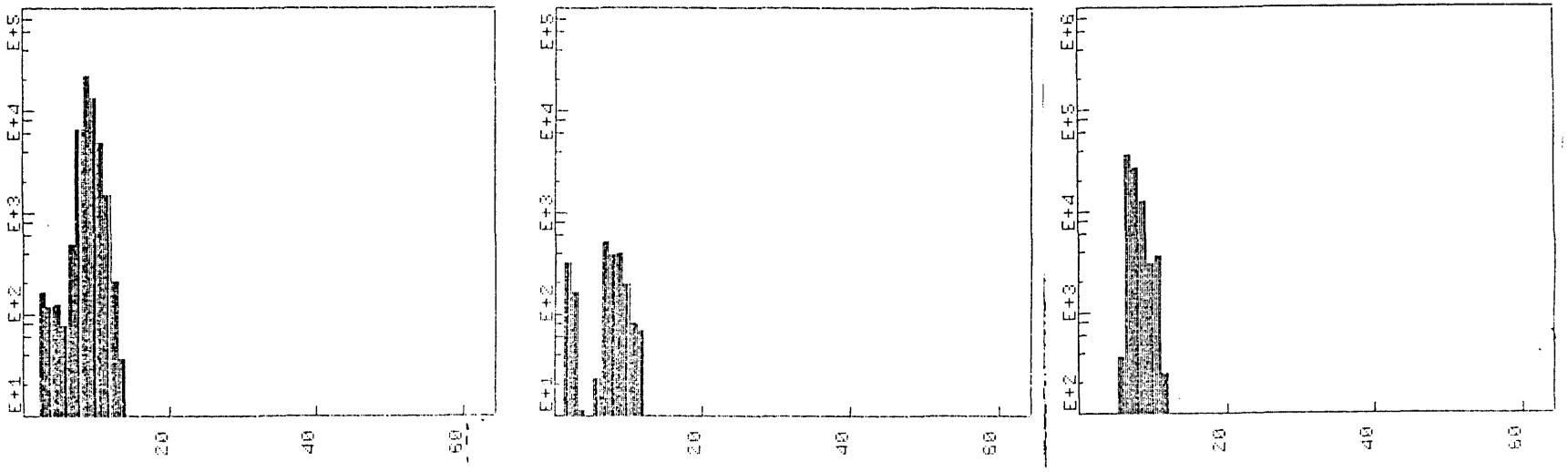

$k = 10^{-8}$ (m)$^{-1}$ $k = 10^{-7}$ (m)$^{-1}$ $k = 6\times10^{-7}$ (m)$^{-1}$

Figure 7.25 The effect of the conductivity is to narrow the size distribution.

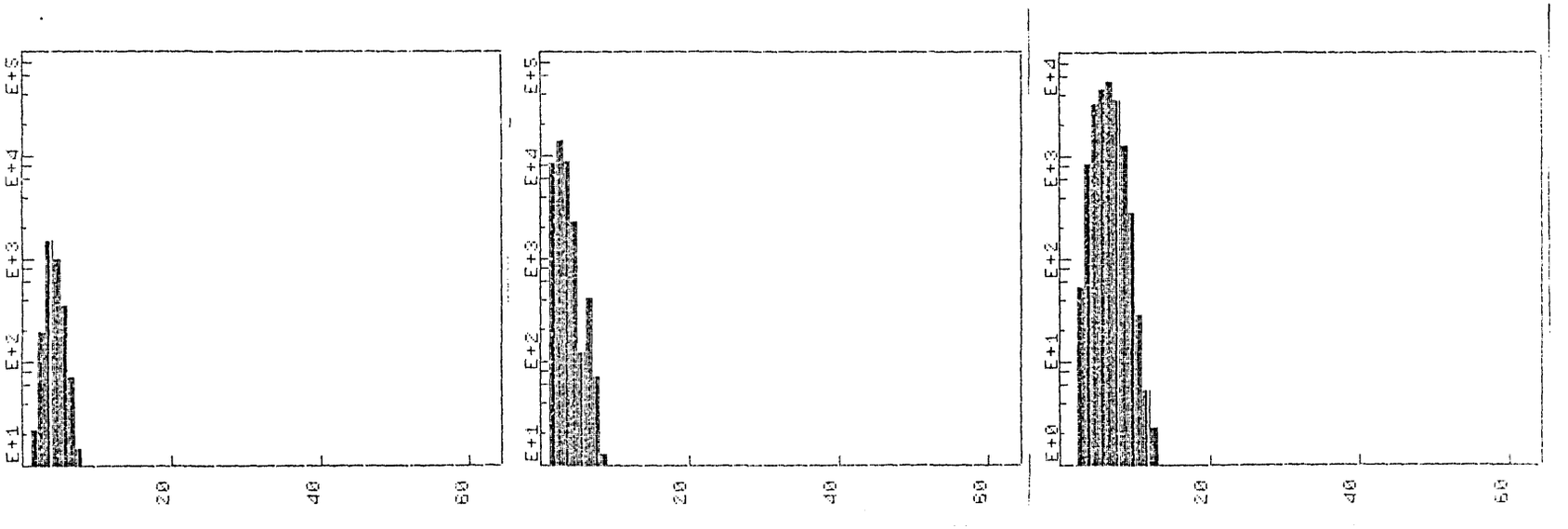

17.4 mPas 30 mPas 57 mPas

Figure 7.26 Bar charts showing a wider range of sizes as the viscosity is raised.

CHAPTER EIGHT

GENERAL DISCUSSION AND SUGGESTIONS FOR FURTHER WORK

General Discussion

The production of charged sprays is of great interest both scientifically and for several branches of industry. Different applications utilise different characteristics of electrostatic spraying. In the particular application to crop spraying, the enhanced deposition of the formulation on the undersides of the target is one of the advantages offered by the process.

Investigations conducted in the past on the subject have illustrated that the manner in which a liquid disrupts into drops is a strong function of the electric field applied. The way in which the liquid interacts with the field depends on the properties of the liquid, amongst which the electrical conductivity is claimed to be the most important factor. Several publications refer to the formation of steady jets of liquid which disintegrate into charged drops of uniform size. Although theories are available for analysing the electric forces which cause a jet to form, many questions about the behaviour of jets remain unanswered. Furthermore, little is known regarding the spray cloud produced from a jet.

A theoretical approach has been combined here with correlations of measurements to provide a better understanding of the process. The need to quantify the appropriate values by measurement rather than by theoretical prediction arises from the complex form of the field. Ions in the liquid move under the influence of the equipotential lines, whilst simultaneously the presence of space charge modifies

the field lines. The effect of the motion of the ions on the motion of the liquid is therefore difficult to describe in complicated geometries. Moreover, the surface of a jet is free from solid boundaries. Hence the boundary conditions, which are used to solve problems in hydrodynamics, cannot easily be specified when electrostatic forces are operative.

The apparatus used consisted of a capillary passing through the centre of a conducting disc, positioned above an earthed collector. This arrangement simplified the electrode geometry, so that theoretical treatment of the electric stresses driving the jet could be carried out. Photographs of a single steady jet issueing from the end of the capillary showed a cone region near the capillary, and a cylindrical portion below the cone which thinned out until a constant diameter was reached. The calculation of the tangential stress on the surface of the cone region and just below it was carried out using two methods. In the first of these, Laplace's equation, which expresses the conservation of potential energy, was solved for the region exterior to the jet. The profile of the liquid interface and the distribution of potentials along it provided one set of boundary conditions. In the second analysis, the momentum equation was derived in spherical co-ordinates and solved for the interior of the cone and the cone surface. Both analyses take into account the convection of the liquid inside the cone.

It was found that the value of the electrical shear stress increases rapidly along the length of the cone, and peaks near its tip. The results from the momentum equation predicted a rapid decline in the tangential stress after the cone tip. However, the conservation of potential energy yielded a more gradual decay in the tangential stress. The deviation of the results for the cylindrical portion of the jet was explained by the difference in the numerical methods

of calculation. Laplace's equation was solved at discrete intervals along the jet surface and at points adjacent to it. In contrast, the momentum equation was solved by continuous integration, and included the forces due to gravity and surface tension. Despite the disagreement, both analyses predict peaks in the tangential stress and the tangential field at or near the tip of cone. The tangential stress was found to vanish at points on the jet above the point of disintegration into drops. In this region all the current is carried by convection on the surface of the jet, and the liquid behaves as an insulator. Near the capillary electrode, the current is carried by conduction through the cone, and the behaviour of the liquid is more like a conductor.

Further work was carried out to assess the factors that cause the jet to disintegrate. Photograghs taken of the end of the jet demonstrated that axisymmetric waves grew due to surface tension. The length of the jet was measured as a function of the flowrate of the liquid, its viscosity and conductivity, and the applied voltage. The viscosity was found to have the greatest effect. The lengthening of the jet at higher flowrates and higher viscosities indicated that hydrodynamics rather than charge effects determine the point of break up. Linear instability theory was used to predict the trend for the length when the flowrate was varied. Increasing the voltage applied to the capillary resulted in an increase in the current and a slight shortening of the jet. However, when the current carried by the jet was increased by raising the conductivity of the liquid, the jet became slightly elongated before drops were formed. This behaviour was found to be due to the increase in the density of charge carried on the surface of the jet at higher conductivity. The results obtained when the

voltage was varied were explained by the constant charge density on the jet surface.

As the voltage applied to the capillary was increased, a value was reached at which the jet became unstable. Photographs showed the jet to waver from one side of the capillary to the other. This behaviour was interpretted in terms of the absence of the stabilising tangential stress. Experiments on a conducting liquid supported this conclusion, when a high normal field on the surface caused rapid charge build up, and resulted in the negation of the tangential stress.

It was of great interest to observe the subsequent behaviour of the liquids at even higher voltages. In order to extend the observations to very high field strengths, an extra electrode was added to the apparatus. When an earthed ring was placed above the capillary tip, the field at the tip was intensified. At high fields, the effect of the sharp metal edges of the capillary became accentuated. The liquid moved towards the point of highest field intensity, and was sprayed from the periphery of the capillary. The extension of points from the annular liquid surface to give stable jets was explained by the high charge imparted to the liquid surface from the capillary. Higher numbers of jets were emitted when the voltage was increased.

These observations prompted the question: what causes spraying from increasing numbers of points on a liquid surface? Clearly, the jets depended critically on the value of the field. Although visual observations of the jets under different conditions of flowrate and conductivity illustrated these effects, they did not explain the changes occuring to the jets. Since the jets are formed primarily by acquiring charge, attention was drawn to investigating the currents carried by the jets. The current was measured on an electrometer by collecting the drops. In earlier work on the

single jet, the density of charge carried on the surface was found to be an important parameter, since it influenced the jet. In the light of this result, emphasis was given to investigating the charge density on the surface when several jets are formed. The charge density was related to the current by the velocity and the radius of the jets. Hence values of the radius were required to estimate the charge density. The photographic techniques were not accessible to measuring the fine jets due to the low field depths at high magnification. Once again the measurements of the drops were related back to the jets. It was assumed that the relation between the drop diameter and the jet diameter, determined for a single jet, remained constant when more than one jet was formed.

Calculation of the charge density led to important conclusions. A plot of the parameter against the numbers of jets emitted from the capillary showed that the charge density remained constant. As the voltage applied to the capillary was increased, the current carried by the jets increased. The liquid reacted to the increase in the current by emitting more jets. Finer jets were formed in order that the increase in the total surface area was comparable to the increase in the total charge carried.

This behaviour also occured at lower field strengths when the liquid was sprayed as a single jet. As the flowrate was raised, the current carried by the jet increased. However, the increase in the current did not correspond to the increase in the flowrate. As a consequence the jet became thicker to maintain constant charge density. The current carried by the jet also rose at higher voltages. Again the final diameter reached by the jet was such that the charge density remained constant. Unlike the experiments in which the flowrate was varied, a rise in the voltage

caused an increase in the charge to mass ratio and therefore a reduction in the final diameter of the jet.

It became clear that when the flowrate and the voltage are varied, a jet accelerates to the value of the final diameter according to the charge carried. The constant charge density on the surface was attributed to the finite charge relaxation time of the liquid.

The conductivity had a different effect on the process. This parameter allowed more charge to reach the surface of the jet, while the diameter was virtually unaffected at lower flowrates. When liquids of higher conductivity were sprayed, higher surface charge densities were carried. A plot of the charge to mass ratio of the drops produced from the break up of a single jet and an ensemble of jets against drop diameter showed that the values approach the Rayleigh limit for a perfect conductor.

The characteristics of the spray cloud are important considerations for a number of applications. The mutual repulsion of the drops determines the width of the cloud; with highly charged drops resulting in sparse deposition. Charging levels also dictate the impact forces on the target. The size distribution of the drops is another important factor. In crop spraying, larger drops are less likely to drift from the plant in windy conditions. Extensive studies have been carried out on the effects of the variables on the charge to mass ratio and average diameter of the cloud. Larger drops were found to carry lower charge to mass ratios. The correlation of the diameter against the ratio was found to depend on the parameter varied. As discussed above, changes in the flowrate and the voltage resulted in an inverse relation between the diameter and the ratio. A weaker dependence of the diameter on the ratio was determined for the case of conductivity variation.

An interesting observation was that the dispersal of the liquid through several jets was a scale up to spraying by the formation of a single jet. For the same liquid, but under different conditions of flowrate and applied voltage, the drop size and the charge to mass ratio for one set of conditions were identical to the values obtained for another set of conditons, provided the flowrate in each jet was constant.

For the single jet, of the parameters investigated, the drop size was found to be the most sensitive to the flowrate. A power balance equating the electrical power consumed by the jet to the sum of the powers for kinetic energy and surface tension energy gave predictions of the diameter close to measured values. The predicted values confirmed that the drop size is proportional to the flowrate to the power 0.63. When multiple jets were formed, the drop size depended on the number of jets formed.

The viscosity of the liquid had a relatively minor influence on the diameter. However, the size distributions of the sprays became more polydisperse as the viscosity was raised. The emission of a wider range of sizes was due to the stretching out of the liquid in the region between an ejected mass and the liquid remaining on the end of the jet. Also, several growths on the end of the jet were pulled off simultaneously under the influence of the external field. The flowrate likewise led to polydispersity. Liquid was observed to be torn from the end of a thick jet by the field before the growth could develop fully into a drop.

Suggestions for further work.

It is hoped that future work will help to study aspects of electrostatic spraying that have not been considered in this thesis or elsewhere. While the conductivity has been investigated extensively, very little is known about the importance of the nature of the ions. Limited results in this thesis show that the stability of several jets at the periphery of the capillary depends on the additive used to raise the conductivity. If spray performance is related to the type of ions, this could have implications for chemical formulations of fertilizers.

Though the concept of the charge relaxation time is used to explain liquid motion, the conductivity is usually the property that is under consideration. The permittivity of the liquid is also important because it partly dictates the field experienced inside the liquid. Permittivity could become significant in cases where the liquid has a low conductivity and a very high field is applied to cause polarization forces.

Since the beginning of investigations into the deformation of drops due to the presence of surface charge, it has been recognised that the cohesive force of surface tension counters electrical effects. Surface tension has not been investigated here, because of the difficulty of keeping the other parameters of the liquid constant. A thorough investigation of this property should be carried out. The results would be not only of interest academically, but also in some industrial applications where interfacial tensions are critical. For example, electric fields are used to enhance mixing in liquid -liquid processes. Surface tension forces play an important role in the spraying of emulsions, as well as their formation in an electric field.

References

1. G.M.Bose, "Recherches sur la cause et sur la veritable theorie de l'electricite." Wittenburg, 1975.

2. J.Zeleny, "On the conditions of instability of electrified drops, with applications to the electrical discharge from liquid points." Proc. Camb. Phil. Soc., vol.18, part 2, p.71, 1914.

3. J.Zeleny, "Electrical discharges from pointed conductors." Phys. Rev., vol.16, no.2, p.102, 1920.

4. J.Zeleny, "Instability of electrified liquid surfaces." The Phys. Rev., vol.10, p.1, 1917.

5. Lord Rayleigh, "On the equilibrium of liquid conducting masses charged with electricity", Phil. Mag., vol.14, p.184, 1882.

6. C.D.Hendricks and J.M.Schneider, "Stability of a conducting droplet under the influence of surface tension and electrostatic forces.", Amer. J. Phys., vol.31, p.450, 1963.

7. Lord Rayleigh, "On the instability of jets.", Proc. Math. Soc., vol.10, p.4, 1878.

8. K.C.Thong, "Electrical control of aerosols in combustion." PhD thesis, Dept. Chem. Eng., Imperial College, London.

9. Lord Rayleigh, "On the instability of a cylinder of viscous liquid under capillary force." Phil. Mag., vol.34, no.207, p.145, 1892.

10. J.N.Schneider, N.R.Linbald, C.D.Hendricks, J.M.Crawley, "Stability of an electrified liquid jet." J. Appl. Pyys., vol.39, no.6, p.2599, 1967.

11. A.B.Basset, "Waves and jets in a viscous liquid." Amer. J. Math., vol.16, p.93, 1894.

12. D.W.Horning, C.D.Hendricks, "Study of an electrically driven jet." J. Appl. Phys., vol.50, no.4, p.2614, 1979.

13. J.R.Melcher, "Field coupled surface waves.", MIT Press, Cambridge, Mass., 1963.

14. G.I.Taylor, "The coalescence of closely spaced drops when they are at different electric potentials." Proc. Roy. Soc., London A, vol.306, p.423, 1968.

15. G.I.Taylor and A.D.McEwan, "Stability of an inetrface under vertical electric field." Fluid Mech., vol.22, p.1, 1965.

16. J.R.Melcher, C.V.Smith,Jr., "Electrohydrodynamic charge relaxation and interfacial perpendicular field instability." Phys. Fluids, vol.12, no.4, p.778, 1967.

17. J.N.Anno, "Mechanics of liquid jets.", Lexington, Mass., Lexington Books, 1977

18. J.R.Melcher, W.J.Shwarz,Jr, "Interfacial relaxation overstability in a tangential electric field." Phys. Fluids, vol.11, p.2604, 1968.

19. N.K.Nayyar, G.S.Murty, "The stability of a dielectric liquid jet in the prescence of a longitudinal electric field." Proc. Roy. Soc., vol.75, p.369, 1960.

20. G.I.Taylor, C.T.R.Wilson, "The bursting of soap bubbles in a uniform electric field." Proc. Camb. Phil. Soc., vol.22, p.728, 1925.

21. W.A.Macky, "Some investigations on the deformation and breaking of water drops in strong electric fields." Proc. Roy. Soc. A, vol.133, p.565, 1931.

22. G.I.Taylor, "Disintegration of water drops in an electric field." Proc. Roy. Soc. A, vol.280, p.383, 1964.

23. G.T.O'Konski, H.C.Thacher, "The distortion of aerosol droplets by an electric field." J. Phys. Chem., vol.57, p.955, 1953

24. J.F.Paddy, "Profiles of axially symmetric menisci." Phil. Trans. Roy. Soc. London, vol.267, p266, 1979.

25. A.G.Bailey, E.Borzabadi, "Natural periodic electrostatic spraying of liquids." IEEE Trans. Ind. Appl., vol.IA-14, no.2, p.162, 1978.

26. A.G.Bailey, E.Borzabadi, "profiles of axially symmetric electrified pendant drops." J. Electrostatics, vol.5, p.369, 1978

27. T.P.Pandya, L.M.Ball, P.Jha, "Stability of speroidal drops in the field of a point charge." J. Coll. and Inter. Sci., vol.99, no.1, 1984.

28. A.Doyle, D.B.Moffett, B.Vonnegut, "Behaviour of evaporating electrically charged droplets." J. Coll. Sci., vol.19, p.136, 1964.

29. M.A.Abbas, J.Latham, "The instability of evaporating charged drops." J. Fluid Mech., vol.30, p.663, 1967.

30. J.W.Schweizer, D.N.Hanson, "Stability limit of charged drops." J. Coll. and Int. Sci., vol.35, no.3, 1971.

31. B.Vonnegut, R.L.Neubauer, "Production of monodisperse liquid particles by electrical atomization." J. Coll. Sci., no.7, p.616, 1952.

32. S.A.Ryce, "An equilibrium value for the charge to mass ratio of droplets produced by electrostatic dispersion." J. Coll. Sci., vol.19, p.490, 1964.

33. R.J.Pfeifer, C.D.Hendricks, "Charge to mass relationships for the electrohydrodynamically sprayed liquid droplets." Phys. Fluids, vol.10, no.10, p.2149, 1967.

34. R.J.Pfeifer, C.D.Hendricks, "Parametric studies of electrohydrodynamic spraying." AIAA J., vol.16, no.3, p.496, 1968

35. V.E.Krohn, "Evidence that the minimum energy state is not accesible to a system of droplets produced by electrohydrodynamic spraying." Appl. Phys. Lett., vol.33, p.220, 1973.

36. W.N.English, "Corona from a water drop." Phys. Rev., vol.74, no.2, 1948.

37. L.B.Loeb, A.F.Kip, V.G.Hanson, "Pulses in negative point to plane corona." Phys. Rev., vol.60, p.714, 1941.

38. L.B.Loeb, "Recent developments in the analysis of the mechanism of corona in air." J. Appl. Phys., vol.19, p.882, 1948

39. G.I.Taylor, "Electrically driven jets." Proc. Roy. Soc. London A, vol.313, p.453, 1969.

40. I.Hayati, "On the mechanism of electrohydrodynamic atomization." PhD thesis, Dept. Chem. Eng., Imperial College, London, 1985.

41. I.Hayati, A.I.Bailey, Th.F.Tadros, "Investigations on the mechanisms of electrohydrodynamic spraying.", J. Coll. Inter. Sci., vol.117, no.1, 1987

42. C.D.Hendricks, R.S.Carson, J.J.Hogan, J.M.Schneider, "Photomicrography of electrically sprayed heavy particles." AIAA J., vol.2, no.4, 1964.

43. V.G.Drozin, "The electrical dispersion of liquids as aerosols." J. Coll. Sci., vol10, p.159, 1955.

44. K.S.Robinson, R.J.Turnball, K.Kim, "Electrostatic spraying of liquid insulators." IEEE Trans. Ind. Appl., vol.IA-16, no.2, 1980.

45. S.B.Sample, R.Bollini, "Production of liquid aerosols by harmonic electrical spraying." J. Coll. and Inter. Sci., vol.41, no.2, 1972.

46. J.F.Hoburg, J.R.Melcher, "Current driven corona terminated water jets as sources of charged drops and audible noise." IEEE Trans. Power Appl. Sys., PAS94, p.128, 1975.

47. J.A.Cross, "Electrostatics, principles, problems and applications." Adam Hilger, Bristol, 1987.

48. J.E.Sickles, T.C.Anestos, "Electrostatic generation of fine paint droplets." IEEE Trans. Ind. Appl., vol.IA-15, no.3, 1979.

49. K.Kim, R.J.Turnball, "Generation of charged drops of insulating liquids by electrostatic spraying." J. Appl. Phys., vol.47, no.5, 1976.

50. J.P.Woosley, R.J.Turnball, K.Kim, "Electrostatic spraying of insulating liquids:H_2." IEEE Trans. Ind. Appl., vol.IA-18, no.3, 1982.

51. A.J.Kelly, "Electrostatic spray theory." J. Appl. Phys., vol.49, no.5, 1978.

52. C.D.Hendricks, "Charged droplet experiments." J. Coll. Sci., vol17, p.249, 1962.

53. J.F.Hughes, I.D.Pavey, "Electrostatic emulsification." J. Electrostatics, vol.10, p.45, 1981.

54. M.A.Nawab, S.G.Mason, "The preparation of uniform emulsions by electrical dispersion." J. Coll. Sci., vol.13, p.179, 1958.

55. M.Arimoto, "Some experimental results on electrostatic emulsion." Res. Rep. Nagaroka Tech. Coll., vol.17, no.2, 1981.

56. A.Watanabe, K.Higashitsuji, N.Nishizawa, "Studies on electrocapillary emulsification." J. Coll. Inter. Sci., vol.64, no.2, 1978.

57. S.A.Ryce, Phys. Fluids, vol.16, p.452, 1973

58. V.I.Kozhenkov, N.A.Fuks, "Electrohydrodynamic atomization of liquids." Rusian Chem. Rev., vol.45, no.12, 1976.

59. A.G.Bailey, W.Balachandran, " The disruption of electrically charged jets of viscous liquid." J. Electrostatics, vol.10, p.99, 1981.

60. J.R.Melcher, E.P.Warren, "Electrohydrodynamics of a current carrying semi-insulating jet." J. Fluid Mech., vol.47, part1, p.127, 1971.

61. N.R.Lindbald, J.M.Schneider, "Production of uniform sized liquid droplets." J. of Sci. Instruments, vol.42, p.635, 1965.

62. A.Neukermans, "Stability criteria of an electrified liquid jet." J. Appl. Phys., vol.44, no.10, 1973.

63. A.G.Bailey, "The importance of capillarity in an electrostatic liquid sprayer." J. Electrostatics, vol.2, p.79, 1976.

64. G.C.Bell Jr., J.Hochburg, "Mechanics of eleoctrostatic atomization, transport, and deposition." Proc. second int. conf. on liquid atomization and sprays, ICLASS 1982

65. R.L.Hines, "Electrostatic atomization and spray painting." J. Appl. Phys., vol.37, no.7, 1966.

66. G.S.P.Castle, II.I.Inculent, "Space charge effects in orchard spraying." IEEE Trans. Ind. Appl., vol.IA-19, no.3, 1983

67. A.R.Jones, K.C.Thong, "The production of charged monodisperse fuel droplets by electrical dispersion." J. Phys. D; Appl. Phys., vol4, p.1159, 1971.

68. W.Balachandran, A.G.Bailey, "Dispersion of liquids using centrifugal and electrostatic forces.", IEEE Trans. Ind. Appl., vol.IA-20,p.68, 1984.

69. M.Mori, T.Sato, H.Amano, A.Watanabe, M.Fujimoto, "Division des liquides en particules dans le champs electro-statique." Proc. Fujihara Memorial Faculty of Eng., Keio Univ., Tokyo, vol.16, no.63, p.1, 1963.

70. R.S.Carson, C.D.Hendricks, "Natural pulsations in electrical spraying of liquids." AIAA J., vol.2, p.733, 1964.

71. T.C.Anestos, J.E.Sickles, R.M.Tepper, "Charge to mass distributions in electrostatic sprays." IEEE Trans. Ind. Appl., vol.IA-13, 1977.

72. S.Ogata, "A study on the charge to mass ratio of polydisperse droplets electrohydrodynamically produced." Japan. J. Appl. Phys., vol.17, no.7, p.1275, 1978.

73. G.I.Taylor, "The force exerted by an electric field on a long cylindrical conductor." Proc. Roy. Soc. London A, vol.291, p.145, 1966.

74. G.I.Taylor, "The circulation produced in a drop by an electric field." Proc. Roy. Soc. London A, vol.291, p.159, 1966.

75. J.R.Melcher, G.I.Taylor, "Electrohydrodynamics: A review of the role of interfacial shear stresses." Annual Review Fluid Mech., vol.1, p.111, 1969.

76. W.F.Pickard, "Progress in dielectrics" London, Academic Press, 1965.

77. S.J.Vellenga, A.Klinkenberg, "On the rate of discharge electrically charged hydrocarbon liquids." Chem. Eng. Sci., vol.20, p.923, 1965.

78. R.A.Coffee, "Electrodynamic energy-A new approach to pesticide application." Proc. Brit. Crop Protection Conf.- Pests and deseases. p.777, 1979.

79. R.A.Coffee, "Electrodynamic crop spraying." Outlook on Agriculture, vol.10, no.7, p.350, 1981.

Appendix 1

```
      PROGRAM VMDCOR(INPUT,TAPE5,OUTPUT,TAPE6)
C
      REAL CM(10),V(10),CON(10),VF(10),E(10),VMD(10)
      REAL PERA,PERL,DEN,CR,Z,D,ST,CONST
      INTEGER I,J,N
      READ(5,10)(V(I),I=1,7)
   10 FORMAT(7E10.5)
      WRITE(6,101)(V(I),I=1,7)
  101 FORMAT(7E10.5)
      READ(5,15)DEN,CR,Z,D
   15 FORMAT(4E10.5)
      WRITE(6,102)DEN,CR,Z,D
  102 FORMAT(4E10.5)
      READ(5,20)(VF(I),I=1,7)
   20 FORMAT(7E10.5)
      WRITE(6,103)(VF(I),I=1,7)
103   FORMAT(7E10.5)
      READ(5,25)(CON(I),I=1,7)
   25 FORMAT(7E10.5)
      WRITE(6,104)(CON(I),I=1,7)
104   FORMAT(7E10.5)
      ST=0.024
      PERA=8.85E-12
      PERL=3.5*PERA
      WRITE(6,220)
  220 FORMAT(4X,"  SINGLE JET VF VARIATION 10% LIQ",//)
C  CALCULATING CM USING HINES SINGLE JET EQUATION
C
      WRITE(6,99991)
99991 FORMAT(5X//," CHARGE TO MASS BY HINES ")
      N=6
      DO 100 I=1,N
      E(I)=V(I)*299.3
      CM(I)=(PERL**2.0)/((3.1416*2.0)*(DEN**3.0))
      CM(I)=((CM(I)*CON(I))/VF(I))**3
      CM(I)=E(I)*CM(I)
      WRITE(6,99992)CM(I),PERL,DEN,CON(I),VF(I),E(I)
99992 FORMAT(4X,E10.5,2X,E10.5,2X,E10.5,2X,E10.5,2X,E10.5,2X,E10.5)
  100 CONTINUE
C  CALCULATING CM ACCORDING TO HENDRICKS MODEL AND MIN ENERGY THEORY
C
      WRITE(6,99995)
99995 FORMAT(5X//," CHARGE TO MASS BY HENDRICKS AND MIN. ENERGY ",//)
C  CALCULATING CM ACCORDING TO HENDRICKS
C
      CONST=(((4*3.1416/PERL)**3.0)*((2*ST)**2.0)
     &*((PERA**5.0)/(DEN**4.0)))**0.143
      WRITE(6,201)CONST
  201 FORMAT(E10.5)
      DO 200 I=1,N
      CM(I)=CONST*((CON(I)*E(I))/(DEN*VF(I)))**0.429
      WRITE(6,99997)CM(I)
99997 FORMAT(5X,E10.5)
  200 CONTINUE
      READ(5,30)(VMD(I),I=1,7)
   30 FORMAT(7E10.5)
      WRITE(6,99999)
99999 FORMAT(5X//,"CHARGE TO MASS BY HENDRICKS MODEL ",//)
C  CALCULATING CM ACCORDING TO HENDRICKS MODEL ONLY
C
      CONST=(4*3.1416*PERA)/(PERL*DEN)
      DO 300 I=1,N
      CM(I)=(CONST*((VMD(I)/2.)**2.)*CON(I)*E(I))/VF(I)
      WRITE(6,9991)CM(I),VMD(I)
 9991 FORMAT(5X,E10.5,4X,E10.5)
  300 CONTINUE
C  USING HINES EQUATION FOR JET RADIUS
C
      WRITE(6,992)
  992 FORMAT(3X,"VMD BY HINES ",//)
      DO 350 I=1,N
      VMD(I)=4.*(((PERL*VF(I))/(CON(I)*(3.1416**2.)*4.)))
     &**0.3333
```

```
      WRITE(6,993)VMD(I)
  993 FORMAT(4X,E10.5)
  350 CONTINUE
C  CALCULATION USING JONES RESULTS
C
      READ(5,505)(CM(I),I=1,7)
  505 FORMAT(7E10.5)
      WRITE(6,9993)
 9993 FORMAT(5X//," VMD BY JONES ",/)
      CONST=(27.*(2.**0.5)*PERA)/(4.0*DEN)
      DO 400 I=1,N


      VMD(I)=(CONST*E(I))/(CM(I)/2.)
      WRITE(6,9995)VMD(I),CM(I)
 9995 FORMAT(5X,E10.5,4X,E10.5)
  400 CONTINUE
C  CALCULATION BASED ON MIN. ENEGY THEORY ,RAYLEIGHLIMIT,MIN.LIMIT
C
      WRITE(6,9996)
 9996 FORMAT(5X//,"VMD BY MIN. ENERGY ",/)
      CONST=(3*(PERA*ST)**0.5)/DEN
      DO 500 I=1,N
      VMD(I)=((CONST/CM(I))**0.6666)*2.0
      WRITE(6,569)VMD(I)
  569 FORMAT(5X,E10.5)
  500 CONTINUE
      WRITE(6,570)
  570 FORMAT(5X//," VMD BY RAYLEIGH LIMIT",/)
      CONST=2.*CONST
      DO 600 I=1,N
      VMD(I)=(((CONST/CM(I)))**0.6666)*2.0
      WRITE(6,575)VMD(I)
  575 FORMAT(5X,E10.5)
  600 CONTINUE
      WRITE(6,580)
  580 FORMAT(5X//,"VMD MIN. LIMIT",/)
      CONST=CONST*(1.34/6.0)
      DO 700 I=1,N
      VMD(I)=(((CONST/CM(I)))**0.6666)*2.0
      WRITE(6,585)VMD(I)
  585 FORMAT(5X,E10.5)
  700 CONTINUE
C  CALCULATING VMD ACCORDING TO ANNO
C
      WRITE(6,590)
  590 FORMAT(5X//," VMD ACCORDING TO ANNO",/)
      N=6
      DO 800 I=1,N
      VMD(I)=4.0*(((4.*PERA*ST)/((CM(I)*DEN)**2.0))**0.333)
      WRITE(6,595)VMD(I)
  595 FORMAT(5X,E10.5)
  800 CONTINUE
C  COMPARING CHARGE RELATION AND DROPLET FORMATION TIMES
C
      WRITE(6,596)
  596 FORMAT(4X,"VMD BASED ON CHARGE RELATION TIME ",/)
      DO 850 I=1,N
      VMD(I)=2.*((PERL*VF(I)*3.)/(4.*3.1416*CON(I)))**0.3333
      WRITE(6,597)VMD(I)
  597 FORMAT(5X,E10.5)
  850 CONTINUE
      STOP
      END
```

```
      PROGRAM PDE(INPUT,TAPE5,OUTPUT,TAPE6,TAPE7)
C
C     .. LOCAL SCLARS ..
      REAL APARAM,CONCHN,CONPES
      INTEGER I,IFAIL,ITCOUN,ITMAX,ITUSED,IXN,IYN,J,N1,
     * N1M,N2,NDIR
C     .. LOCAL ARRAYS ..
      REAL A(15,36),B(15,36),C(15,36),CHNGS(25),D(15,36),E(15,36),
     * F(15,36),RESIDS(25),T(15,36),WRKSP1(15,36),WRKSP2(15,36),
     * WRKSP3(15,36),X(15),Y(36),V(36),CI(36),RC(36),EN(36),
     * VEL(36),CIN(36),JR(36),VD(36),VC(36),ED(36),YL(36)
C     .. FUNCTION REFERENCES ..
      REAL COS,EXP
C     .. SUBROUTINE REFERENCES ..
CC    D03ERF
C
      N1=15
      N2=36
      ND1=7
      ND2=5
      ND6=3
      ND3=4
      ND4=6
      ND5=25
C
CCC
C-----N1= NUMBER OF NODAL POINTS ON X-AXIS.
C-----N2= NUMBER OF NODAL POINTS ON Y-AXIS.
C-----ND1= NUMBER OF NODAL POINTS ON SYRINGE RADIUS.
C-----ND2= NUMBER OF INTERVALS BEYOND SYRINGE RADIUS.
C-----ND3= NUMBER OF NODAL POINTS ON SYRINGE.
C-----ND4= NUMBER OF INTERVALS ON CONE SECTION.
C-----ND5= NUMBER OF INTERVALS ON JET.
C-----N1= ND1+ND2
C-----N2= ND3+ND4+ND5
C-----ND4= ND1-1
C
CCC
C-----HC= LENGTH OF CONICAL SECTION.
C-----HJ= LENGTH OF JET.
C-----HS= LENGTH OF SYRINGE.
C-----HD= DISTANCE BETWEEN ELECTRODE PLATES.
C-----RS= RADIUS OF SYRINGE.
C-----RJ= RADIUS OF JET.
CCC
C
      ND34=ND3+ND4
      NDM34=ND34-1
      ND41=ND34+1
      ND31=ND3+1
      ND12=ND1+ND2
      ND21=ND12+1
      READ(5,9)VOLT,CUR,CON,FLO
    9 FORMAT(F10.3,3E14.5)
      READ(5,11)TH,TH1,RS,RJ1,RJ2,HJP,HJC
      PER=8.85E-12
   11 FORMAT(2F10.5,5E10.3)
      READ(5,12)VISC,DIE,DEN
   12 FORMAT(E14.5,2F10.5)
      PI=22/7
      READ(5,13)R,HD,HS
   13 FORMAT(3E14.5)
      WRITE(6,99999)
      HD=HJC*TAN(TH1)
      RJ=RJ1
      RJX=RJ+HD
      HC=(RS-RJX)/TAN(TH)
      HJ=HD-(HS+HC+HJC)
      H1=(RS-RJX)/(ND1-2)
      RM=(R-RS)/2
      H2=RM/ND2
      H6=RM/ND6
      H3=HS/(ND3-1)
      H4=HC/(ND4-1)
      H45=HJC
      H5=HJ/(ND5-1)
      NJM=15
      APARAM=1.0
      ITMAX=35
      ITCOUN=0
      NDIR=1
      CONPES=0.1E-5
      CONCHN=0.1E-5
      CON=CON*8.0
C
C
```

```
C-----SPECIFYING X-COORDINATES.
C
      X(1)=RJ
      X(2)=RJX
      DO 300 I=3,ND1
      X(I)=X(I-1)+H1
  300 CONTINUE
      ND11=ND1+1
      DO 310 I=ND11,ND12
      X(I)=X(I-1)+H2
  310 CONTINUE
C
      DO 305 I=ND21,N1
      X(I)=X(I-1)+H6
  305 CONTINUE
C
C-----SPECIFYING Y-COORDINATES.
C
      Y(1)=0.0
      DO 320 I=2,ND3
      Y(I)=Y(I-1)+H3
  320 CONTINUE
      DO 330 I=ND31,NDM34
      Y(I)=Y(I-1)+H4
  330 CONTINUE
      Y(ND34)=Y(NDM34)+H45
      Y(ND41)=Y(ND34)+H5/2
      DO 340 I=ND41+1,N2-1
      Y(I)=Y(I-1)+H5
  340 CONTINUE
      Y(N2)=Y(N2-1)+H5/2
      WRITE(6,220)(X(I),I=1,N1)
  220 FORMAT (5F7.5)
      WRITE(6,230)(Y(I),I=1,N2)
  230 FORMAT (10F7.5)
      JR(1)=RJX
      JR(2)=RJ1
      DO 1000 J=3,ND5+1
      IF(J.EQ.3)H5=H5/2
      IF(J.EQ.4) H5=H5*2
      JR(J)=JR(J-1)-(H5*(RJ1-RJ2)/HJP)
      IF(JR(J).LT.RJ2) GO TO 1032
 1000 CONTINUE
 1032  LH=J
      WRITE(6,1007) LH
 1007 FORMAT(14)
      DO 1031 J=LH,ND5+1
      JR(J)=RJ2
 1031 CONTINUE

C
C
C-----SPECIFYING CONICAL RADII.
C
      RC(1)=RJ/SIN(TH1)
      RC(2)=RC(1)+(0.5*H0/SIN(TH1))
      RZ=RC(2)+(0.5*H0/SIN(TH1))
      RC(3)=RJX/SIN(TH)
      ND4T=2*ND4+1
      DO 200 I=4,ND4T
      RC(I)=RC(I-1)+(0.5*H1)/SIN(TH)
      WRITE(6,194)RC(I)
  194 FORMAT(E14.4)
  200 CONTINUE
      M=0
C
      DL=HD-HS
      EP=(2*VOLT)/(DIE*LOG10(4*DL/RS))
      DO 1021 I=ND3,N2
      YL(I)=Y(I)-HS
 1021 CONTINUE
      DO 1022 I=ND31,N2
      ED(I)=EP*LOG((RS+YL(I))/(RS+YL(I-1)))
 1022 CONTINUE
C
      DO 1023 I=ND31,N2
      WRITE(6,1024) YL(I),ED(I)
 1024 FORMAT(E14.5,F10.4)
 1023 CONTINUE
      DO 199 I=1,N2-1
      CI(I)=0.
  199 CONTINUE
C
      LK=36
   10 M=M+1
```

```
      IF(M.EQ.1) GO TO 197
      DO 198 I=ND3,N2-1
      CI(I)=CIN(I)
  198 CONTINUE
C
  197 DO 185 I=1,ND3
      V(I)=VOLT
  185 CONTINUE
      EF=VOLT/HD*H5
      THI=TH
      DO 202 I=ND31,ND34
      K=2*(ND34-I)+1
      IF(K.EQ.1) RC(3)=RZ
      IF(K.EQ.1) TH=TH1
      CONST=(CUR-CI(I-1))
      CONST=CONST/(2*PI*CON*(1-COS(TH)))
      CONST=CONST*(1/RC(K)-1/RC(K+2))
      CONX=(V(I-2)-V(I-1))
      IF((M.EQ.1).AND.(CONST.GT.EF*.8)) GO TO 1006
      V(I)=V(I-1)-CONST
      CONX=V(I-1)-V(I)
      WRITE(6,1009) CONST,ED(I),V(I),V(I-1)
 1009 FORMAT(4F14.4)
  202 CONTINUE
      GO TO 73
 1006 LN=I
      DO 1017 I=LN,ND34
      V(I)=V(I-1)-(CONX*2.5)
 1017 CONTINUE
      WRITE(6,1009) CONST,ED(ND34),V(ND34),V(NDM34)
   73 TH=THI
      RC(3)=RJX/SIN(TH)
      DO 207 I=ND3,NDM34
      K=2*(NDM34-I)+2
      IF(K.EQ.2) TH=TH1
      IF(K.EQ.2) RC(3)=RZ
      CONST=CUR-CI(1)
      CONST=CONST/(2*PI*CON*(1-COS(TH)))
      CONST=CONST*(1/RC(K)-1/RC(K+1))
      IF((M.EQ.1).AND.(CONST.GT.EF/2)) GO TO 1018
      VC(I)=V(I)-CONST
      WRITE(6,1011) VC(I),V(I),CONST,ED(I)
 1011 FORMAT(4F14.4)
  207 CONTINUE
      GO TO 74
 1018  LN=I
      DO 1019 I=LN,ND34
      VC(I)=V(1)-(CONX*2.5/2)
 1019 CONTINUE
   74 TH=THI
      RC(3)=RJX/SIN(TH)
C
C
      DO 1039 I=ND41,N2-1
      IF(I.EQ.ND41) H5=H5/2
      IF(I.EQ.ND41+1) H5=H5*2
      L=I-ND34+2
      CONST=((CUR-CI(I))/(CON*PI*(JR(L))**2))*H5
      IF((M.EQ.1).AND.(CONST.GT.EF)) CONST=CONX*1.0
      IF(I.GT.LK) CONST=EF/1.5
      V(I)=V(I-1)-CONST
 1039 CONTINUE
      V(N2)=0.
      EF=VOLT/HD
C     SET UP DIFFERENCE EQUATION COEFFICIENTS, SOURCE TERMS AND
C     INITIAL CONDITIONS.
      DO 60 J=1,N2
      DO 40 I=ND1,N1
      IF (J.EQ.1) GO TO 410
      IF (J.EQ.N2) GO TO 400
      IF ((I.EQ.ND1).AND.(J.LE.ND3)) GO TO 410
      IF (I.EQ.N1) GO TO 420
      CALL INNER(A,B,C,D,E,Q,T,X,Y,N1,N2,I,J)
      GO TO 40
  400 Q(I,J)=0.0
      GO TO 450
  410 Q(I,J)=VOLT
      GO TO 450
  420 Q(I,J)=VOLT-(EF*Y(J))
  450 CALL BOUND(A,B,C,D,E,T,N1,N2,I,J)
   40 CONTINUE
   60 CONTINUE
C
C
      NDM1=ND1-1
```

```
      IF(M.EQ.1) GO TO 197
      DO 198 I=ND3,N2-1
      CI(I)=CIN(I)
  198 CONTINUE
C
  197 DO 185 I=1,ND3
      V(I)=VOLT
  185 CONTINUE
      FF=VOLT/HJ*H5
      THI=TH
      DO 202 I=ND31,ND34
      K=2*(ND34-1)+1
      IF(K.EQ.1) RC(3)=RZ
      IF(K.EQ.1) TH=TH1
      CONST=(CUR-CI(I-1))
      CONST=CONST/(2*PI*CON*(1-COS(TH)))
      CONST=CONST*(1/RC(K)-1/RC(K+2))
      CONX=(V(I-2)-V(I-1))
      IF((M.EQ.1).AND.(CONST.GT.FF*.8)) GO TO 1006
      V(I)=V(I-1)-CONST
      CONX=V(I-1)-V(I)
      WRITE(6,1009) CONST,ED(I),V(I),V(I-1)
 1009 FORMAT(4F14.4)
  202 CONTINUE
      GO TO 73
 1006 LN=I
      DO 1017 I=LN,ND34
      V(I)=V(I-1)-(CONX*2.5)
 1017 CONTINUE
      WRITE(6,1009) CONST,ED(ND34),V(ND34),V(NDM34)
   73 TH=THI
      RC(3)=RJX/SIN(TH)
      DO 207 I=ND3,NDM34
      K=2*(NDM34-I)+2
      IF(K.EQ.2) TH=TH1
      IF(K.EQ.2) RC(3)=RZ
      CONST=CUR-CI(1)
      CONST=CONST/(2*PI*CON*(1-COS(TH)))
      CONST=CONST*(1/RC(K)-1/RC(K+1))
      IF((M.EQ.1).AND.(CONST.GT.FF/2)) GO TO 1018
      VC(I)=V(I)-CONST
      WRITE(6,1011) VC(I),V(I),CONST,ED(I)
 1011 FORMAT(4F14.4)
  207 CONTINUE
      GO TO 74
 1018  LN=I
      DO 1019 I=LN,ND34
      VC(I)=V(1)-(CONX*2.5/2)
 1019 CONTINUE
   74 TH=THI
      RC(3)=RJX/SIN(TH)
C
C
      DO 1039 I=ND41,N2-1
      IF(I.EQ.ND41) H5=H5/2
      IF(I.EQ.ND41+1) H5=H5*2
      L=I-ND34+2
      CONST=((CUR-CI(I))/(CON*PI*(JR(L))**2))*H5
      IF((M.EQ.1).AND.(CONST.GT.FF)) CONST=CONX*1.0
      IF(I.GT.LK) CONST=FF/1.5
      V(I)=V(I-1)-CONST
 1039 CONTINUE
      V(N2)=0.
      FF=VOLT/HD
C     SET UP DIFFERENCE EQUATION COEFFICIENTS, SOURCE TERMS AND
C     INITIAL CONDITIONS.
      DO 60 J=1,N2
      DO 40 I=ND1,N1
      IF (J.EQ.1) GO TO 410
      IF (J.EQ.N2) GO TO 400
      IF ((I.EQ.ND1).AND.(J.LE.ND3)) GO TO 410
      IF (I.EQ.N1) GO TO 420
      CALL INNER(A,B,C,D,E,D,T,X,Y,N1,N2,I,J)
      GO TO 40
  400 D(I,J)=0.0
      GO TO 450
  410 D(I,J)=VOLT
      GO TO 450
  420 D(I,J)=VOLT-(FF*Y(J))
  450 CALL BOUND(A,B,C,D,E,T,N1,N2,I,J)
   40 CONTINUE
   60 CONTINUE
C
C
      NDM1=ND1-1
```

```
      DO 500 J=ND34,N2
      DO 550 I=1,NDM1
      IF (J.EQ.N2) GO TO 510
      IF ((I.EQ.1).AND.(J.LT.N2)) GO TO 520
      CALL INNER(A,B,C,D,E,Q,T,X,Y,N1,N2,I,J)
      GO TO 550
  510 Q(I,J)=0.0
      GO TO 540
  520 Q(I,J)=V(J)
  540 CALL ROUND(A,B,C,D,E,T,N1,N2,I,J)
  550 CONTINUE
  500 CONTINUE
C
      DO 560 J=1,ND3
      DO 570 I=1,NDM1
      CALL ROUND(A,B,C,D,E,T,N1,N2,I,J)
      Q(I,J)=0.0
  570 CONTINUE
  560 CONTINUE
C
      DO 600 J=ND31,NDM34
      DO 650 I=1,NDM1
      L=ND34-J+1
      IF(I.LT.L) GO TO 610
      IF(I.EQ.L) GO TO 620
      CALL INNER(A,B,C,D,E,Q,T,X,Y,N1,N2,I,J)
      GO TO 650
  610 CALL ROUND(A,B,C,D,E,T,N1,N2,I,J)
      Q(I,J)=0.0
      GO TO 650
  620 CALL ROUND(A,B,C,D,E,T,N1,N2,I,J)
      Q(I,J)=V(J)
  650 CONTINUE
  600 CONTINUE
      WRITE (6,99996)
      IFAIL=1
      CALL D03EBF(N1,N2,N1M,A,B,C,D,E,Q,T,APARAM,ITMAX,
     * ITCOUN,ITUSED,NDIR,IXN,IYN,CONRES,CONCHN,RESIDS,
     * CHNGS,WRKSP1,WRKSP2,WRKSP3,IFAIL)
      WRITE(6,99997)(I,RESIDS(I),CHNGS(I),I=1,ITUSED)
C     CHECK ERROR FLAG
      IF (IFAIL.NE.0) GO TO 160
      WRITE(6,99996)
      DO 80 J=1,N2
      WRITE(6,99995) J,(T(I,J),I=1,N1)
   80 CONTINUE
C
      H4H=H4
C
      DO 559 J=ND31,ND34
      IF(J.EQ.ND34) TH=TH1
      IF(J.EQ.ND34) H4=H45
      L=ND34-J+1
      K=L+1
      I=2*(ND34-J)+2
      DV=VC(J-1)-T(K,J)
      EN(J)=(VC(J-1)-T(K,J))/(SIN(TH)*H4)
      CTM=PER*EN(J)*(CUR-CI(J-1))
      CTM=CTM/(4*PI*CON*(1-COS(TH))*VISC)
      CTK=FLO/(2*PI*(1-COS(TH)))
      CTB=CTM*(SIN(TH)/(1-COS(TH)))
      CTC=CTM/SIN(TH)
      VEL(J)=1/RC(I)
      VEL(J)=VEL(J)*(CTB-2*CTC*COS(TH))
      IF(J.EQ.ND34)VELX=VEL(J)
      VEL(J)=VEL(J)+CTK/(RC(I)**2)
      CIN(J-1)=PER*EN(J)*2*PI*RC(I)*SIN(TH)*VEL(J)
      WRITE(6,561) VC(J-1),T(L,J),T(K,J),DV,EN(J),VEL(J),CIN(J-1)
  561 FORMAT (4F9.0,3E12.5)
  559 CONTINUE
C
      TH=TH1
      H4=H44
      DO 558 J=ND41,N2-1
      L=J-ND34+2
      DV=T(1,J)-T(2,J)
      VEL(J)=FLO/(PI*(JR(L))**2)
      IF(JR(L).GT.PJ2) VEL(J)=VEL(J)+VELX
      EN(J)=DV/H0
      CIN(J)=PER*EN(J)*2*PI*(JR(L))*VEL(J)
      WRITE(6,562) T(1,J),T(2,J),DV,EN(J),VEL(J),CIN(J)
  562 FORMAT(6E12.4)
  558 CONTINUE
      DO 576 J=ND41,N2-1
      IF(CIN(J).GT.CUR) GO TO 577
```

```
      IF(M.EQ.1) GO TO 197
      DO 198 I=ND3,N2-1
      CI(I)=CIN(I)
198   CONTINUE
C
197   DO 185 I=1,ND3
      V(I)=VOLT
185   CONTINUE
      EF=VOLT/HJ*H5
      THI=TH
      DO 202 I=ND31,ND34
      K=2*(ND34-I)+1
      IF(K.EQ.1) RC(3)=RZ
      IF(K.EQ.1) TH=TH1
      CONST=(CUR-CI(I-1))
      CONST=CONST/(2*PI*CON*(1-COS(TH)))
      CONST=CONST*(1/RC(K)-1/RC(K+2))
      CONX=(V(I-2)-V(I-1))
      IF((M.EQ.1).AND.(CONST.GT.FE*.8)) GO TO 1006
      V(I)=V(I-1)-CONST
      CONX=V(I-1)-V(I)
      WRITE(6,1009) CONST,ED(I),V(I),V(I-1)
1009  FORMAT(4F14.4)
202   CONTINUE
      GO TO 73
1006  LN=I
      DO 1017 I=LN,ND34
      V(I)=V(I-1)-(CONX*2.5)
1017  CONTINUE
      WRITE(6,1009) CONST,ED(ND34),V(ND34),V(NDM34)
 73   TH=THI
      RC(3)=RJX/SIN(TH)
      DO 207 I=ND3,NDM34
      K=2*(NDM34-I)+2
      IF(K.EQ.2) TH=TH1
      IF(K.EQ.2) RC(3)=RZ
      CONST=CUR-CI(1)
      CONST=CONST/(2*PI*CON*(1-COS(TH)))
      CONST=CONST*(1/RC(K)-1/RC(K+1))
      IF((M.EQ.1).AND.(CONST.GT.FE/2)) GO TO 1018
      VC(I)=V(I)-CONST
      WRITE(6,1011) VC(I),V(I),CONST,ED(I)
1011  FORMAT(4F14.4)
207   CONTINUE
      GO TO 74
1018   LN=I
      DO 1019 I=LN,ND34
      VC(I)=V(I)-(CONX*2.5/2)
1019  CONTINUE
 74   TH=THI
      RC(3)=RJX/SIN(TH)
C
C
      DO 1039 I=ND41,N2-1
      IF(I.EQ.ND41) H5=H5/2
      IF(I.EQ.ND41+1) H5=H5*2
      L=I-ND34+2
      CONST=((CUR-CI(I))/(CON*PI*(JR(L))**2))*H5
      IF((M.EQ.1).AND.(CONST.GT.FE)) CONST=CONX*1.0
      IF(I.GT.LK) CONST=FE/1.5
      V(I)=V(I-1)-CONST
1039  CONTINUE
      V(N2)=0.
      EF=VOLT/HD
C     SET UP DIFFERENCE EQUATION COEFFICIENTS, SOURCE TERMS AND
C     INITIAL CONDITIONS.
      DO 60 J=1,N2
      DO 40 I=ND1,N1
      IF (J.EQ.1) GO TO 410
      IF (J.EQ.N2) GO TO 400
      IF ((I.EQ.ND1).AND.(J.LE.ND3)) GO TO 410
      IF (I.EQ.N1) GO TO 420
      CALL INNER(A,B,C,D,E,Q,T,X,Y,N1,N2,I,J)
      GO TO 40
400   Q(I,J)=0.0
      GO TO 450
410   Q(I,J)=VOLT
      GO TO 450
420   Q(I,J)=VOLT-(EF*Y(J))
450   CALL BOUND(A,B,C,D,E,T,N1,N2,I,J)
40    CONTINUE
60    CONTINUE
C
C
      NDM1=ND1-1
```

```
      IF(M.EQ.1) GO TO 197
      DO 198 I=ND3,N2-1
      CI(I)=CIN(I)
  198 CONTINUE
C
  197 DO 185 I=1,ND3
      V(I)=VOLT
  185 CONTINUE
      EE=VOLT/HJ*H5
      THI=TH
      DO 202 I=ND31,ND34
      K=2*(ND34-I)+1
      IF(K.EQ.1) RC(3)=RZ
      IF(K.EQ.1) TH=TH1
      CONST=(CUR-CI(I-1))
      CONST=CONST/(2*PI*CON*(1-COS(TH)))
      CONST=CONST*(1/RC(K)-1/RC(K+2))
      CONX=(V(I-2)-V(I-1))
      IF((M.EQ.1).AND.(CONST.GT.EE*.8)) GO TO 1006
      V(I)=V(I-1)-CONST
      CONX=V(I-1)-V(I)
      WRITE(6,1009) CONST,ED(I),V(I),V(I-1)
 1009 FORMAT(4F14.4)
  202 CONTINUE
      GO TO 73
 1006 LN=I
      DO 1017 I=LN,ND34
      V(I)=V(I-1)-(CONX*2.5)
 1017 CONTINUE
      WRITE(6,1009) CONST,ED(ND34),V(ND34),V(NDM34)
   73 TH=THI
      RC(3)=RJX/SIN(TH)
      DO 207 I=ND3,NDM34
      K=2*(NDM34-I)+2
      IF(K.EQ.2) TH=TH1
      IF(K.EQ.2) RC(3)=RZ
      CONST=CUR-CI(1)
      CONST=CONST/(2*PI*CON*(1-COS(TH)))
      CONST=CONST*(1/RC(K)-1/RC(K+1))
      IF((M.EQ.1).AND.(CONST.GT.EE/2)) GO TO 1018
      VC(I)=V(I)-CONST
      WRITE(6,1011) VC(I),V(I),CONST,ED(I)
 1011 FORMAT(4F14.4)
  207 CONTINUE
      GO TO 74
 1018  LN=I
      DO 1019 I=LN,ND34
      VC(I)=V(I)-(CONX*2.5/2)
 1019 CONTINUE
   74 TH=THI
      RC(3)=RJX/SIN(TH)
C
C
      DO 1039 I=ND41,N2-1
      IF(I.EQ.ND41) H5=H5/2
      IF(I.EQ.ND41+1) H5=H5*2
      L=I-ND34+2
      CONST=((CUR-CI(I))/(CON*PI*(JR(L))**2))*H5
      IF((M.EQ.1).AND.(CONST.GT.EE)) CONST=CONX*1.0
      IF(I.GT.LK) CONST=EE/1.5
      V(I)=V(I-1)-CONST
 1039 CONTINUE
      V(N2)=0.
      EE=VOLT/HD
C     SET UP DIFFERENCE EQUATION COEFFICIENTS, SOURCE TERMS AND
C     INITIAL CONDITIONS.
      DO 60 J=1,N2
      DO 40 I=ND1,N1
      IF (J.EQ.1) GO TO 410
      IF (J.EQ.N2) GO TO 400
      IF ((I.EQ.ND1).AND.(J.LE.ND3)) GO TO 410
      IF (I.EQ.N1) GO TO 420
      CALL INNER(A,B,C,D,E,Q,T,X,Y,N1,N2,I,J)
      GO TO 40
  400 Q(I,J)=0.0
      GO TO 450
  410 Q(I,J)=VOLT
      GO TO 450
  420 Q(I,J)=VOLT-(EE*Y(J))
  450 CALL BOUND(A,B,C,D,E,T,N1,N2,I,J)
   40 CONTINUE
   60 CONTINUE
C
C
      NDM1=ND1-1
```

```
      IF(M.EQ.1) GO TO 197
      DO 198 I=ND3,N2-1
      CI(I)=CIN(I)
  198 CONTINUE
C
  197 DO 185 I=1,ND3
      V(I)=VOLT
  185 CONTINUE
      EE=VOLT/HJ*H5
      TH1=TH
      DO 202 I=ND31,ND34
      K=2*(ND34-I)+1
      IF(K.EQ.1) RC(3)=RZ
      IF(K.EQ.1) TH=TH1
      CONST=(COR-CI(I-1))
      CONST=CONST/(2*PI*CON*(1-COS(TH)))
      CONST=CONST*(1/RC(K)-1/RC(K+2))
      CONX=(V(I-2)-V(I-1))
      IF((M.EQ.1).AND.(CONST.GT.EE*.8)) GO TO 1006
      V(I)=V(I-1)-CONST
      CONX=V(I-1)-V(I)
      WRITE(6,1009) CONST,ED(I),V(I),V(I-1)
 1009 FORMAT(4F14.4)
  202 CONTINUE
      GO TO 73
 1006 LN=I
      DO 1017 I=LN,ND34
      V(I)=V(I-1)-(CONX*2.5)
 1017 CONTINUE
      WRITE(6,1009) CONST,ED(ND34),V(ND34),V(NDM34)
   73 TH=TH1
      RC(3)=RJX/SIN(TH)
      DO 207 I=ND3,NDM34
      K=2*(NDM34-I)+2
      IF(K.EQ.2) TH=TH1
      IF(K.EQ.2) RC(3)=RZ
      CONST=COR-CI(1)
      CONST=CONST/(2*PI*CON*(1-COS(TH)))
      CONST=CONST*(1/RC(K)-1/RC(K+1))
      IF((M.EQ.1).AND.(CONST.GT.EE/2)) GO TO 1018
      VC(I)=V(I)-CONST
      WRITE(6,1011) VC(I),V(I),CONST,ED(I)
 1011 FORMAT(4F14.4)
  207 CONTINUE
      GO TO 74
 1018  LN=I
      DO 1019 I=LN,ND34
      VC(I)=V(1)-(CONX*2.5/2)
 1019 CONTINUE
   74 TH=TH1
      RC(3)=RJX/SIN(TH)
C
C
      DO 1039 I=ND41,N2-1
      IF(I.EQ.ND41) H5=H5/2
      IF(I.EQ.ND41+1) H5=H5*2
      L=I-ND34+2
      CONST=((COR-CI(I))/(CON*PI*(JR(L))**2))*H5
      IF((M.EQ.1).AND.(CONST.GT.EE)) CONST=CONX*1.0
      IF(I.GT.LK) CONST=EE/1.5
      V(I)=V(I-1)-CONST
 1039 CONTINUE
      V(N2)=0.
      EE=VOLT/HD
C     SET UP DIFFERENCE EQUATION COEFFICIENTS, SOURCE TERMS AND
C     INITIAL CONDITIONS.
      DO 60 J=1,N2
      DO 40 I=ND1,N1
      IF (J.EQ.1) GO TO 410
      IF (J.EQ.N2) GO TO 400
      IF ((I.EQ.ND1).AND.(J.LE.ND3)) GO TO 410
      IF (I.EQ.N1) GO TO 420
      CALL INNER(A,B,C,D,E,Q,T,X,Y,N1,N2,I,J)
      GO TO 40
  400 Q(I,J)=0.0
      GO TO 450
  410 Q(I,J)=VOLT
      GO TO 450
  420 Q(I,J)=VOLT-(EE*Y(J))
  450 CALL BOUND(A,B,C,D,E,T,N1,N2,I,J)
   40 CONTINUE
   60 CONTINUE
C
C
      NDM1=ND1-1
```

```
      IF(M.EQ.1) GO TO 197
      DO 198 I=ND3,N2-1
      CI(I)=CIN(I)
  198 CONTINUE
C
  197 DO 185 I=1,ND3
      V(I)=VOLT
  185 CONTINUE
      EE=VOLT/HJ*H5
      THI=TH
      DO 202 I=ND31,ND34
      K=2*(ND34-1)+1
      IF(K.EQ.1) RC(3)=RZ
      IF(K.EQ.1) TH=TH1
      CONST=(COR-CI(I-1))
      CONST=CONST/(2*PI*CON*(1-COS(TH)))
      CONST=CONST*(1/RC(K)-1/RC(K+2))
      CONX=(V(I-2)-V(I-1))
      IF((M.EQ.1).AND.(CONST.GT.EE*.8)) GO TO 1006
      V(I)=V(I-1)-CONST
      CONX=V(I-1)-V(I)
      WRITE(6,1009) CONST,ED(I),V(I),V(I-1)
 1009 FORMAT(4F14.4)
  202 CONTINUE
      GO TO 73
 1006 LN=I
      DO 1017 I=LN,ND34
      V(I)=V(I-1)-(CONX*2.5)
 1017 CONTINUE
      WRITE(6,1009) CONST,ED(ND34),V(ND34),V(NDM34)
   73 TH=THI
      RC(3)=RJX/SIN(TH)
      DO 207 I=ND3,NDM34
      K=2*(NDM34-I)+2
      IF(K.EQ.2) TH=TH1
      IF(K.EQ.2) RC(3)=RZ
      CONST=COR-CI(1)
      CONST=CONST/(2*PI*CON*(1-COS(TH)))
      CONST=CONST*(1/RC(K)-1/RC(K+1))
      IF((M.EQ.1).AND.(CONST.GT.EE/2)) GO TO 1018
      VC(I)=V(I)-CONST
      WRITE(6,1011) VC(I),V(I),CONST,ED(I)
 1011 FORMAT(4F14.4)
  207 CONTINUE
      GO TO 74
 1018  LN=I
      DO 1019 I=LN,ND34
      VC(I)=V(1)-(CONX*2.5/2)
 1019 CONTINUE
   74 TH=THI
      RC(3)=RJX/SIN(TH)
C
C
      DO 1039 I=ND41,N2-1
      IF(I.EQ.ND41) H5=H5/2
      IF(I.EQ.ND41+1) H5=H5*2
      L=I-ND34+2
      CONST=((COR-CI(I))/(CON*PI*(JR(L))**2))*H5
      IF((M.EQ.1).AND.(CONST.GT.EE)) CONST=CONX*1.0
      IF(I.GT.LK) CONST=EE/1.5
      V(I)=V(I-1)-CONST
 1039 CONTINUE
      V(N2)=0.
      EE=VOLT/HD
C     SET UP DIFFERENCE EQUATION COEFFICIENTS, SOURCE TERMS AND
C     INITIAL CONDITIONS.
      DO 60 J=1,N2
      DO 40 I=ND1,N1
      IF (J.EQ.1) GO TO 410
      IF (J.EQ.N2) GO TO 400
      IF ((I.EQ.ND1).AND.(J.LE.ND3)) GO TO 410
      IF (I.EQ.N1) GO TO 420
      CALL INNER(A,B,C,D,E,Q,T,X,Y,N1,N2,I,J)
      GO TO 40
  400 Q(I,J)=0.0
      GO TO 450
  410 Q(I,J)=VOLT
      GO TO 450
  420 Q(I,J)=VOLT-(EE*Y(J))
  450 CALL BOUND(A,B,C,D,E,T,N1,N2,I,J)
   40 CONTINUE
   60 CONTINUE
C
C
      NDM1=ND1-1
```

```
C
      DO 500 J=ND34,N2
      DO 550 I=1,NDM1
      IF (J.EQ.N2) GO TO 510
      IF ((I.EQ.1).AND.(J.LT.N2)) GO TO 520
      CALL INNER(A,B,C,D,E,Q,T,X,Y,N1,N2,I,J)
      GO TO 550
  510 Q(I,J)=0.0
      GO TO 540
  520 Q(I,J)=V(J)
  540 CALL BOUND(A,B,C,D,E,T,N1,N2,I,J)
  550 CONTINUE
  500 CONTINUE
C
      DO 560 J=1,ND3
      DO 570 I=1,NDM1
      CALL BOUND(A,B,C,D,E,T,N1,N2,I,J)
      Q(I,J)=0.0
  570 CONTINUE
  560 CONTINUE
C
      DO 600 J=ND31,NDM34
      DO 650 I=1,NDM1
      L=ND34-J+1
      IF(I.LT.L) GO TO 610
      IF(I.EQ.L) GO TO 620
      CALL INNER(A,B,C,D,E,Q,T,X,Y,N1,N2,I,J)
      GO TO 650
  610 CALL BOUND(A,B,C,D,E,T,N1,N2,I,J)
      Q(I,J)=0.0
      GO TO 650
  620 CALL BOUND(A,B,C,D,E,T,N1,N2,I,J)
      Q(I,J)=V(J)
  650 CONTINUE
  600 CONTINUE
      WRITE (6,99998)
      IFAIL=1
      CALL D03EBF(N1,N2,N1M,A,B,C,D,E,Q,T,APARAM,ITMAX,
     * ITCOUN,ITUSED,NDIR,IXN,IYN,CONRES,CONCHN,RESIDS,
     * CHNGS,WRKSP1,WRKSP2,WRKSP3,IFAIL)
      WRITE(6,99997)(I,RESIDS(I),CHNGS(I),I=1,ITUSED)
C     CHECK ERROR FLAG
      IF (IFAIL.NE.0) GO TO 160
      WRITE(6,99996)
      DO 80 J=1,N2
      WRITE(6,99995) J,(T(I,J),I=1,N1)
   80 CONTINUE
C
      H4H=H4
C
      DO 559 J=ND31,ND34
      IF(J.EQ.ND34) TH=TH1
      IF(J.EQ.ND34) H4=H45
      L=ND34-J+1
      K=L+1
      I=2*(ND34-J)+2
      DV=VC(J-1)-T(K,J)
      EN(J)=(VC(J-1)-T(K,J))/(SIN(TH)*H4)
      CTM=PER*EN(J)*(COR-CI(J-1))
      CTM=CTM/(4*PI*CON*(1-COS(TH))*VISC)
      CTK=FLO/(2*PI*(1-COS(TH)))
      CTB=CTM*(SIN(TH)/(1-COS(TH)))
      CTC=CTM/SIN(TH)
      VEL(J)=1/RC(I)
      VEL(J)=VEL(J)*(CTB-2*CTC*COS(TH))
      IF(J.EQ.ND34)VELX=VEL(J)
      VEL(J)=VEL(J)+CTK/(RC(I)**2)
      CIN(J-1)=PER*EN(J)*2*PI*RC(I)*SIN(TH)*VEL(J)
      WRITE(6,561) VC(J-1),T(L,J),T(K,J),DV,EN(J),VEL(J),CIN(J-1)
  561 FORMAT (4F9.0,3E12.5)
  559 CONTINUE
C
      TH=TH1
      H4=H4H
      DO 558 J=ND41,N2-1
      L=J-ND34+2
      DV=T(1,J)-T(2,J)
      VEL(J)=FLO/(PI*(JR(L))**2)
      IF(JR(L).GT.RJ2) VEL(J)=VEL(J)+VELX
      EN(J)=DV/H0
      CIN(J)=PER*EN(J)*2*PI*(JR(L))*VEL(J)
      WRITE(6,562) T(1,J),T(2,J),DV,EN(J),VEL(J),CIN(J)
  562 FORMAT(6E12.4)
  558 CONTINUE
      DO 576 J=ND41,N2-1
      IF(CIN(J).GT.CUR) GO TO 577
```

```
  576   CONTINUE
  577   LK=J
        DO 578 J=LK,N2-1
        CIN(J)=CUR*0.99
  578   CONTINUE
        V(N2)=0.
        EN(N2)=0.
        NM2=N2-1
        IF(M.EQ.4) GO TO 574
        GO TO 10
  574   WRITE(6,573) M
  573   FORMAT(I4)
        STOP
C       ERROR IN DO3EBF
  160   WRITE(6,99993) IFAIL
        STOP
99999 FORMAT (4(1X/), 31H D03EBF EXAMPLE PROGRAM RESULTS/1X)
99998 FORMAT (37H ITERATION      RESIDUAL       CHANGE   /
     *38H         NO              MAX.            MAX. /)
99997 FORMAT(2X,I2,10X,E11.4,4X,E11.4)
99996 FORMAT(//36H TABLE OF CALCULATED FUNCTION VALUES//
     *6OH     1           1           2           3           4           5        6/
     * 3H   J)
99995 FORMAT(1X,I2,1X,15(F6.0,1X))
99993 FORMAT (24H ERROR IN D03EBF  IFAIL=, I4)
        END
        SUBROUTINE INNER(A,B,C,D,E,Q,T,X,Y,N1,N2,I,J)
        DIMENSION A(N1,N2),B(N1,N2),C(N1,N2),D(N1,N2),E(N1,N2),Q(N1,N2)
       *  ,T(N1,N2),X(N1),Y(N2)
C
C
        A(I,J)=2./((Y(J)-Y(J-1))*(Y(J+1)-Y(J-1)))
        E(I,J)=2./((Y(J+1)-Y(J))*(Y(J+1)-Y(J-1)))
        B(I,J)=2./((X(I)-X(I-1))*(X(I+1)-X(I-1)))
        D(I,J)=2./((X(I+1)-X(I))*(X(I+1)-X(I-1)))
        C(I,J)=-A(I,J)-B(I,J)-D(I,J)-E(I,J)
        B(I,J)=B(I,J)-1./((X(I))*(X(I+1)-X(I-1)))
        D(I,J)=D(I,J)+1./((X(I))*(X(I+1)-X(I-1)))
        Q(I,J)=0.0
        T(I,J)=0.0
C
        RETURN
        END

        SUBROUTINE BOUND(A,B,C,D,E,T,N1,N2,I,J)
        DIMENSION A(N1,N2),B(N1,N2),C(N1,N2),D(N1,N2),E(N1,N2),T(N1,N2)
C
C
        A(I,J)=0.0
        B(I,J)=0.0
        C(I,J)=0.0
        D(I,J)=0.0
        E(I,J)=0.0
        T(I,J)=0.0
C
        RETURN
        END
```

```
      PROGRAM FIELDS(INPUT,TAPE5,OUTPUT,TAPE6)
C    MAINFILE D02EBF
C       THIS PROGRAM SOLVES THE EQUATION OF MOTION IN ORDER TO EVALUATE
C   THE SHEAR AND NORMAL ELECTRICAL STRESSES OPERATING ON THE JET
      REAL TOL,X,XEND
C       LOCAL SCALARS
      INTEGER IFAIL,IRELAB,N,J,MPED,IW
C  LOCAL ARRAYS
      REAL W(3,70),Y(7)
C
C       D02EBF,OUTPUT
      EXTERNAL FCN,OUTPUT,PEDERV
      WRITE (6,99999)
      N=3
C  N NUMBER OF EQUATIONS
      WRITE (6,99998)
      IW=70
      MPED=0
C  SETTING A MIXTURE OF ERROR EVALUATION
      IRELAB=1
      WRITE(6,99991)
      DO 200 J=2,7
      TOL=10.**(-J)
      WRITE(6,99997) TOL
      X=0.2127E-2
      XEND=0.7025E-1
      Y(1)=1.299E+5
      Y(2)=6.7E+4
      Y(3)=0.71726E-2
      IFAIL=1
      CALL D02EBF(X,XEND,N,Y,TOL,IRELAB,FCN,MPED,PEDERV,
     &OUTPUT,W,IW,IFAIL)
      WRITE(6,99996)IFAIL
      IF(TOL.LT.0)WRITE(6,99994)
  200 CONTINUE
      STOP
99999 FORMAT(4(1X/),35H FIELDS PROGRAM RESULTS REAR METHOD/1X)
99998 FORMAT(8HO IFAIL=,I1)
99996 FORMAT (1X/ 17H JET SOLUTION)
99997 FORMAT (14H0/22H CALCULATION WITH TOL=,E10.5,/)
99994 FORMAT (24H RANGE TOO SHORT FOR TOL)
99991 FORMAT(10X,31H CALCULATING JACOBIAN BY PEDERV,/)
      END
      SUBROUTINE FCN(T,Y,F)
      REAL T
      REAL F(7),Y(3)
      F(1)=-(0.12495/((T**5.)*Y(1)))-(2.*Y(2)/T)
     &-(3.063E+14/Y(1))-(5.56E+9/((T**2.)*Y(1)))
      F(2)=(((2.62E-8*Y(1)/(T**2.))-((T*F(1))*((1.62E-10*
     &T*Y(1)*Y(2))+(2.02E-8/(T**3.)))))/((T**2.0)*(3.905E+7
     &+(3.1E-11*(Y(1)**2.0)))))-(2.*Y(2)/T)
      F(3)=(8.11E-11*Y(1)*Y(2))+(8.1E-11*T*((Y(2)*F(1))+
     &(Y(1)*F(2))))-(5.252E-8/(T**3.))
      END
C PEDERV EVALUATES THE JACOBIAN OF THE SYSTEM
      SUBROUTINE PEDERV(T,Y,PW)
      REAL T,PW(1,1),Y(1)
      IF(T.GE.1.561E-03)GO TO 200
      PW(1,1)=-(5.36E-08/((Y(1)**0.5)*((2.053E-03-T)**3)))
     &+(1.04E-12/((2.053E-03-T)**4))
      IF(T.LT.1.561E-03)GO TO 100
  200 PW(1,1)=-(0.57E-06/((Y(1)**0.5)*((2.644E-03-T)**3)))
     &+(2.45E-11/((2.644E-03-T)**4))
  100 RETURN
      END

      SUBROUTINE OUTPUT(XSOL,Y)
      REAL XSOL,CIN,TH
      INTEGER J
      REAL Y(7)
      TH=0.0722
      CIN=3.85E-12*2.0*XSOL*SIN(TH)*Y(3)*Y(1)
      WRITE (6,99995) XSOL,Y(1),Y(2),Y(3),CIN
      XSOL=XSOL-2.0E-04
      RETURN
99995 FORMAT("R    EN    ET    VS    CIN",
     &1X/,E10.5,4X,E10.5,4X,E10.5,4X,E10.5,4X,E10.5,/)
      END
```